Synthesis and Characterization of Amide and Urea Receptor Systems for Anion and Metal Complexation and the Synthesis and Use of Block Copolymers for Optoelectronic Crystal Growth

By

Jessica Lohrman

Submitted to the graduate degree program in Chemistry and the Graduate Faculty of the University of Kansas in partial fulfillment of the requirements for the degree of Doctor of Philosophy.

_____

Chair: Dr. Kristin Bowman-James

_____

Dr. Mikhail Barybin

_____

Dr. Timothy Jackson

_____

Dr. David Benson

_____

Dr. Candan Tamerler

Date Defended: 28 June 2017

The dissertation committee for Jessica Lohrman certifies that this is the approved version of the following dissertation:

Synthesis and Characterization of Amide and Urea Receptor Systems for Anion and Metal Complexation and the Synthesis and Use of Block Copolymers for Optoelectronic Crystal Growth

Chair: Dr. Kristin Bowman-James

Date Approved: 25 July 2017

Abstract

The content of this dissertation is divided into two parts, as a result of projects from two research groups during the course of my research at the University of Kansas. The first five chapters detail my work with Dr. Bowman-James which has focused on host-guest chemistry ranging from ligand synthesis to anion and metal binding. I joined the Bowman-James group after my fourth year at KU and have been a member from 2015 to 2017.

Ditopic pyrazine pincers or "duplex" pincers were synthesized and investigated for both their anion binding and their metal binding merit. Chapter 2 will investigate duplex hosts as anion binding hosts, the duplex receptors were synthesized with R group functionalizations that permit a range of solubilities in various solvents. Their anion binding capabilities will be discussed in comparison to their monotopic counterparts. The duplex pincers were also studied for transition metal binding capabilities which will be detailed in Chapter 5. Palladium complexes were made and characterized with the duplex pincers and some of the interesting features of these compounds will be discussed. Aside from the duplex hosts, urea macrocyclic receptors were also synthesized and characterized for their anion host capabilities, which will be discussed in Chapter 3. Variations in macrocycle size and urea components were explored and binding merit was determined on these receptor complexes.

The final two chapter of this dissertation highlight one of my projects in the Ren group from my first year of graduate school in 2011 up through my fourth year in 2015. I joined the Bowman-James group after Dr. Ren moved to Temple University. Chapter 6 will include a review on the field of organic photovoltaic and optoelectronic devices. Chapter 7 will detail my work synthesizing block copolymers for use as compatibilizing agents for P3HT and C_{60}

interfaces. These organic photovoltaic devices exhibited an interesting magnetoconductive behavior that can be observed at room temperature in these charge transfer systems.

Acknowledgements

Firstly, I would like to thank Dr. Bowman-James, from the bottom of my heart, for accepting me into her group after my fourth year. Kristin, you have been the best mentor I could ask for! When working with you, the science is more exciting and there is always something to discuss and figure out. Thank you for always being there when I went through hard times and always helping to pull me through. I will really miss talking to you every day, whether about chemistry or just general ridiculous things. You single handedly restored my appreciation for chemistry and I cannot thank you enough.

Dr. Benson, thank you for being a great TA boss! I learned so much about teaching, how to run a classroom, how to construct fair tests, and how to always strive always improve a class from you. I also enjoyed our opera conversations. I cannot thank you enough. My thanks, also, to Tim Jackson and Misha Barybin. Whenever I had a question over the past 6 years, you both would always have an open door and would try to help me out. Thank you Cindy Berrie for helping me with AFM. Rich Givens and Mike Clift, thank you for helping me when I had organic chemistry questions. Victor Day, thank you for all the help with my crystal structures and for the moral support! Thank you Candan Tamerler for agreeing to be on my defense committee.

My thanks to the Bowman-James group, both current and former members who have made every day in the lab more fun. Hanumaiah Telikepalli, thank you for the synthetic help and for our small political chats. Sun Ok Kang, than you for helping me with crystal growth and making sense of my endless titration data. Emran Haque, I'm so happy you joined the group, it has been great getting to know you over the past year. Kara Motley, you are a fantastic undergraduate researcher and I know you will be great wherever you end up.

The former Ren group Dan, Alec, and Phil, you guys made every day better. I've never laughed harder than when I was with you three and you always stood by me when times were tough, for which, I cannot thank you enough. Though we never knew where our conversations started, we could always be sure it would end with an argument about which teenage mutant ninja turtle villain was the main boss. Dan and Phil: you are still wrong, it's Shredder. Phil, thank you teaching me spectroscopy and for always having my back. Alec, thank you for having patients when I would be going crazy and for being the best lab mate I could ask for. Dan, I'm still impressed you know all the words to "Let it go", and I really miss our absurd conversations. I gained three brothers from the Ren group and I am very thankful for that.

Thank you to the current and past generations of grad students Hannah, Nate, Chris, Cassie, Jason, Derek, Allyssa, Melissa, Josh, Brad, Theresa, Tom, Indeewara, Pubudu, and Kelci, you are all like family to me. John Meyers and Andy Speath in particular, thank you for mentoring me. John, you make me want to be a better chemist at all times. You also taught me I'm never too old for slip-n-slides, so I'm appreciative for that too. Andy, I'm sorry for glittering your desk. I owe so much to you for all the help and advice you gave me! Mason Hart, you have been one of my best friends here for 5 years. I really don't know what I'm going to do without game night. Probably be a calmer person since I don't have to feel like a recess monkey for losing to you every time. Mary Smith, we did this whole thing together, through good times and bad. You've supported me so much and I will miss our elaborate dressage dancing. Thank you for making me laugh.

Wei Qin, thank you for teaching me about multiferroic materials and for having a good sense of humor. Thank you to Shenqiang Ren for making me a much stronger person and introducing me to materials chemistry. Justin and Sarah, thank you for all the help with NMR

over the years. My thanks to Simon Lang for helping me whenever I needed help learning new organic set ups.

Lastly, I would like to thank my sister Sara and Mom and Dad, without whom I could never have made this far in life. Sara, you are the best role model of a strong women. Nothing can stop you and I've always looked up to that. Mom, you brought me from a vaguely illiterate and extremely stubborn 10 year old with poor grades, to a chemistry PhD program. You supported me every time I thought I couldn't do it, pushed to do better because you knew I could, and then sent me snacks when I wasn't eating properly. You have always been my emotional rock and biggest fan. I can never finish saying thank you! Dad, you taught me it's ok to be a bit weird. You've supported me this whole time, both financially and emotionally, despite the fact that I've been I college 11 years now. Thank you for always making me laugh when I needed it and for always finding new adventures for us to go on! Thank you for believing there was nothing I couldn't do, and always telling me that my entire life. The three of you mean the world to me and I am thankful every day for each of you.

Table of Contents

List of Figures

Chapter 2

Chapter 3

Chapter 5

Chapter 6

Chapter 7

List of Tables

Chapter 2

Chapter 3

Chapter 5

Chapter 7

List of Schemes

Chapter 2

Chapter 3

Chapter 5

Chapter 7

Abbreviations

AFM – Atomic force microscopy

BCP – Block copolymer

BHJ – Bulk heterojunction

CH_3CN – Acetonitrile

CT – Charge transfer

CTC – Charge transfer crystal

DCB – 1,2-Dichlorobenzene

DEH-PPV - poly[(2,5-di(2′-ethyl)hexyloxy)-1,4-phenylenevinylene]

DMF – Dimethylformamide

DMSO – Dimethylsulfoxide

DOE – Department of energy

FTIR – Fourier transform infrared spectroscopy

HOMO – Highest occupied molecular orbital

HRMS – High resolution mass spectrometry

ITO – Indium tin oxide

LBHB – Low barrier hydrogen bond

LUMO – Lowest unoccupied molecular orbital

MC – Magnetoconductance

MEM-PPV - Poly[2- methoxy,5-(2'-ethyl-hexyloxy)-p-phenyl-ene vinylene]

MFE – Magnetic field effect

MMA – Methyl methacrylate

MOF – Metal organic framework

NMR – Nuclear magnetic resonance

OPV – Organic photovoltaic

P3AT – Poly-3-alkylthiophene

PBr3HT - Poly-6-bromo-3-hexylthiophene

PCE – Power conversion efficiency

P3HT – Poly-3-hexylthiophene

PCBM - Phenyl-C_{61}-butyric acid methyl ester

PDOT:PSS – Poly(3,4-etylenediaminedioxythiophene) polystyrene sulfonate

PL – Photoluminescence

PLA - Polylactide

PPV - p-phenylenevinylene

PS – Polystyrene

TBA – Tetrabutylammonium

TEA - Tetraethylammonium

TEA – Triethylamine

THF – Tetrahydrofuran

XRD – X-ray diffraction

CHAPTER 1

Supramolecular Anion Receptor Review

1.0.0 Supramolecular Chemistry

Supramolecular chemistry was described by one of the founders of the field, Jean-Marie Lehn, as "…the chemistry of the intermolecular bond, covering the structures and functions of the entities formed by association of two or more chemical species."[1] Early works in this field were dedicated to the study of the interaction of these molecular assemblies and the forces that drive them. The field evolved into host-guest complexes that could be used for the recognition of ions in solution which has since proven to be important to environmental and biological sustainability.

The first example of a supramolecular host-guest system was reported by Charles Pedersen in 1967 concerning macrocyclic crown ethers. He showed that crown receptors were able to stabilize alkali metals through ion-dipole interactions between the cation and the oxygens in the macrocycle. A particular compound of note was 18-crown-6, **1**, that was capable of capturing K^+ selectively over Li^+, Na^+, Cs^+, or Rb^+ based its size to fit in the ring cleft.[2-3] Jean-Marie Lehn advanced this work by developing higher order inclusion complexes composed of more than one macrocyclic ring system referred to as cryptands, **2**. Cryptands were demonstrated to capture alkali and alkaline earth metals within the cavity center like a crypt. These receptors were seen to enhance cation binding in comparison to monocyclic macrocycles by a factor of 10^5 in a 95:5 methanol:water mixture.[4-5] Park and Simmons' bicyclic quaternized amine receptor, **3**, was the first example of a host that was capable of sequestering anions internally. These advancements in cation and anion capture have evolved into a significant collection of supramolecular hosts catering to ionic guests.

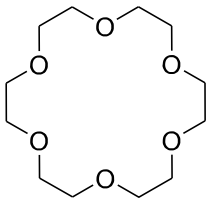

1

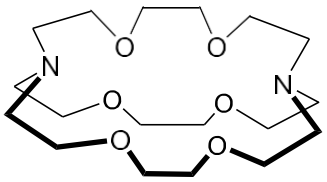

2

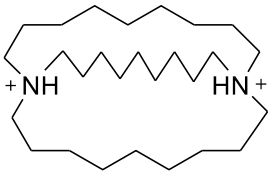

3

The field of supramolecular chemistry received its first major accolades in 1987 in the form of a Nobel Prize awarded to the works of Lehn, Pedersen, and also to Donald Cram. Amongst Cram's notable accomplishments were spherands, **4**, which targeted spherical cations by utilizing a constrictive ring system with six methoxy groups converging towards the central cavity extending above and below the molecular plane.[6] Applications for supramolecular chemistry are still growing, from simple hosts for ions to applications in separations, sensors, catalysis, and materials. Recently, the advancement of supramolecular chemistry has been recognized with another Nobel Prize. In 2016, Sir J. Fraser Stoddart, Ben Feringa, and Jean-Pierre Sauvage were awarded for their work with supramolecular systems as molecular machines.[7-9]

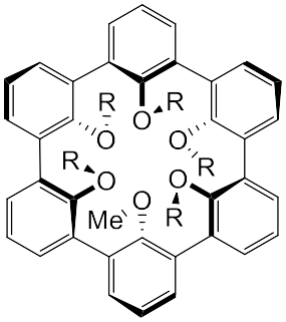

4

1.1.0 Importance of Anions

Anions have an impact on many facets of life including environmental and biological systems. Halides are of particular interest in the biological field where Cl^- acts as an electrolyte and maintains potential across cell membranes. These Cl^- levels are sensitive and essential to body function and misregulation has been linked to the cause of neuromuscular diseases such as cystic fibrosis.[10] In the United States, fluoridation of tap water is a common practice. While some believe in the benefits of F^- to oral hygiene, high fluoride concentrations will negate any positive value and cause fluorosis of dental and skeletal structures.[11-12]

Nutrient anions such as phosphate and nitrate are ubiquitous in both biological and environmental systems. Due to their agriculturally significant contribution in fertilizer, nutrient anions used on fields can lead to an overabundance that contaminates freshwater rivers and lakes leading to eutrophication. Eutrophication of lake and river systems can produce heavy algae blooms that can negatively impact the natural environment and its inhabitants.[13] Utilization of anion sensors and receptors in crop fertilization and management can help control optimal nutrient levels for successful crop yields.[14] The use of sensors can also aid in the prevention of over fertilization to minimize agricultural pollution of fresh water.[15] Meanwhile, capture and repurposing of these agriculturally significant anions could impact crop growth needed to feed an ever growing global population.

Hazardous anions that have a detrimental impact on the environment are not limited to agricultural fertilizers but can also be found in nuclear waste products. A major issue for the Department of Energy (DOE) is that of nuclear waste remediation. Cold-war era nuclear waste is stored in large containment tanks at the Hanford Site, Idaho National Laboratory, the Savannah

River Site, and Oak Ridge National Laboratory. While over 94 million gallons of nuclear waste is stored at these sites, recently there has been a push to address environmental concerns from the long term storage of these materials as the tanks begin to fail.[16] Tank waste contains problematic ions such as most actinides, lanthanides, and the radioactive nuclides $^{137}Cs^{+}$ and $^{90}TcO_4^{-}$. While many of these ions are well known as radioactive contaminants, anions such as phosphate, nitrate, hydroxide and carbonate all cause substantial separation issues as well as contribute to tank corrosion.[17] Sulfate, another anionic component of the waste, poses even further issues to the prolonged containment of waste materials. The proposed method of storage for these materials is immobilization of waste via a vitrification process which will contain the waste materials in glass. Insolubility of sulfate in a borosilicate matrix creates voids within the glass infrastructure that hinder the glass structural integrity. Sulfate also exhibits high leach rates, which can increase the leach rate of actinides from the glass. Furthermore, during vitrification, sulfate tends to separate as a molten salt. This leads to the corrosion of melter components which has the potential for harmful effects. In order to safely process and store these waste materials, the anionic components need to be addressed.

Anions are ever present and can pose substantial health and environmental issues if left unchecked. Therefore it is imperative that anion content and concentrations be regulated. Supramolecular chemistry can provide solutions to these problems.

1.2.0 Anionic Hosts

Anions are more elusive in their capture when compared to their cation counterparts for a few reasons. Anion size tends to be larger than that of cations which causes their charge to radius ratio to be lower. Lower charge to radius ratios can decrease their electrostatic interactions with a

host system of similar counter charge. This can also be followed by the fact that anions come in a multitude of geometries. From spherical guests such as halides to trigonal planar ions like nitrate, geometry variation presents difficulties in shaping idealized binding pockets for each anion. Another important factor to consider is that anions can be susceptible to the pH of their surrounding environment. Oxo anions, such as phosphate and sulfate, risk becoming protonated depending upon the environmental pH, which may alter their charged state.[18]

Solvation is another key factor that influences both enthalpies and entropies of binding. The interactions of solute within the solvent matrix can greatly affect the binding capability of a host-guest system. Competition for binding can arise depending on properties of the solvent, such as polarity and hydrogen bonding ability, which affects how it interacts with the host and guest. Protic solvents interact strongly with negatively charged anions through hydrogen bonding and will compete with host hydrogen bonding. If the anion interaction with the solvent is stronger than that of the host-guest complex, the binding will be ineffective and weak. Strongly polar aprotic solvents such as dimethyl sulfoxide (DMSO) are also competitive with host compounds. As a hydrogen bond acceptor, DMSO can compete with anions for hydrogen bond donors provided by host systems and thus weaken the host-anion complexation. Weaker hydrogen bond acceptors such as acetonitrile (CH_3CN) display less competitive behavior so association constants are typically higher in comparison to DMSO.[19] All of the aforementioned considerations must be taken into account when designing anion receptor systems. Therefore, it is important to tailor the host to the anion of interest through the geometry of the receptor as well as the environment in which it resides for success in sequestration.

1.2.1 Early Anionic Hosts

The first report of supramolecular encapsulation of an anion in a simple host was by Park and Simmons in 1968. This was accomplished by using a bicyclic ammonium macrocycle known as a katapinand. The word katapinand comes from the Greek work katapinosis meaning to engulf, which is a good description of how the macrocycle encompasses an anion inside its binding cavity. The katapinand, **5**, was composed of protonated tertiary amines linked by three nine-membered aliphatic chains. Positively charged ammonium groups electrostatically trap an anionic halide guest within the central cavity. Encapsulation is further aided by isomerization of the outward pointing ammonium hydrogen bonds in **5**, to face inward in the presence of chloride, **5a**. The ammonium groups are then able to act as hydrogen bond donors to further stabilize halides.[20]

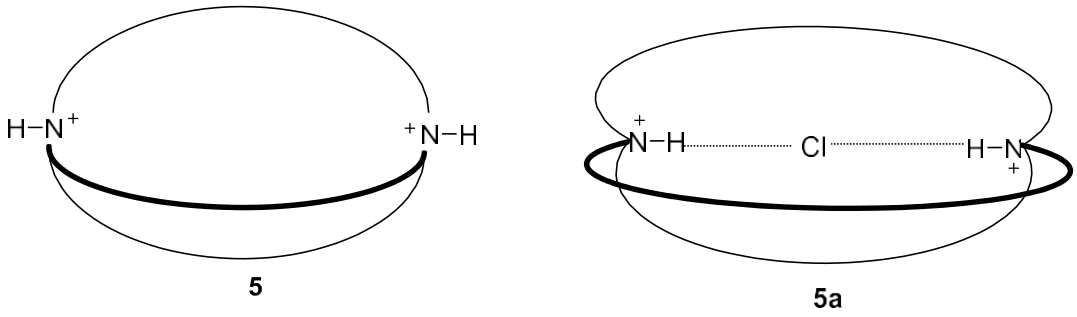

5 **5a**

Jean-Marie Lehn continued the focus on anion encapsulation with his own form of katapinand which he termed as cryptands. Originally applied to cations, cryptands could also be modified into effective halide hosts by the protonation of four linking tertiary amines into quaternary ammonium groups, **6**. These ammonium hydrogens were anticipated to point inward towards the cavity center, thus hydrogen bonding to the encapsulated halide in a similar fashion to Park and Simmons' katapinand-chloride complex. The addition of two extra hydrogen bond donors and a decrease in cavity size caused the cryptate complex to exhibit Cl^-/Br^- selectivity

>1000 in water and displayed the outright exclusion of I^-.[21] Another example by Lehn a few years later was adapted from an octaamine cryptand that was originally studied for binuclear metal binding. Cryptand **7** was reported to be an effective anion receptor aided by the hexaprotonation of the six amines.[22-23] It was shown to have a substantial affinity not only for Cl^- and F^-, but it also for N_3^-. The crystal structure revealed that the linear anion, N_3^-, extends down the center of the cavity where terminal nitrogen lone pairs act as hydrogen bond acceptors to three separate hydrogen bond donors each, **7a**.

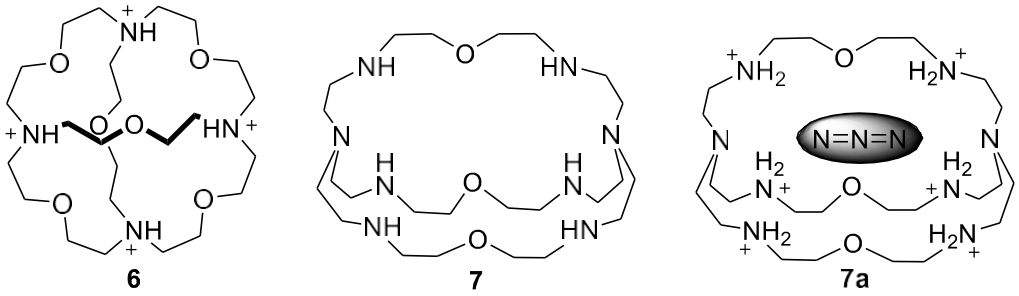

6 **7** **7a**

Schmidtchen took the method of using quaternary amines for anion binding a step further by creating a tetra-quaternary tricycle, **8**. Due to the use of methyl group to generate the positive charge instead of protons, the binding could be solely attributed to charge and not hydrogen bonding. The crystal structure showed that the tetrahedron contained a spherical cavity ideally sized to fit spherical halide ions which proved to be selective for bromide and iodide over chloride in water. Coulombic interactions between the tetraammonium points and negatively charged iodide caused it to be held perfectly in the center of the cavity equidistant from all N points of the tetrahedron at ~4.45 Å.[24] Though **8** was capable of encapsulating halides through charge alone, the binding was still weaker than for compound **7** that additionally benefited from hydrogen bonding.

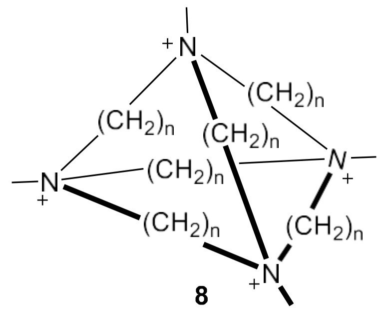

8

A Bowman-James collaboration with Jean-Marie Lehn in France lead to the start of the Bowman-James group into receptor systems. Their studies demonstrated a hexaprotonated ammonium macrocycle [24]N_6O_2, **9,** is capable of not only binding ATP, **9a**, but was also capable of catalyzing phosphoryl transfer. This causes the macrocycle to form a phosphoramidate intermediate followed by hydrolysis of phosphoramidate to adenosine diphosphate (ADP), **9b**. This demonstrated the utility of complex **9** not only as an anion receptor but also as a simple enzyme mimic of ATPase by its catalytic ability.[25-26] With DOE funding the Bowman-James group has since expanded to synthesizing supramolecular hosts as anion capture agents.

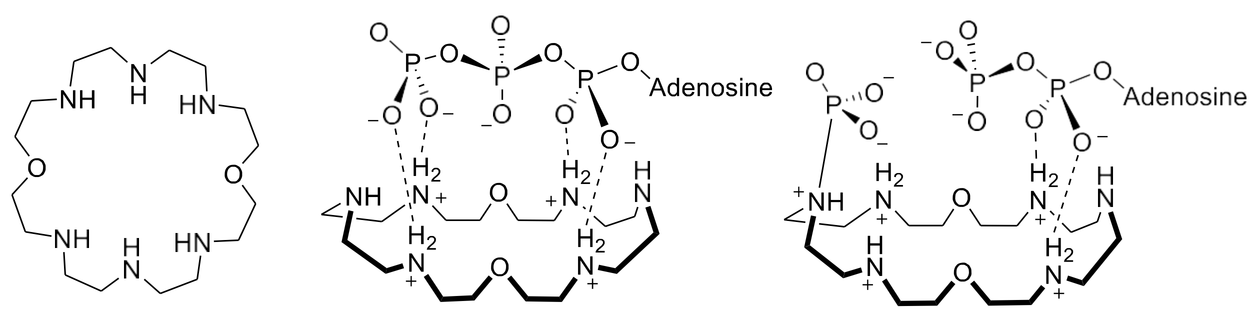

9 **9a** **9b**

The Bowman-James group next demonstrated macrocycle **9** could be used to bind other oxoanions, specifically, to envelop NO_3^- by folding around the anion encapsulated in the central pocket.[27] The bicycle, **10**, also demonstrated an affinity for NO_3^- by using an octaamine ring system with *m*-phenyl bridging units promoting C_3 symmetry. In the crystal structure it was

revealed that two NO_3^- anions were encapsulated within the bicyclic cavity on either side of the phenyl bridges. Each oxygen is aligned perfectly with two N-H bonds, thereby effectively tying them back on either side of the cavity. Alignment in this fashion allowed the dual nitrates, whose unusual crystal structure revealed an eclipsed conformation, to overcome electron repulsion between the two anions, **10a**.

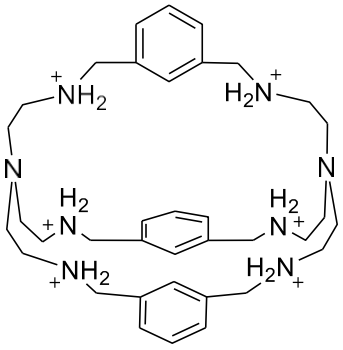

10

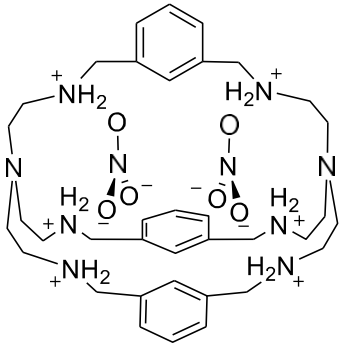

10a

The previously discussed receptors in this section all depend on charge as a key factor in their ability to bind anion guests. However, there are some limitations to charged receptors as anion hosts. Many of these systems depend upon protonated ammonium groups to sequester anions, which makes them highly reliant on the pH of the environment to function. Quaternized systems that don't rely on protonation and are pH independent, like those reported by Schmidtchen, displayed only weak binding without the support of hydrogen bonding. Moreover, because these complexes are charged, they can typically only be employed in protic solvents such as water, thereby limiting the environments in which they can function. It is for this reason, interest in the field of neutral receptor systems was cultivated and has been on the rise since the 1980's.

1.2.2 Amide Hosts

Neutral hosts that depend on hydrogen bonding for anion capture arose after Quiocho, in 1985, demonstrated the sulfate binding protein of *Salmonella tryphimurium* was capable of sequestering sulfate within a 7 Å deep cleft. Solvent and cations were inaccessible inside the cleft, so it was concluded that hydrogen bonding was the primary force holding the sulfate in place.[28] Neutral hydrogen bonding subunits, such as amides, have since been shown to be affective components in receptors due to their generous hydrogen bond donating nature.

The first example of an amide functionalized receptor was reported by Pascal in 1986, in which a biphenyl-anchored bicyclic species with three amide bridging units formed a cylindrical cavity, **11**. After NMR studies with tetrabutylammonium (TBA) fluoride, it was suggested that F^- was likely sequestered internally by the three amide groups whose NH hydrogen bond donors pointed inward towards the cavity center.[29] From here, amide receptors took off as excellent hydrogen bond donors for the purposes of anion recognition and capture. In 1993 Reinhoudt modeled a simple tripodal acyclic amide receptor, **12**, after the protein binding of sulfate described by Quiocho.[30] Depending on R group functionalization, this early acyclic amide receptor was shown to have selectivity for oxoanion $H_2PO_4^-$ over Cl^- by a factor of nine in the case of **12c**.

A major advancement to this field, by Crabtree, was the introduction of a diamide receptor system with a phenyl or pyridyl backbone. A benefit of these receptors is the structured backbone of either a isophthalamide or pyridine-2,6-dicarboxamide which creates a binding pocket that is preorganized for coordination. The isophthalamide receptor with phenyl appendages, **13**, showed bound bromide in the binding pocket between the two amide groups in

the crystal structure.[31-32] Diamide subunits have since been vastly expanded upon with great success into macrocycles and higher dimensions of cyclic systems by the Bowman-James group.

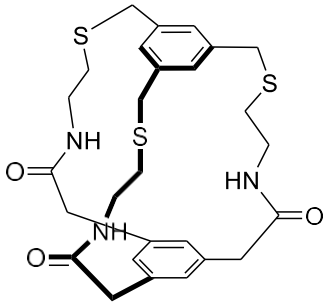

11

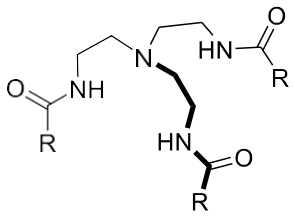

12a R = CH_2Cl
12b R = $(CH_2)_4CH_3$
12c R = C_6H_5
12d R = 4-$MeOC_6H_4$

12

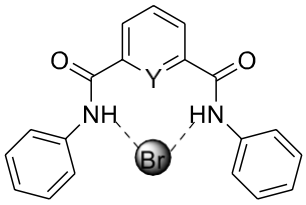

13

With respect to neutral receptors, a major interest in the Bowman-James group has been the utilization of diamide subunits, **14**, to construct anion receptors. The versatile anion coordination subunit can be employed using a phenyl or pyridyl core with either simple amides or thioamides in a *meta* relationship on the ring. From here, the diamide subunit can be further tailored into receptors of variable geometry such as acyclic ligands, monocycles, bicycles, tricycles, and various other host compounds with the addition of bridging groups.

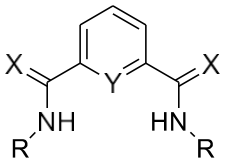

14

X = O or S
Y = CH or N

The first monocyclic diethylamine bridged system linking two isophthalamide or, later, pyridine-2,6-dicarboxamides, **15**, subunits was reported by the Bowman-James group in 2001.[33] Receptor **16** is composed of tertiary amine bridging units and isophthalamide anchors, where the amines are capable of acting as basic sites that can deprotonate anions with acidic protons. This was shown to have high selectivity for $H_2PO_4^-$ and HSO_4^- over Cl^- showing binding constants that were 90 and 63 times greater than for Cl^- respectively. The crystal structure of **15** with

sulfate revealed a unique sandwich complex (**16**) where the two macrocycles are related by pseudo-S_4 symmetry atop one another in order to accommodate the tetrahedral sulfate shape. In this complex, each sulfate oxygen is hydrogen bonded to two macrocyclic amides.

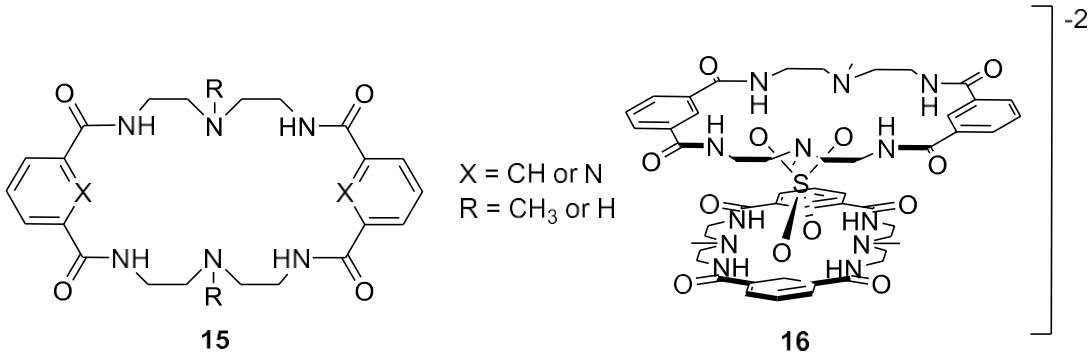

15 **16**

The Bowman-James group was also able to produce higher dimension macrocycles such as bicycles and tricycles using pyridine-2,6-dicarboxamide as anchoring units which could be tailored to different geometries of various guests. Bicycle **17** displayed a significant affinity for F^- and Cl^- with K_a's greater than the 10^5 M^{-1} limitation for NMR titrations. Crystal structures showed F^- at the center of the cavity associated with all six hydrogen bond donors symmetrically.[34] An even higher degree of macrocycle was synthesized as tricycles **18** and **19.** Receptor **18** showed a selectivity for linear anions like N_3^- and FHF^-, which were encapsulated down the center of the cylindrical cavity. As opposed to the linear tricycle **18**, the tetrahedron, **19**, showed encapsulation of a tetrahedrally-hydrated F^-, where each of the four water molecules associate with the receptor's amides.[35-36] Other early examples utilizing the diamide subunit include Jurzcak's acyclic and monomacrocyclic systems and Ansyln's bicyclic cyclophanes.[37-39]

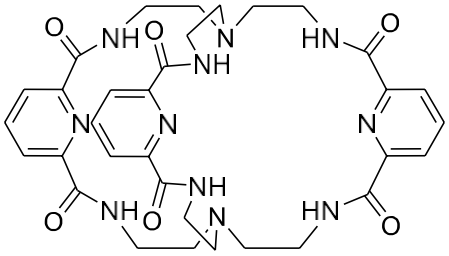

17

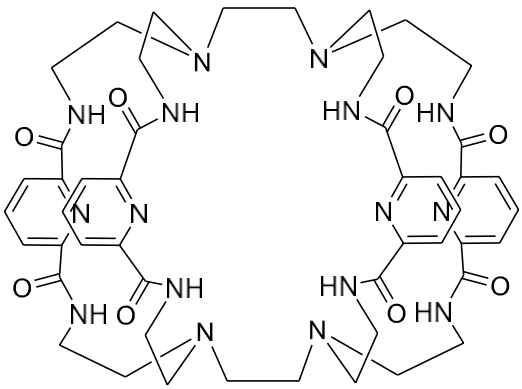

18

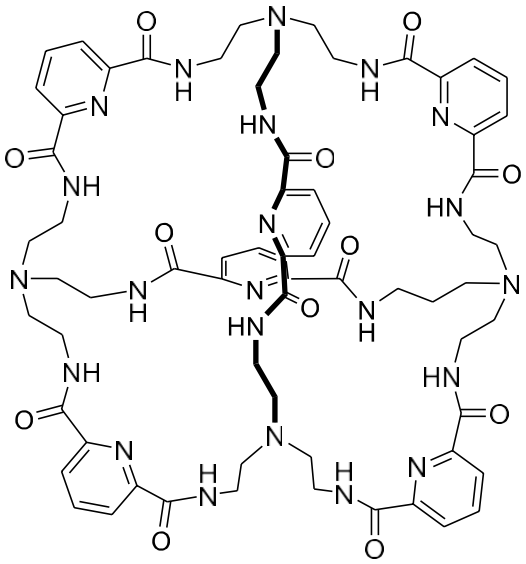

19

1.2.3 Urea Hosts

Urea groups are another important subunit in neutral receptors. While amide groups provide only one hydrogen bond donor per unit, a urea contributes two parallel hydrogen bond donors. In 1992 Wilcox reported the affinity of a monourea receptor for phosphate and sulfate appended phenyl groups, **20**.[40] The urea's parallel hydrogen bond donors align well with oxygens in oxoanions making them effective for oxoanion binding. Hamilton and coworkers further demonstrated mono and bis-urea anion recognition with carboxylates.[41] The dual hydrogen bonding NH units in **20** are complementary to the positioning of the carboxylate oxygens. Binding was shown to be enhanced significantly by the progression to thioureas due to increased acidity of the hydrogen bond donors from greater polarizability of sulfur.[42]

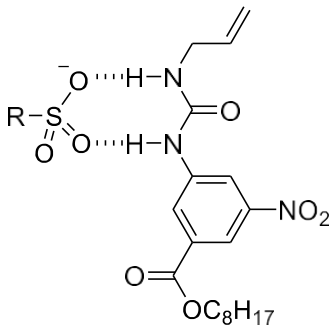

20

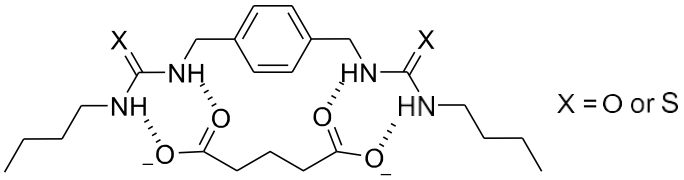

21

Ureas and thioureas have been employed widely in anion receptors.[43-46] Reinhoudt has reported some notable advances in both acyclic and macrocyclic urea host systems, **22**. Core receptor **22** was examined with both terminal R groups for acyclic compounds as well as bridging groups to create macrocyclic urea receptors. Binding of $H_2PO_4^-$ was found to be bind selective in comparison to other anions such as Cl^-, NO_3^-, Br^-, and HSO_4^-. Interestingly, through titrations and Job plots it was determined that the acyclic compound displays a 1:2 binding mode whereas the macrocyclic complex showed 1:1 binding. This is likely due to the more rigid, compact, and less flexible nature of the macrocycles. Continuous efforts in these urea based systems have broken ground into applications for selective anion sensors as well as porous columnar materials and is still expanding with further investigation.[47-51]

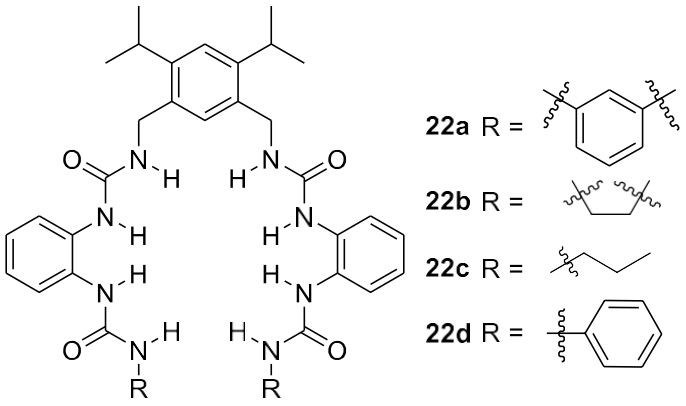

22

More recently the Bowman-James group has investigated simple acyclic urea and amide pincers in a comparison of the chelate effect influence on the two functional groups. It was shown that the urea chelate systems were superior anion hosts in comparison to the pyridine-2,6-diacarboxamide-based receptors by possessing twice the NH hydrogen bond donating capabilities. It was reported that selective binding occurred for SO_4^{2-} relative to $H_2PO_4^-$, Cl^-, NO_3^-, OAc^-, ClO_4^-, and N_3^-. The urea hosts demonstrated SO_4^{2-} binding capabilities in DMSO and DMSO/water solvents mixtures which are known to be highly solvating. An interesting aspect of this work was the analysis of the additional urea NH hydrogen bonding units in the receptors. As the possible coordination given by NH groups increased from two in receptor **23**, to four in receptor **24**, and to six in receptor **25,** so did the anion affinity where **25** displayed a large K_a of 7,025 M^{-1} in a 25% H_2O mixture in DMSO.[52]

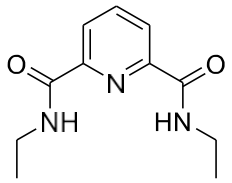

23

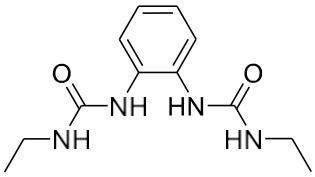

24

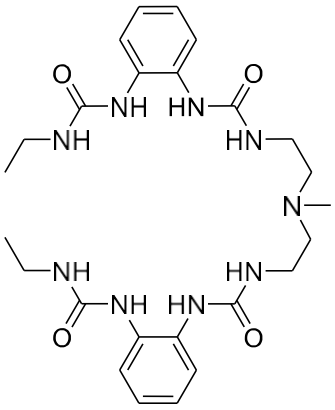

25

1.3.0 Continuation of Anion Receptor Work in the Bowman-James Group

Amide and urea-based subunits have been of great interest to the Bowman-James group due to their versatility. Ease of functionalization in the amide and urea R groups gives them an

inherent ability to be designed to accommodate specific anion guests through hydrogen bonding systems that match anion geometries. The following two Chapters, 2 and 3, will include work in supramolecular anion receptor chemistry. Work in Chapter 2 will focus on the synthesis and investigation of anion binding properties of pyrazine-2,3,5,6-tetracarboxamide based receptors. Variation of arm appendages on these receptors yielded a series of hosts with tunable solubility. These new tetra-substituted pyrazine hosts will be evaluated in comparison to simple pyridine-2,6-dicarboxamide corollaries with the corresponding arm groups. The subsequent research in Chapter 3 will examine urea-based macrocycles and their anion host capabilities. Urea-based macrocycles were synthesized with *m*-xylene backbones and alkyl amine bridging units of different length and number of urea groups. Anion affinity of these simple urea macrocyclic receptors was evaluated and will be discussed therein.

References

1. Lehn, J.-M., Supramolecular Chemistry—Scope and Perspectives Molecules, Supermolecules, and Molecular Devices (Nobel Lecture). *Angewandte Chemie International Edition in English* **1988,** *27* (1), 89-112.
2. Pedersen, C. J., Cyclic Polyethers and their Complexes with Metal Salts. *Journal of the American Chemical Society* **1967,** *89* (10), 2495-2496.
3. Pedersen, C. J., Cyclic Polyethers and their Complexes with Metal Salts. *Journal of the American Chemical Society* **1967,** *89* (26), 7017-7036.
4. Lehn, J. M., Cryptates: the Chemistry of Macropolycyclic Inclusion Complexes. *Accounts of Chemical Research* **1978,** *11* (2), 49-57.
5. Konopelski, J. P.; Kotzyba-Hibert, F.; Lehn, J.-M.; Desvergne, J.-P.; Fages, F.; Castellan, A.; Bouas-Laurent, H., Synthesis, Cation Binding, and Photophysical Properties of Macrobicyclic Anthraceno-Cryptands. *Journal of the Chemical Society, Chemical Communications* **1985,** (7), 433-436.
6. Cram, D. J.; Kaneda, T.; Helgeson, R. C.; Lein, G. M., Spherands - Ligands whose Binding of Cations Relieves Enforced Electron-Electron Repulsions. *Journal of the American Chemical Society* **1979,** *101* (22), 6752-6754.
7. Bissell, R. A.; Cordova, E.; Kaifer, A. E.; Stoddart, J. F., A Chemically and Electrochemically Switchable Molecular Shuttle. *Nature* **1994,** *369* (6476), 133-137.
8. Livoreil, A.; Dietrich-Buchecker, C. O.; Sauvage, J.-P., Electrochemically Triggered Swinging of a [2]-Catenate. *Journal of the American Chemical Society* **1994,** *116* (20), 9399-9400.
9. Koumura, N.; Zijlstra, R. W. J.; van Delden, R. A.; Harada, N.; Feringa, B. L., Light-driven Monodirectional Molecular Rotor. *Nature* **1999,** *401* (6749), 152-155.
10. Puljak, L.; Kilic, G., Emerging Roles of Chloride Channels in Human Diseases. *Biochimica et Biophysica Acta (BBA) - Molecular Basis of Disease* **2006,** *1762* (4), 404-413.
11. Cametti, M.; Rissanen, K., Recognition and Sensing of Fluoride Anion. *Chemical Communications* **2009,** (20), 2809-2829.
12. Ayoob, S.; Gupta, A. K., Fluoride in Drinking Water: A Review on the Status and Stress Effects. *Critical Reviews in Environmental Science and Technology* **2006,** *36* (6), 433-487.
13. Moss, B., A Land Awash with Nutrients - the Probem of Eutrophication. *Chemistry & Industry* **1996,** (11), 407-411.
14. Forde, B. G., Nitrate Transporters in Plants: Structure, Function and Regulation. *Biochimica et Biophysica Acta (BBA) - Biomembranes* **2000,** *1465* (1), 219-235.
15. Watt, M. M.; Zakharov, L. N.; Haley, M. M.; Johnson, D. W., Selective Nitrate Binding in Competitive Hydrogen Bonding Solvents: Do Anion–π Interactions Facilitate Nitrate Selectivity? *Angewandte Chemie International Edition* **2013,** *52* (39), 10275-10280.
16. Moyer, B. A.; Custelcean, R.; Hay, B. P.; Sessler, J. L.; Bowman-James, K.; Day, V. W.; Kang, S.-O., A Case for Molecular Recognition in Nuclear Separations: Sulfate Separation from Nuclear Wastes. *Inorganic Chemistry* **2013,** *52* (7), 3473-3490.
17. Clark, S.; Buchanan, M.; Wilmarth, B., Basic Research Needs for Environmental Management. Energy, U. S. D. o., Ed. February 2016.

18. Beer, P. D.; Gale, P. A., Anion Recognition and Sensing: The State of the Art and Future Perspectives. *Angewandte Chemie International Edition* **2001,** *40* (3), 486-516.
19. Fundamentals and Applications of Anion Separations. Moyer, B. A.; Singh, R. P. Eds.; Springer: New York, 2004.
20. Park, C. H.; Simmons, H. E., Macrobicyclic Amines. III. Encapsulation of Halide Ions by in,in- 1,(k + 2)-diazabicyclo[k.l.m.]alkane Ammonium Ions. *Journal of the American Chemical Society* **1968,** *90* (9), 2431-2432.
21. Graf, E.; Lehn, J. M., Anion Cryptates: Highly Stable and Selective Macrotricyclic Anion Inclusion Complexes. *Journal of the American Chemical Society* **1976,** *98* (20), 6403-6405.
22. Lehn, J. M.; Pine, S. H.; Watanabe, E.; Willard, A. K., Binuclear Cryptates. Synthesis and Binuclear Cation Inclusion Complexes of Bis-tren Macrobicyclic Ligands. *Journal of the American Chemical Society* **1977,** *99* (20), 6766-6768.
23. Dietrich, B.; Guilhem, J.; Lehn, J.-M.; Pascard, C.; Sonveaux, E., Molecular Recognition in Anion Coordination Chemistry. Structure, Binding Constants and Receptor-Substrate Complementarity of a Series of Anion Cryptates of a Macrobicyclic Receptor Molecule. *Helvetica Chimica Acta* **1984,** *67* (1), 91-104.
24. Schmidtchen, F. P.; Muller, G., Anion Inclusion without Auxiliary Hydrogen Bonds: X-ray Structure of the Iodide Cryptate of a Macrotricyclic Tetra-quaternary Ammonium Receptor. *Journal of the Chemical Society, Chemical Communications* **1984,** (16), 1115-1116.
25. Hosseini, M. W.; Lehn, J. M.; Jones, K. C.; Plute, K. E.; Mertes, K. B.; Mertes, M. P., Supramolecular Catalysis: Polyammonium Macrocycles as Enzyme Mimics for Phosphoryl Transfer in ATP Hydrolysis. *Journal of the American Chemical Society* **1989,** *111* (16), 6330- 6335.
26. Hosseini, M. W.; Lehn, J. M.; Maggiora, L.; Mertes, K. B.; Mertes, M. P., Supramolecular Catalysis in the Hydrolysis of ATP Facilitated by Macrocyclic Polyamines: Mechanistic Studies. *Journal of the American Chemical Society* **1987,** *109* (2), 537-544.
27. Papoyan, G.; Gu, K.-j.; Wiorkiewicz-Kuczera, J.; Kuczera, K.; Bowman-James, K., Molecular Dynamics Simulations of Nitrate Complexes with Polyammonium Macrocycles: Insight on Phosphoryl Transfer Catalysis. *Journal of the American Chemical Society* **1996,** *118* (6), 1354- 1364.
28. Pflugrath, J. W.; Quiocho, F. A., Sulphate Sequestered in the Sulphate-Binding Protein of Salmonella Typhimurium is Bound Solely by Hydrogen Bonds. *Nature* **1985,** *314* (6008), 257- 260.
29. Pascal Jr, R. A.; Spergel, J.; Van Engen, D., Synthesis and X-ray Crystallographic Characterization of a (1,3,5)cyclophane with Three Amide N-H groups Surrounding a Central Cavity. A Neutral Host for Anion Complexation. *Tetrahedron Letters* **1986,** *27* (35), 4099-4102.
30. Valiyaveettil, S.; Engbersen, J. F. J.; Verboom, W.; Reinhoudt, D. N., Synthese und Komplexierungsverhalten Ungeladener Anionen-Rezeptoren. *Angewandte Chemie* **1993,** *105* (6), 942-944.
31. Kavallieratos, K.; de Gala, S. R.; Austin, D. J.; Crabtree, R. H., A Readily Available Non-preorganized Neutral Acyclic Halide Receptor with an Unusual Nonplanar Binding Conformation. *Journal of the American Chemical Society* **1997,** *119* (9), 2325-2326.

32. Kavallieratos, K.; Bertao, C. M.; Crabtree, R. H., Hydrogen Bonding in Anion Recognition: A Family of Versatile, Nonpreorganized Neutral and Acyclic Receptors. *The Journal of Organic Chemistry* **1999,** *64* (5), 1675-1683.
33. Hossain, M. A.; Llinares, J. M.; Powell, D.; Bowman-James, K., Multiple Hydrogen Bond Stabilization of a Sandwich Complex of Sulfate between Two Macrocyclic Tetraamides. *Inorganic Chemistry* **2001,** *40* (13), 2936-2937.
34. Kang, S. O.; Llinares, J. M.; Powell, D.; VanderVelde, D.; Bowman-James, K., New Polyamide Cryptand for Anion Binding. *Journal of the American Chemical Society* **2003,** *125* (34), 10152- 10153.
35. Kang, S. O.; Day, V. W.; Bowman-James, K., Tricyclic Host for Linear Anions. *Inorganic Chemistry* **2010,** *49* (18), 8629-8636.
36. Wang, Q.-Q.; Day, V. W.; Bowman-James, K., Supramolecular Encapsulation of Tetrahedrally Hydrated Guests in a Tetrahedron Host. *Angewandte Chemie International Edition* **2012,** *51* (9), 2119-2123.
37. Szumna, A.; Jurczak, J., A New Macrocyclic Polylactam-Type Neutral Receptor for Anions − Structural Aspects of Anion Recognition. *European Journal of Organic Chemistry* **2001,** *2001* (21), 4031-4039.
38. Szumna, A.; Jurczak, J., Unusual Encapsulation of Two Anions in the Cavity of Neutral Macrocyclic Octalactam, Preliminary Communication. *Helvetica Chimica Acta* **2001,** *84* (12), 3760-3765.
39. Bisson, A. P.; Lynch, V. M.; Monahan, M.-K. C.; Anslyn, E. V., Recognition of Anions through NH·π Hydrogen Bonds in a Bicyclic Cyclophane—Selectivity for Nitrate. *Angewandte Chemie International Edition in English* **1997,** *36* (21), 2340-2342.
40. Smith, P. J.; Reddington, M. V.; Wilcox, C. S., Ion Pair Binding by a Urea in Chloroform Solution. *Tetrahedron Letters* **1992,** *33* (41), 6085-6088.
41. Fan, E.; Van Arman, S. A.; Kincaid, S.; Hamilton, A. D., Molecular Recognition: Hydrogen- Bonding Receptors that Function in Highly Competitive Solvents. *Journal of the American Chemical Society* **1993,** *115* (1), 369-370.
42. Hossain, M. A.; Kang, S. O.; Llinares, J. M.; Powell, D.; Bowman-James, K., Elite New Anion Ligands: Polythioamide Macrocycles. *Inorganic Chemistry* **2003,** *42* (17), 5043-5045.
43. Bühlmann, P.; Nishizawa, S.; Xiao, K. P.; Umezawa, Y., Strong Hydrogen Bond-mediated Complexation of H_2PO^- by Neutral Bis-thiourea Hosts. *Tetrahedron* **1997,** *53* (5), 1647-1654.
44. Brooks, S. J.; Gale, P. A.; Light, M. E., Carboxylate Complexation by 1,1'-(1,2-phenylene)bis(3- phenylurea) in Solution and the Solid State. *Chemical Communications* **2005,** (37), 4696-4698.
45. César, R.; Marta, A.; Mercedes, M.; Volker, W.; Luisa, M. M.; Victoria, A.; Cruz, C. M.; Joaquín, R. M., Tris(2-aminoethyl)amine, a Suitable Spacer for Phosphate and Sulfate Receptors. *Chemistry Letters* **1995,** *24* (9), 759-760.
46. Brooks, S. J.; García-Garrido, S. E.; Light, M. E.; Cole, P. A.; Gale, P. A., Conformational Control of Selectivity and Stability in Hybrid Amide/Urea Macrocycles. *Chemistry – A European Journal* **2007,** *13* (12), 3320-3329.
47. Tresca, B. W.; Zakharov, L. N.; Carroll, C. N.; Johnson, D. W.; Haley, M. M., Aryl C-H···Cl- Hydrogen Bonding in a Fluorescent Anion Sensor. *Chemical Communications* **2013,** *49* (65), 7240-7242.

48. Vonnegut, C. L.; Shonkwiler, A. M.; Zakharov, L. N.; Haley, M. M.; Johnson, D. W., Harnessing Solid-state Packing for Selective Detection of Chloride in a Macrocyclic Anionophore. *Chemical Communications* **2016,** *52* (61), 9506-9509.
49. Lee, D. H.; Lee, H. Y.; Lee, K. H.; Hong, J.-I., Selective Anion Sensing based on a Dual-Chromophore Approach. *Chemical Communications* **2001,** (13), 1188-1189.
50. Shimizu, L. S.; Smith, M. D.; Hughes, A. D.; Shimizu, K. D., Self-Assembly of a Bis-urea Macrocycle into a Columnar Nanotube. *Chemical Communications* **2001,** (17), 1592-1593.
51. Roy, K.; Wang, C.; Smith, M. D.; Dewal, M. B.; Wibowo, A. C.; Brown, J. C.; Ma, S.; Shimizu,
L. S., Guest Induced Transformations of Assembled Pyridyl Bis-urea Macrocycles. *Chemical Communications* **2011,** *47* (1), 277-279.
52. Jia, C.; Wang, Q.-Q.; Begum, R. A.; Day, V. W.; Bowman-James, K., Chelate Effects in Sulfate Binding by Amide/Urea-based Ligands. *Organic & Biomolecular Chemistry* **2015,** *13* (25), 6953-6957.

CHAPTER 2

Synthesis and Anion Binding Properties of Pyrazine-2,3,5,6-Tetracarboxamide "Duplex" Receptors

2.1.0 Introduction

Receptors such as pyridine-2,6-dicarboxamide and isophthalamide have been reported as useful anion binding hosts as well as subunits that can be incorporated into macrocyclic anion receptors.[1-8] While simple dicarboxamides have been extensively studied, there have been few examples of tetra-substituted hosts with dual binding pockets on a single aromatic heterocyclic ring aside from a few notable exceptions. Mataka and Gale reported a tetra-substituted urea host 1-phenyl-3-[2,4,5-tris(3-phenylureido)-phenyl]urea receptor capable of binding isophthalate between the *o*-urea appended arms of two independent units (Figure 1a). This complex was shown to generate a hydrogen bonding array between multiple molecules.[9-10]

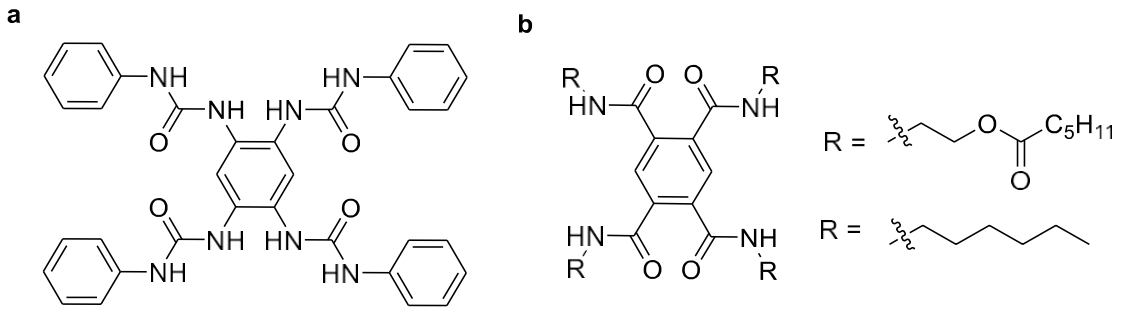

Figure 1. Tetra-substituted pincers 1-phenyl-3-[2,4,5-tris(3-phenylureido)-phenyl]urea (a) and N,N′,N″,N‴-1,2,4,5-tetra(ethylhexanoate) pyromellitamide (b).[9-12]

Another interesting example of a tetra-substituted aryl anion-responsive compound was developed by Thordarson and coworkers in the form of benzene-1,2,4,5-tetracarboxamide known as pyromellitamide receptors. The pyromellitamide complex, seen in Figure 1a, was synthesized and shown to readily form low molecular mass organic gelators. Gel formation was found to be the product of a dense network of intermolecular hydrogen bonding. An exciting facet of these

gel systems is that they can be disrupted upon the introduction of anions to the material. This was the first example of an anion-responsive organic gelator. Anions were thought to overcome the hydrogen bonding network by supposedly positioning themselves in the binding pockets. This causes the amide NH hydrogen bonds to be donated to the anion instead of participating in an intermolecular hydrogen bonding network.[11-12]

Anion responsive behavior exhibited in pyromellitamide pincers gels has opened the door to an exciting new materials of induced organic extended arrays through their hydrogen bonding capabilities. By utilizing a pyrazine-2,3,5,6-tetracarboxamide platform, it has been our goal to further explore tetra-substituted amide hosts in regard to their anion binding properties. Considering Thordarson's studies with the pyromellitamides, further explorations of tetra-substituted pyrazines can focus on their ability to form supramolecular self-assemblies and to stabilize metal ions. These efforts will be discussed further in Chapter 5.[3]

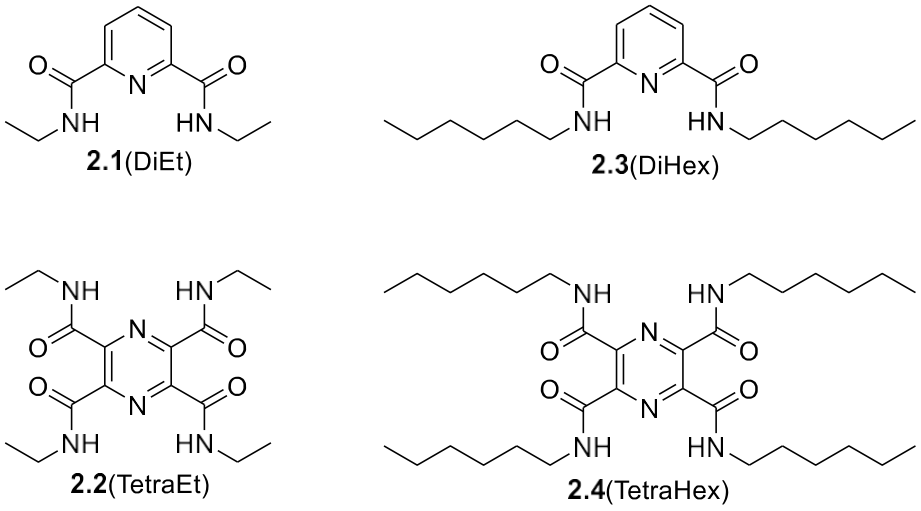

Figure 2. Pyridine-2,6-dicarboxamide and pyrazine-2,3,5,6-tetracarboxamide pincers substituted with hydrophobic ethyl and hexyl R groups.

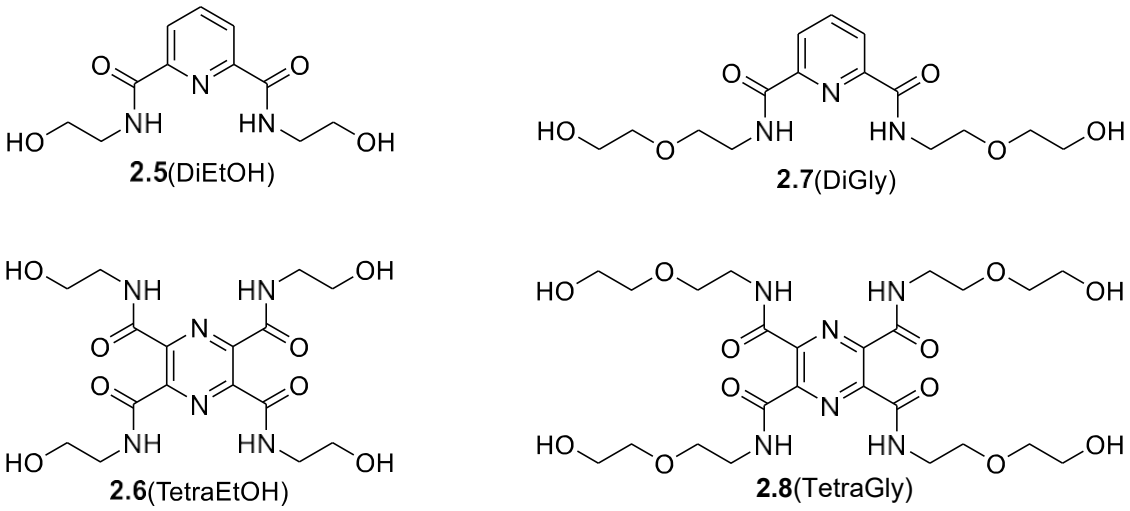

Figure 3. Pyridine-2,6-dicarboxamide and pyrazine-2,3,5,6-tetracarboxamide pincers substituted with hydrophilic hydroxylethyl and glycol R groups.

This chapter will focus on the synthesis and anionic bonding properties of a series of dual cavity "duplex" pincers. Often, receptors are limited to a small range of solvents due to solubility restrictions. We synthesized a diverse set of duplexes with R groups that are functionalized to be either hydrophobic or hydrophilic as shown in Figure 2. This allowed us to generate receptor systems that are versatile in a range of environments.

2.2.0 Experimental

2.2.1 Synthesis

General synthesis

^{1}H and ^{13}C NMR spectra were acquired on 400 or 500 MHz Bruker NMR spectrometers in molecular sieve-dried DMSO-d_6 and $CDCl_3$. Synthesis of **2.3**(DiHex**)**, **2.5**(DiEtOH), and **2.8**(TetraGly) which are shown below, was accomplished with help from Dr. Hanumaiah

Telikepalli, a resident scientist. Compound **2.2**(TetraEt) was first synthesized by Tommy Johnson, a former Bowman-James group member. Compounds were prepared with reagent grade solvents unless indicated otherwise.

Synthesis of tetramethyl pyrazine-2,3,5,6-tetracarboxylate. 2.b.

Scheme 1. Synthesis of **2.b**.

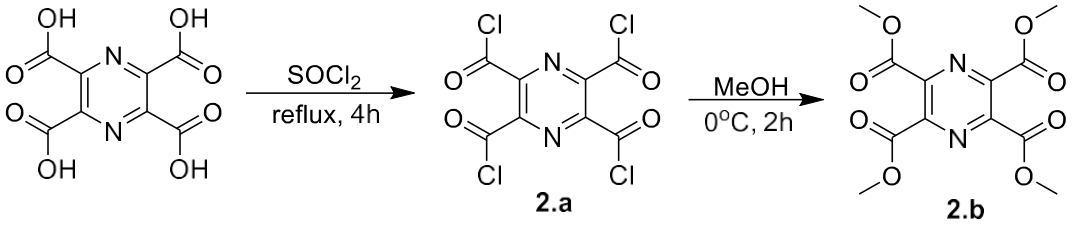

Pyrazine-2,3,5,6-tetracarboxylic acid (1.05 g, 4.10 mmol) was weighed into a 100 mL round bottom flask. Thionyl chloride (10.00 mL, 137.80 mmol) was added slowly along with 2 drops of DMF. The reaction was stirred at reflux for 4 hours after which it was cooled to room temperature and excess thionyl chloride was removed with a rotovap. A yellow-white solid resulted which was then immediately used or converted to tetracarboxylate by addition of 100 mL of MeOH while cooling the vessel in an ice bath. Pyrazine-2,3,5,6-tetracarbonyl tetrachloride (**2.a**) was added over a two-hour time period and allowed to warm up to room temperature while stirring. The white solid was then heated in MeOH and subjected to hot filtration and washed four times with hot methanol. The filtrate was rotovapped to yield a yellowish white solid which was then suspended and washed in DCM and filtered once again. The yellow filtrate was discarded and the white solid was dried under vacuum to give compound **2.b**. Yield (755 mg, 59.0%). ^{1}H NMR (400 MHz, DMSO-d_6) δ 3.95 (s, 12H) ppm. ^{13}C NMR (125 MHz, DMSO-d_6), δ 163.23, 144.23, 53.73 ppm.

Synthesis of N^2,N^6-diethylpyridine-2,6-dicarboxamide. 2.1(DiEt).

Scheme 2. Synthesis of **2.1**(DiEt).

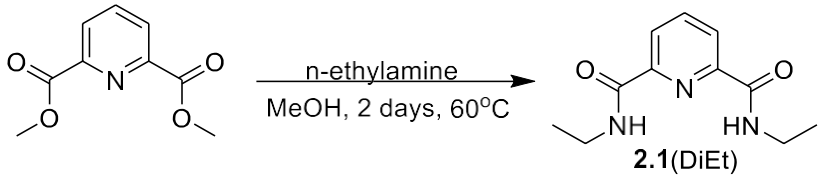

This compound has been previously reported in literature.[13-14] Dimethyl pyridine-2,6-dicarboxylate (0.31 g, 1.57 mmol) was added to a sealable vial with 10 mL of methanol. A 2.0 M solution of ethylamine (3.14 mL, 6.28 mmol) was added to the reaction vessel which was then sealed and stirred at 60°C for 2 days. Solvent was removed under reduced pressure to yield a white solid **2.1**(DiEt). (0.32 g, yield 96%). ^{1}H NMR (400 MHz, DMSO-d_6) δ 9.33 (t, 2H), 8.17 (d, 2H), 8.15 (t, 1H), 3.40 (m, 4H), 1.18 (t, 6H) ppm. ^{13}C NMR (125 MHz, DMSO-d_6), δ 162.83, 148.80, 139.41, 124.05, 33.64, 15.15 ppm. Exact mass for $C_{11}H_{15}N_3O_2$ + Na^+ 244.1164, found (HREIMS+) 244.0972.

Synthesis of N^2,N^3,N^5,N^6-tetraethylpyrazine-2,3,5,6-tetracarboxamide. 2.2(TetraEt)**.**

Scheme 3. Synthesis of **2.1**(TetraEt).

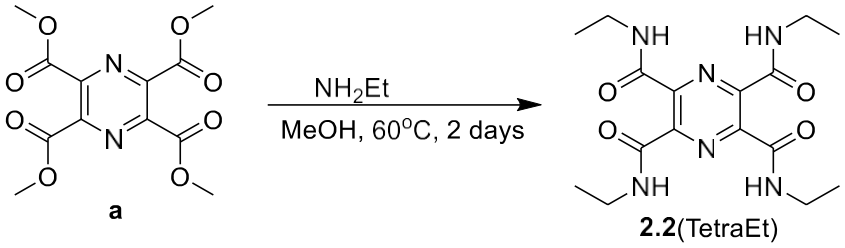

Pyrazine-2,3,5,6-tetracarboxylate (0.11 g, 0.35 mmol) was placed in a sealable vial with 8 mL of MeOH and ethylamine (1.10 mL, 2.11 mmol). The vial was sealed and heated to 60°C

while stirring for 2 days. The reaction progress was monitored using TLC to watch the disappearance of the carboxylate starting material. Excess ethylamine was removed via rotovap to yield a white solid **2.2**(TetraEt) (0.11 g, yield 86.6%). ^{1}H NMR (400 MHz, DMSO-d_6) δ 8.76 (t, 4H), 1.58 (q, 8H), 1.14 (t, 12H) ppm. ^{13}C NMR (125 MHz, DMSO-d_6), δ 163.19, 145.39, 33.81, 14.60 ppm. Exact mass for $C_{16}H_{24}N_6O_2$ + H^+ 365.1859, found (HREIMS+) 365.1908.

Synthesis of N^2,N^6-dihexylpyridine-2,6-dicarboxamide. 2.3(DiHex).

Scheme 4. Synthesis of **2.3**(DiHex).

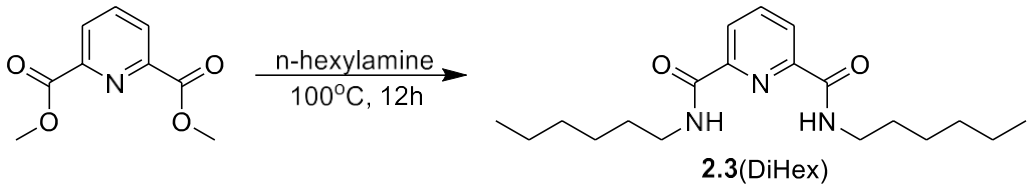

2.3(DiHex)

This compound has been previously reported in literature.[15] Dimethyl pyridine-2,6-dicarboxylate (5.00 g, 25.64 mmol) was added to hexylamine (10.37 g, 102.50 mmol) and heated at 100°C for 12 hours. Pure product was obtained by column chromatography using a gradient of hexane-DCM (1:1) to DCM followed by crystallization from ether to afford **2.3**(DiHex) as white fluffy solid (3.67 g, yield 43%).^{1}H NMR (400 MHz, DMSO-d_6) δ 9.29 (t, 2H), 8.17 (m, 3H), 3.35 (m, 4H), 1.58 (m, 4H), 1.31 (m, 12H), 0.86 (t, 6H) ppm. ^{13}C NMR (125 MHz, DMSO-d_6), δ 163.91, 148.76,139.38, 124.05, 38.85, 31.05, 24.48, 26.23, 22.07, 13.92 ppm. Exact mass for $C_{19}H_{31}N_3O_2$ + Na^+ 356.2314, found (HREIMS+) 356.2295.

Synthesis of N^2,N^3,N^5,N^6-tetrahexylpyrazine-2,3,5,6-tetracarboxamide. 2.4(TetraHex).

Scheme 5. Synthesis of **2.4**(TetraHex).

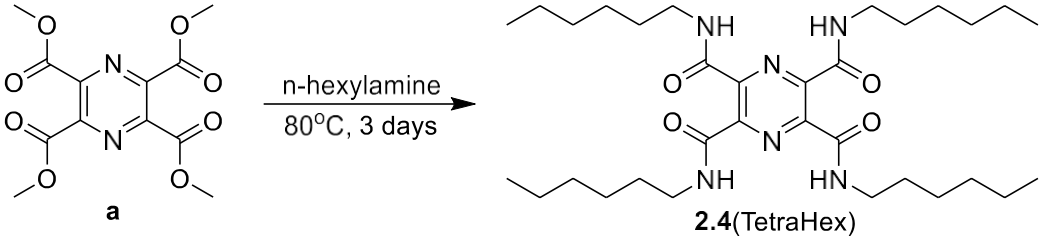

Hexylamine (1.90 mL, 14.30 mmol) was added to **2.1** (742.00 mg, 2.38 mmol) in a 50 mL round bottom flask. The suspension was heated to 80°C and stirred for 3 days. Solvent was removed via rotovap yielding a yellow solid. The mixture was suspended in cold acetone and filtered to yield a white solid **2.4**(TetraHex) (278 mg, 20%). ^{1}H NMR (400 MHz, $CDCl_3$): δ 7.94, (s, 4H), 3.37 (q, 8H), 1.66 (m, 8H), 1.84 (s, 8H), 1.40 (m, 8H), 1.36 (m, 16H), 0.92 (t, 12H) ppm. ^{13}C NMR (125 MHz, DMSO-d6), δ 163.37, 144.88, 40.35, 31.81, 28.99, 27.05, 22.84, 14.24 ppm. Exact mass for $C_{32}H_{56}N_6O_4$ + Na^+ 611.4261, found (HREIMS+) 611.4185.

Synthesis of N^2,N^6-bis(2-hydroxyethyl)pyridine-2,6-dicarboxamide. 2.5(DiEtOH).

Scheme 6. Synthesis of **2.5**(DiEtOH).

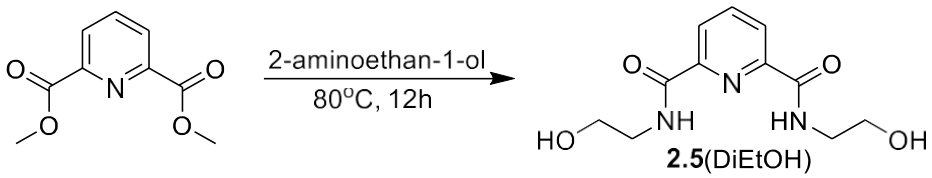

This compound has been previously reported in literature.[16] Dimethyl pyridine-2,6-dicarboxylate (5.00 g, 25.64 mmol) was added to aminoethanol (6.26 g, 102.60 mmol) and heated at 80°C for 12 hours in a sealed tube. The reaction mixture poured in to DCM (200 mL) stirred at room for 30 minutes. Solids were filtered, washed and dried to afforded N,N-bis(2-hydroxyethyl)pyridine-2,6-dicarboxamide as white solid (3.2 g, yield 49%). ^{1}H NMR (400

MHz, DMSO-d_6) δ 9.36 (t, 2H), 8.18 (m, 3H), 4.83 (t, 2H), 3.57 (q, 4H), 3.44 (q, 4H) ppm. ^{13}C NMR (125 MHz, DMSO-*d6*), δ 163.26, 148.75, 139.36, 124.14, 59.75, 41.76 ppm. Exact mass for $C_{11}H_{15}N_3O_4$ + Na 276.0960, found (HREIMS+) 276.0954.

Synthesis of N^2,N^3,N^5,N^6-tetrakis(2-hydroxyethyl)pyrazine-2,3,5,6-tetracarboxamide. 2.6(TetraEtOH).

Scheme 7. Synthesis of **2.6**(TetraEtOH).

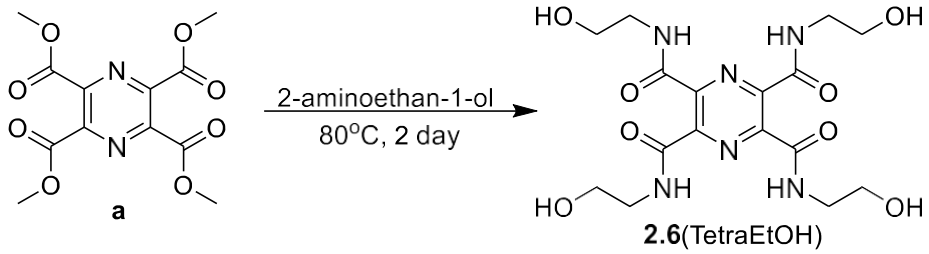

Compound **a** (198.40mg, 0.62 mmol) was charged into a round bottom flask with 2-aminoethan-1-ol (2.00 mL, 33.40 mmol) and stirred at 80°C for 2 days. The solution was allowed to cool and then ether was diffused in overnight wherein a white precipitate evolved. Following filtration of the solid, the product **2.6**(TetraEtOH) was collected as a white powder (53.02 mg, 20%). ^{1}H NMR (400 MHz, DMSO-d_6): δ 8.96 (t, 4H), 4.78 (t, 4H), 3.55 (q, 8H), 3.36 (m overlapped, 8H) ppm. ^{13}C NMR (125 MHz, DMSO-*d6*), δ 163.58, 145.19, 59.50, 41.85 ppm. Exact mass for $C_{16}H_{25}N_6O_8$ + H^+ 429.1734, found (HREIMS+) 429.1863.

Synthesis of N^2,N^6-bis(2-(2-hydroxyethoxy)ethyl)pyridine-2,6-dicarboxamide. 2.7(DiGly)**.**

Scheme 8. Synthesis of **2.7**(DiGly).

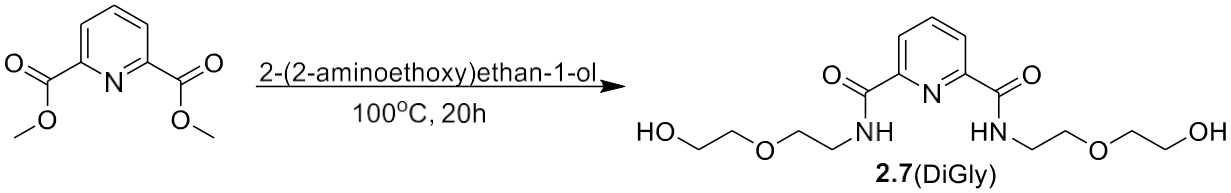

This compound has been previously reported in literature.[17] A solution of dimethyl pyridine-2,6-dicarboxylate (374.27 mg, 1.92 mmol) was prepare in 2-(2-aminoethoxy)ethan-1-ol (6 mL, 54 mmol) in a round bottom flask and was heated to 100°C for 20 hours. The resulting viscous yellow oil was purified by column chromatography in a 9:1 DCM:MeOH to yield **2.7**(DiGly) (374 mg, 57.6%). ^{1}H NMR (500 MHz, DMSO-d_6): 9.37 (s, 3H), 8.19 (m, 3H), 4.61 (t, 4H), 3.59 (t, 4H), 3.54 (t, 4H), 3.50 (t, 4H), 3.47 (t, 4H) ppm. ^{13}C NMR (125 MHz, DMSO-d_6): δ 168.46, 153.83, 144.69, 129.48, 77.42, 74.23, 65.40, 44.16 ppm. Exact mass found for $C_{15}H_{23}N_3O_4 + Na^+$ 364.1485, found (HREIMS+) 364.1470.

Synthesis of N^2,N^3,N^5,N^6-tetrakis(2-(2-hydroxyethoxy)ethyl)pyrazine-2,3,5,6-tetracarboxamide. 2.8(TetraGly).

Scheme 9. Synthesis of **2.8**(TetraGly).

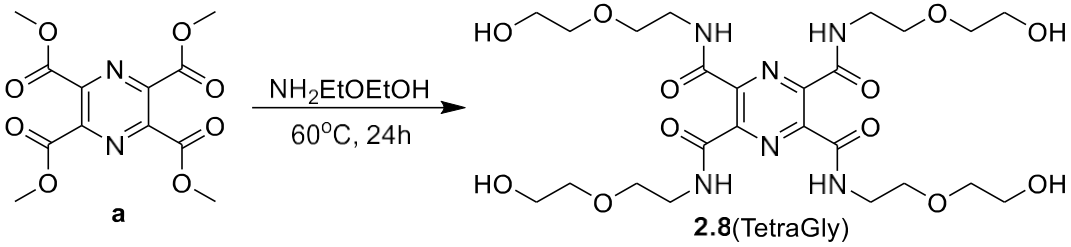

A solution of **a** (0.70 g, 2.24 mmol) in 2-(2-aminoethoxy)ethanol (5.00 g, 47.60 mmol) was prepared in a and heated at 100°C for 15 hours. The reaction mixture poured in to methanol and stirred and the solid filtered off. The filtrate concentrated and crystallized from acetonitrile to provide tetrakis(2-(2-hydroxyethoxy)ethyl)pyrazine-2,3,5,6-tetracarboxamide as a white solid (0.4 g, yield 29%). ^{1}H NMR (500 MHz, DMSO-d_6): δ 8.94 (s, 4H), 4.16 (t, 4H), 3.57 (t, 8H), 3.51 (t, 8H), 3.45 (m, 16H) ppm. ^{13}C NMR (125 MHz, DMSO-d_6), δ 163.50, 145.16, 77.21,

68.89, 60.17, 38.98 ppm. Exact mass for $C_{24}H_{40}N_6O_{12}$ + Na^+ 627.2602, found (HREIMS+) 627.2601.

2.2.2 ^{1}H NMR Anion Binding Studies

For qualitative anion binding screenings, 2 mM solutions of each host were prepared in 9:1 CD_3CN:DMSO-*d*$_6$ for compounds **2.1**(DiEt), **2.2**(TetraEt), **2.3**(DiHex), **2.5**(DiEtOH), **2.7**(DiGly), and **2.8**(TetraGly). Due to solubility constraints, compound **2.4**(TetraHex) was prepared as a 2 mM solution in DMF-*d*$_6$ and compound **2.6**(TetraEtOH) was prepared as a 2 mM solution in DMSO-*d*$_6$. Ten equivalents (0.1 mmol) tetrabutylammonium (TBA) salt of HSO_4^-, Cl^-, F^-, $H_2PO_4^-$, NO_3^- and tetraethylammonium (TEA) OAc^- were each respectively added to a 0.5 mL solution of each host and the ^{1}H NMR spectra were recorded to monitor NH amide shifting.

Binding stoichiometry was analyzed by Job plot analysis, which was conducted for **2.7**(DiGly) and **2.8**(TetraGly) with 5 mM stock solutions of both host and TEAOAc salt. NMR tubes were prepped with a constant total concentration of host and guest with variation of host ratios of 0.17, 0.20, 0.25, 0.33, 0.50, 0.67, 0.75, 0.80, and 0.83 to anion guest. ^{1}H NMR spectra were obtained and amide shifts were recorded and plotted as change in shift, $\Delta\delta$, over total concentration against host ratio.

Quantitative anion binding studies were accomplished with ^{1}H NMR titrations. Stock solutions of each host were prepared at 2 mM concentrations in 9:1 CD_3CN:DMSO-*d*$_6$ for compounds **2.1**(DiEt), **2.2**(TetraEt), **2.3**(DiHex), **2.5**(DiEtOH), **2.7**(DiGly), and **2.8**(TetraGly) while compound **2.4**(TetraHex) was prepared as a 2 mM solution in DMF-*d*$_6$ and compound **2.6**(TetraEtOH) was prepared as a 2 mM solution in DMSO-*d*$_6$. Cleaned and dried NMR tubes were prepared with 0.5 mL of the 2 mM host solution. Solutions at a concentration of 20 mM of

each anion using $TBAF^-$, $TBAH_2PO_4^-$, and $TEAOAc^-$ were prepared using the same solvent or solvent combination as the host to be titrated. ^1H NMR spectra were recorded after every addition of anion to the host solution. Following normalization of each spectrum to the solvent peak, the amide NH downfield shift of each host was recorded and analyzed in EQNMR2 by fitting a binding curve to each data set that allowed the determination of binding constants for each host complex.[18] All binding constants were determined at <15% error.

Binding Spectra

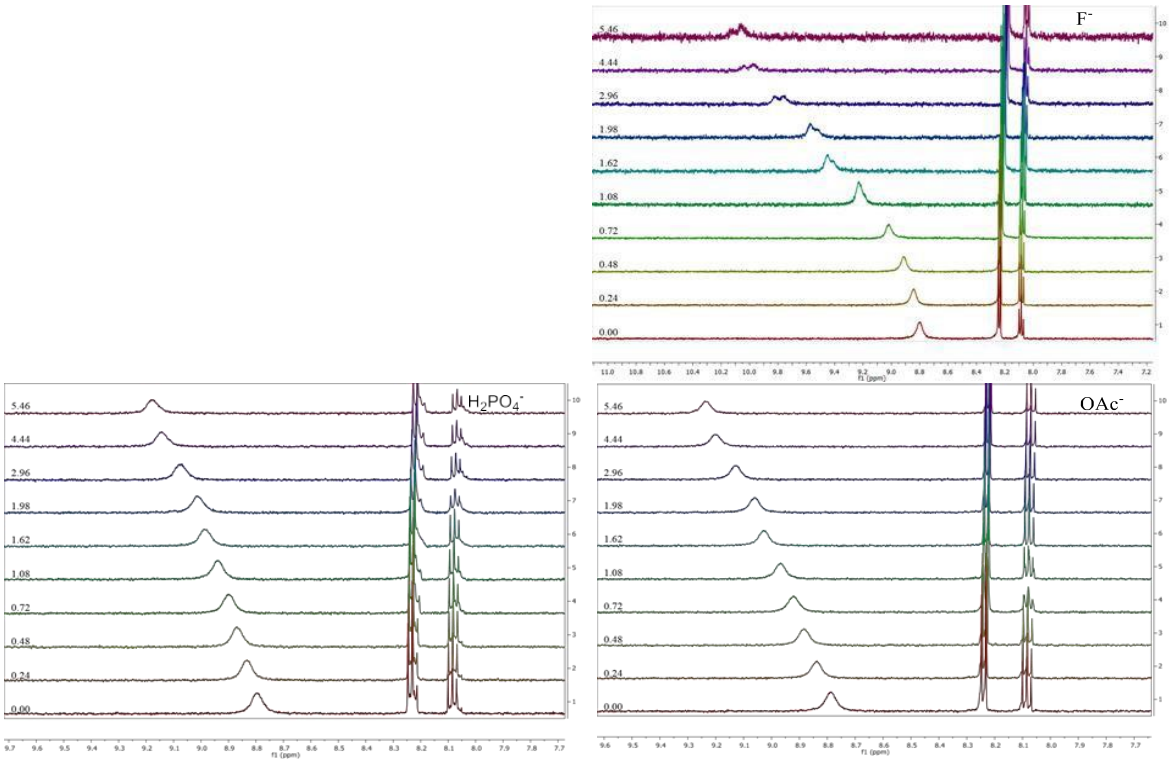

Figure 4. ^1H NMR anion binding titration for compound **2.1**(DiEt) with F^-, $H_2PO_4^-$, and OAc^- in 9:1 CD_3CN:DMSO-d_6.

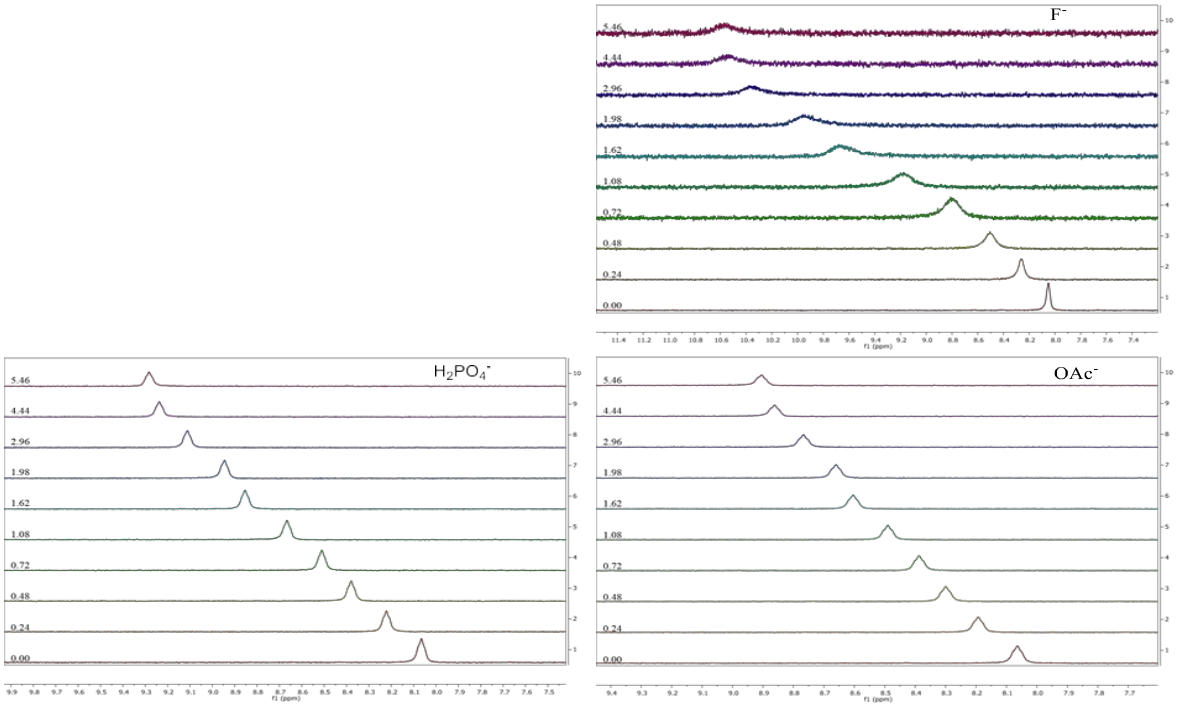

Figure 5. ^{1}H NMR anion binding titration for compound **2.2**(TetraEt) with F^-, $H_2PO_4^-$, and OAc^- in 9:1 CD_3CN:DMSO-*d*$_6$.

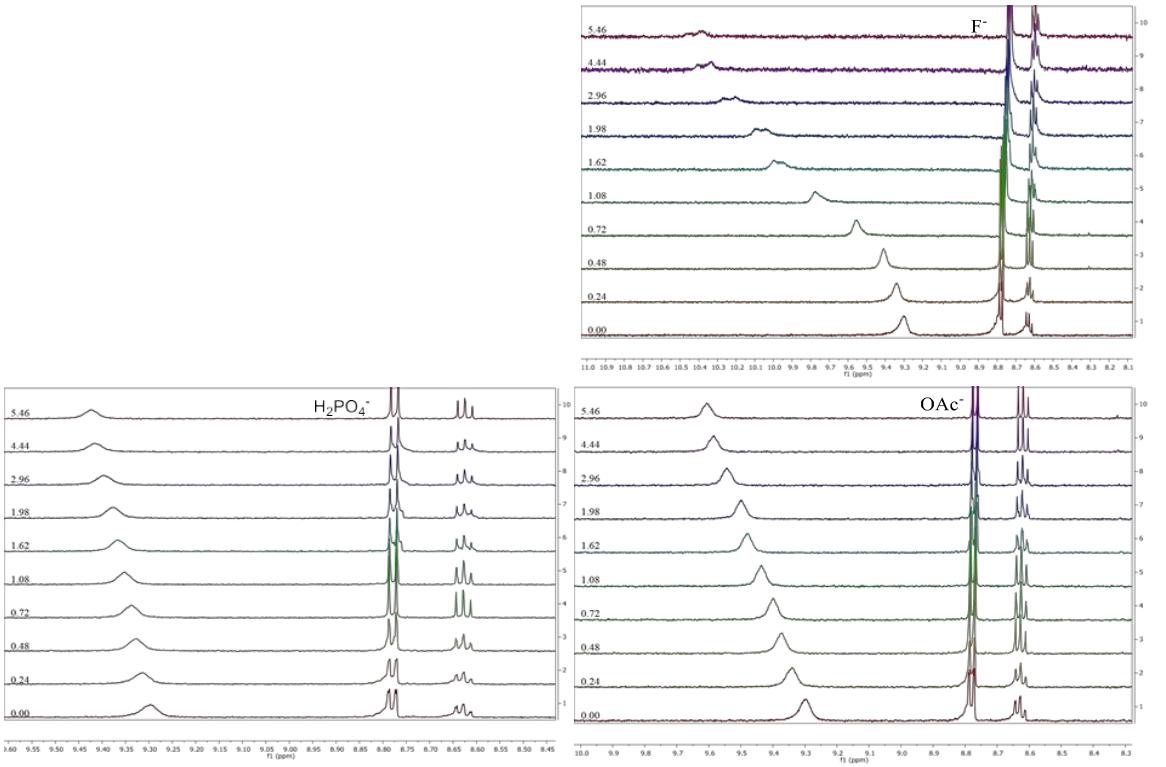

Figure 6. ^{1}H NMR anion binding titration for compound **2.5-MonoHex** with F^-, $H_2PO_4^-$, and OAc^- in 9:1 CD_3CN:DMSO-*d*$_6$..

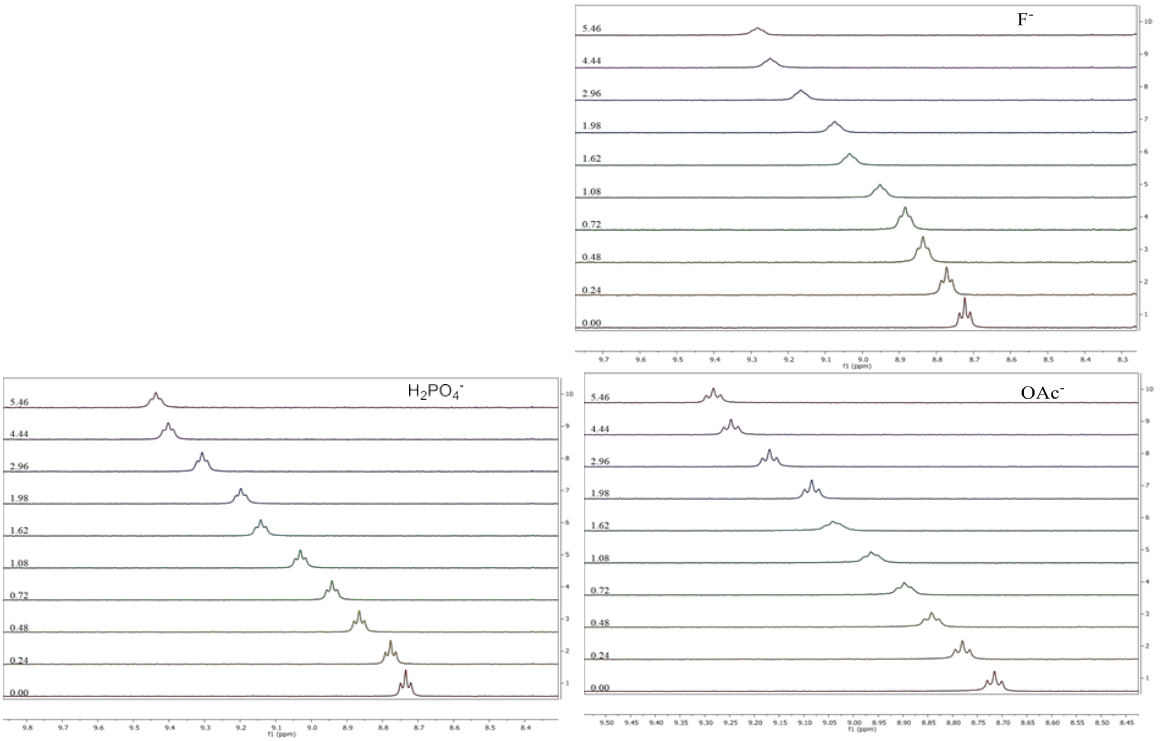

Figure 7. ^{1}H NMR anion binding titration for compound **2.4**(TetraHex) with F^-, $H_2PO_4^-$, and OAc^- in 9:1 CD_3CN:DMSO-*d*$_6$.

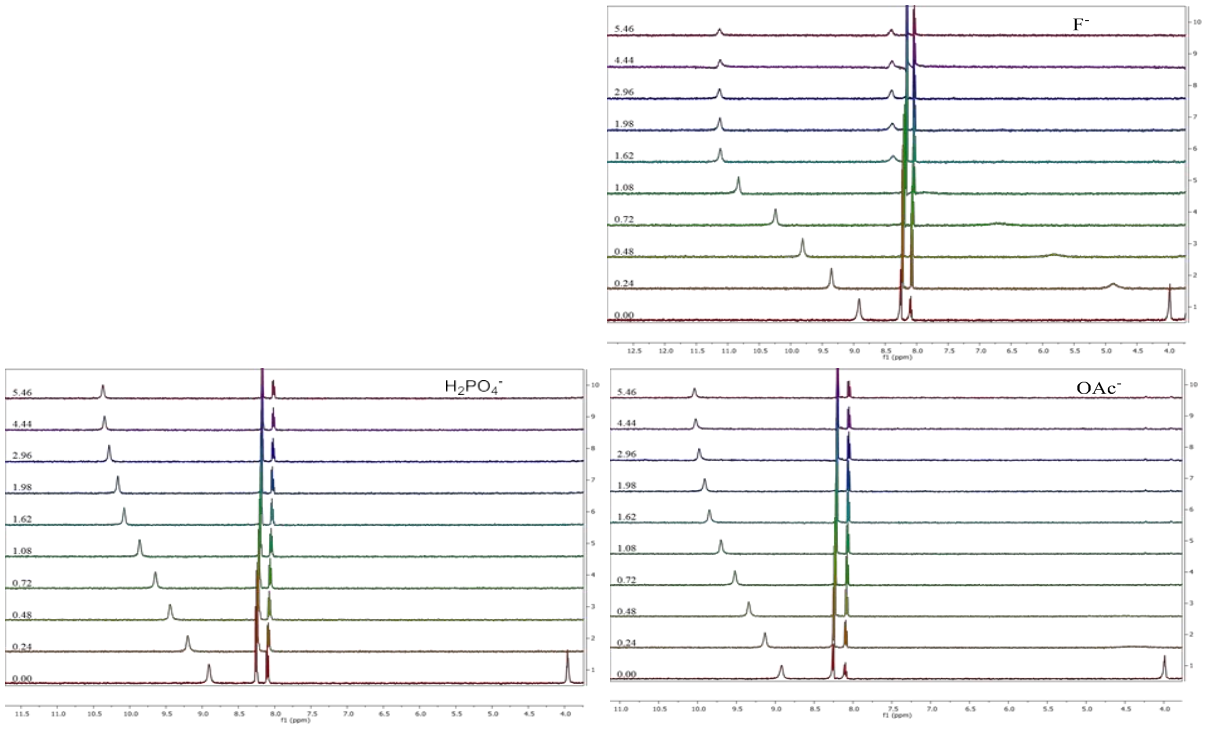

Figure 8. ^{1}H NMR anion binding titration for compound **2.5**(DiEtOH) with F^-, $H_2PO_4^-$, and OAc^- in 9:1 CD_3CN:DMSO-*d*$_6$.

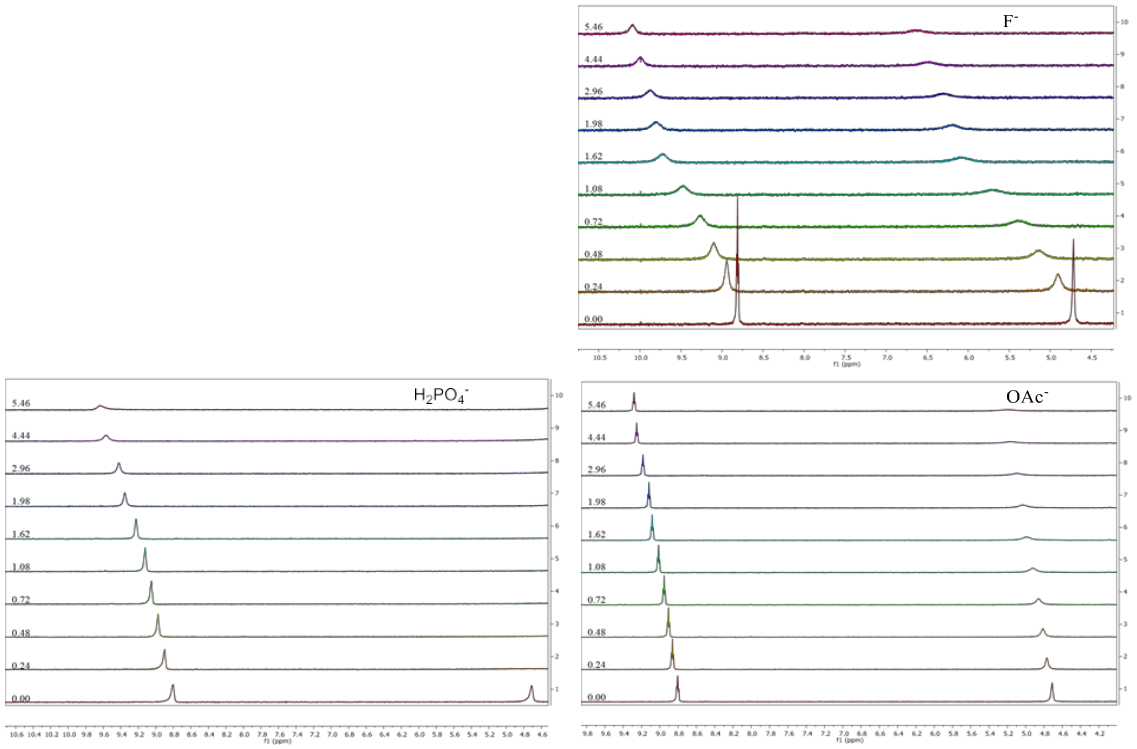

Figure 9. ^{1}H NMR anion binding titration for compound **2.6**(TetraEtOH) with F^-, $H_2PO_4^-$, and OAc^- in 9:1 CD_3CN:DMSO-d_6.

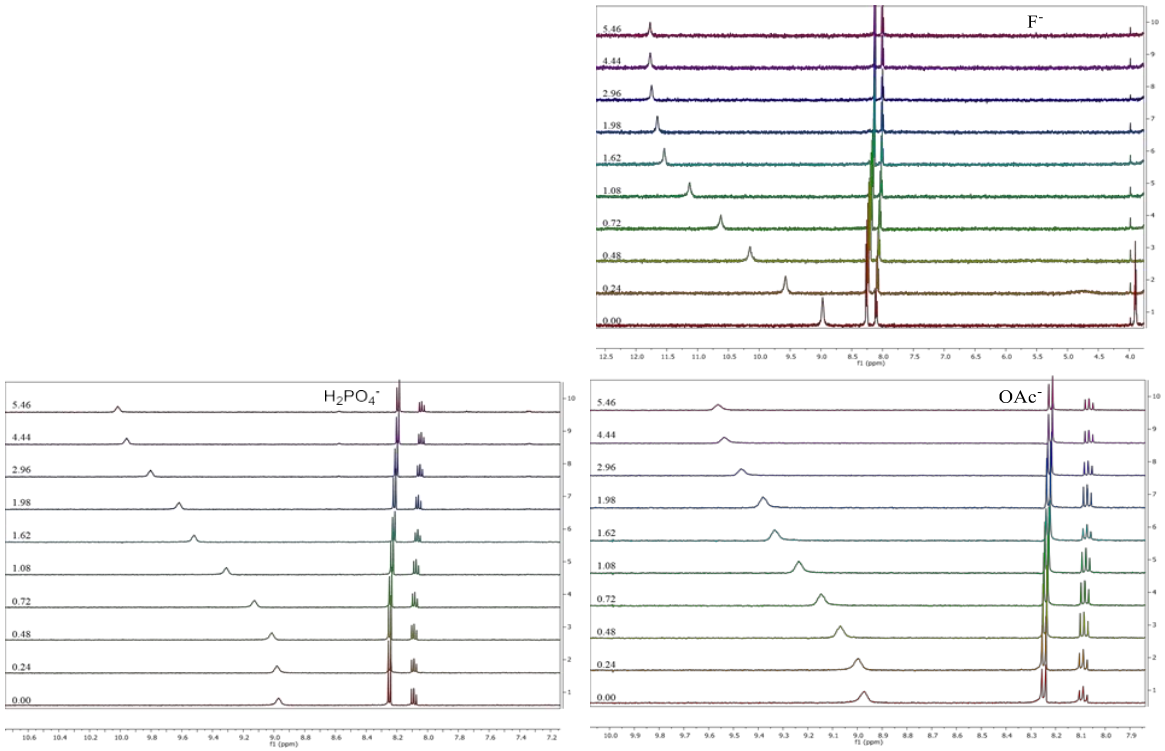

Figure 10. ^{1}H NMR anion binding titration for compound **2.7**(DiGly) with TBAF, $TBAH_2PO_4$, and TEAOAc in 9:1 CD_3CN:DMSO-d_6.

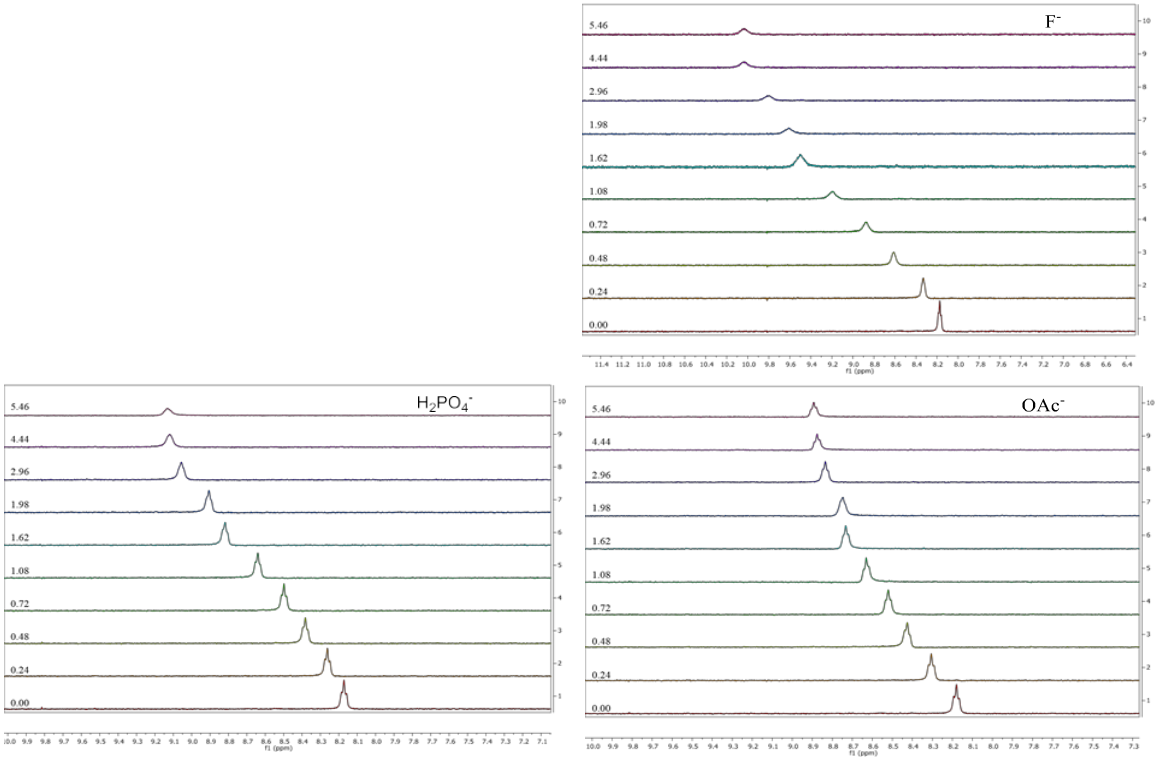

Figure 11. ^{1}H NMR anion binding titration for compound **2.8**(TetraGly) with F^-, $H_2PO_4^-$, and OAc^- in 9:1 CD_3CN:DMSO-d_6.

2.3.0 Results and Discussion

2.3.1 Duplex Synthesis and Properties

Solubility of the duplex host system can be seen as a function of its arm group appendages. Two sets of pincers of each pyridine-2,6-dicarboxamide and pyrazine-2,3,5,6-tetracarboxamide with matching R groups were synthesized. This allowed for direct comparison between monotopic and ditopic host's anion affinity comparison studies. It also allowed for comparisons between hydrophobic arm groups and hydrophilic arm groups (Figure 12).

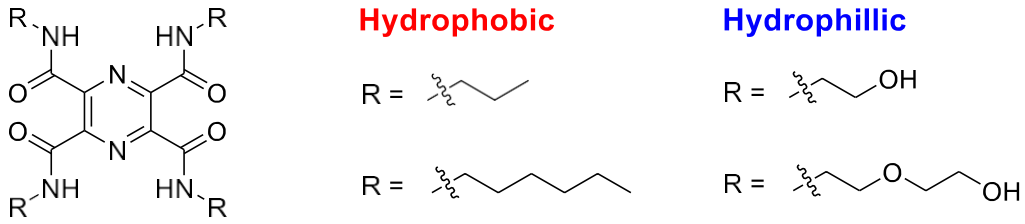

Figure 12. Pyrazine-2,3,5,6-tetracarboxamide duplex variants with hydrophobic and hydrophilic appended R groups.

Through careful selection of R groups, a series of pincers was synthesized that are soluble across a range of solvents. This included water for the complexes with terminal hydroxyl groups such as **2.6**(TetraEtOH) to chloroform and hexane for the long chained aliphatic arms of **2.4**(TetraHex). The duplex ligands were synthesized with variable R group substituents from tetramethyl pyrazine-2,3,5,6-tetracarboxylate, **2.b**. Compound **2.b**, was synthesized from pyrazine-2,3,5,6-tetracarboxylic acid by reacting it with thionyl chloride to produce pyrazine-2,3,5,6-tetracarbonyl tetrachloride, **2.a**. The acid chloride derivative was then treated with methanol yielding compound **2.b**. While duplexes **2.2**(TetraEt) and **2.4**(TetraHex) could also have been synthesized from the corresponding acid chloride, the hydroxide appended **2.6**(TetraEtOH) and **2.8**(TetraGly) ran the risk of unwanted side products from nucleophilic attack of the hydroxyl at the acyl chlorides. Therefore, the tetramethyl ester starting material was required for the hydrophilic receptors. Since the tetraester is also much more stable than the acyl chloride it was used for all of the duplex syntheses. Crystals were grown of **2.2**(TetraEt) and **2.8**(TetraGly), however, the structures will be discussed in Chapter 5.

Hot filtration of the tetracarboxylate, **2.b**, is an important purification step that was discovered when synthesizing compound **2.6**(TetraEtOH). Initial ^{1}H NMR titrations of **2.6**(TetraEtOH) with anion guests were unsuccessful due to an excess of the titrant signal by integration, however no impurities were seen in the NMR nor mass spectrometry (MS). It was

determined that the starting material pyrazine-2,3,5,6-tetracarboxylic acid, which cannot be seen by NMR or MS, was contaminating **2.6**(TetraEtOH) and throwing off mass measurements for titrations. Since the other duplexes were readily soluble in methanol, they were easy to extract from tetracarboxylic acid impurities. On the other hand, **2.6**(TetraEtOH) is only soluble in the same solvents as the impurity making them very difficult to purify. To obtain a pure sample of **2.6**(TetraEtOH), it was necessary to remove tetracarboxylic acid from **2.b** before the amidation reaction by hot filtration.

A key goal was to assess anion binding affinities of the duplex pincer with different arm groups. It was also important to compare the duplex host anion binding capabilities with the single cavity pincer analogs of each duplex. For this, the monotopic pyridine-2,6-dicarboxamide counterpart of each duplex was synthesized for direct comparison of properties of the ditopic vs monotopic hosts.

Scheme 10. General synthesis for pyrazinetetraamide pincers.

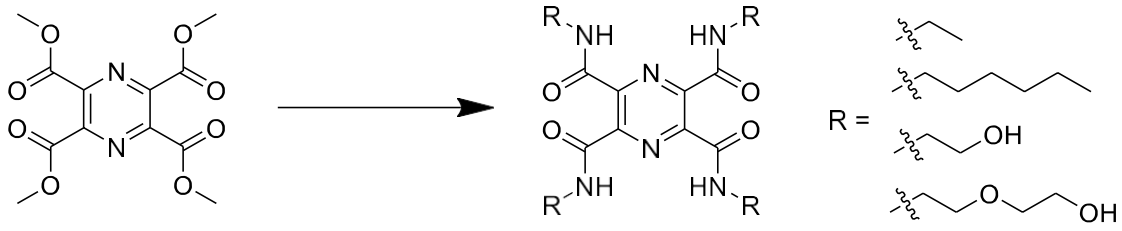

The monotopic hosts were found to be soluble in a large variety of solvents shown in Table 1. Duplex compounds were more selective to specific solvents which was dependent on the R group. While most duplex compounds showed some degree of solubility in methanol, **2.4**(TetraHex) was the only duplex to dissolve readily in nonpolar solvents such as

dichloromethane, chloroform and to some degree in hexanes. On the other end of the spectrum is the short-chained hydroxyethyl armed duplex, **2.6**(TetraEtOH), which showed solubility limited to highly solvating polar solvents DMF, DMSO, and water. The duplex compound is therefore tunable to a desired environment, either hydrophobic or hydrophilic, depending on the R group substitution.

Table 1. Solubility chart for mono and ditopic pincers where (S is soluble, L is low solubility, and N is non-soluble).

Solvent	2.1 (DiEt)	2.2 (TetraEt)	2.3 (DiHex)	2.4 (TetraHex)	2.5 (DiEtOH)	2.6 (TetraEtOH)	2.7 (DiGly)	2.8 (TetraGly)
Acetone	S	N	S	N	S	N	S	Low
Acetonitrile	S	N	S	N	Low	N	S	Low
Methanol	S	S	S	S	S	Low	S	S
Ethanol	S	S	S	S	S	N	S	S
Toluene	Low	N	S	S	Low	N	N	Low
Hexane	N	N	N	S	N	N	N	N
Chloroform	S	S	S	S	Low	N	S	Low
DMF	S	S	S	S	S	S	S	S
DMSO	S	S	S	Low	S	S	S	S
THF	S	Low	S	S	Low	N	S	N
Cyclohexane	N	N	N	S	N	N	N	N
Water	N	N	N	N	S	S	S	S

2.3.2 Anion Binding

Both monotopic and ditopic hosts were screened for qualitative affinity for the following anions: F^-, Cl^-, NO_3^-, HSO_4^-, OAc^-, and $H_2PO_4^-$. This was determined by an observed downfield shift of the amide protons in ^1H NMR spectra in comparison to the free base NH signal. The anions demonstrating the highest degree of interaction with the amide hydrogens were F^-, $H_2PO_4^-$, and

OAc^-. The largest degree of NH shift was seen in the interaction with F^- by a difference typically a $\Delta\delta$ of > 1 ppm with each monotopic and ditopic receptor.

Anion binding stoichiometry

When determining anion binding stoichiometry with both the monotopic and ditopic hosts it was expected that the monotopic hosts would bind in a 1:1 ratio which has been previously reported for similar receptors.[3] However, the dual cavity duplex hosts could potentially bind anions in a 1:2 ratio with the host receptor. It must also be considered that the binding of two anions into the duplex receptor may be unfavorable due to the close proximity of the anions across the pyrazine core. Findings by Thordarson and coworkers supported the 1:2 host-guest binding stoichiometry in their work with pyromellitamide receptors.[11] Binding modes for 1:1 or 1:2 guest to host binding were analyzed by ^{1}H NMR Job plots for **2.7**(DiGly) and **2.8**(TetraGly) with TEAOAc, wherein molar ratios of anion and host were varied at constant total concentrations. In Figure 13, the Job plot for **2.7**(DiGly) shows the binding curve is at its apex at 0.5 molar fraction when host and guest concentrations are equivalent. This verifies the expected 1:1 stoichiometry of host to guest binding for the monotopic pincers.

The Job plot analysis of **2.8**(TetraGly) revealed a more ambiguous binding stoichiometry. The apex of the binding plot is clearly before the 0.5 molar fraction ratio which supports the 1:2 guest to host ratio, however, the plot apex falls between the 1:1 and 1:2 stoichiometries. Thordarson and coworkers noted this issue with Job plots when analyzing pyromellitamides and attributed it to aggregation of the hydrogen bonding network. This can limit the effectiveness of Job plots for these systems. They found a slight break of symmetry of the aromatic CH in the ^{1}H NMR titration spectrum. Further addition of anion past 2 equivalents of anion restored the symmetry, indicating 1:2 binding for the tetracarboxamide hosts.[11] Fitting the data to both 1:1

and 1:2 modes in EQNMR2 supports the 1:2 binding mode as a better fit through generally lower error in the fit.

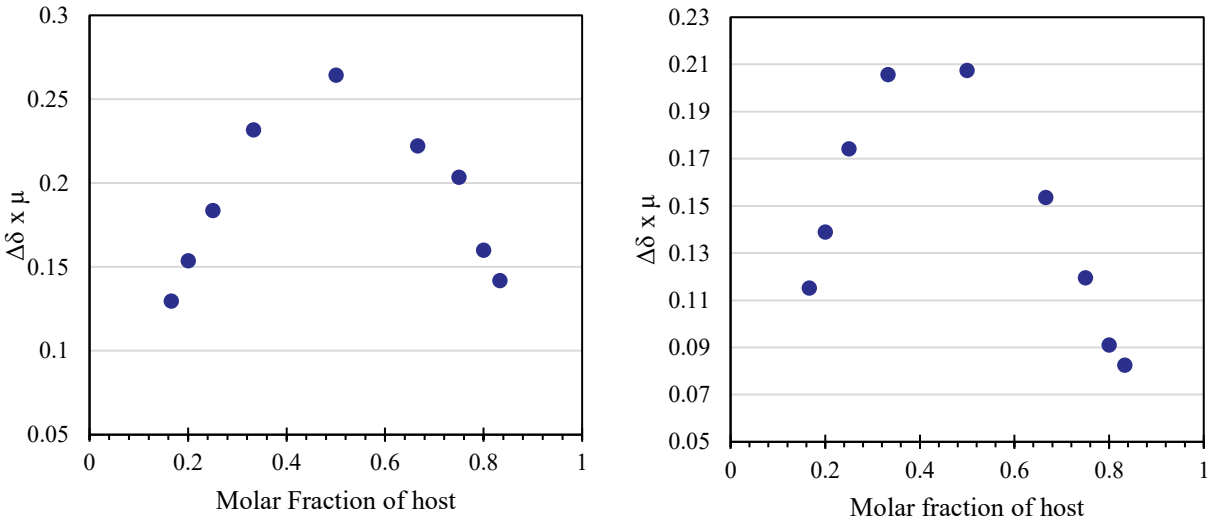

Figure 13. Job plots for **2.7**(DiGly) (left) and **2.8**(TetraGly) (right) with TEAOAc.

Binding constant determination

An interesting aspect of the binding affinity of duplex receptors is their comparison to their monotopic corollaries. Table 2 contains the binding constants for each duplex pincer and the analogous monotopic receptor with identical R appendages. Ka's were obtained by EQNMR least-squares analysis from ^{1}H NMR titrations.[18] Monotopic host binding constants were calculated using a 1:1 stoichiometry model while duplex hosts were calculated from a 1:2 model. The binding constant data in Table 2 unilaterally show that the duplex receptors demonstrate a slight increase in binding strength when compared to the monotopic complexes. Since the titrations for the ethyl and hydroxyethyl ether appended complexes were both performed in the 9:1 CD_3CN:DMSO-d_6 solution, they can be used as a direct comparison between the single and dual cavity hosts.

Table 2. Binding constants (M^{-1}) in determined by ^1H NMR titration.

Anion	**2.1**[a,d] (DiEt)	**2.2**[a,e] (TetraEt)	**2.3**[a,d] (DiHex)	**2.4**[b,e] (TetraHex)	**2.5**[a,d] (DiEtOH)	**2.6**[c,e] (TetraEtOH)	**2.7**[a,d] (DiGly)	**2.8**[a,e] (TetraGly)
$H_2PO_4^-$	437	K_{1a} 758 K_{2a} 162	43	K_{1a} 537 K_{2a} 126	1,950	K_{1a} 708 K_{2a} 52	513	K_{1a} 708 K_{2a} 1,740
OAc^-	145	K_{1a} 1,318 K_{2a} 62	148	K_{1a} 589 K_{2a} 83	2,750	K_{1a} 1050 K_{2a} 123	562	K_{1a} 2,090 K_{2a} 22
F^-	115	K_{1a} 501 K_{2a} 5,370	209	K_{1a} 501 K_{2a} 83	18,200	K_{1a} 110,000 K_{2a} 5,750	1,550	K_{1a} 26,600 K_{2a} 431

(Binding constants determined in: [a] CD_3CN:DMSO-d_6, [b] DMF-d_6, [c]DMSO-d_6. Results in binding model [d] 1:1 and [e] 1:2)

In comparison to Thordarson's pyromellitamides, our complexes bound F^-, OAc^-, and $H_2PO_4^-$ as opposed to Cl^-, OAc^-, Br^-, NO_3^- and I^-.[11] While Cl^- chemical shifts were present in the qualitative screenings, the degree was minimal and we did not observe any interaction from Br^-, NO_3^- and I^-. Binding constants for pyromellitamide determined in acetone-d_6 (Figure 1b) showed high binding constants for Cl^- and OAc^- in excess of 100,000 M^{-1} which surpasses what was found for most of pyrazine receptors in Table 2, aside from **2.6**(TetraEtOH). However, since the pyrazine duplex hosts were titrated in part if not entirely in highly solvating DMSO-d_6 and DMF-d_6, it is expected that the binding would be lower. The use of pyrazine core groups could also lower the binding in comparison to pyromellitamide due to the electron repulsion from pyrazine nitrogens on the anion guest as previously shown by Crabtree with monotopic pyridine hosts.[3]

Cooperative binding was assessed by cooperativity parameters, ($\alpha = 4K_{2a}/K_{1a}$) to determine if binding of the first anion affects the binding of the second.[19] Pyromellitamide was reported to exhibit a negative cooperativity on anion guests evidenced by the lower K_{2a}'s

yielding α values < 1. This was explained by the need for amide hydrogens to be pointing inward towards the binding pocket in order to receive an anion. For the tetracarboxamide host to bind two anions, both binding sites must adopt the inward oriented amides, which causes the outward facing adjacent carbonyls to experience electrostatic repulsion from one another. It is, therefore, energetically less favorable to bind the second anion after the first.[11] Cooperativity parameters calculated from the pyrazine tetracarboxamide binding data also generally demonstrated negative cooperativity for each of the anion complexes where α values were < 1(Table 3). Anomalous data points in the cooperativity study were **2.2**(TetraEt) with F^- and **2.8**(TetraGly) with $H_2PO_4^-$ that remain outliers to previous reports and the rest of the obtained data. It is unclear why these pyrazine receptors deviated from the trend of negative cooperativity observed by Thordarson and coworkers and thus requires a further study.

Table 3. Cooperativity parameters, α, for **2.2**(TetraEt), **2.4**(TetraHex), **2.6**(TetraEtOH), and **2.8**(TetraGly).

Anion	**2.2**(TetraEt)	**2.4**(TetraHex)	**2.6**(TetraEtOH)	**2.8**(TetraGly)
$H_2PO_4^-$	0.83	0.94	0.29	9.83
OAc^-	0.19	0.56	0.47	0.04
F^-	42.86	0.66	0.21	0.35

Comparing the binding curves for **2.1**(DiEt) and **2.2**(TetraEt) seen in Figure 14 suggests a stronger association between host and guest for **2.2**(TetraEt) as equilibrium is reached at 2 equivalents of anion added. The single cavity **2.1**(DiEt) shows a much weaker interaction between anion and host amide overall which is reflected in the binding constants for the interaction. Comparatively, the binding constants for OAc^- with **2.1**(DiEt) and **2.2**(TetraEt) were found to be 145 M^{-1} and 1,320 M^{-1} respectively, which is an improvement of over 1,200 M^{-1}.

Similar results are seen in OAc^- binding with **2.7**(DiGly) and **2.8**(TetraGly) where an increase from 562 to 2090 M^{-1} is seen with a difference of over 1,500 M^{-1}. Despite the fact that the anions are in close proximity to one another across the pyrazine core, the duplexes demonstrate a slightly higher degree of binding.

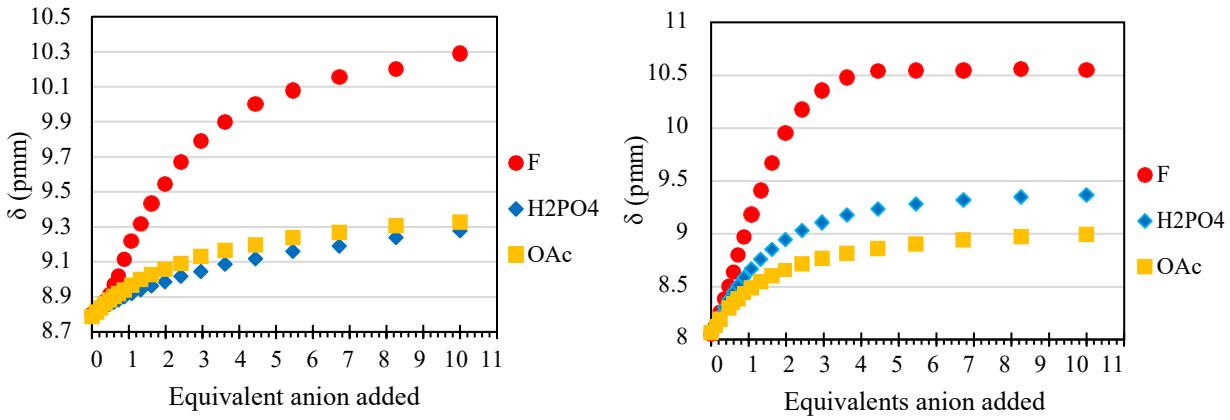

Figure 14. Plots for NH chemical shifts for compounds **2.1**(DiEt) (left) and **2.2**(TetraEt) (right) upon increasing concentration of anions: F^- (red), OAc^- (yellow), and $H_2PO_4^-$ (blue) in 9:1 CD_3CN:DMSO-d_6.

Receptors **2.4**(TetraHex) and **2.6**(TetraEtOH) displayed limited solubility in the 9:1 solvent mixture of CD_3CN:DMSO-d_6, requiring that titrations to be performed in DMF-d_6 and DMSO-d_6 respectively. Since both DMSO and DMF are prone to stronger solvation effects on the receptor for anion binding, they typically lead to lower binding affinity. However, despite the greater solvation effects present in the binding medium, **2.4**(TetraHex) was still competitive with the monotopic **2.3**(DiHex) receptor with an increase in binding by 500 M^{-1} for $H_2PO_4^-$. With the low binding affinity seen with receptor **2.3**(DiHex) in the CD_3CN:DMSO-d_6 solvent mixture, it could not be compared directly to **2.4**(TetraHex) due to the greater solvation effects from the solvent.

The most interesting anion binding comparison between monotopic and ditopic hosts was that of **2.5**(DiEtOH) and **2.6**(TetraEtOH). Receptor **2.5**(DiEtOH) demonstrated a staggering increase in anion affinity in comparison to other monotopic pincers with binding constants for $H_2PO_4^-$, OAc^- and F^- of 1,950, 2,750, and 18,200 M^{-1} respectively. The red F^- curve in Figure 15 shows a steep increase until equilibrium is achieved at 1 equivalent of anion added, indicating a strong interaction between host and guest. Based on the trend observed for the monotopic and ditopic compounds, it is reasonable to expect that **2.6**(TetraEtOH) would outperform the already impressive **2.5**(DiEtOH) as a receptor.

Aside from monotopic vs ditopic binding affinities, further comparisons can be made between duplexes with aliphatic R substitution such as **2.2**(TetraEt) and hydrophilic arms like **2.8**(TetraGly). Additional binding groups have been previously reported to provide more stability to the guest anion. It can be expected that the hydrophilic hosts will gain an advantage on binding ability.[14] The binding constants in Table 2 for hydrophobic host **2.2**(TetraEt) and hydrophilic host **2.8**(TetraGly) were revealed to be surprisingly similar for OAc^- and $H_2PO_4^-$. Despite the four extra hydrogen bond donors on **2.8**(TetraGly), similar binding could be due to the longer glycol chains having to reorient to aid in hydrogen bonding. The longer chains likely cause additional crowding that further hampers anion binding. However, the F^- binding for **2.8**(TetraGly) showed significant improvement on **2.2**(TetraEt). With this in mind, a dramatic difference could be expected with shorter chain lengths that align better with the binding pocket on hydrophilic **2.6**(TetraEtOH). Despite the requirement for titrations to be performed in highly solvating DMSO, the binding constants were competitive or exceeded all other duplex receptors in Table 2.

Titrations of **2.6**(TetraEtOH) with $H_2PO_4^-$ and OAc^- yielded binding constants of 780 M^{-1} and 1050 M^{-1} respectively**.** These values appeared to be lower than that of **2.5**(DiEtOH) (titrated in 9:1 CD_3CN:DMSO-d_6) which exhibited binding constants of 1950 M^{-1} for $H_2PO_4^-$ and 2750 M^{-1} for OAc^- but this, again, can be attributed to DMSO solvation effects. However, in regard to F^-, **2.6**(TetraEtOH) demonstrated a significant increase over the monotopic counterpart with a binding constant of 110,000 M^{-1} when calculated up to ~5 equivalents of anion added. To be able to compare the F^- binding of **2.6**(TetraEtOH) in DMSO to its monotopic counterpart directly, an additional titration was run with **2.5**(DiEtOH) in DMSO-d_6. A binding constant of 5,890 M^{-1} was obtained which demonstrates a decrease by a factor of 23 from the duplex host. An important aspect in regards to F^- binding in **2.6**(TetraEtOH) can be seen in the binding curve in Figure 15. An interesting feature is found where there is clearly a sharp initial binding event which levels off at 9.8 ppm and remains at equilibrium until 4.5 equivalents of anion is reached, then a second curve initiates.

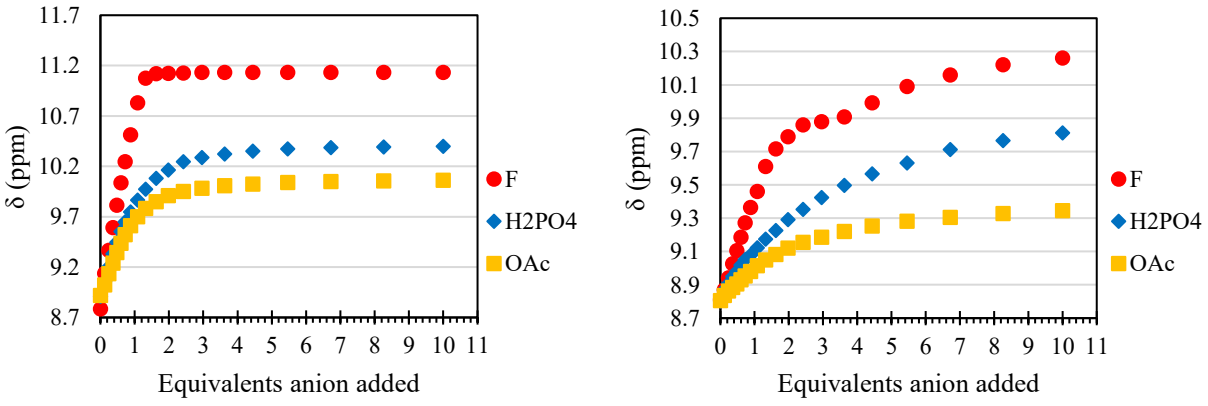

Figure 15. Plot for NH chemical shift for compounds **2.5**(DiEtOH) in 9:1 CD_3CN:DMSO-d_6 (left) and **2.6**(TetraEtOH) in DMSO-d_6 (right) upon increasing concentration of anions F^- (red), OAc^- (yellow), and $H_2PO_4^-$ (blue).

Referencing the ^{1}H NMR spectra from the **2.6**(TetraEtOH) titration with F^-,a set of peaks grows in after 4.5 equivalents was added at 16.15 ppm which is indicative of the presence of bifluoride, FHF^- (Figure 16).[20] The integration from the NMR reveals that the deprotonation of the amide starts occurring as the amide integration recedes and the FHF^-, signal rises after 4.5 equivalents of F^- was added.

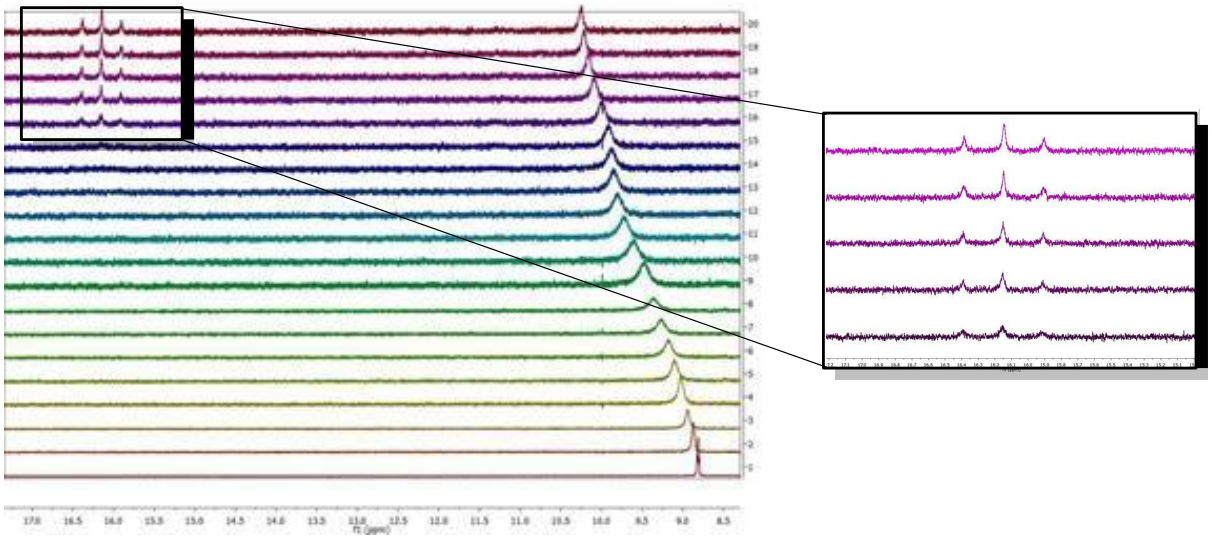

Figure 16. ^{1}H NMR spectra for **2.6**(TetraEtOH) showing the presence of bifluoride, FHF^-.

The crystal structure of **2.6**(TetraEtOH) in Figure 17 shows the preorganized binding pocket capable to readily accept anions with the carbonyls pointed away while the amide nitrogens point inward toward the binding pocket center. The short hydroxyethyl chains are of amiable size for wrapping around small anions and supporting the anion with a second set of hydrogen bond donors from the tail hydroxyl groups. Methanol was found to be sitting in the binding cavity of the pincer, which demonstrates the binding capabilities of **2.6**(TetraEtOH).

Amide NHs are preorganized pointing inward toward the binding pocket due to NH-N interactions with the pyrazine nitrogens. Compound **2.6**(TetraEtOH) forms intermolecular hydrogen bonds with adjacent molecules as well so that the pyrazine rings are offset instead of being in a columnar stack as was seen in Thordarson's work.[11]

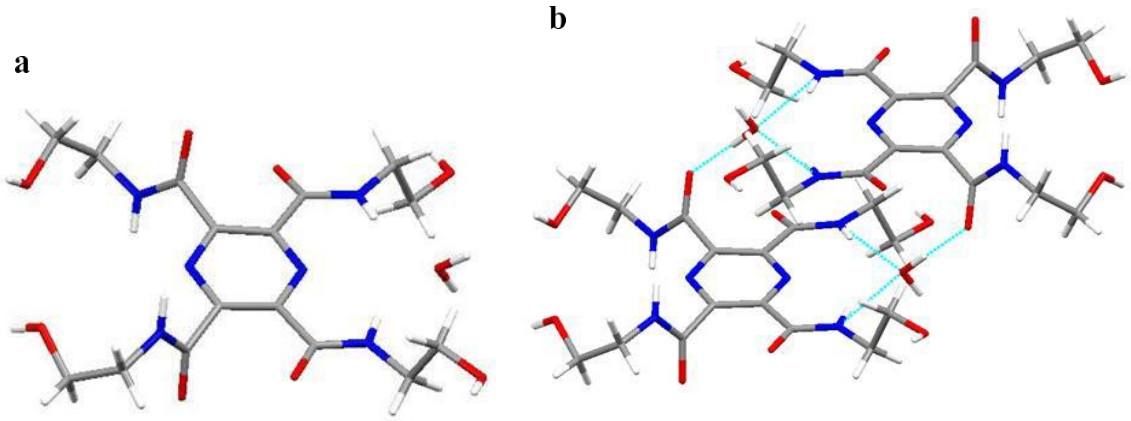

Figure 17. Crystal structure of **2.6**(TetraEtOH) showing single molecule (a) and two molecules stacked (b).

2.4.0 Conclusions

Pyrazine-2,3,5,6-tetracarboxamide duplex receptors were synthesized with a variety of different R groups to give a series of compounds with varied solubility due to hydrophobic and hydrophilic functionalization. For example, the hexyl R group appended **2.4**(TetraHex) led to compound solubility in chloroform and hexanes while the hydroxyl terminating R groups of **2.6**(TetraEtOH) restricted solubility to DMSO and water. The versatile host systems were then evaluated for anion host capabilities. All duplex hosts, regardless of R group substitution, were found to bind F^-, $H_2PO_4^-$, and OAc^- at least to some extent.

Binding affinities for duplex receptors and their monotopic 2,6-pyridinedicarboxamide counterparts were analyzed by ^1H NMR titrations. These studies revealed a trend in which the

duplex receptors generally displayed a higher degree of binding affinity than the single cavity hosts in a 1:2 host-guest stoichiometry. This is despite the proximity of the anion on either side of the cavity. Comparing single cavity **2.1**(DiEt) with dual cavity **2.2**(TetraEt) a significant increase in binding affinity is present, with a 9 times [1] increase in the binding constant for OAc^-.

The hydrophilic receptors with terminal hydroxide arms provided four extra hydrogen bond donors which further increased the affinity for anion guests. This was especially evident when comparing **2.2**(TetraEt) and **2.4**(TetraHex) to **2.6**(TetraEtOH) and **2.8**(TetraGly). Despite being restricted to highly solvating DMSO, **2.6**(TetraEtOH) demonstrated significant and competitive binding to the other duplex hosts. Most remarkable was the affinity for F^- in comparison to all other receptors both monotopic and ditopic. The short hydroxyl chains have the potential to wrap around the F^- guest, further stabilizing it and increasing binding strength. The binding curve for F^- with **2.6**(TetraEtOH) revealed a second binding curve beginning after equilibrium had been reached. This was attributed to FHF^- generation after 4.5 equivalents were added which was facilitated by the deprotonation of amides after this point. This new anionic species in the medium produces a second series of shifting in the remaining amide hydrogens.

Duplex hosts have shown great versatility and ease of functionalization of the R groups that contribute tunable solubility to desired environments. Further work on this project could expand into ion pair hosts with heterogeneous R appendages. This would facilitate dual anion and cation binding in unison across the pyrazine spacer and could benefit from cooperative binding.

References

1. Kavallieratos, K.; de Gala, S. R.; Austin, D. J.; Crabtree, R. H., A Readily Available Non-preorganized Neutral Acyclic Halide Receptor with an Unusual Nonplanar Binding Conformation. *Journal of the American Chemical Society* **1997,** *119* (9), 2325-2326.
2. Hossain, M. A.; Llinares, J. M.; Powell, D.; Bowman-James, K., Multiple Hydrogen Bond Stabilization of a Sandwich Complex of Sulfate between Two Macrocyclic Tetraamides. *Inorganic Chemistry* **2001,** *40* (13), 2936-2937.
3. Kavallieratos, K.; Bertao, C. M.; Crabtree, R. H., Hydrogen Bonding in Anion Recognition: A Family of Versatile, Nonpreorganized Neutral and Acyclic Receptors. *The Journal of Organic Chemistry* **1999,** *64* (5), 1675-1683.
4. Bisson, A. P.; Lynch, V. M.; Monahan, M.-K. C.; Anslyn, E. V., Recognition of Anions through NH-π Hydrogen Bonds in a Bicyclic Cyclophane—Selectivity for Nitrate. *Angewandte Chemie International Edition in English* **1997,** *36* (21), 2340-2342.
5. Dorazco-González, A.; Höpfl, H.; Medrano, F.; Yatsimirsky, A. K., Recognition of Anions and Neutral Guests by Dicationic Pyridine-2,6-dicarboxamide Receptors. *The Journal of Organic Chemistry* **2010,** *75* (7), 2259-2273.
6. Yamnitz, C. R.; Negin, S.; Carasel, I. A.; Winter, R. K.; Gokel, G. W., Dianilides of dipicolinic acid function as synthetic chloride channels. *Chemical Communications* **2010,** *46* (16), 2838-2840.
7. Kumar, P.; Gupta, R., The wonderful world of pyridine-2,6-dicarboxamide based scaffolds. *Dalton Transactions* **2016,** *45* (47), 18769-18783.
8. Atkins, J. L.; Patel, M. B.; Daschbach, M. M.; Meisel, J. W.; Gokel, G. W., Anion Complexation and Transport by Isophthalamide and Dipicolinamide Derivatives: DNA Plasmid Transformation in E. coli. *Journal of the American Chemical Society* **2012,** *134* (33), 13546-13549.
9. Mataka, S.; Irie, T.; Ikezaki, Y.; Tashiro, M., Preparation of Benzo-diimidazoles and Benzo-triimidazoles. *Chemische Berichte* **1993,** *126* (8), 1819-1822.
10. Light, M. E.; Gale, P. A.; Brooks, S. J., Bis(tetrabutylammonium) isophthalate 1-phenyl-3-[2,4,5-tris(3-phenylureido)phenyl]urea: a synchrotron study. *Acta Crystallographica Section E* **2006,** *62* (5), o1905-o1907.
11. Webb, J. E. A.; Crossley, M. J.; Turner, P.; Thordarson, P., Pyromellitamide Aggregates and Their Response to Anion Stimuli. *Journal of the American Chemical Society* **2007,** *129* (22), 7155-7162.
12. Tong, K. W. K.; Dehn, S.; Webb, J. E. A.; Nakamura, K.; Braet, F.; Thordarson, P., Pyromellitamide Gelators: Exponential Rate of Aggregation, Hierarchical Assembly, and Their Viscoelastic Response to Anions. *Langmuir* **2009,** *25* (15), 8586-8592.
13. Bartczak, T. J.; Michalska, Z. M.; Ostaszewski, B.; Sobota, P.; Strzelec, K., Synthesis, characterization and X-ray structures of the model ligand for a coordination polymer: diethyl-2,6-pyridine dicarboxamide and its complex with PdCl2. *Inorganica Chimica Acta* **2001,** *319* (1–2), 229-234.
14. Jia, C.; Wang, Q.-Q.; Begum, R. A.; Day, V. W.; Bowman-James, K., Chelate effects in sulfate binding by amide/urea-based ligands. *Organic & Biomolecular Chemistry* **2015,** *13* (25), 6953-6957.

15. Horino, H.; Sakaba, H.; Arai, M., Facile Preparation of 6-Bromopyridine-2-carboxamide and Pyridine-2,6-dicarboxamide: Partial Aminocarbonylation of 2,6-Dibromopyridine. *Synthesis* **1989,** *1989* (09), 715-718.
16. Kumar, S.; Singh, R.; Singh, K., Silver selective pyridine based diamide-diester 18-membered macrocycle- Syntheis and ionophore character. *Bioorganic & Medicinal Chemistry Letters* **1993,** *3* (2), 363-364.
17. Costero, A. M.; José Bañuls, M.; José Aurell, M.; Ward, M. D.; Argent, S., Biphenyl macrolactams in anion complexation. Selective naked-eye fluoride recognition. *Tetrahedron* **2004,** *60* (42), 9471-9478.
18. Hynes, M. J., EQNMR: a computer program for the calculation of stability constants from nuclear magnetic resonance chemical shift data. *Journal of the Chemical Society, Dalton Transactions* **1993,** (2), 311-312.
19. Connors, K. A.; Pendergast, D. D., Microscopic binding constants in cyclodextrin systems: complexation of .alpha.-cyclodextrin with sym-1,4-disubstituted benzenes. *Journal of the American Chemical Society* **1984,** *106* (24), 7607-7614.
20. Goursaud, M.; De Bernardin, P.; Dalla Cort, A.; Bartik, K.; Bruylants, G., Monitoring Fluoride Binding in DMSO: Why is a Singular Binding Behavior Observed? *European Journal of Organic Chemistry* **2012,** *2012* (19), 3570-3574.

CHAPTER 3

m-Xylyl Urea Macrocyclic Hosts for Anion Binding

3.1.0 Introduction

Urea macrocycles have been reported to produce interesting supramolecular assemblies as well as demonstrated an affinity for anionic species due to their strong hydrogen bonding capabilities.[1-3] Linda Shimizu has extensively shown the ability of urea macrocycles to form dense hydrogen bonding networks (Figure 1). In simple bis-urea macrocycles, intermolecular stacking resulted in columnar tubules.[4] The crystallized tubules reported by Shimizu were capable of CO_2 and H_2 gas absorption within the columns and some asymmetric urea macrocycles were found to be capable of gel formation.[5] Crystallized columnar urea macrocycles composed of hydrogen bonding arrays have also been reported to act as solid state host systems wherein the organic guest can be diffused. After diffusion, these tubules can act as cavities to facilitate guest photoreactions, making urea macrocycles an exciting area of interest for host-guest chemistry. [2, 6]

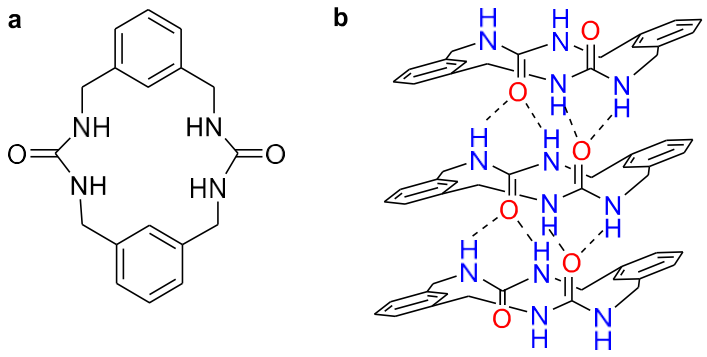

Figure 1. Shimizu's bis-urea macrocycle (a) and columnar hydrogen bond stacking (b).[7]

The strong hydrogen bonding nature of ureas can not only be applied to the structural assembly of macrocycles but also for the purpose of anion sequestration. Ureas and thioureas are popular subunits in anion hosts because each urea subunit can donate two hydrogen bonds to the guest ion.[3, 8] Increasing the number of hydrogen bond donors can help stabilize anions if positioned in synergistic locations that can enhance binding. Macrocyclic urea hosts are particularly attractive because they provide multiple hydrogen bond donors within a constrained pre-organized cavity.[9-12] From large urea macrocycles to simple thiourea cyclophanes, these receptors have demonstrated substantial anion binding capabilities.[10, 13-15] In this chapter, synthesis and characterization of asymmetric amine-bridged urea macrocycles will be detailed and their anion binding abilities will be assessed. The urea macrocycles of interest, shown in Figure 2, consist of different degrees of pocket rigidity and size which will be evaluated through anion binding studies.

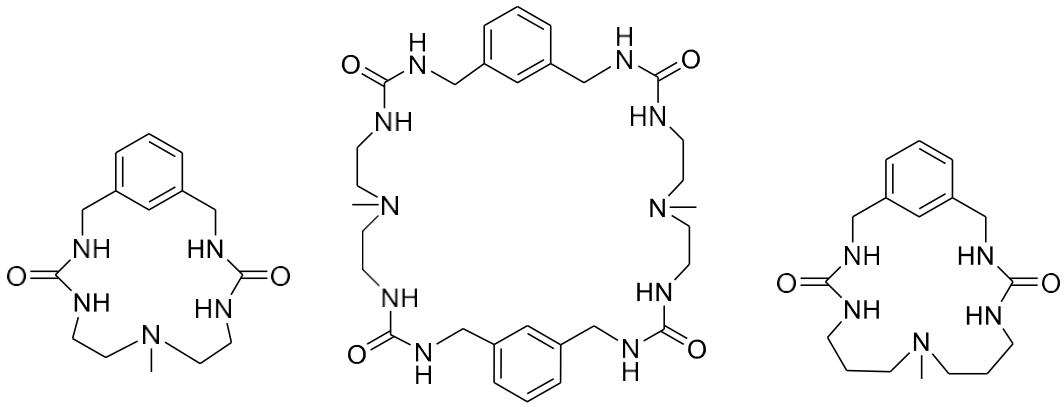

Figure 2. Urea *m*-xylyl macrocycles **3.1**, **3.2**, and **3.3**.

3.2.0 Experimental

3.2.1 Synthesis

General synthesis

Compounds **3.1**, **3.2**, and **3.3** were all synthesized by methods previously established by Hanumaiah Telikepalli, a former resident scientist in the Bowman-James group. ^{1}H and ^{13}C NMR spectra were acquired on a 400 or 500 MHz Bruker NMR spectrometer in molecular sieve-dried DMSO-d_6.

Synthesis of 1+1 ethyl urea macrocycle and 2+2 ethyl urea macrocycle. 3.1 and 3.2.

Scheme 1. Synthesis of **3.1** and **3.2** macrocycles.

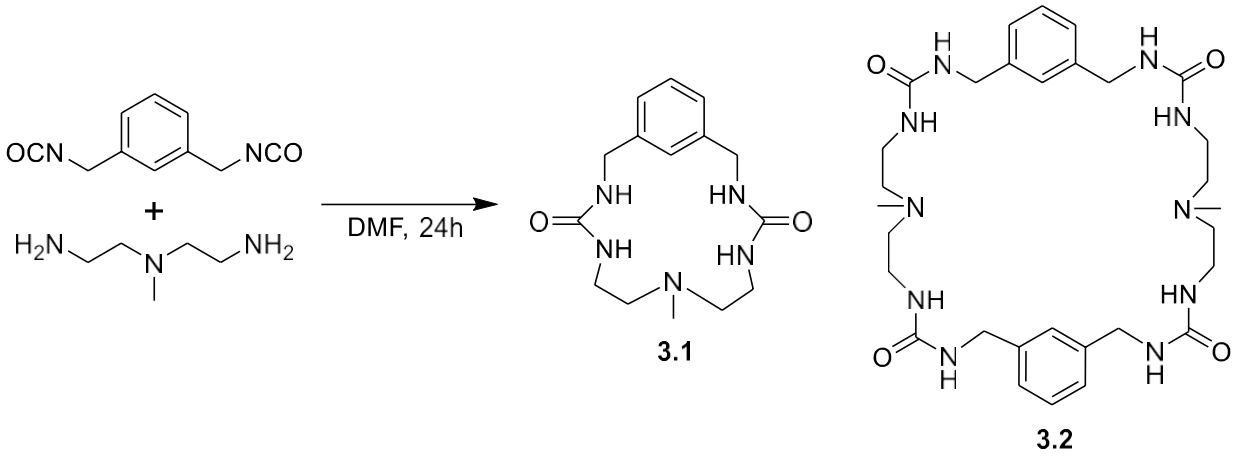

Into a 200 mL round bottom flask was added 1,3-bis(isocyanatomethyl)benzene (1.60 g, 8.51 mmol) and 50 mL of pyridine and stirred. In a separate flask, 2,2′-diamino-*N*-methyldiethylamine (1.00 g, 8.54 mmol) was added to 50 mL of pyridine then charged into an addition funnel. The amine solution was then added dropwise to the initial solution of 1,3-bis(isocyanateomethyl)benzene. The reaction was stirred at room temperature and within 10 minutes a white solid formed. The reaction was further stirred for 24 hours. Solvent was removed and the resulting mixture of **3.1** and **3.2** was stirred in hot ethanol and then subjected to

hot filtration. The filtrate contained **3.1** and the remaining solid was **3.2**. Yield **3.1** (378 mg, 14%). Yield **3.2** (1.9 g, 37.4%). Crystals of **3.1** were grown by slow evaporation in methanol.

3.1 ^{1}H NMR (400 MHz, $CDCl_3$): δ 7.16, (s, 1H), 7.15 (t, 1H), 7.00 (d, 2H), 6.32 (t, 2H), 5.31 (t, 2H), 4.24 (td 4H), 3.11 (d, 4H), 2.44 (t, 4H), 2.19 (s, 3H) ppm. ^{13}C NMR (125 MHz, DMSO-d6), δ 158.54, 142.09, 127.94, 124.89, 123.13, 57.66, 42.63, 41.49, 37.88 ppm. Exact mass for $C_{32}H_{56}N_6O_4$ + H^+ 306.1930, found (HREIMS+) 306.1931.

3.2 ^{1}H NMR (400 MHz, $CDCl_3$): δ 7.21, (s, 2H), 7.08 (m, 6H), 6.39 (d, 4H), 5.87 (t, 4H), 4.14 (m, 8H), 3.08 (m, 8H), 2.35 (t, 8H), 2.16 (s, 6H) ppm. ^{13}C NMR (125 MHz, DMSO-d6), δ 158.51, 141.23, 128.58, 126.20, 125.73, 57.55, 43.40, 42.46, 37.78 ppm. Exact mass for $C_{32}H_{56}N_6O_4$ + H^+ 611.3782, found (HREIMS+) 611.3778.

Synthesis of 1+1 propyl urea macrocycle and 2+2 propyl macrocycle. 3.3.

Scheme 2. Synthesis of **3.3** macrocycle.

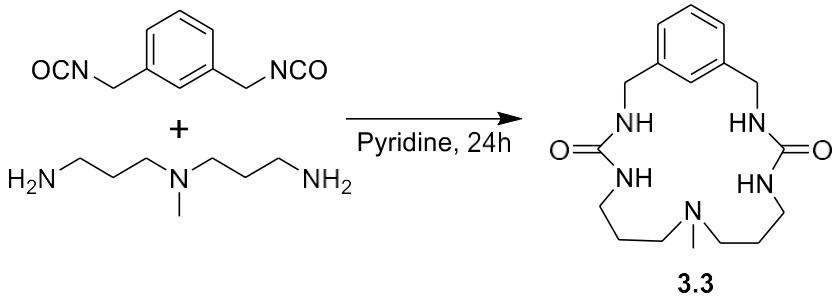

3.3

1,3-Bis(isocyanatomethyl)benzene (800 mg, 4.26 mmol) was added into 30 mL of pyridine and stirred. 3,3′-Diamino-*N*-methyldipropylamine (682 mg, 4.28 mmol) was added to 40 mL of pyridine and added dropwise to the initial solution of 1,3-bis(isocyanatomethyl)benzene. The reaction was stirred at room temperature and within 15 minutes a white solid formed. The reaction was further stirred for 24 hours. Solvent was removed and the white solid was washed with a solvent mixture of methanol/acetonitrile/ether to

yield a white solid upon drying. (803 mg, 56.6%) ^{1}H NMR (400 MHz, DMSO-d_6): δ 7.23, (s, 1H), 7.18 (t, 1H), 7.04 (d, 2H), 6.38 (t, 2H), 5.99 (t, 2H), 4.22 (d 4H), 3.05 (m, 4H), 2.29 (t, 4H), 2.14 (s, 3H), 1.53 (t, 4H) ppm. ^{13}C NMR (125 MHz, DMSO-d_6), δ 158.51, 141.94, 127.97, 125.72, 124.29, 55.12, 43.02, 38.28, 27.99 ppm. Exact mass for $C_{32}H_{56}N_6O_4$ + H^+ 334.2243, found (HREIMS+) 334.2210.

3.2.2 ^{1}H NMR Anion Binding Studies

For qualitative anion binding studies, 2 mM solutions were prepared in DMSO-d_6 for compounds **3.1**, **3.2**, and **3.3**. TBA salts (10 eq, 0.1 mmol) of hydrogen sulfate, bromide, chloride, fluoride, dihydrogen phosphate, nitrate, acetate and tetramethylammonium oxalate ($TMA_2C_2O_4$) were added to 0.5 mL solutions of each host, and the ^{1}H NMR spectra was recorded to monitor NH amide signal shifting.

For quantitative anion binding titrations, 2 mM solutions of each host were prepared in DMSO-d_6 for compounds **3.1**, **3.2**, and **3.3**. Cleaned and dried NMR tubes were prepared with 0.5 mL of the 2 mM host solution. Solutions of each anion using TBA fluoride, TBA dihydrogen phosphate, TBA acetate, and TBA hydrogen sulfate were prepared using the DMSO-d_6 at 20 mM each. ^{1}H NMR spectra were recorded after every addition of anion to the host solution. After normalization of each spectrum to the solvent peak, the amide NH downfield signal shift of each host was recorded and analyzed in EQNMR2 by fitting a least-squares binding curve to each data set that allowed the determination of binding constants for each host complex.[16] All binding constants were determined at <15% error.

Binding Spectra

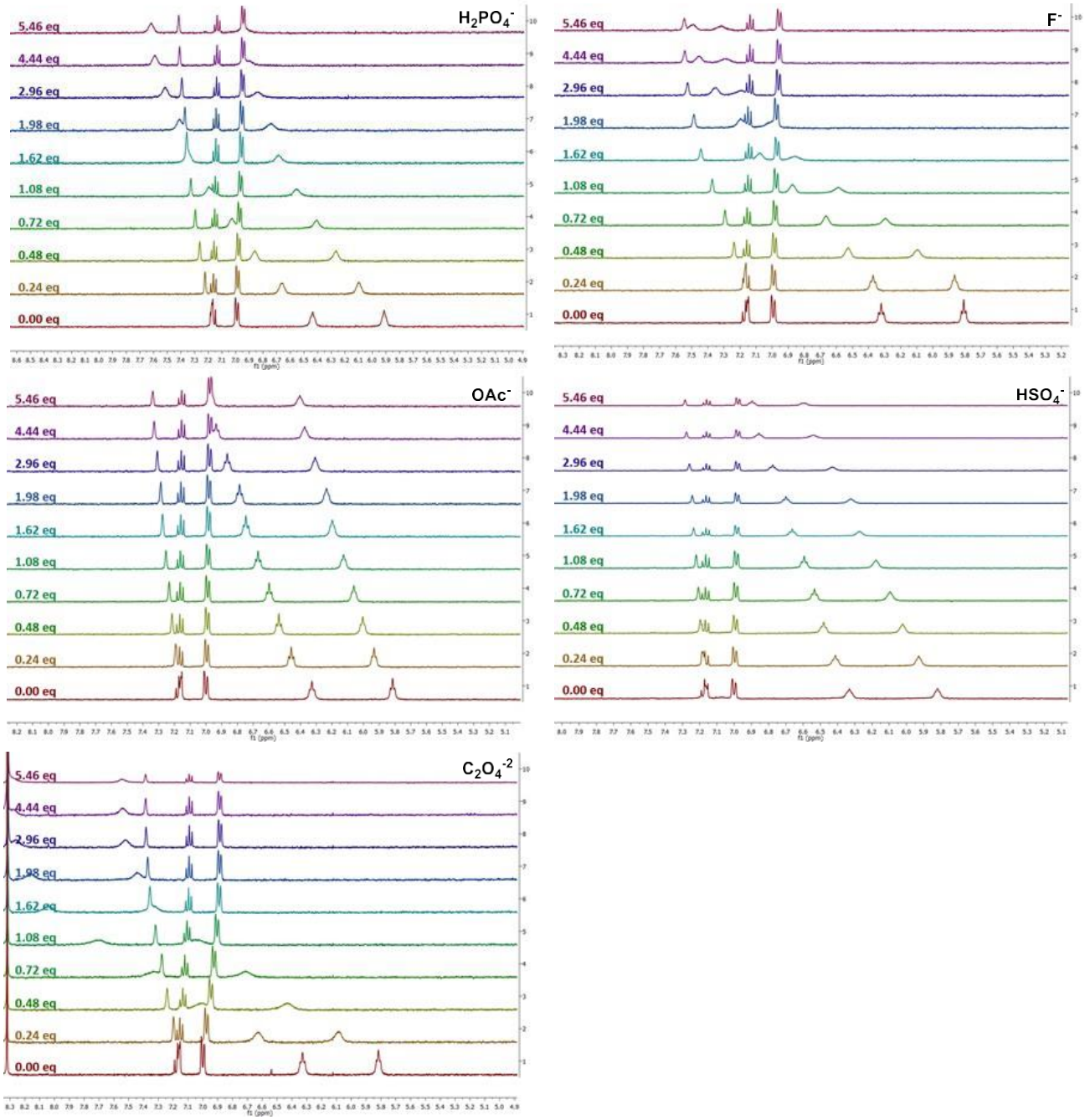

Figure 3. ^{1}H NMR titration spectra for **3.1** with F^-, $H_2PO_4^-$, OAc^-, HSO_4^-, and $C_2O_4^{-2}$.

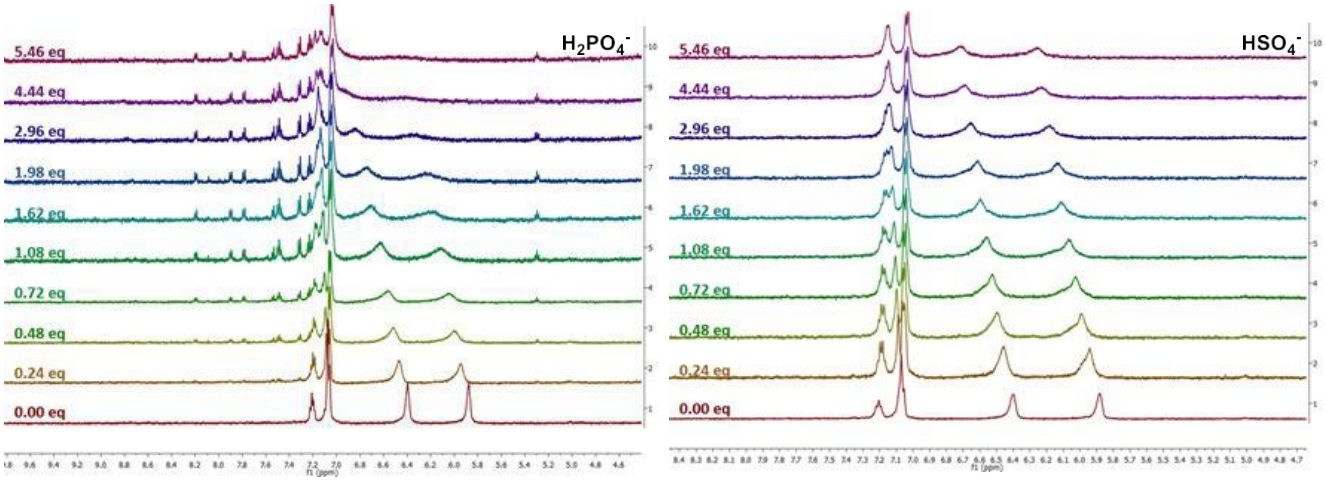

Figure 4. ^{1}H NMR titration spectra for **3.1** with $H_2PO_4^-$ and HSO_4^-.

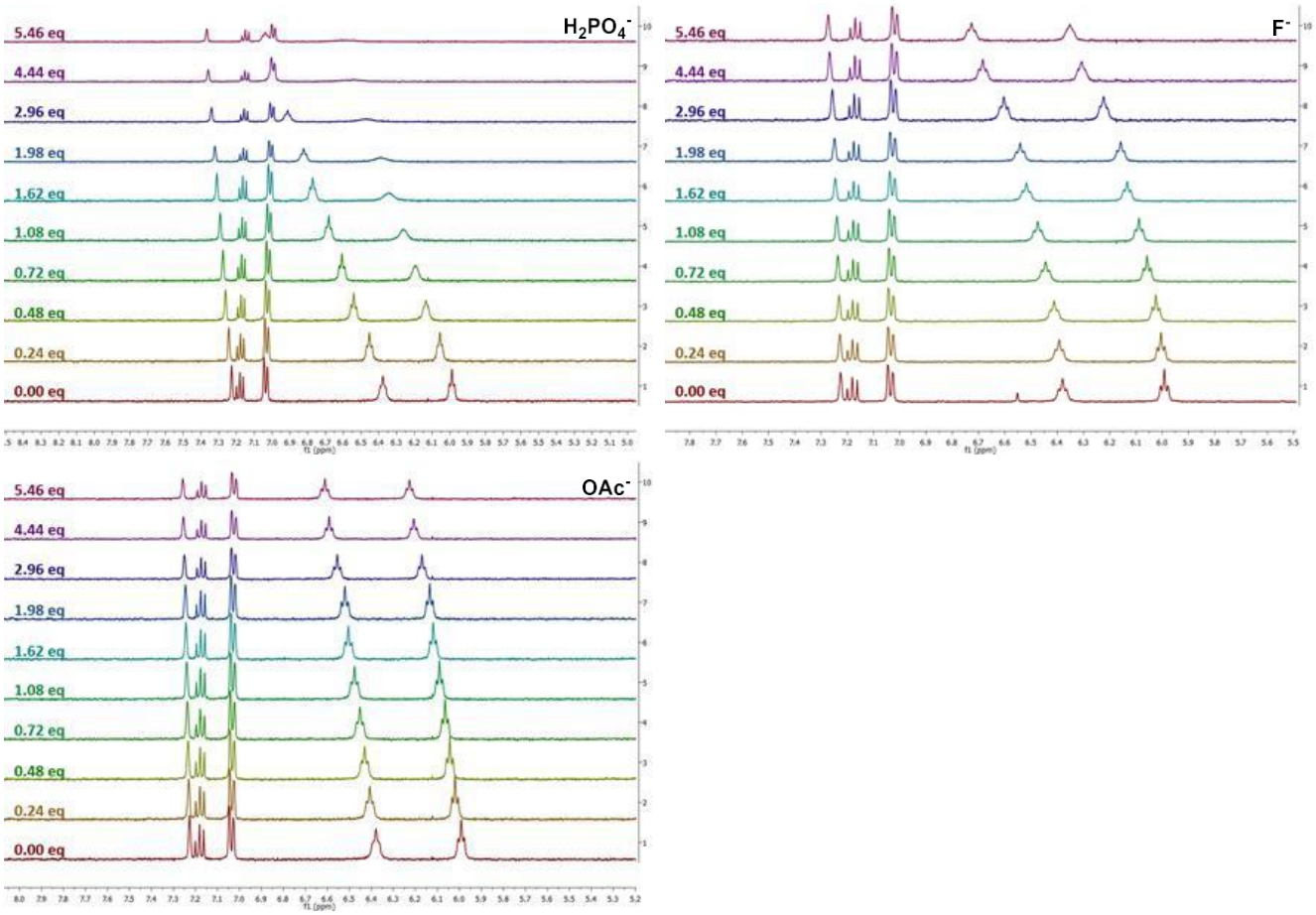

Figure 5. ^{1}H NMR titration spectra for **3.1** with F^-, $H_2PO_4^-$, and OAc^-.

3.3.0 Results and Discussion

3.3.1 Urea Macrocycle Synthesis and Characterization

Urea macrocyclic receptors were all synthesized with 1,3-bis(isocyanatomethyl)benzene and amine bridging unit 2,2′-diamino-*N*-methyldiethylamine for both **3.1** and **3.2** or 3,3′-diamino-*N*-methyldipropylamine for **3.3** (Figure 2). The use of isocyanates for the synthesis of asymmetric urea macrocycles enabled facile preparations without the use of protecting groups, as was previously reported by Shimizu.[7] The reactions yielded a simplified 1+1 product composed of one *m*-xylene head group and one tertiary amine bridging group, **3.1** and **3.3**. The reaction 2+2 side product was synthesized alongside the 1+1 product composed of two *m*-xylene head groups and two tertiary amine bridging groups. The 2+2 ethyl urea macrocycle, **3.2**, that was isolated displayed limited solubility in all solvents except for DMSO. The 2+2 propyl urea side product has yet to be fully isolated so it is not discussed herein.

Crystals of compound **3.1** were grown by slow evaporation in methanol. In the crystal structure of **3.1** the urea NH groups and the carbonyl oxygens twist to orient above and below the molecular plane allowing for intermolecular hydrogen bonding with adjacent molecules (Figure 6). The receptors stack in an antiparallel conformation where the aromatic *m*-xylyl heads overlay with the amine bridging groups in an alternating pattern. This is similar to what was reported by Shimizu with asymmetric glycol-bridged urea macrocycles that did not exhibit the π-π stacking that was seen in Figure 1.[4, 7] The intermolecular distance between carbonyl and urea on adjacent molecules (N···O) was found to be 2.884 – 2.910 Å. The pocket diameter between (N···N) of the bis-ureas ranges from 4.960 Å nearest the *m*-xylyl head and 4.098 Å toward the bridging unit.

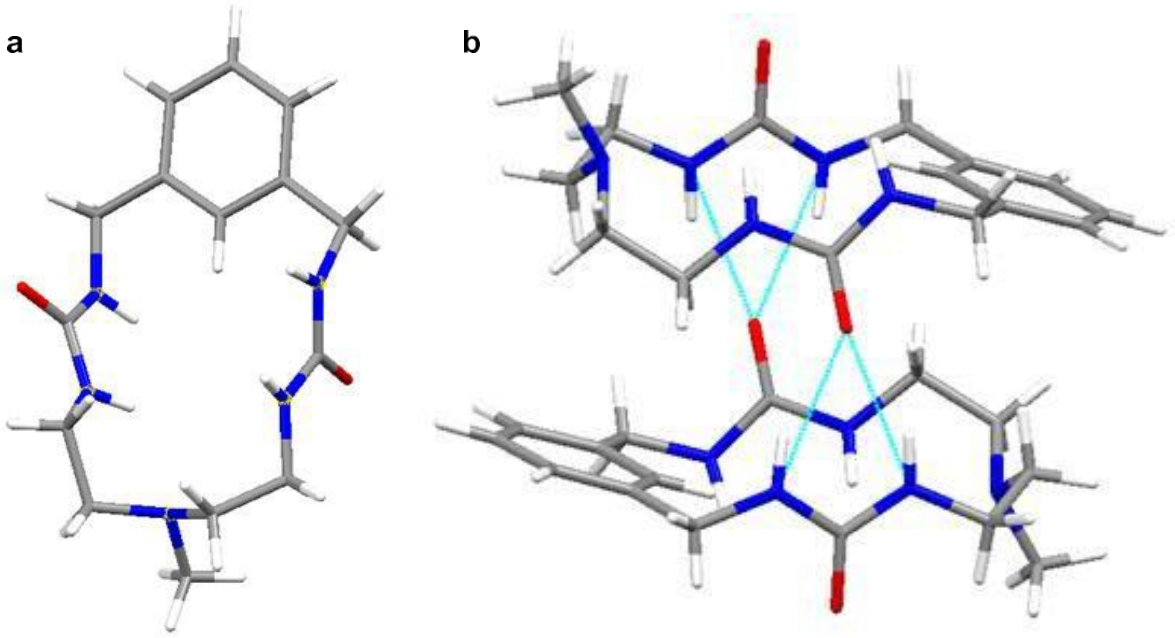

Figure 6. Crystal structure of a single **3.1** molecule (a) and two stacked **3.1** molecules with hydrogen bonding (b).

Crystallization of **3.2** was unsuccessful due to its insolubility in most solvents and its propensity for forming gels upon heating in DMF and DMSO (Figure 7). It was found to form a gel in a 40 mM solution of DMSO after being heated to boiling and then allowed to cool to room temperature. Diffusion of acetone and methanol into a solution of **3.2** in DMSO also led to formation of a gel after a few days. Similar behavior was reported by Shimizu for asymmetric urea macrocycles with ether bridges.[7]

Figure 7. Inverted vial containing gel formed from **3.2** in DMSO.

3.3.2 Anion Binding Studies

Binding affinities were qualitatively assessed for **3.1** by ^{1}H NMR additions with TMA, TEA, and TBA salts in DMSO-d_6. The **3.1** macrocycle has two urea NHs and the CH on the phenyl group that orient inward toward the cavity center which are capable of anion association. Out of the anions introduced to **3.1**, anions: F^-, $H_2PO_4^-$, OAc^-, HSO_4^- and ox^{-2} were all determined to form host-guest complexes as indicated by downfield shifts of the CH and both NH signals in the NMR spectra. NH signals labeled "**d**" and "**e**" in Figure 8 were assigned by ^{1}H COSY NMR. The chemical shifts of the internal cavity CH, labeled as "**a**" in Figure 8, was monitored in comparison to the other external aromatic hydrogens (**b** and **c**). For anions Br^- and NO_3^-, little to no hydrogen shifting was observed and very minimal shifts from Cl^- indicated poor binding.

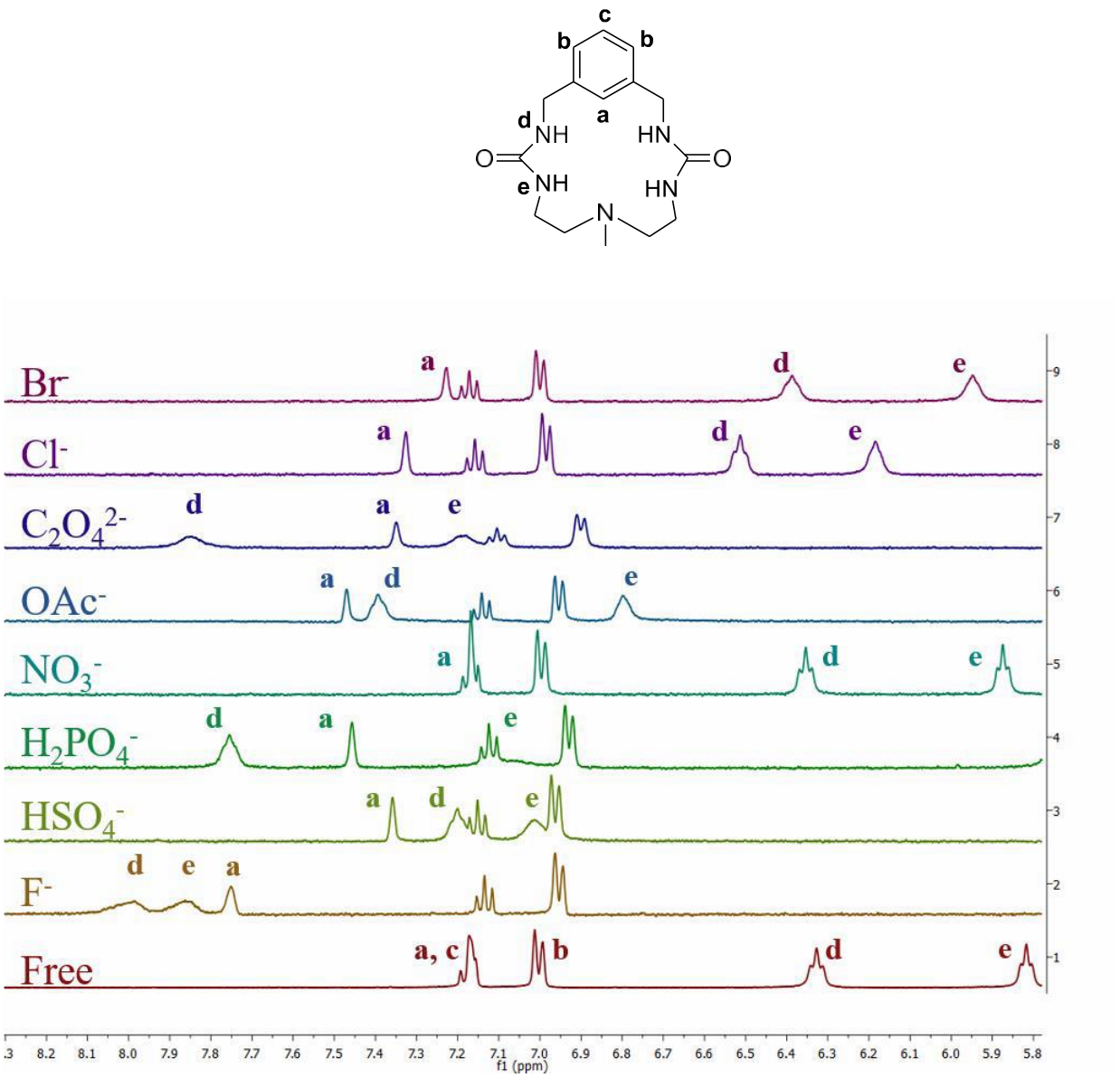

Figure 8. Screening of 10 equivalents of anion salts of: F^-, HSO_4^-, $H_2PO_4^-$, NO_3^-, OAc^-, $C_2O_4^{-2}$, Cl^- and Br^- in a 2 mM solution of host **3.1** in DMSO-*d*$_6$.

Due to broadening of the NH signals, shifts of the aromatic CH (**a**) were used to calculate binding constants in ^{1}H NMR titrations (Figure 9). The largest affinity observed for receptor **3.1** was towards the dianionic species, $C_2O_4^{-2}$, and was found to have the largest association constant at over 3,700 M^{-1}. As previously mentioned, the pocket of receptor **3.1** shows urea N···N

distances of 4.960 Å nearest the *m*-xylyl head and 4.098 Å toward the bridging unit. Oxalate is known to have an O···O distance of 2.69 Å for oxygens on adjacent carbons and a distance of 2.18 Å for oxygens on the same carbon.[17] Binding of $C_2O_4^{-2}$ with receptor **3.1** could potentially occur above the cavity by bridging between the two ureas. Another possibility is that $C_2O_4^{-2}$ extends vertically from the pocket causing it to be sandwiched between two macrocyclic hosts, however, a crystal structure is needed to confirm the binding motif. With respect to the monoanionic species, competitive binding for $H_2PO_4^-$ and F^- is seen with binding constants of 1,410 M^{-1} and 1,700 M^{-1}, respectively. However, these are both bound to a greater extent when compared to other monoanionic oxoanions like HSO_4^- and OAc^- (Table 1).

Interestingly, Figure 8 shows that the two urea hydrogen signals shift to different extents for some of the anion species introduced. The best examples are both F^- and $H_2PO_4^-$ anion complexes. Binding constants calculated for $H_2PO_4^-$ derived from shifts for both urea hydrogen signals and the CH signal all produce binding constants within 100 M^{-1}. However, F^- binding produced three different binding constants depending on which hydrogen bond donor shifts the constant was calculated from. The NH signal "**d**" generated a binding constant of 730 M^{-1}, the NH "**e**" showed a binding constant of 1185 M^{-1} and the CH signal, a shifting resulted in a binding constant of 1680 M^{-1}. This is attributed to stronger interactions with certain hydrogens donors over others. Similar shifting differences have been reported in literature.[9, 18]

Table 1. Anion binding constants (M^{-1}) obtained for **3.1** with anions: F^-, $H_2PO_4^-$, OAc^-, HSO_4^-, and $C_2O_4^{-2}$ in DMSO-d_6. (*Binding constant determined from CH chemical shifts*)

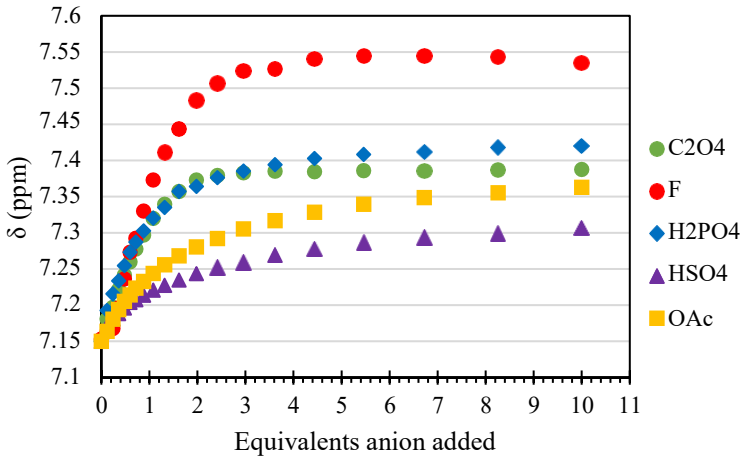

Anion	3.1
$H_2PO_4^-$	1,410
F^-	1,700
OAc^-	347
HSO_4^-	219
$C_2O_4^{-2}$	3,720

Figure 9. CH chemical shifts obtained **3.1** ^{1}H NMR titrations with F^-, $H_2PO_4^-$, OAc^-, HSO_4^-, and $C_2O_4^{-2}$ in DMSO-d_6.

Macrocycle **3.1** forms a tight binding pocket between two opposite urea groups with four hydrogen bond donors total. Complexes **3.2** and **3.3**, both have larger less-rigid pockets, so we wanted to compare their binding capabilities to those of receptor **3.1** to determine any changes in anion affinity and selectivity. While the 1+1 propyl urea macrocycle, **3.3**, only has a slight increase in cavity size by the replacement of ethyl bridging groups to propyl groups, macrocycle **3.2** contains a much larger binding pocket. Although the separation of the urea groups in **3.2** is greater, it also contains four extra hydrogen bond donors that could potentially aid in binding.

Anion binding ^{1}H NMR titrations of the larger cavity receptors **3.2** and **3.3** demonstrated a significant drop in chemical shifting when compared to **3.1**. The decrease in amide NH interaction tends to indicate a lower degree of anion association. Urea shifts in receptor **3.2** were substantially lower in the case of OAc^- and F^- with binding being too low to calculate. $H_2PO_4^-$ and HSO_4^- still bound strong enough to produce binding curves (Figure 10). Titrations for $H_2PO_4^-$, F^-, and OAc^- were also performed with receptor **3.3,** however, since the degree of NH

shift seen in the qualitative studies with HSO_4^- was so low, a binding constant could not be obtained for that species. The decrease in anion affinity is reflected in the lower degree of urea shifting with **3.3** when compared to **3.1** is seen in the binding curve where the more gradual sloping curve indicates weaker interaction (Figure 10).

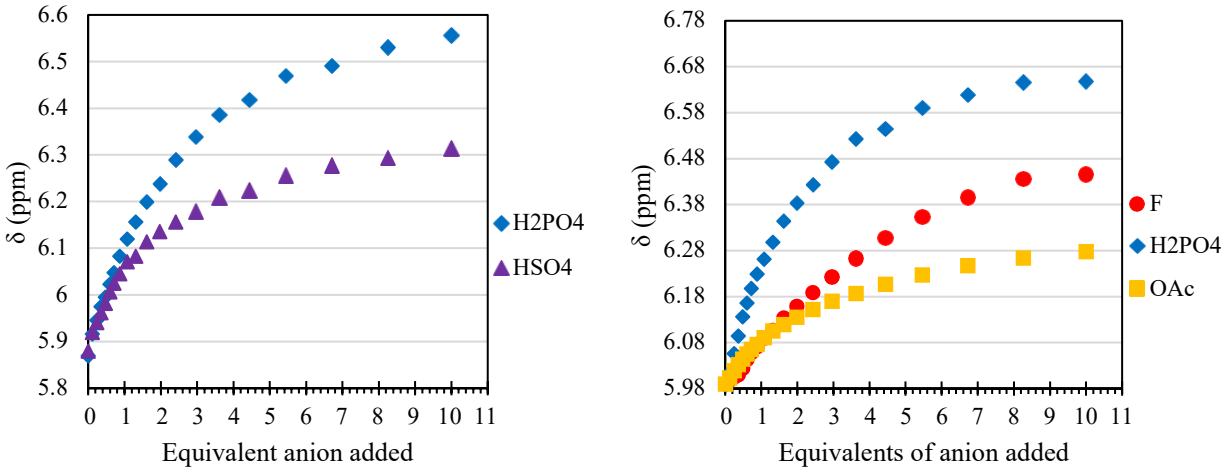

Figure 10. Anion binding curves from ^{1}H NMR titrations for **3.2** with $H_2PO_4^-$ and HSO_4^- (left) in **3.3** and with F^-, $H_2PO_4^-$, and OAc^- (right) in DMSO-d_6.

In comparison to the anion binding capabilities of **3.1**, the expanded pocket size of **3.2** and **3.3** dramatically decreases binding of the urea macrocyclic receptors (Table 2). Receptor **3.2** showed a lower binding constant for 200 M^{-1} for $H_2PO_4^-$, and only a slight increase in HSO_4^-. Despite the addition of two extra urea groups yielding four additional hydrogen bond donors, the larger cavity keeps the anion binding capabilities low due to the separation of urea groups. While slight selectivity for $H_2PO_4^-$ binding is observed for **3.3** over OAc^- and F^- anions, the binding constant significantly drops by over 1000 M^{-1} in comparison to **3.1**. The F^- binding was also seen to decrease heavily in comparison to **3.1** by a factor of 17. The replacement of the ethyl linkages

in the bridging chain with propyl linkers makes a less rigid structure and wider cavity that decreases the receptors ability to hydrogen bond with anions.

Table 2. Binding constants (M^{-1}) for **3.1**, **3.2**, and **3.3** in DMSO-d_6.

Anion	3.1	3.2	3.3
$H_2PO_4^-$	1,410	200	339
F^-	1,700	[B]	42
OAc^-	347	[B]	145
HSO_4^-	214	316	[b]

([a] All constants were calculated from urea hydrogens. [b] Binding data were too low to fit)

3.4.0 Conclusions

Bis-urea macrocycles were synthesized with *m*-xylene head groups and ethyl and propyl amine-based bridging groups yielding receptors **3.1** and **3.3** respectively. The side product **3.2** with two *m*-xylyl heads and two amine bridging groups was also isolated and evaluated. The crystal structure for receptor **3.1** shows a stacked intermolecular hydrogen bonding network with a rigid structure. It also exhibited affinity for monoanionic $H_2PO_4^-$, F^-, HSO_4^-, and OAc^- and dianionic ox^{-2}. Binding affinities for monoanionic $H_2PO_4^-$ and F^- are shown to be similar to one another and demonstrate a larger degree of binding in comparison to OAc^- and HSO_4^-. However, out of all anions introduced to **3.1**, the highest binding affinity was obtained in the presence of $C_2O_4^{-2}$.

The smaller **3.1** pocketed receptor displayed stronger anion affinity in comparison to the expanded **3.2** and **3.3** receptors. Lower anion affinity was observed with almost every anion when complexed with the larger pocketed receptors. Macrocycle **3.1** bound $H_2PO_4^-$ four times stronger than receptor **3.3** and seven times stronger than **3.2**. The longer bridging unit in **3.3**

could cause further separation of urea subunits across the cavity, thereby decreasing the chelation of anions between all four possible hydrogen bond donors. The expanded **3.2** receptor has also shown a decrease in binding with the exception of HSO_4^-, which demonstrated a very slight increase in affinity. The larger binding pocket and extensive separation between urea groups were shown to limit overall anion affinity, despite the addition of two extra urea subunits in **3.2**. In future works, testing the binding of oxalate with compounds **3.2** and **3.3** might afford more competitive results; however their wider structures ultimately made them poor anion hosts. Longer polyanionic species such as pyrophosphate could potentially lead to strong anion affinity in these urea macrocyclic hosts, which could be a future direction for these systems.

References

1. Amendola, V.; Fabbrizzi, L.; Mosca, L., Anion recognition by hydrogen bonding: urea-based receptors. *Chemical Society Reviews* **2010,** *39* (10), 3889-3915.
2. Shimizu, L. S.; Salpage, S. R.; Korous, A. A., Functional Materials from Self-Assembled Bis-urea Macrocycles. *Accounts of Chemical Research* **2014,** *47* (7), 2116-2127.
3. Fan, E.; Van Arman, S. A.; Kincaid, S.; Hamilton, A. D., Molecular recognition: hydrogen-bonding receptors that function in highly competitive solvents. *Journal of the American Chemical Society* **1993,** *115* (1), 369-370.
4. Shimizu, L. S.; Smith, M. D.; Hughes, A. D.; Shimizu, K. D., Self-assembly of a bis-urea macrocycle into a columnar nanotube. *Chemical Communications* **2001,** (17), 1592-1593.
5. Roy, K.; Wang, C.; Smith, M. D.; Dewal, M. B.; Wibowo, A. C.; Brown, J. C.; Ma, S.; Shimizu, L. S., Guest induced transformations of assembled pyridyl bis-urea macrocycles. *Chemical Communications* **2011,** *47* (1), 277-279.
6. Salpage, S. R.; Xu, Y.; Som, B.; Sindt, A. J.; Smith, M. D.; Shimizu, L. S., Pyridyl-phenylethynylene bis-urea macrocycles: self-assembly and utility as a nanoreactor for the selective photoreaction of isoprene. *RSC Advances* **2016,** *6* (100), 98350-98355.
7. Yang, J.; Dewal, M. B.; Sobransingh, D.; Smith, M. D.; Xu, Y.; Shimizu, L. S., Examination of the Structural Features That Favor the Columnar Self-Assembly of Bis-urea Macrocycles. *The Journal of Organic Chemistry* **2009,** *74* (1), 102-110.
8. Smith, P. J.; Reddington, M. V.; Wilcox, C. S., Ion pair binding by a urea in chloroform solution. *Tetrahedron Letters* **1992,** *33* (41), 6085-6088.
9. Brooks, S. J.; García-Garrido, S. E.; Light, M. E.; Cole, P. A.; Gale, P. A., Conformational Control of Selectivity and Stability in Hybrid Amide/Urea Macrocycles. *Chemistry – A European Journal* **2007,** *13* (12), 3320-3329.
10. Snellink-Ruel, B. H. M. A., Martijn M. G.; Engbersen, Johan F. J.; Timmerman, Peter; Reinhoudt, David N., Neutral Anion Receptor with Multiple Urea-Binding Sites. *European Journal of Organic Chemistry* **2000**, 165-170.
11. Jia, C.; Wang, Q.-Q.; Begum, R. A.; Day, V. W.; Bowman-James, K., Chelate effects in sulfate binding by amide/urea-based ligands. *Organic & Biomolecular Chemistry* **2015,** *13* (25), 6953-6957.
12. Schneider, H.-J., Binding Mechanisms in Supramolecular Complexes. *Angewandte Chemie International Edition* **2009,** *48* (22), 3924-3977.
13. Sasaki, S.-i.; Mizuno, M.; Naemura, K.; Tobe, Y., Synthesis and Anion-Selective Complexation of Cyclophane-Based Cyclic Thioureas. *The Journal of Organic Chemistry* **2000,** *65* (2), 275-283.
14. Lee, K. H.; Hong, J.-I., C3-Symmetric metacyclophane-based anion receptors with three thiourea groups as linkers between aromatic groups. *Tetrahedron Letters* **2000,** *41* (32), 6083-6087.
15. Meshcheryakov, D.; Arnaud-Neu, F.; Bohmer, V.; Bolte, M.; Hubscher-Bruder, V.; Jobin, E.; Thondorf, I.; Werner, S., Cyclic triureas-synthesis, crystal structures and properties. *Organic & Biomolecular Chemistry* **2008,** *6* (6), 1004-1014.

16. Hynes, M. J., EQNMR: a computer program for the calculation of stability constants from nuclear magnetic resonance chemical shift data. *Journal of the Chemical Society, Dalton Transactions* **1993,** (2), 311-312.
17. Jeffrey, G. A.; Parry, G. S., The Crystal Structure of Sodium Oxalate. *Journal of the American Chemical Society* **1954,** *76* (21), 5283-5286.
18. Watt, M. M.; Zakharov, L. N.; Haley, M. M.; Johnson, D. W., Selective Nitrate Binding in Competitive Hydrogen Bonding Solvents: Do Anion–π Interactions Facilitate Nitrate Selectivity? *Angewandte Chemie International Edition* **2013,** *52* (39), 10275-10280.

CHAPTER 4

Dicarboxamide Pincer Ligand Applications

4.1.0 Pincer ligands

Typically, pincer ligands are composed of an aryl backbone as seen in **1** with two arms extending from the molecule with electron donor units, E, used to pinch and hold a metal ion in a tridenate chelate. Both of the electron donor arms are *ortho* to a central group on the aryl ring that also participates in binding, shown as X. An attractive feature of pincer ligands is that they are highly tunable by manipulating E, X, R, and thus can bind a variety of metals and serve multiple purposes.[1]

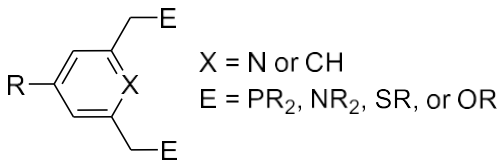

1

The electron donors, E, in the arms of the ligand can influence metal electronic properties. Examples of pendant arms include NR_2, SR, OR, and PR_2 and may be symmetric or asymmetric.[2] For the purposes of this discussion, focus will remain on symmetric donor systems. The R groups attached to the electron donor play an important role in properties of the metal complexes, depending on electron withdrawing or donating nature as well as inducing steric components to the ligand. The central aryl chelate group also has a large impact on whether the deprotonated carbon contributes an anionic site to the metal in the case of a *m*-xylyl backbone, or a neutral nitrogen in the case of pyridine. The external functionalization positioned away from the binding cavity, such as R, can be used for fine electronic tuning at a remote position. It can also act as a tethering group for immobilization to broaden the applications of the pincer into materials.[3]

The first examples of pincer ligand complexes were reported in 1976 by Moulton and Shaw. The initial complex was composed of *m*-xylenyldiphosphine, **2**, which binds various metals between the two phosphoryl groups and the central anionic carbon after deprotonation (**2a)**.[4] Ni(II), Pd(II), and Pt(II) square planar complexes were made with chloride metal salts of each and underwent metathesis upon introduction of sterically unhindered ligands such as cyanide, hydrides, or carbonyl groups at the fourth coordination site. Ir(III) and Rh(III) were also found to react with the PCP pincer to form a 5-coordinate hydride complex. Since the initial results from Moulton and Shaw, the PCP pincer has been applied to an outstanding range of catalytic reactions in organic synthesis and the scope of pincer chemistry has grown significantly with structural diversity producing a variety of functions.

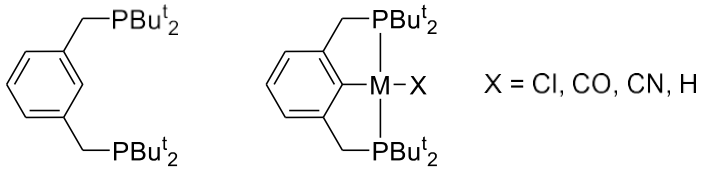

2 **2a**

A particular type of pincer that has been the interest of the Bowman-James group, for not only anion binding as mentioned in Chapters 1 and 2, but also their use for metal binding are diamide and dithioamide pincers, **3**. Amide based pincers are becoming more recognized in the pincer ligand field due their facile synthesis as well as their capability of metal chelation. They are particularly attractive as transition metal hosts as they are capable of binding metals either as an anionic or a neutral ligand depending on whether the metal is bound between the two anionic deprotonated amides or by two sulfurs on thioamide sulfurs which can bind anionically or in a neutral fashion. In rare cases, transition metal guest can be held between neutral amide oxygens.[5] Specifically, a large amount of interest has centered on the development of pyridine-2,6-

dicarboxamide ligands which form a NNN chelate with a neutral donor from the pyridine nitrogen and two anionic donors from the deprotonated amides. The two deprotonated amides act as two anionic σ-donors which allows binding of metal ions and have been shown to stabilize metals at higher oxidation states.[6] The R groups on the pyridine-2,6-dicarboxamide pincer are also a tunable component that can sterically affect the environment around the metal center and the adjacent fourth coordinate group.

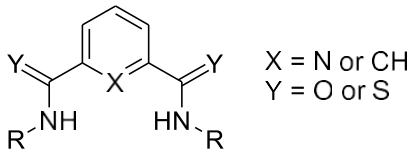

3

This chapter will highlight the different applications of metal pincer complexes with emphasis on dicarboxamide pincer examples. Alteration of the pincer core and R group functionalizations will open the door to host versatility. It is also important in the following sections to call attention to dicarboxamide pincers and the diverse way they've been applied to advance the respective fields of study and their functions.

4.2.0 Metal Pincers in Literature and Dicarboxamides

Since the 1970s, pincer complexes have been used in a wide range of applications. Initially, pincer ligands were used for catalysis in a range of organic synthetic reactions.[7] Over the last 20 years as technology has advanced, pincers have expanded their use into the fields of sensors and receptors, materials, and biomimetics, to name just a few.[1, 3, 6, 8-9]

Pincer compounds are featured heavily in catalysis applications and have been reported in numerous accounts in literature. The tridentate structure aids in stabilization of metal complexes so they may be used in a wealth of organic synthetic reactions with benefits including stability in

air, thermal stability, and have been shown at times to have shorter turnover rates. In the classic pincer, **1**, M-C σ-bonding helps stabilize the catalytic site while the electron donor arm groups can be tuned to alter the catalytic site properties.[7] Functionalization of the donor groups can also contribute a steric influence on catalytic selectivity as well as asymmetrical catalysis.[1] C-C coupling by the Heck reaction and Suzuki coupling have been widely explored but pincer catalysts have also been used for Kharasch additions as well as Stille, Sonagashira, Hiyama, and Negishi couplings.[2, 6, 10-14] While a number of metal pincers have demonstrated utility in both Heck and Suzuki reactions, some of the most widely applied complexes are palladium pincers.[15]

An interesting amide-based catalytic pincer system from the Bowman-James group showed application for Heck reaction catalysis. They developed the first thioamide ditopic pincer macrocycle, **4**, which was shown to bind two palladiums in each of the SCS binding cavities between the two sulfurs and a deprotonated phenyl carbon.[16] The crystal structure of complex **4** showed that these macrocycles stack over each other in an anti-conformation. The resulting complex, **4a**, was able to catalyze coupling between 4-iodotoluene and styrene while demonstrating stability in presence of water and oxygen. It also showed stability at high temperatures and was able to produce significant turnover results.

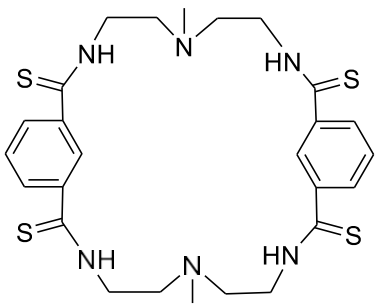

4

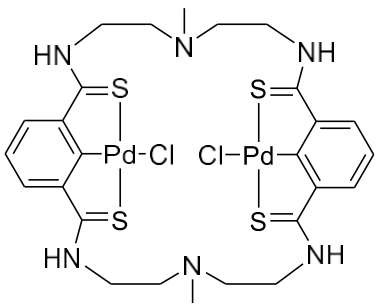

4a

Metal pincer receptors, depending on the components, have been shown to bind substrates both irreversibly and reversibly. Upon substrates binding to metal centers in the cavity, they have pronounced effect on the pincers properties which can be detected by a range of methods including NMR, UV-Vis, electrochemistry, or by sight. Selective capture and sensing of particular substrates is a highly desirable trait for both the recognition of potentially hazardous materials as well as sequestration of useful substrates for repurposing.

Diamide and thioamide metal bound pincers have also been demonstrated by the Bowman-James group to act as receptors. One substrate of interest that has shown affinity for palladium and platinum bound pincers has been the half-mustard derivative chloroethyl ethyl sulfide (CEES). The sulfur mustards are classified as chemical warfare agents and are most commonly known for their usage in World War I due to their cytotoxic effects which are extremely hazardous. Due to these detrimental effects, there is an interest in their capture and degradation. CEES is often used as a surrogate in laboratory studies where mustard agents are examined. It was shown that the palladium pyridine-2,6-diamide complex can bind CEES by displacing fourth coordinate acetonitrile in an irreversible metathesis, **5**.[17] A surprising feature seen in the crystal structures that directly influence the CEES binding is the increasing steric bulk at the phenyl amide arms. By substituting naphthalene and then anthracene groups the binding is significantly increased. The anthracene-appended crystal structure shows that CEES was captured in a cage-like complex where the sulfur is directly bound to the palladium and the anthracene units act as walls protectively enclosed around it, **6**.

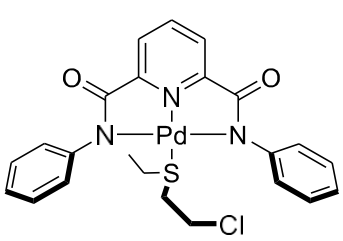

5

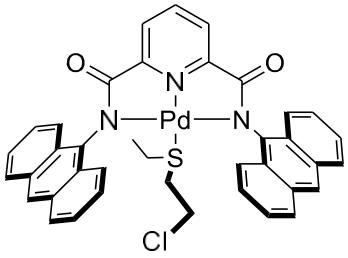

6

Thioamide pincers bound platinum between the sulfurs in a SNS configuration instead of binding through the deprotonated nitrogens in the typical NNN.[18] Introduction of CEES to the SNS platinum complex, **7**, showed no binding initially but after deprotonation of the amide NH to yield the iminothiolate complex, a pronounced upfield shift is observed in the ^{1}H NMR indicating binding (**8**). An interesting facet of the platinum iminothiolate complex is that it exhibits capture and release control based on pH. Addition of acid reprotonates the thioamide nitrogens and CEES is released thus making it a completely switchable receptor for the hazardous mustards.[19] This on-off switchable binding of the metal pincer complexes is a desirable trait in which both capture and release of substrates can be mediated.

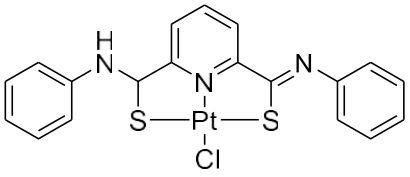

7

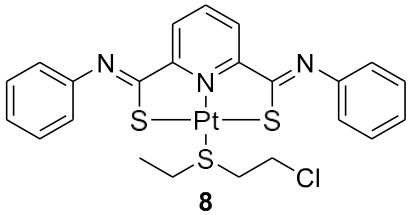

8

Metalloenzymes perform a large range of functions, in which the mechanisms, properties, and intermediate structures can be difficult to elucidate. A better understanding of metalloenzymes and their mechanistic pathways could help produce new selective and high-functioning catalysts. Metal pincer complexes afford an opportunity to study complex mechanisms found in nature on a simplified scale in the form of biomimics. One set of intermediates that are difficult to stabilize in metalloenzyme pathways include those involved in

oxidations such as terminal hydroxides, superoxides, and alkylperoxides as well as bridging hydroxides and oxo groups.[6]

Demonstrating metal pincer complexes' ability to stabilize these reactive intermediates, Tolman and coworkers used the 2,6-diisopropylphenyl-pyridine-2,6-dicarboxamide ligand to stabilize the copper(III) hydroxo species, **9**.[20] The intermediate produced has similarities to those produced in oxidation reactions by enzymes, such as dopamine β-monooxygenase.[6] The Tolman group investigated the electronic and oxidative properties of complex **9**. It was found to be capable of oxidizing dihydroanthracene to produce anthracene and a copper(II)-augua complex at very high rates giving insight into the hydrogen abstraction capabilities of the oxidative intermediate.

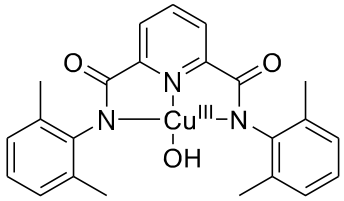

9

Work on terminal hydroxide-metal species has also been explored by Holm and coworkers with nickel(II) pyridine-2,6-dicarboxamide pincer ligands. The terminal hydroxide coordinated to the nickel complex showed significant ability toward CO_2 fixation. CO_2 is a noted greenhouse gas but has the potential to be converted to renewable fuel.[21] Using a pyridine-2,6-dicarboxamide pincer, Holm was able to synthesize a four coordinate nickel(II) hydroxo species, **10**. In the presence of CO_2 gas, the terminal hydroxide rapidly take up the gas and is converted to a bicarbonate product, **10a**. This reaction was shown to be reversible, going through a five-coordinate intermediate by the bicarbonate upon dissolution back to the four-coordinate nickel(II) hydroxo complex **10**.

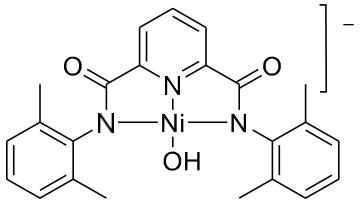

10

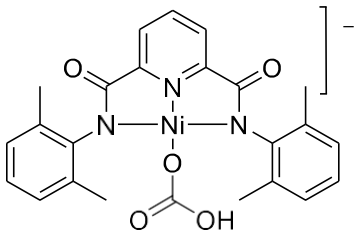

10a

The ability to work on these smaller scale systems through metal pincer complexes aids in unraveling different mechanistic pathways. These pathways and intermediates can then be redesigned into new and functional catalysts and receptor systems.

Recently, metal pincer complexes have expanded into the field of materials.[3, 22] Metal carboxamide pincer complexes can be incorporated into larger nanostructural arrays such as metal organic frameworks, dendrimers, and polymer systems as either a linking unit or as a functional unit. The three different ways into forming these array systems with metal pincer complexes is by being a sole component through self-assembly, incorporated into a polymer as a structural component, or tethered to the structural unit of a framework such as a polymer system.

Certain pincer backbones can naturally lead to the self-assembly of multiunit arrays. The Bowman-James group demonstrated this with their cyclization of palladium pyrazine-2,6-diamide pincers, which have a tendency to form extended structural arrays as opposed to a monomeric complex.[2] Specifically a pyridine-2,6-dicarboxamide pincer was shown to form a NNN chelated square planar palladium complex with acetonitrile in the fourth coordinate group when introduced to palladium(II) acetate, **11**. Sitting in chloroform overnight caused the loosely-bound acetonitrile to be displaced by the oxygen carbonyl of an adjacent complex with Pd – O distances of 2.05 Å. The self-assembly proceeded in a continuous manner forming a nanoarray composed of a cyclic hexameric complex labeled the palladawheel, **12**.[23] This self-assembly

behavior of complex **11** which generates nanostructures is an attribute that could be utilized further in materials chemistry in higher order array systems.

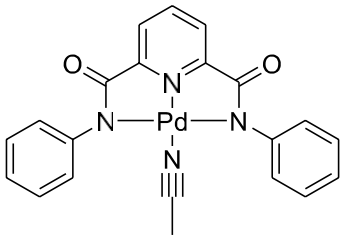

11

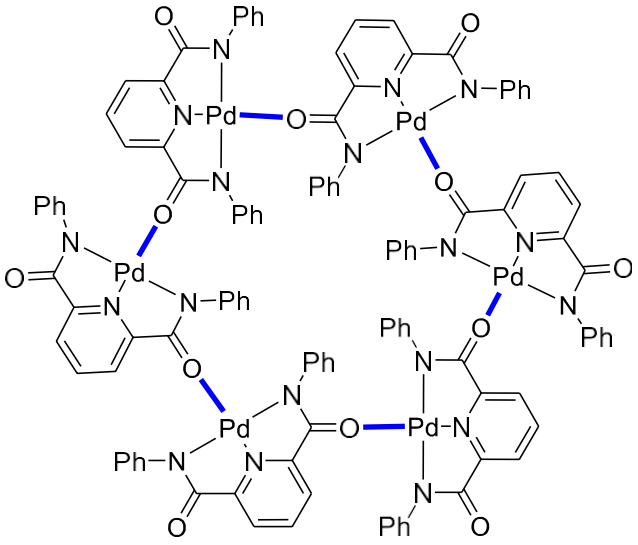

12

4.3.0 Tetra-substituted Aryl Pincers

Tetra-substituted ditopic pincers have the potential to expand pincer application into the fields of coordination polymers and metal organic frameworks (MOFs); however, there have been few examples of these complexes in literature. Some examples of tetra-substituted aryl pincers have been reported by Shimizu, van Koten, and Shionoya. These compounds ranged from a dual SCS platinum pincer used as a coordination polymers (**13**), a NCN dual pincer that showed catalytic properties (**14**), and a remarkable dual NCN platinum pincer, **15**, from Shionoya was applied as molecular ball bearings in molecular rotors systems.[24-26]

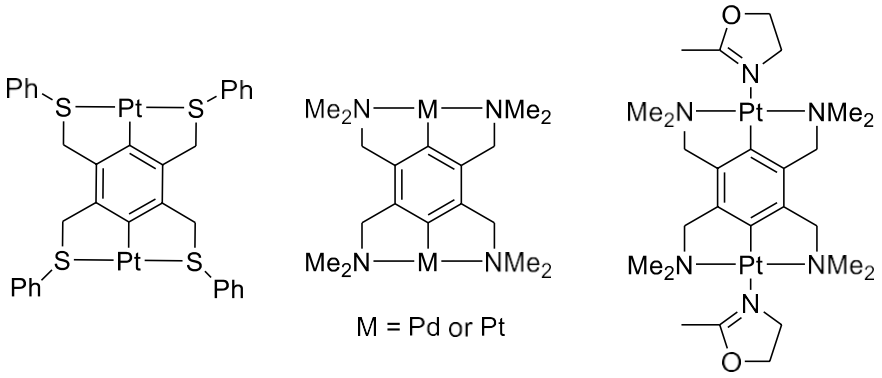

13 **14** **15**

Though tetracarboxamide pincers have been synthesized by Thordarson and coworkers, as was discussed in Chapter 2, at this point they have not been explored for metal compelation.[27-28] The facile functionalization of amide R groups allows amide-based pincers to be versatile hosts that can whose properties can be tuned depending on the nature of their pendant groups. With this tunable nature of the amide ligand in mind, tetra-substituted amide ligands can be applied to metal binding and, therefore, provide new possiblilities for further advancement in the fields of catalysis, biomimetric, sensors, receptors, and materials. The ditopic coordination sites also have the potential to be used as MOF scaffolds as well as coordination polymer units.

4.4.0 Continuation of metal pincer work in the Bowman-James group

Pyridine-2,6-diamide metal pincers have been of great interest in the Bowman-James group and advancing these systems into new areas of utility is a continuous goal. The following Chapter 5 expands upon work in synthesizing and analyzing new pyrazine-2,3,5,6-tetracarboxamide metal complexes. Dimetallated square planar palladium complexes of the tetracarboxamide ligands will be discussed along with some interesting features exhibited by these metal complexes. Variable appended carboxamide R group functionalization will be shown to enhance solubility in these complexes and their characterization will be discussed.

References

1. Albrecht, M.; van Koten, G., Platinum Group Organometallics Based on "Pincer" Complexes: Sensors, Switches, and Catalysts. *Angewandte Chemie International Edition* **2001,** *40* (20), 3750-3781.
2. *Pincer and Pincer-Type Complexes*. 1 ed.; John Wiley & Sons, Incorporated: Boschstr. 12, 69469 Weinheim, Germany, 2014; p 320.
3. Moughton, A. O.; O'Reilly, R. K., Noncovalently Connected Micelles, Nanoparticles, and Metal-Functionalized Nanocages Using Supramolecular Self-Assembly. *Journal of the American Chemical Society* **2008,** *130* (27), 8714-8725.
4. Moulton, C. J.; Shaw, B. L., Transition metal-carbon bonds. Part XLII. Complexes of nickel, palladium, platinum, rhodium and iridium with the tridentate ligand 2,6-bis[(di-t-butylphosphino)methyl]phenyl. *Journal of the Chemical Society, Dalton Transactions* **1976,** (11), 1020-1024.
5. Rajput, A.; Mukherjee, R., Coordination chemistry with pyridine/pyrazine amide ligands. Some noteworthy results. *Coordination Chemistry Reviews* **2013,** *257* (2), 350-368.
6. Kumar, P.; Gupta, R., The wonderful world of pyridine-2,6-dicarboxamide based scaffolds. *Dalton Transactions* **2016,** *45* (47), 18769-18783.
7. Ohff, M.; Ohff, A.; van der Boom, M. E.; Milstein, D., Highly Active Pd(II) PCP-Type Catalysts for the Heck Reaction. *Journal of the American Chemical Society* **1997,** *119* (48), 11687-11688.
8. Bedford, R. B.; Draper, S. M.; Noelle Scully, P.; Welch, S. L., Palladium bis(phosphinite) 'PCP '-pincer complexes and their application as catalysts in the Suzuki reaction. *New Journal of Chemistry* **2000,** *24* (10), 745-747.
9. Gossage, R. A.; van de Kuil, L. A.; van Koten, G., Diaminoarylnickel(II) "Pincer" Complexes: Mechanistic Considerations in the Kharasch Addition Reaction, Controlled Polymerization, and Dendrimeric Transition Metal Catalysts. *Accounts of Chemical Research* **1998,** *31* (7), 423-431.
10. Inés, B.; SanMartin, R.; Churruca, F.; Domínguez, E.; Urtiaga, M. K.; Arriortua, M. I., A Nonsymmetric Pincer-Type Palladium Catalyst In Suzuki, Sonogashira, and Hiyama Couplings in Neat Water. *Organometallics* **2008,** *27* (12), 2833-2839.
11. Wasilke, J.-C.; Wu, G.; Bu, X.; Kehr, G.; Erker, G., Ruthenium Carbene Complexes Featuring a Tridentate Pincer-type Ligand. *Organometallics* **2005,** *24* (17), 4289-4297.
12. Szabó, K. J., Palladium-Pincer-Complex-Catalyzed Transformations Involving -Organometallic Species. *Synlett* **2006,** *2006* (06), 811-824.
13. Wang, Q.-Q.; Begum, R. A.; Day, V. W.; Bowman-James, K., Chemical Mustard Containment Using Simple Palladium Pincer Complexes: The Influence of Molecular Walls. *Journal of the American Chemical Society* **2013,** *135* (45), 17193-17199.
14. Begum, R. A.; Powell, D.; Bowman-James, K., Thioamide Pincer Ligands with Charge Versatility. *Inorganic Chemistry* **2006,** *45* (3), 964-966.
15. Wang, Q.-Q.; Ara Begum, R.; Day, V. W.; Bowman-James, K., Molecular Thioamide ↔ Iminothiolate Switches for Sulfur Mustards. *Inorganic Chemistry* **2012,** *51* (2), 760-762.
16. Donoghue, P. J.; Tehranchi, J.; Cramer, C. J.; Sarangi, R.; Solomon, E. I.; Tolman, W. B., Rapid C–H Bond Activation by a Monocopper(III)–Hydroxide Complex. *Journal of the American Chemical Society* **2011,** *133* (44), 17602-17605.

17. Wei, J.; Ge, Q.; Yao, R.; Wen, Z.; Fang, C.; Guo, L.; Xu, H.; Sun, J., Directly converting CO2 into a gasoline fuel. **2017,** *8*, 15174.
18. Albrecht, M.; van Koten, G., Gas Sensor Materials Based on Metallodendrimers. *Advanced Materials* **1999,** *11* (2), 171-174.
19. Wang, Q.-Q.; Day, V. W.; Bowman-James, K., Hexagonal molecular "palladawheel". *Chemical Communications* **2013,** *49* (73), 8042-8044.
20. Loeb, S. J.; Shimizu, G. K. H., Dimetallated thioether complexes as building blocks for organometallic coordination polymers and aggregates. *Journal of the Chemical Society, Chemical Communications* **1993,** (18), 1395-1397.
21. Steenwinkel, P.; Kooijman, H.; Smeets, W. J. J.; Spek, A. L.; Grove, D. M.; van Koten, G., Intramolecularly Stabilized 1,4-Phenylene-Bridged Homo- and Heterodinuclear Palladium and Platinum Organometallic Complexes Containing N,C,N-Coordination Motifs; η1-SO2 Coordination and Formation of an Organometallic Arenium Ion Complex with Two Pt−C σ-Bonds. *Organometallics* **1998,** *17* (24), 5411-5426.
22. Hiraoka, S.; Hisanaga, Y.; Shiro, M.; Shionoya, M., A Molecular Double Ball Bearing: An AgI–PtII Dodecanuclear Quadruple-Decker Complex with Three Rotors. *Angewandte Chemie International Edition* **2010,** *49* (9), 1669-1673.
23. Webb, J. E. A.; Crossley, M. J.; Turner, P.; Thordarson, P., Pyromellitamide Aggregates and Their Response to Anion Stimuli. *Journal of the American Chemical Society* **2007,** *129* (22), 7155-7162.
24. Tong, K. W. K.; Dehn, S.; Webb, J. E. A.; Nakamura, K.; Braet, F.; Thordarson, P., Pyromellitamide Gelators: Exponential Rate of Aggregation, Hierarchical Assembly, and Their Viscoelastic Response to Anions. *Langmuir* **2009,** *25* (15), 8586-8592.

CHAPTER 5

Duplex Metal Complex Synthesis and Characterization

Parts reproduced with permission from: Lohrman, J.; Telikepalli, H.; Johnson, T. S.; Jackson, T. A.; Day, V. W.; Bowman-James, K., *Inorganic Chemistry* **2016,** *55* (11), 5098-5100. DOI: 10.1021/acs.inorgchem.6b00594

5.1.0 Introduction

While examples of tetra-substituted ditopic pincers are quite scarce in the literature, they provide an excellent opportunity to further expand pincer complex application and utilize their full metal binding potential. Metal binding in dual sided pincers can not only be utilized in catalysis but has also led to new applications in coordination polymers and molecular machines.[1-3] As previously discussed in Chapter 2, Thordarson and coworkers developed tetra-substituted pyromellitamide pincers which displayed a unique extended structure through intermolecular bonds.[4-5] However, metal ion binding has yet to be explored in the pyrazine-2,3,5,6-tetracarboxamide system.

Pincer ligands are particularly attractive hosts for transition metals due to their tridentate chelate system that can stabilize metal ions. Specifically, pyridine-2,6-dicarboxamides have been shown to bind metals anionically, where the metal center is bound between two deprotonated amides resulting in an NNN chelate, as shown in Figure 1. While more rare, there are also cases of these pincers binding as a neutral ligand where the metal is held between the two carbonyl oxygens in an ONO chelate.[6] The versatility of these pincers can be expanded by the modification of the R groups of the amides. This includes tuning the solubility or the steric hindrance. These modifications allow for the introduction of different metal ions, which can ultimately expand both the application and utility of this family of pincer complexes.

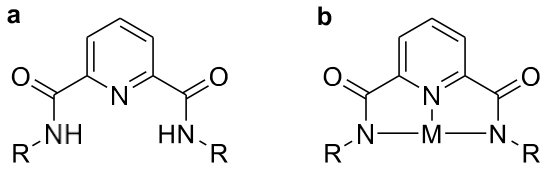

Figure 1. 2,6-dicarboxamide pincer ligand as a free complex (a), with a metal in NNN chelate (b).

Utilizing a pyrazine ring in place of the phenyl ring as the core of the tetracarboxamide pincers promotes opportunities for metal binding which opens the door to a new set of dimetallated pincers. The work in this chapter focuses on the synthesis and characterization of square planar dimetallated duplex pincers as seen in Figure 2, some of which has been published by the Bowman-James group.[7] As previously shown in Chapter 2, functionalization of the amide groups allows for duplexes with versatile solubility. Additionally, the nature of the R group substitution can be used to influence other properties that pertain to metal binding or function of the pincer. Potential applications can then be extended to use in catalysis, organometallic arrays, or MOF systems in the future.

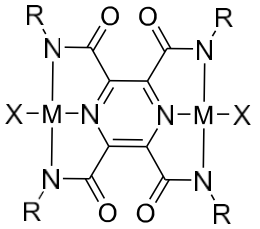

Figure 2. Dimetallated pyrazine-2,3,5,6-tetracarboxamide ligand.

5.2.0 Experimental

5.2.1 Synthesis

General synthesis

^{1}H and ^{13}C NMR spectra was acquired on a 400 or 500 MHz Bruker in molecular sieve dried DMSO-d_6 and $CDCl_3$. IR spectra were acquired by a PerkinElmer Spectrum 100 FTIR. UV-Vis spectra was acquired with a Shimazu UV-3600 spectrometer in DMSO.

Synthesis of 5.1.

Scheme 1. Synthesis of **5.1**.

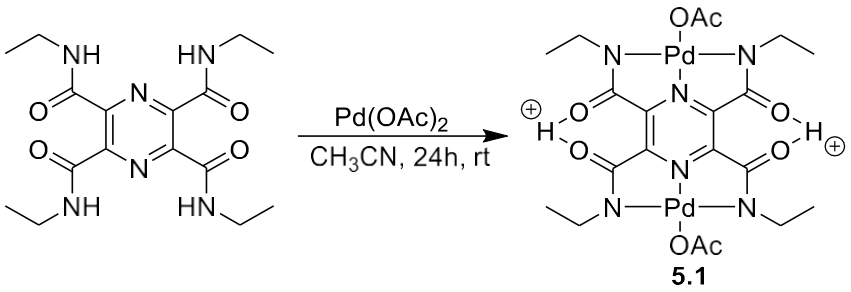

5.1

A white suspension of **2.2**(DiEt) (73.5 mg , 0.202 mmol) in 10 mL of acetonitrile was stirred at room temperature. $Pd(OAc)_2$ (102.8 mg, 0.459 mmol) was added in one solid portion and stirred at room temperature for 24 hours to yield a red suspension. Solvent was removed by rotovap to yield **5.1** as a dark red solid, which then dissolved in MeOH and filtered. Deep red crystals were grown from the filtrate by slow evaporation at 0°C. ^{1}H NMR (400 MHz, DMSO-d_6): δ 19.57, (s, 1H), 3.17 (q, 4H), 2.92 (q, 4H), 1.84 (s, 6H), 1.08 (t, 6H), 0.98 (t, 6H) ppm. ^{13}C NMR (125 MHz, DMSO-d_6), δ 175.03, 172.06, 166.15, 165.66, 148.58, 146.90, 41.27, 23.21, 21.10, 14.54, 13.68 ppm. Exact mass for $C_{20}H_{28}N_6O_8Pd_2 + H^+$ 693.0117, found (HREIMS$^+$) 689.0480.

Synthesis of 5.2.

Scheme 2. Synthesis of **5.2**.

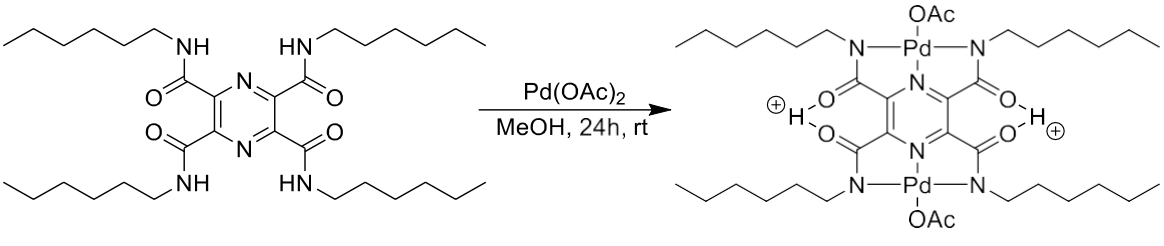

5.2

To a solution of **2.4**(TetraHex) (40.6 mg, 0.0689 mmol) in 4 mL of MeOH was added $Pd(OAc)_2$ (33.98 mg, 0.152 mmol) in one portion. The reaction was stirred at room temperature for 18 hours to yield a deep red solution. Solvent was removed with a rotovap and dried yielding **5.2** as a red powder (41.0 mg, 65.2%). ^{1}H NMR (400 MHz, $CDCl_3$): δ 19.43, (s, 2H), 3.26 (t, 8H), 2.05 (s, 6H), 1.61 (m, 8H), 1.3 (m, 24H) 0.89 (t, 12H) ppm. ^{13}C NMR (125 MHz, $CDCl_3$), δ 177.80, 165.65, 147.57, 48.53, 31.57, 28.99, 27.15, 22.72, 14.20 ppm. Exact mass for $C_{36}H_{58}N_6O_8Pd_2 + H^+$ 916.2542, found (HREIMS+) 915.3051.

Synthesis of 5.3.

Scheme 2. Synthesis of **5.3**.

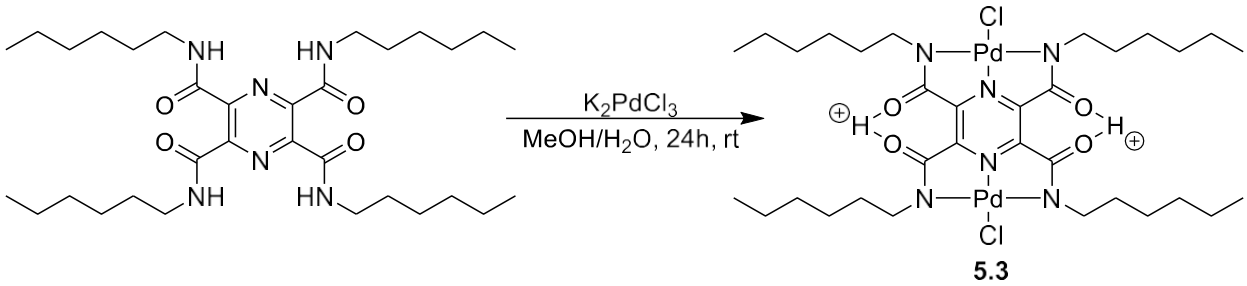

5.3

To a solution of **2.4**(TetraHex) (42.5 mg, 0.072 mmol) in 13 mL of methanol, K_2PdCl_4 in a 6 mL solution in DI water was added dropwise. The solution was stirred at room temperature for 20 hours and a brown precipitate resulted. The mixture was filtered and washed with water and methanol, then dried under vacuum to yield **5.3** as a brown powder (52.5 mg, 80.2%). ^{1}H NMR (400 MHz, $CDCl_3$, ppm): δ 19.44 (s, 0.36H), 3.42 (t, 8H), 1.64 (m, 8H), 1.31 (m, 24H), 0.89 (t, 12H). ^{13}C NMR (125 MHz, $CDCl_3$), δ 166.79, 147.39, 48.94, 31.62, 29.46, 26.86, 22.68, 14.18. Exact mass for $C_{32}H_{53}Cl_2N_6NaO_4Pd_2Cl_2 + Na^+$ 913.1370, found (HREIMS+) 913.332

Synthesis of 5.4.

Scheme 4. Synthesis of **5.4**.

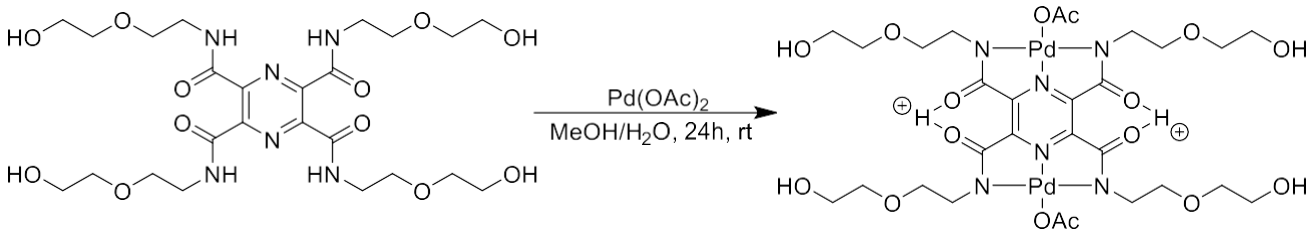

Into a suspension of **2.8**(TetraGly) (21 mg, 0.035 mmol) in 8 mL of acetonitrile was added $Pd(OAc)_2$ (23.5 mg, 0.105 mmol) in one portion. The reaction was stirred for 16 hours at room temperature, resulting in a red precipitate. After filtering with excess acetonitrile and ether, compound **5.4** was dried under reduced pressure and isolated as a red solid. Yield (25.7 mg, 78.7%). ^{1}H NMR (500 MHz, DMSO-d_6): 19.51 (s, 2H), 118.19 (m, 3H), 4.60 (t, 4H), 3.39-3.49 (m, 32H), 1.91 (s, 3H), 1.84 (s, 3H) ppm. ^{13}C NMR (125 MHz, DMSO-d_6), δ 168.46, 153.83, 144.69, 129.48, 77.42, 74.23, 65.40, 44.16 ppm.

Synthesis of 5.5.

Scheme 5. Synthesis of **5.5**.

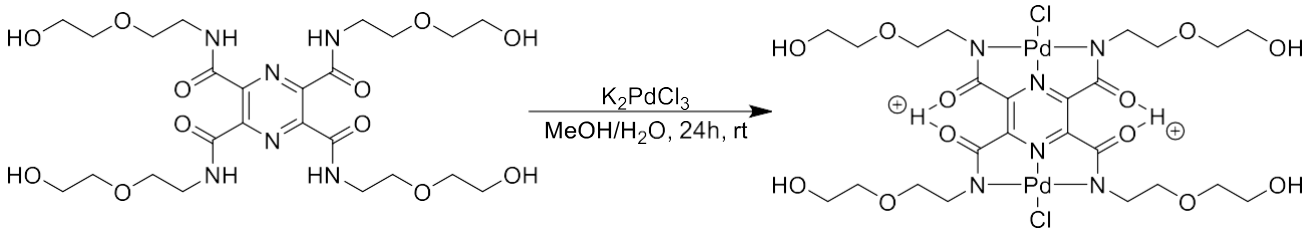

A solution of **2.9**(TetraGly) (62.4 mg, 0.103 mmol) was prepared in 1 mL of water to which a solution of K_2PdCl_4 (78.1 mg, 0.239 mmol) in 1 mL of water was added. Reaction was stirred at room temperature for 14 hours which resulted an orange precipitate. The precipitate, was filtered with excess acetonitrile and ether, then dried under reduced pressure to give **5.5** as an orange solid. Yield (56.0 mg, 61.4%). ^{1}H NMR (500 MHz, DMSO-d_6): 19.57 (s, 2H), 4.59 (s, 4H), 3.40-3.54 (m, 32H) ppm. ^{13}C NMR (125 MHz, DMSO-d_6), δ 168.46, 153.83, 144.69, 129.48, 77.42, 74.23, 65.40, 44.16 ppm. Exact mass found for $C_{24}H_{38}C_{l2}N_6O_{12}Pd_2$ + Na^+ 906.9892, found (HREIMS+) 907.0085.

Synthesis of N^2,N^3,N^5,N^6-tetrakis(2,6-methylphenyl)pyrazine-2,3,5,6-tetracarboxamide. 5.6(TetraDMP)**.**

Scheme 6. Synthesis of **5.6**(TetraDMP).

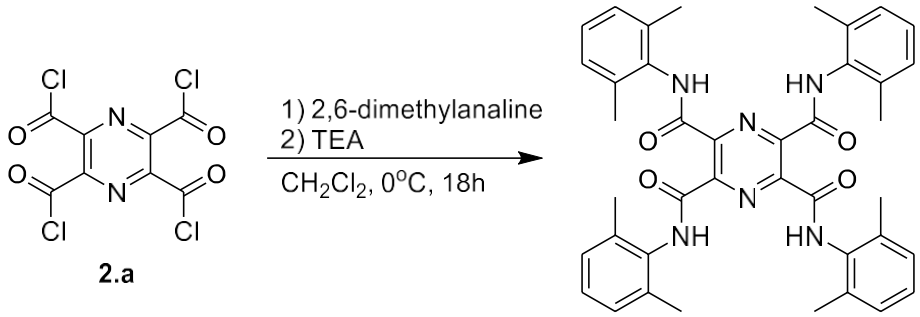

A solution of pyrazine-2,3,5,6-tetracarbonyl tetrachloride (1.4 g, 4.2 mmol) was prepared in 20 mL of DCM. 2,6-diethylanaline (5 mL, 33.9 mmol) was added dropwise. Triethylamine (TEA) (2.34 mL, 16.8 mmol) was added dropwise and stirred at room temperature for 18 hours. The product was precipitated in MeOH and filtered to yield **5.6**(TetraDMP) as a white powder. Yield (624.1 mg, 20.5%) ^{1}H NMR (500 MHz, DMSO-d_6): 10.42 (s, 4H), 7.17 (t, 4H), 7.16 (d, 8H), 2.32 (s, 24H) ppm. ^{13}C NMR (125 MHz, DMSO-d_6), δ 168.42, 144.69, 129.48, 77.42,

74.23, 65.40, 44.16 ppm. Exact mass found for $C_{40}H_{40}N_6O_4 + K^+$ 707.2748, found (HREIMS+) 707.2743.

Synthesis of N^2,N^3,N^5,N^6-tetrakis(2-aminoethyl)pyrazine-2,3,5,6-tetracarboxamide. 5.7(TetraDEA).

Scheme 7. Synthesis of **5.7**(TetraDEA).

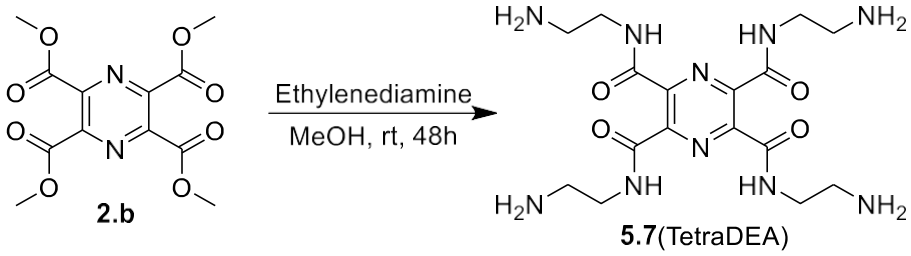

A solution of **2.b** (241.7 mg, 0.774 mmol) in 10 mL methanol was prepared. Ethylenediamine (3.0 mL, 44.9 mmol) was added and stirred at room temperature for 48 hours. The reaction was rotovapped to remove methanol, and diethyl ether was added to precipitate out a viscous yellow oil. After excess diethylamine and ether was decanted, the viscous oil was washed with ether an additional three times and then dried under reduced pressure to yield a viscous yellow oil. Yield (271.8 mg, 82.7%) ^{1}H NMR (500 MHz, DMSO-*d*$_6$): 8.94 (s, 4H), 3.33 (d, 8H), 2.70 (d, 8H) ppm. ^{13}C NMR (125 MHz, DMSO-*d*$_6$), δ 164.13, 145.84, 42.94, 41.53 ppm. Exact mass found for $C_{48}H_{56}N_6O_4 + H^+$ 425.2373, found (HREIMS+) 425.2369.

5.2.2 Anion Additions

A stock solution of 0.226 mM **5.5** was prepared in DMSO by diluting from a 2 mM solution. 113 µL of palladium duplex was added to a quartz cuvette to which an equivalent of anion was added from a 2 mM stock solution of either TBAF or $TBAH_2PO_4$. Varied anion equivalence of 0.0, 0.25, 0.5, 0.75, 1.0, 1.5, 2.0, 3.0 were added for TBAF and anion equivalence

of 0.0, 0.5, 1.0, 2.0 and 3.0 were added for $TBAH_2PO_4$. This was follows by addition of DMSO until the volume was equal to 1 mL. UV-Vis spectra were obtained for each sample.

For mass analysis of **5.5** in the presence of anions, a solution was prepared of **5.5** (13 mg, 0.014 mmol) was stirred in 1 mL H_2O. To this solution, NaH_2PO_4 was added and stirred. The solution turned a darker red in color after 1 day and mass spectrometry was used to analyze the resultant compound.

5.3.0 Results and Discussion

5.3.1 Ethyl Duplex Metal Binding

The ethyl duplex pincer **2.2**(TetraEt) was synthesized as previously mentioned in Chapter 2 from **2.b**. Crystals of **2.2**(TetraEt) were grown through slow evaporation of methanol. The crystal structure revealed that the amide carbonyls twist out of plane with the pyrazine core as shown in Figure 3a. Repulsion between adjacent carbonyls leads to an O2 – O3 separation from 3.184-3.238 Å (Figure 3a), which promotes the out of plane twisting and aids in intermolecular hydrogen bonding.

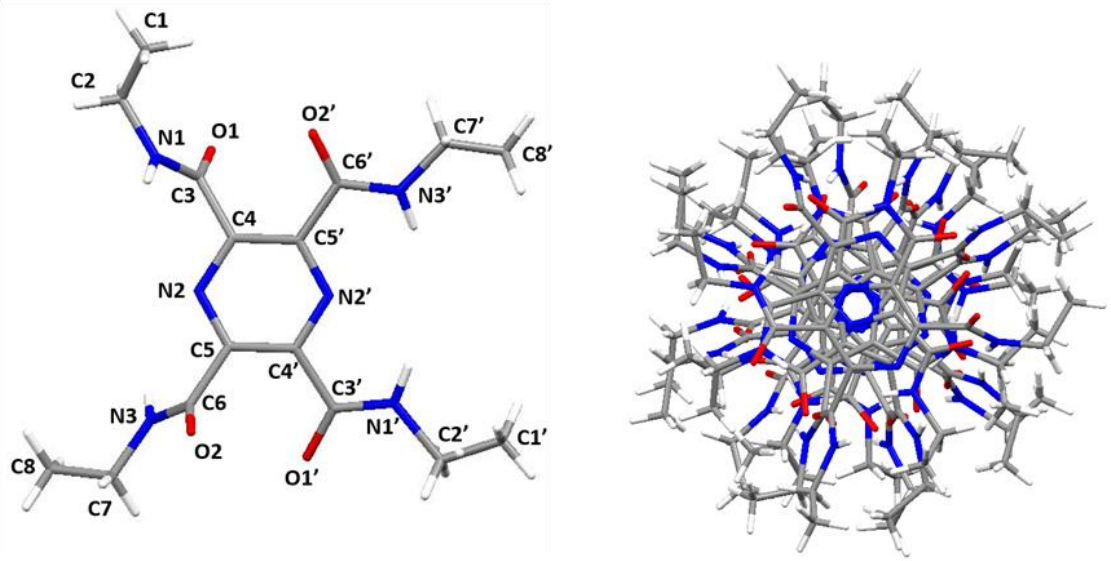

Figure 3. Crystal structures of free ethyl duplex pincer **2.2**(TetraEt) both single molecule (**a**) and hydrogen bond stacked (**b**).

This twisting of the amides allows for a dense network of intermolecular hydrogen bonding to form leading to large disorganized columns as shown in Figures 3b. Figure 4a shows a side view of the 11 independent **2.2**(TetraEt) molecules in the crystal structure intertwined by hydrogen bonds. Following solubilization in heated acetonitrile, the mixture was sonicated and then cooled slowly, producing an opaque gel as seen in Figure 4b. The gel shown in Figure 4b was made with only 2 mg in 1 mL of acetonitrile. Similar results were reported by Thordarson and coworkers with pyromellitamide complexes.[4-5]

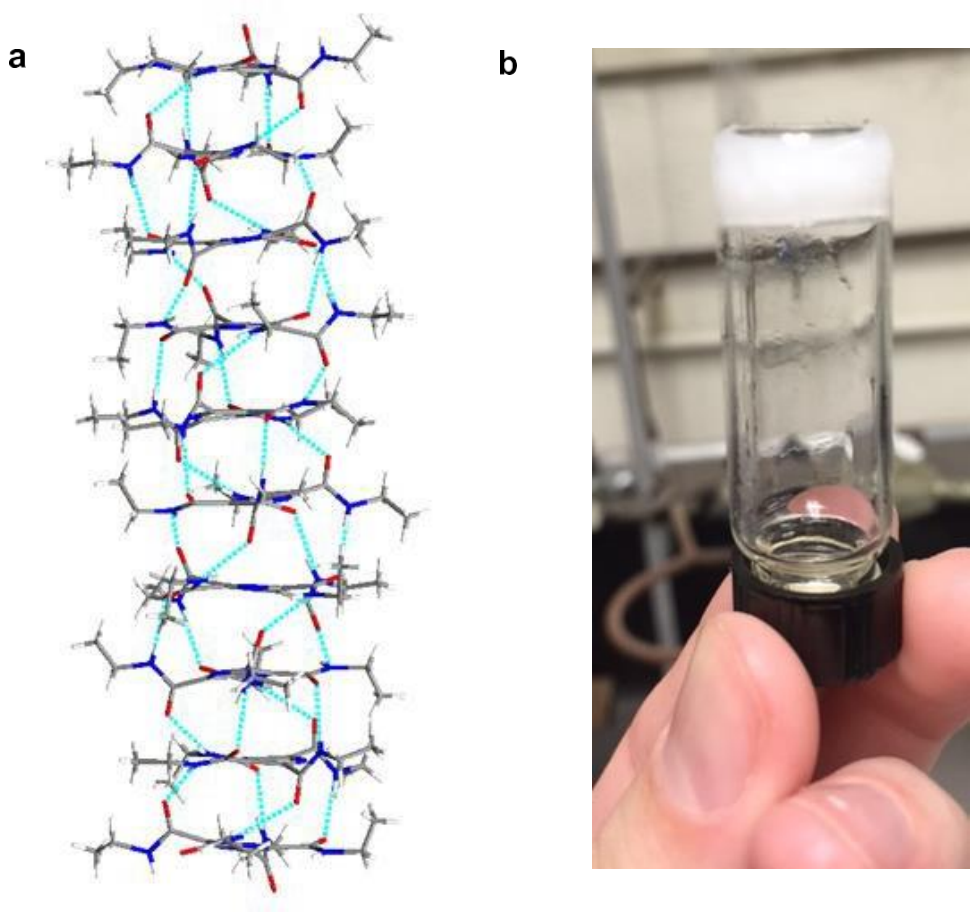

Figure 4. Columnar stacking of **2.2**(TetraEt) hydrogen bonding network (a) and inverted vial with gel formation in acetonitrile.

The introduction of $Pd(OAc)_2$ into pyridine-2,6-dicarboxamide pincers has been previously reported. Deprotonation of the amides causes the Pd(II) to be held in a NNN chelate by the amides and the pyridine nitrogen in a square planar geometry. A labile ligand such as acetonitrile is seen bound to the fourth coordinate position in Figure 5a.[8-11] Similar to the monotopic pincers, when two equivalents of $Pd(OAc)_2$ were introduced to duplex **2.2**(TetraEt) the amides are deprotonated resulting in a dimetallated palladium complex (**5.1)** which is seen in Figure 5b. Preliminary results for this complex were collected by former Bowman-James group

member Tommy Johnson, however it was unclear at the time what was the actual complex composition.

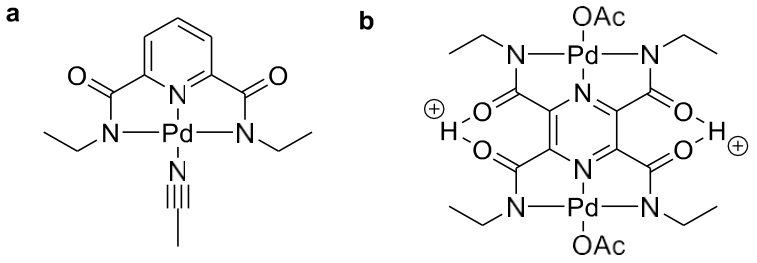

Figure 5. Palladium complexes of pincer complexes **2.1**(DiEt) (a) and duplex pincer **2.2**(TetraEt) yielding complex **5.1** (b).

The growth of dark red crystals by slow evaporation of methanol was able to shed light on the formerly ambiguous nature of the fourth coordinate ligands. The crystal structure of **5.1** revealed that, instead of neutral ligands, the fourth coordinate positions were occupied by negatively charged acetates. This was unexpected considering the two anionic amides already bound to palladium. Because of this, two counter ions must be present in the complex, though none were initially evident in the crystal structure. However, further investigation into the crystal structure lead to some surprising observations.

To accommodate the square planar geometry of each palladium, the amide groups twisted into planar alignment with the pyrazine ring. This conformation forces adjacent carbonyl oxygens into close proximity, shown in Figure 6a, and causes the ligand to abandon the web-like hydrogen bonding network. Ordered packing is seen, where each molecule is slightly offset to the one underneath it, much like a descending staircase along the *a* axis (Figures 6b, c).

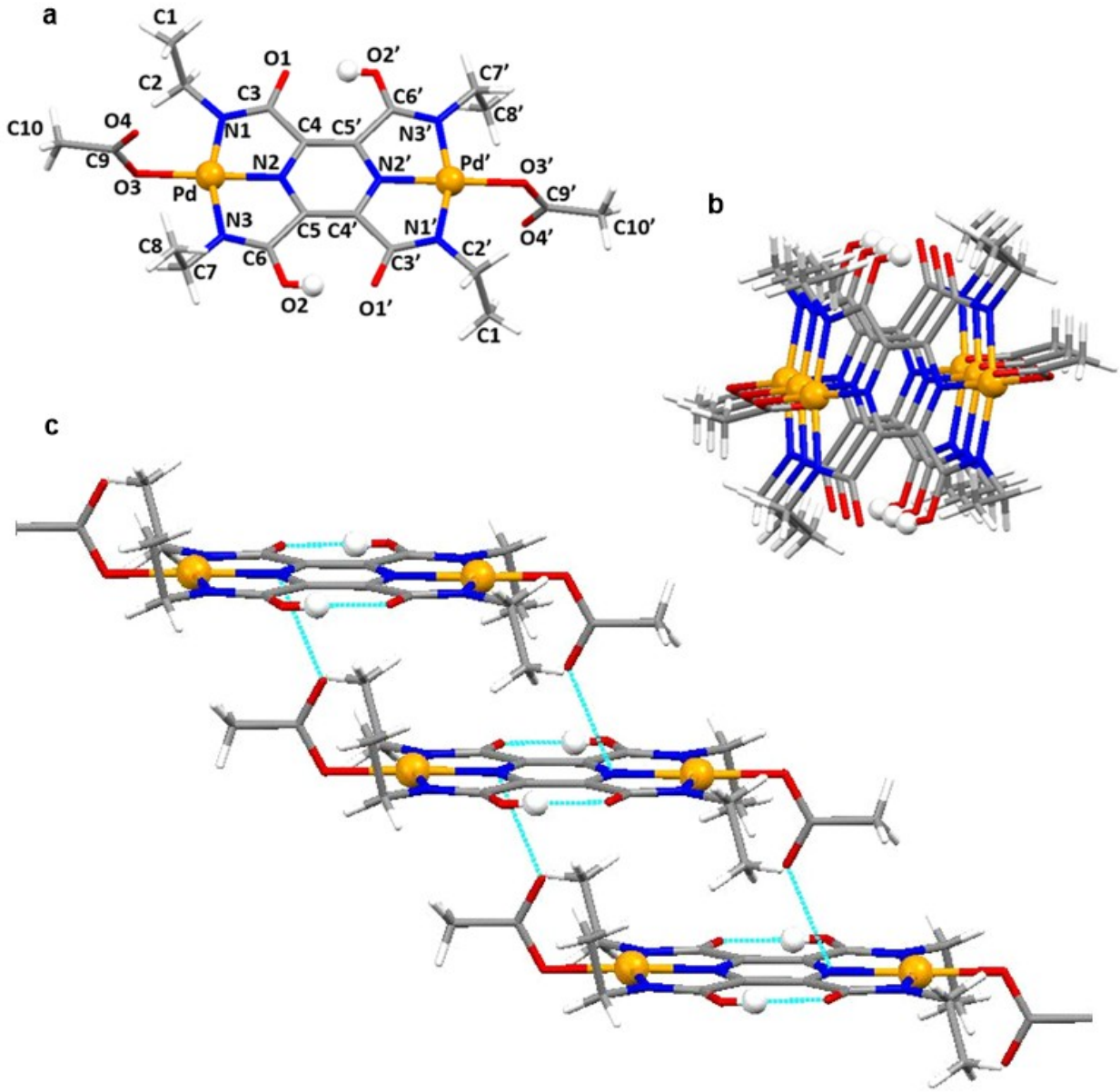

Figure 6. Crystal structures of compound **5.1** with fourth coordinate acetate in ethyl duplex single molecule (**a**) and stacked (**b, c**).

As previously mentioned, the O···O distance of the ortho carbonyls in free ligand **2.2**(TetraEt) have a separation of 3.194 Å when they are twisted out of the plane from one another. When the carbonyls lock into a planar conformation due to palladium binding, the

O···O distance decreases to 2.435 Å. It was then realized the close proximity of the adjacent carbonyls facilitated short hydrogen bonds between the two oxygens, with the protons acting as counter ions within the complex. Similar proton counter ions were noted by the groups of Fleisher, Stoeckli-Evans and Brooker using N,N'-bis(2-pyridylmethyl)pyrazine-2,3-dicarboxamide ligands with copper(II) and nickel(II). The adjacent carbonyls share a proton between the two, allowing it to act as a counter ion to the metal complex when the carbonyls are locked into close proximity.[12-18]

Scheme 8. Tautomerism of amide – iminol.

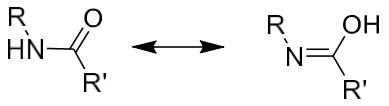

The crystal structure of complex **5.1** revealed other structural changes due to the presence of hydrogen bonded counter ions. Particularly, shortening of the N – C and lengthening of the C = O bond length is seen with **5.1** when compared to the free ligand **2.2**(TetraEt). An average bond length of the C – N bonds was decreased from 1.320 Å to 1.299 Å while the C = O bonds were elongated from 1.227 Å in **2.2**(TetraEt) to 1.278 Å. Similar results were observed by Stoeckli-Evans in *o*-dicarboxamide derivatives and was attributed to amide – iminol tautomerism, seen in Scheme 8, which results in shorter C-N bonds and longer C = O bonds.[12]

Table 1. Selected atomic distances (Å) from **2.2**(TetraEt) and **5.1**.

Atoms	**2.2**(TetraEt)	**5.1**
O1-O2'	3.184(3)	2.435(5)
O1-C3	1.221(3)	1.275(4)
O2-C6	1.219(3)	1.296(5)
N1-C3	1.329(4)	1.301(5)
N3-C6	1.321(4)	1.296(4)

Examples of similar short hydrogen bonds in nature are known as Low Barrier Hydrogen Bonds (LBHBs). LBHBs have been reported as important intermediates in biological enzymatic pathways but have proved difficult to study due to their rarity. They can be characterized by ^{1}H NMR with signals between 17-21 ppm. LBHBs occur when a hydrogen donor and acceptor with similar pKa values are found at a separation of < 2.5 Å. Typical hydrogen bonding is described by a double well system where a potential energy barrier separates the protons movement causing localization on the donor and association with the acceptor. With LBHBs, the potential energy barrier is low lying, allowing for the hydrogen to exist more freely between the donor and acceptor and causes it to be shared almost equally.[19] Capability of generating these biologically significant hydrogen bonds in a reproducible and controllable setting can help to further elucidate enzymatic pathways and mechanisms.

The short hydrogen bonds in **5.1** were confirmed by ^{1}H NMR. The NMR spectrum revealed a signal at 19.66 ppm which falls within the range of previously reported LBHB that are typically observed between 17-21 ppm (Figure 7). Another interesting feature seen in the ^{1}H

NMR that the ethyl CH signals appear as a duo of signals instead of just one peak. When the temperature is raised to 100°C and the spectrum revealed that these signals merge into a single signal for each of the expected peaks. This could potentially be due to the tautomerization process. Another possibility is an equilibrium between protonated acetate (acetic acid) and the short hydrogen bond causing the generation of the dual signals.

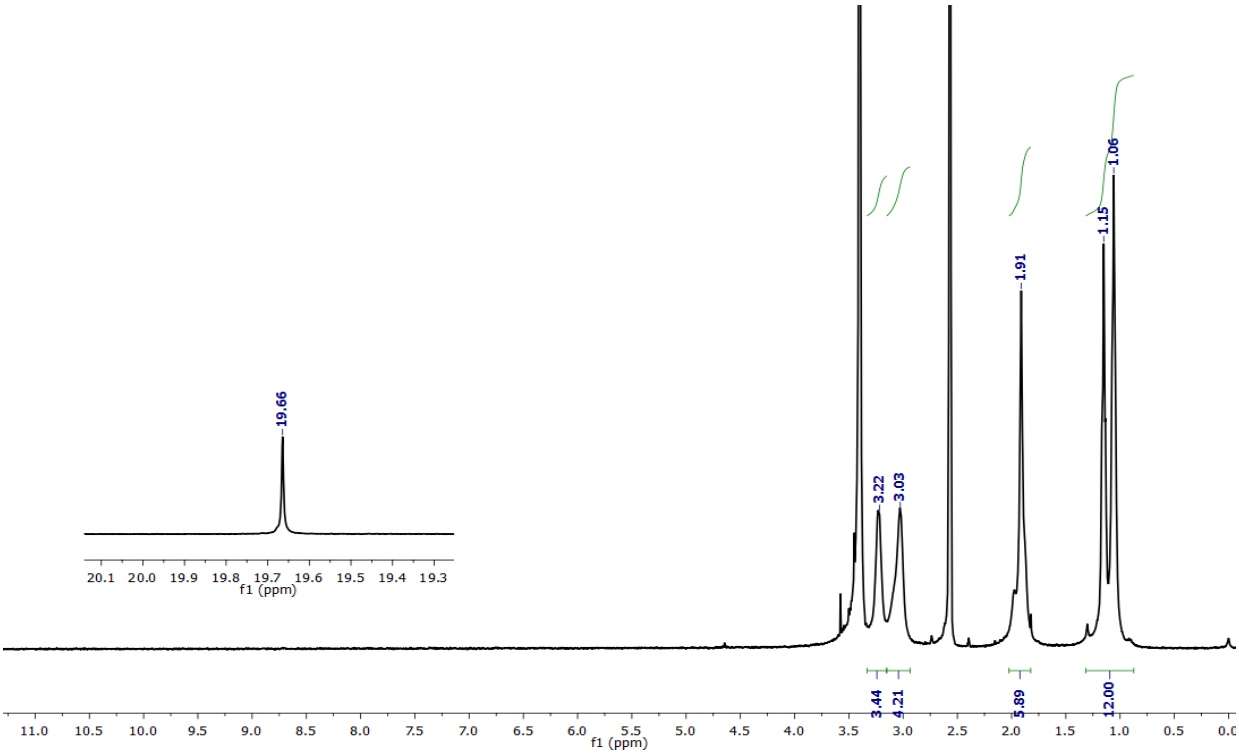

Figure 7. ^{1}H NMR spectra of **5.1** showing a peak at 19.60 ppm.

Further confirmation of the bond length adjustments to accommodate the short hydrogen bond in **5.1** is seen in the IR spectra. The spectra in Figure 8 shows a comparison of the free and metallated species. This supports the tautomerization effects previously described as the carbonyl stretch shifts from 1669 cm^{-1} to a lower wave number of 1623 cm^{-1}, indicating increasing bond length.[12]

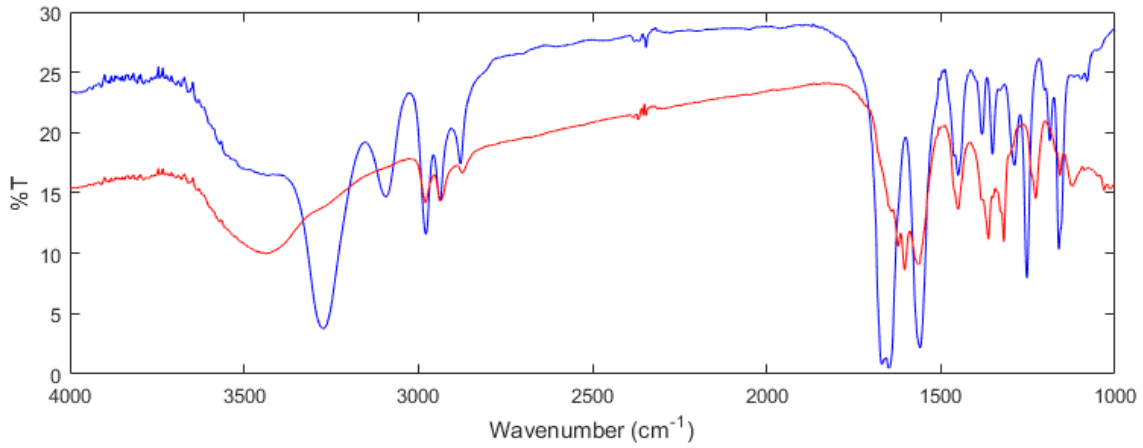

Figure 8. IR spectra of **2.2**(TetraEt) (blue) and **5.1** Pd complex (red).

The prospect of dimetallated duplex systems being used in coordination polymers and in MOF systems is a promising goal. However, these applications for **5.1** are limited by solubility in only short list of solvents including MeOH, DMF and DMSO. Due to the susceptibility of palladium acetate to be reduced in MeOH, a more robust complex was devised using of K_2PdCl_4 in place of $Pd(OAc)_2$ as a Pd(II) source.[20-21] This would hopefully yield a complex with chloride as the fourth coordinate group which could increase stability. The reaction yielded a red solid; however, this solid exhibited incredibly poor solubility making it difficult to characterize. To expand on the scope and utility of these compounds in more diverse applications, it was necessary to synthesize duplex ligands that would be not only robust, but also hospitable to a wider range of solvents. As shown in Chapter 2, the solubility could be tuned by the functionalization of the arm groups. The hexyl chain arms on **2.4**(TetraHex) provides potential for metal complex solubility in organic solvents such as chloroform and hexanes, while the glycol arms on **2.8**(TetraGly) permitted solubility in alcohols and water (Figure 9).

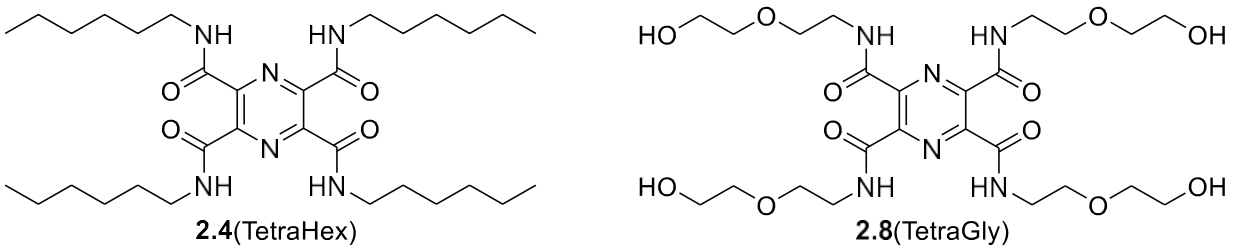

Figure 9. Duplex functionalized with hexyl arms **2.4**(TetraHex) and glycol arms on **2.8**(TetraGly).

5.3.2 Extended Arm Duplex Metal Binding

Reacting **2.4**(TetraHex) and **2.8**(TetraGly) with $Pd(OAc)_2$ yielded dimetallated complexes similar to **5.1** with tridentate NNN bound palladium in the binding cavity with acetates bound in the fourth coordinate position (Scheme 9). Complexes **5.2** and **5.4** both showed solubility in a wider range of solvents not accessible to **5.1**. Complex **5.2** proved to be soluble in chloroform and DCM while **5.4** was soluble in water and alcohols. ^{1}H NMR spectra of both compounds displayed the short strong hydrogen bond previously seen in **5.1**. Since **5.2** was soluble in chloroform, it was found to be less susceptible to reduction in aprotic solvent systems, however; the complex still undergoes degradation if dissolved in an alcohol. Because complex **5.4** has hydroxyl appended R groups, it decomposes regardless of the solvent system and also decomposes to a rapid extent if heated. The ^{1}H NMR spectrum shows the acetate signals for **5.4** at 2.82 ppm however, mass spectrum of complex **5.4** showed only the dichloride complex with a mass of 884.9937. This is likely due to decomposition of the acetate complex in the mass spectrum leaving only the chloride exchanged product from the column.

Scheme 9. Palladium complexes made with ligands **2.4**(TetraHex) and **2.8**(TetraGly).

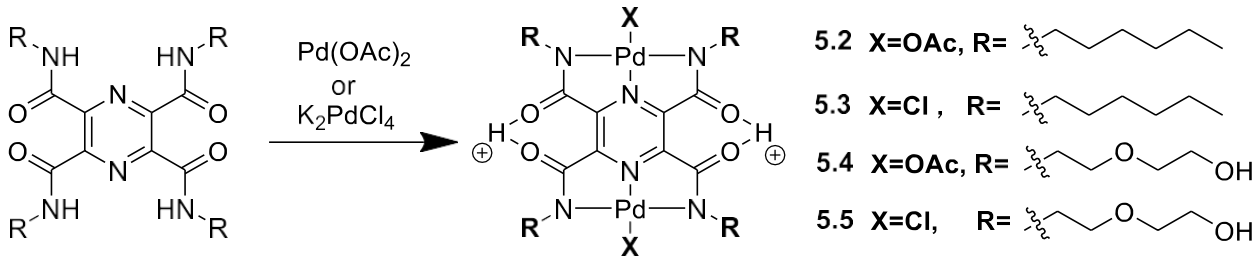

As was previously attempted with **2.2(**TetraEt), a goal was to make more stable complexes using K_2PdCl_4 as the palladium source in place of $Pd(OAc)_2$. Compounds **5.3** and **5.5** were obtained as red and orange powders respectively. However, the products in these reactions showed greater solubility and therefore could be characterized. Complex **5.3** demonstrated solubility in chloroform, while complex **5.5** was soluble in methanol, DMSO, and water. This increased solubility also increases their application range by being stable in a greater amount of environments. Complexes **5.3** and **5.5** also showed the proton counter ions with signals in their ^1H NMR spectrum at around 19 ppm, despite not having been made with $Pd(OAc)_2$. This shows that the short proton counter ion can be generated regardless of fourth coordinate group composition.

The crystal structure of **2.8**(TetraGly) shows the twisting of the amides out of the plane as was shown in compound **2.2**(TetraEt) where an intermolecular hydrogen bonding network is possible. However, the long glycol arms hang above and below the plane and can also participate in intermolecular hydrogen bonding with the amides (Figure 10a). The added interaction of the hydroxyl groups leads to a herringbone edge to face packing structure of the ring system as opposed to the columnar packing displayed by complex **2.2(**TetraEt) which discourages its ability to from columnar gel matrices (Figure 10b).

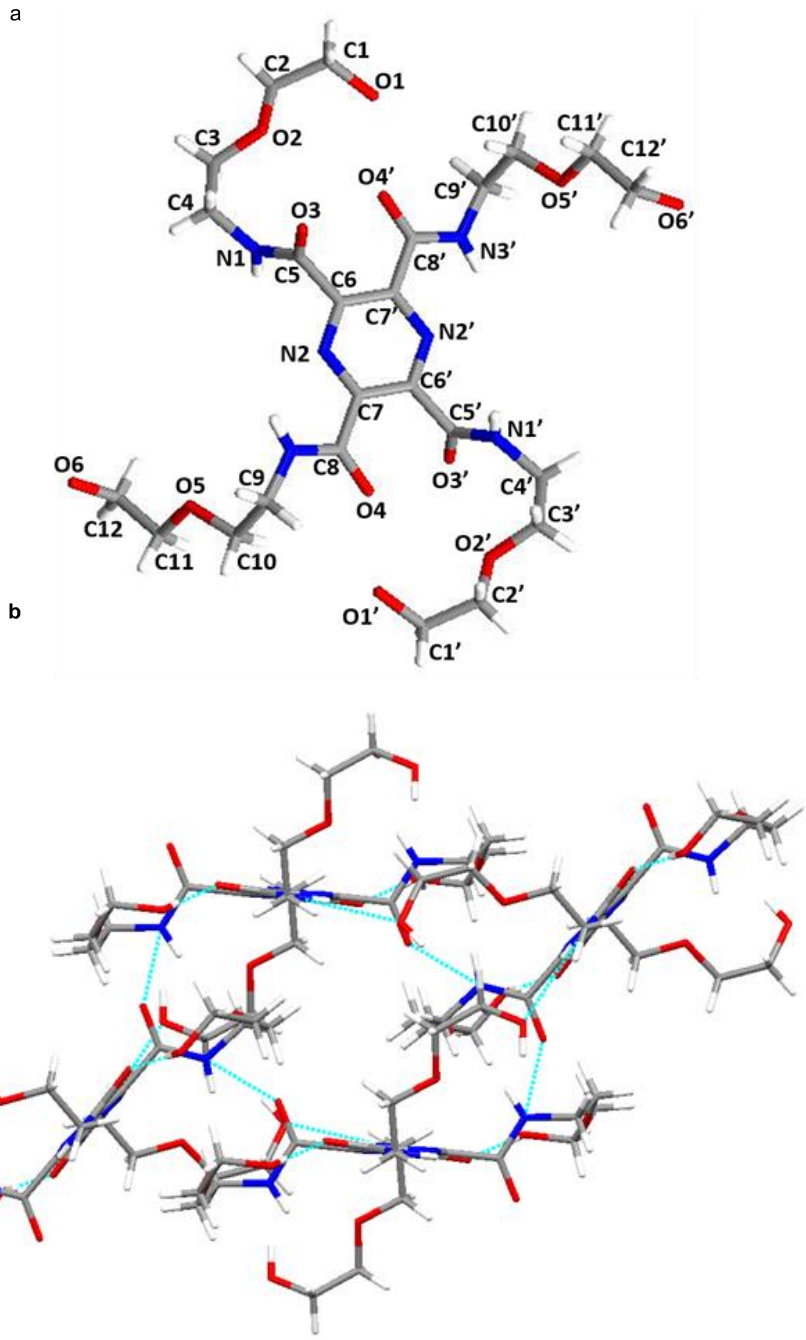

Figure 10. Crystal structure of free base **2.8**(TetraGly) as a single molecule (*a*) and four molecules stacked (*b*). (Crystals of 2.8(TetraGly) grown by Hanumaiah Telikepalli)

The addition of palladium within the duplex cavity locks the amides in a planar conformation. This allows a counter ion of the short intramolecular hydrogen bond between

adjacent carbonyls shortening the O···O distance to 2.415 Å (Table 2). When compared to the free form **2.8**(TetraGly) which had an O···O distance of 2.986 Å, it was shown to be much shorter suggesting LBHB-like behavior (Figure 11a). The N – C and C = O bonds tend to shorten and lengthen respectively due to the tautomerism that was mentioned above. Glycol appendages still extend above and below the plane of the molecule which as was seen in the free base, which lead to the sheet-like packing seen in Figure 11b. The terminal hydroxyl arms extending above form intermolecular hydrogen bonds with adjacent molecule hydroxyl functionalizations that extend below the pyrazine plane in a repeating fashion. This network thus results in a scaffold of two-dimensional sheets.

Table 2. Selected atomic distances (Å) from **2.8**(TetraGly) and **5.5**.

Atoms	**2.8**(TetraGly)	**5.5**
O3-O4'	2.986(2)	2.415(4)
O3-C5	1.222(2)	1.272(4)
O4'-C8'	1.233(2)	1.279(4)
N1-C5	1.346(2)	1.304(4)
N3'-C8'	1.333(2)	1.319(3)

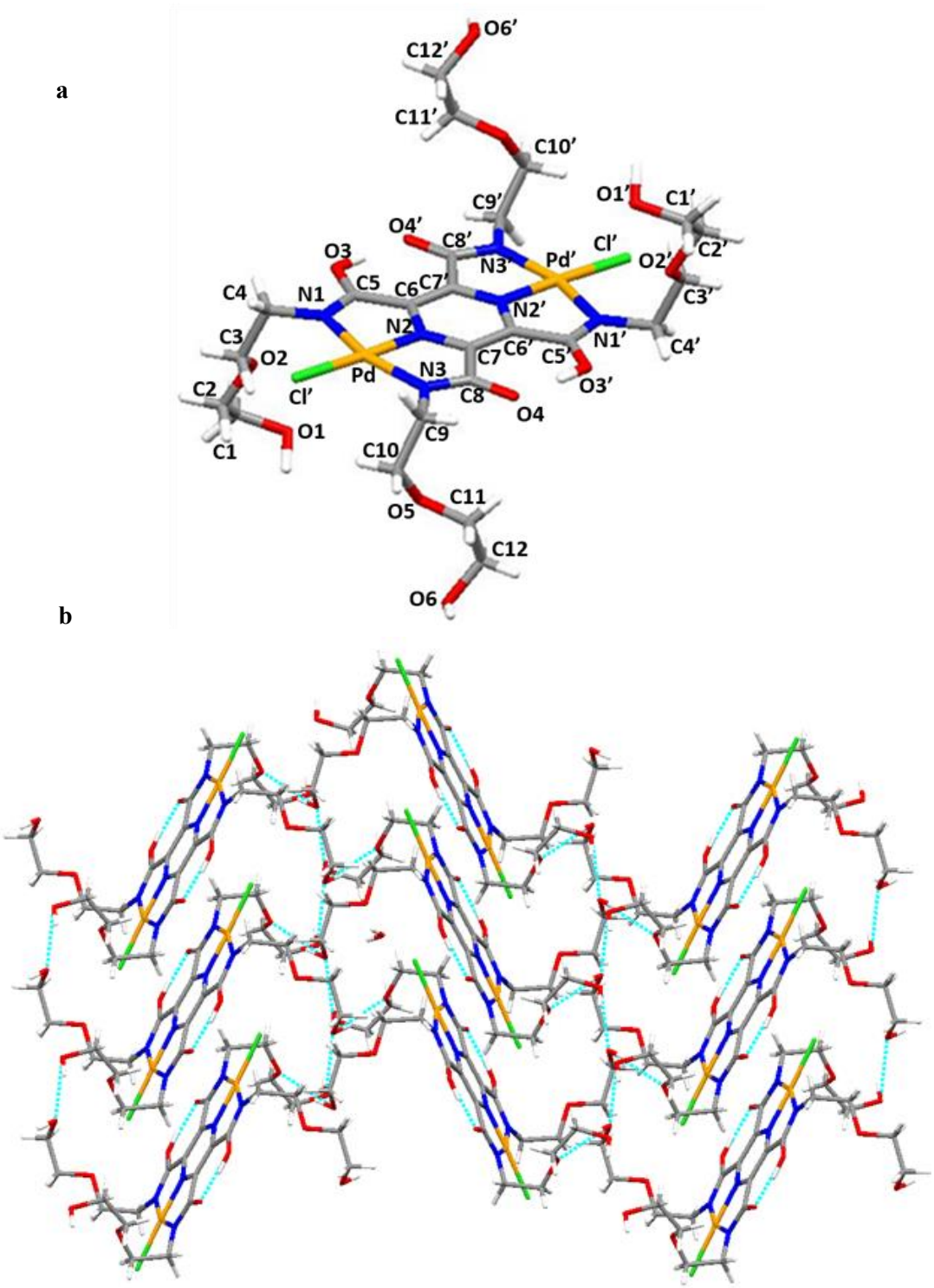

Figure 11. Crystal structure of **5.5** as a single molecule (*a*) and multiple complexes stacked (*b*).

5.3.3 Anion Addition

Additional interest was placed in how **5.5** would interact with anions in solution due to the hydroxyl tails on the R groups and the short hydrogen bonds counter ions. We also wanted to see if we could potentially exchange the anionic ligand in the fourth coordinate position. Anions Cl^-, NO_3^-, NO_2^-, SO_4^{-2}, F^-, and $H_2PO_4^-$ in the forms of TBA salts were all introduced to **5.5** in DMSO to determine if there would be any binding or sensing properties observed. A solution of **5.5** in DMSO exhibited a visible color change upon the addition of F^- and $H_2PO_4^-$ from an orange-yellow color to an orange-red color, but a change was not present with the other anions tested (Figure 12).

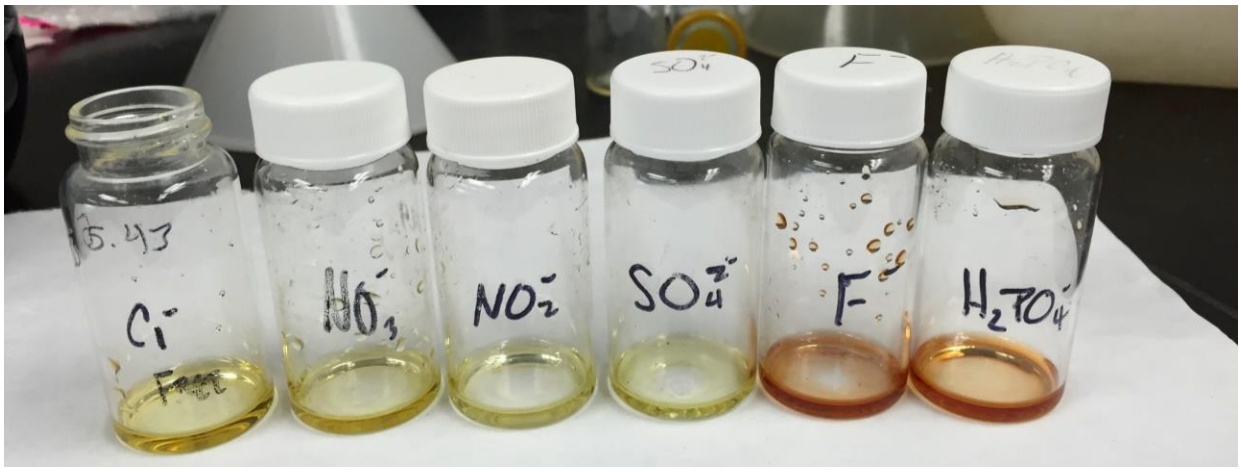

Figure 12. Anions added to **5.5** in DMSO with fluoride and dihydrogen phosphate with reddened color change.

UV-Vis spectra were recorded for both anions at various equivalents. It is shown in both cases that the initial compound has a weak feature at 475 nm (Figure 13). As anion is added, the peak becomes more defined and shifts to 492 nm with a shoulder extending to 500 nm which accounts for the visible color change observed. The absorption shift is observed in the presence

of both fluoride and dihydrogen phosphate. The shift in the feature does not shift further after two equivalents of the anion are added. This color change was thought to have been caused by replacement of the fourth coordinate chloride group, but unfortunately, attempts at crystal growth of these complexes were unsuccessful.

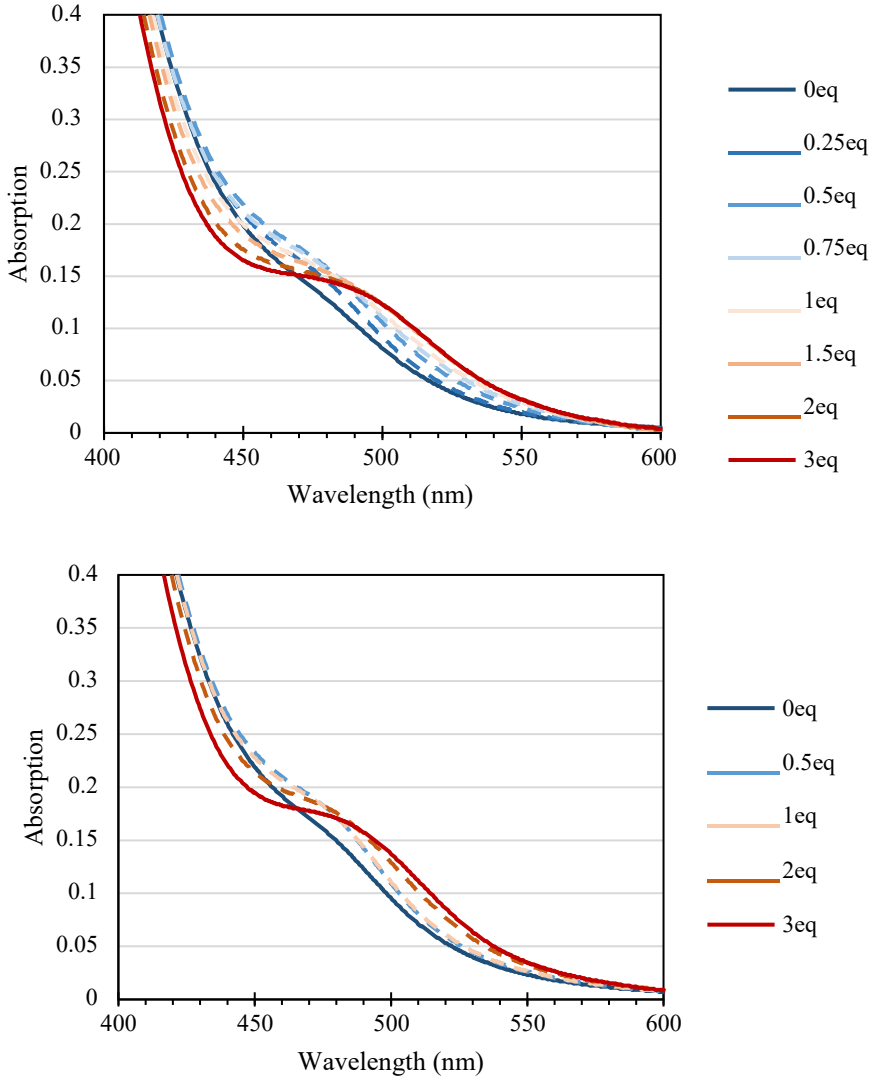

Figure 13. Absorption spectra **5.5** in DMSO with TBAF (top) and $TBAH_2PO_4$ (bottom).

To further investigate the spectral shift seen in Figure 13, a solution of **5.5** was prepared in water with NaH_2PO_4. A reddening of the solution was observed and high resolution mass

spectrometry (HRMS) was performed on the sample. Interestingly, the mass obtained shows a mass peaks at 966.9565 (Figure 14). This could suggest the replacement of the deprotonated LBHB counter ions with K^+ and Na^+ counter ions leading to an expected mass of 966.9270, which may be causing the spectral change that is being observed. Similar color changes are observed when base is added to the complex in solution and NMR titration run with TBAF and complex **5.1** has also shown the disappearance of the peak at 19.56 ppm after 2 equivalence of anion is added.

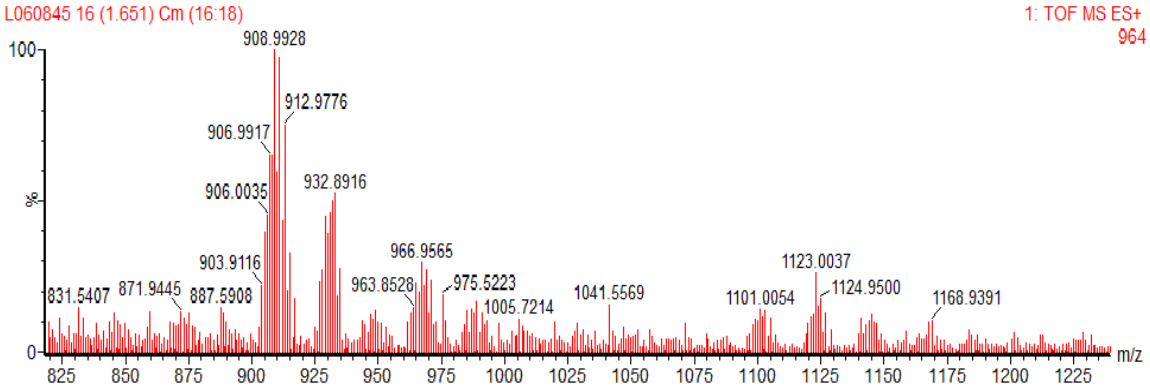

Figure 14. HREIMS(+) of complex **5.5** after the introduction of NaH_2PO_4.

5.3.4 Aryl and Amine Substituted Duplexes

Attempts to metallate **2.2**(TetraEt), **2.4**(TetraHex), and **2.8**(TetraGly) transition metals other than palladium, such as Pt(II), Ni(II), and Cu(II), were unsuccessful. However, monotopic pincer ligands with aryl arm substituents have been reported by the Borovik, Mukherjee, Holm, and Tolman groups, which have been shown to more readily stabilize transition metals such as Ni, Cu, Co, Au, and Fe.[22-27] Monotopic pincers with amine appended arm groups have also been shown capable of binding Ni and Cu.[28-29] In order to expand the metal binding capabilities of the duplex pincer, two new ligands were synthesized to enhance metal stabilization.

Duplex ligand **5.6**(DuDMP) was synthesized with 2,6-dimethylphenyl substituted R groups shown in Figure 15. The typical synthetic route that was used for all other duplex ligands syntheses with the carboxylate starting material, **2.b**, was not compatible with 2,6-dimethylaniline due to its lower nucleophilicity. Instead, the compound **5.6**(TetraDMP) was synthesized from pyrazine-2,3,5,6-tetracarbonyl tetrachloride, **2.a**, intermediate via Schotten-Baumann reaction in DCM with 2,6-dimethylaniline and base. This resulted in a 20% yield after isolation. Pincer **5.7**(TetraDEA) was synthesized by a similar method as previously synthesized monotopic corollary with tetramethyl pyrazine-2,3,5,6-tetracarboxylate and ethylenediamine stirred at room temperature. **5.7**(TetraDEA) was isolated in an 82.7% yield as a very viscous liquid. This product was seen to reversibly uptake CO_2 when in solution which has been seen in other amide/amine receptor complexes.[30] Because of this, care had to be taken to limit its exposure to air when solvated.

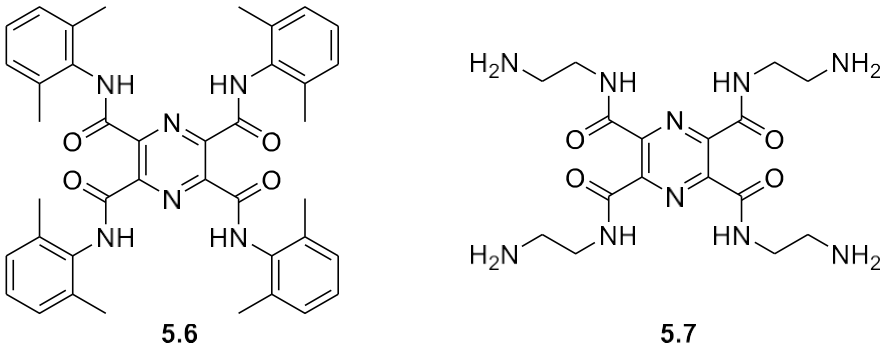

Figure 15. Ligand with aryl appended arms **5.6**(TetraDMP) (left) and amine terminating arms **5.7**(TetraDEA) (right).

Preliminary reactions with both **5.6**(TetraDMP) and **5.7**(TetraDEA) have resulted in dramatic color changes to green and red when introduced to copper and nickel salts respectively,

indicating complexation. However, more analysis is required to fully characterize these potential new complexes.

5.4.0 Conclusions and Future Works

Ditopic tetracarboxamide pincers have the potential to be assets in the field of MOF and coordination polymers by having tunable R appendages that can be adjusted to necessity of the working environment. The pyrazine backbone of the pincer also allows binding palladium(II) salts, which ended up yielding some very interesting complexes. The complex **5.1** displayed an innate organized packing structure in comparison to the hydrogen bonding network inherent to the free ligand **2.1**(TetraEt). Interestingly, this complex produces an unexpected short strong hydrogen bond that mimics LBHBs in a reproducible and controlled fashion. The adjacent carbonyls of the complex are seen, by XRD, to lock into place in plane with the rest of the molecule. The shortened carbonyl distance of 2.415 Å promotes the appearance of the short hydrogen bond, which, can then act as a counter ion for the rest of the molecule, thereby balancing the charge provided by the two acetate groups bound to the fourth coordinate positions on each palladium.

To enhance solubility as well as stability, new palladium complexes were made with ligands **2.4**(TetraHex) and **2.8**(TetraGly). Palladium complexes with **2.4**(TetraHex) both OAc^- and Cl^- fourth coordinate groups yielded complexes **5.2** and **5.3** which demonstrated solubility in chloroform and DCM. Complexes prepared with **2.8**(TetraGly) yielded palladium complexes **5.4** and **5.5** that showed solubility in water and DMSO. Importantly, the chloride coordinated complexes were found to be much more stable in comparison to the OAc counterparts. Complexes **5.2**, **5.3**, **5.4**, and **5.5** all demonstrated the LBHB-like hydrogen bond counter ions as well like the initial **5.1** complex. The crystal structure of the palladium complex **5.5** also

demonstrated the close proximity carbonyls stabilizing the short hydrogen. The crystal structure also revealed an interesting packing structure. Because of the terminal hydroxyl tails, they formed a sheet-like packing between adjacent molecules.

The palladium bound duplex **5.5** was also shown to display a distinct color change upon introduction of fluoride and phosphate anions. Upon addition of NaH_2PO_4 salt to a solution of **5.5** and analysis by HRMS, it appears that the salts may be deprotonating the LBHB of the complex which causes them to be replaced with other counter ions. Further work in this project includes the incorporation other transition metals into the duplex ligand system by utilizing more stabilizing aryl and amine appended arm groups that could introduce catalysis application for the duplex pincer. Future work with the stabilizing aryl or amine arms into the pincer scaffold could allow the binding of greater variety of transition metals and expand the scope of potential application for these ditopic pincers. These new complexes could ultimately lead to new applications in catalysis and materials.

References

1. Loeb, S. J.; Shimizu, G. K. H., Dimetallated Thioether Complexes as Building Blocks for Organometallic Coordination Polymers and Aggregates. *Journal of the Chemical Society, Chemical Communications* **1993,** (18), 1395-1397.
2. Steenwinkel, P.; Kooijman, H.; Smeets, W. J. J.; Spek, A. L.; Grove, D. M.; van Koten, G., Intramolecularly Stabilized 1,4-Phenylene-Bridged Homo- and Heterodinuclear Palladium and Platinum Organometallic Complexes Containing N,C,N-Coordination Motifs; η1-SO2 Coordination and Formation of an Organometallic Arenium Ion Complex with Two Pt−C σ-Bonds. *Organometallics* **1998,** *17* (24), 5411-5426.
3. Hiraoka, S.; Hisanaga, Y.; Shiro, M.; Shionoya, M., A Molecular Double Ball Bearing: An AgI–PtII Dodecanuclear Quadruple-Decker Complex with Three Rotors. *Angewandte Chemie International Edition* **2010,** *49* (9), 1669-1673.
4. Webb, J. E. A.; Crossley, M. J.; Turner, P.; Thordarson, P., Pyromellitamide Aggregates and Their Response to Anion Stimuli. *Journal of the American Chemical Society* **2007,** *129* (22), 7155-7162.
5. Tong, K. W. K.; Dehn, S.; Webb, J. E. A.; Nakamura, K.; Braet, F.; Thordarson, P., Pyromellitamide Gelators: Exponential Rate of Aggregation, Hierarchical Assembly, and Their Viscoelastic Response to Anions. *Langmuir* **2009,** *25* (15), 8586-8592.
6. Rajput, A.; Mukherjee, R., Coordination Chemistry with Pyridine/Pyrazine Amide Ligands. Some Noteworthy Results. *Coordination Chemistry Reviews* **2013,** *257* (2), 350-368.
7. Lohrman, J.; Telikepalli, H.; Johnson, T. S.; Jackson, T. A.; Day, V. W.; Bowman-James, K., Pyrazinetetracarboxamide: A Duplex Ligand for Palladium(II). *Inorganic Chemistry* **2016,** *55* (11), 5098-5100.
8. Kaseyama, T.; Takebayashi, S.; Wakabayashi, R.; Shinkai, S.; Kaneko, K.; Takeuchi, M., Supramolecular Assemblies of Polyaniline through Cooperative Bundling by a Palladium-Complex-Appended Synthetic Cross-Linker. *Chemistry – A European Journal* **2009,** *15* (46), 12627-12635.
9. Wang, Q.-Q.; Begum, R. A.; Day, V. W.; Bowman-James, K., Chemical Mustard Containment Using Simple Palladium Pincer Complexes: The Influence of Molecular Walls. *Journal of the American Chemical Society* **2013,** *135* (45), 17193-17199.
10. Guenet, A.; Graf, E.; Kyritsakas, N.; Hosseini, M. W., Porphyrin-Based Switchable Molecular Turnstiles. *Chemistry – A European Journal* **2011,** *17* (23), 6443-6452.
11. Belli Dell'Amico, D.; Calderazzo, F.; Di Colo, F.; Guglielmetti, G.; Labella, L.; Marchetti, F., Coordination Properties towards Palladium(II) of a Tridentate Dianionic Ligand Acting as a N- or a N,O-donor. *Inorganica Chimica Acta* **2006,** *359* (1), 127-135.
12. Cati, D. S.; Ribas, J.; Ribas-Ariño, J.; Stoeckli-Evans, H., Self-Assembly of CuII and NiII [2 × 2] Grid Complexes and a Binuclear CuII Complex with a New Semiflexible Substituted Pyrazine Ligand: Multiple Anion Encapsulation and Magnetic Properties. *Inorganic Chemistry* **2004,** *43* (3), 1021-1030.
13. Cati, D. S.; Stoeckli-Evans, H., Crystal structures of N2,N3,N5,N6-tetrakis(pyridin-2-ylmethyl)pyrazine-2,3,5,6-tetracarboxamide and N2,N3,N5,N6-tetrakis(pyridin-4-ylmethyl)pyrazine-2,3,5,6-tetracarboxamide. *Acta Crystallographica Section E* **2017,** *73* (2), 300-305.

14. Cati, D. S.; Stoeckli-Evans, H., A Mononuclear Cobalt(III) Complex of the Ligand N,N′-Bis(pyridin-2-ylmethyl)pyrazine-2,3-dicarboxamide. *Acta Crystallographica Section E* **2004,** *60* (2), m174-m176.
15. Cati, D. S.; Stoeckli-Evans, H., An Orthorhombic Polymorph of N,N'-bis(2-pyridylmethyl)pyrazine-2,3-dicarboxamide. *Acta Crystallographica Section E* **2004,** *60* (2), 210-212.
16. Hausmann, J.; Jameson, G. B.; Brooker, S., Control of Molecular Architecture by the Degree of Deprotonation: Self-Assembled Di- and Tetranuclear Copper(II) Complexes of N,N'-bis(2-pyridylmethyl)pyrazine-2,3-dicarboxamide. *Chemical Communications* **2003,** (24), 2992-2993.
17. Fleischer, E. B.; Jeter, D.; Florian, R., Structure of the Dimetallic Complex Catena-μ-chloro-dichloro-μ-[N,N'-bis[2-(2-pyridyl)ethyl]-2,3-pyrazinedicarboxamidato-N,NN,N1:N',Nn,N4-dicopper. *Inorganic Chemistry* **1974,** *13* (5), 1042-1047.
18. Fleischer, E. B.; Lawson, M. B., Uni- and Bimetallic Complexes Derived from a Substituted Pyrazine Ligand. *Inorganic Chemistry* **1972,** *11* (11), 2772-2775.
19. Klinman, J. P., Low Barrier Hydrogen Bonds: Getting Close, but Not Sharing. *ACS Central Science* **2015,** *1* (3), 115-116.
20. Ornelas, C.; Aranzaes, J. R.; Salmon, L.; Astruc, D., "Click" Dendrimers: Synthesis, Redox Sensing of Pd(OAc)2, and Remarkable Catalytic Hydrogenation Activity of Precise Pd Nanoparticles Stabilized by 1,2,3-Triazole-Containing Dendrimers. *Chemistry – A European Journal* **2008,** *14* (1), 50-64.
21. Yen, P.-W.; Chou, T.-C., Formation of Palladium Metal Active sites on Styrene–Divinylbenzene Copolymer Catalyst by Alcohol Reduction at Room Temperature. *Applied Catalysis A: General* **1999,** *182* (2), 217-223.
22. Donoghue, P. J.; Tehranchi, J.; Cramer, C. J.; Sarangi, R.; Solomon, E. I.; Tolman, W. B., Rapid C–H Bond Activation by a Monocopper(III)–Hydroxide Complex. *Journal of the American Chemical Society* **2011,** *133* (44), 17602-17605.
23. Kawamoto, T.; Hammes, B. S.; Haggerty, B.; Yap, G. P. A.; Rheingold, A. L.; Borovik, A. S., Synthesis and Structure of Helical Supramolecular Arrays. *Journal of the American Chemical Society* **1996,** *118* (1), 285-286.
24. Kawamoto, T.; Prakash, O.; Ostrander, R.; Rheingold, A. L.; Borovik, A. S., Metallohelices: Effects of Weak Interactions on Helical Morphology. *Inorganic Chemistry* **1995,** *34* (17), 4294-4295.
25. Ray, M.; Ghosh, D.; Shirin, Z.; Mukherjee, R., Highly Stabilized Low-Spin Iron(III) and Cobalt(III) Complexes of a Tridentate Bis-Amide Ligand 2,6-Bis(N-phenylcarbamoyl)pyridine. Novel Nonmacrocyclic Tetraamido-N Coordination and Two Unusually Short Metal−Pyridine Bonds. *Inorganic Chemistry* **1997,** *36* (16), 3568-3572.
26. Huang, D.; Holm, R. H., Reactions of the Terminal NiII−OH Group in Substitution and Electrophilic Reactions with Carbon Dioxide and Other Substrates: Structural Definition of Binding Modes in an Intramolecular NiII···FeII Bridged Site. *Journal of the American Chemical Society* **2010,** *132* (13), 4693-4701.
27. Huang, D.; Makhlynets, O. V.; Tan, L. L.; Lee, S. C.; Rybak-Akimova, E. V.; Holm, R. H., Kinetics and Mechanistic Analysis of an Extremely Rapid Carbon Dioxide Fixation Reaction. *Proceedings of the National Academy of Sciences* **2011,** *108* (4), 1222-1227.

28. Napitupulu, M.; Griggs, B. L.; Luo, S.-X.; Turner, P.; Maeder, M.; Lawrance, G. A., Symmetrical Diamides based on 2,6-bis(methoxycarbonyl)pyridine: Syntheses and Metal Ion Binding Studies. *Journal of Heterocyclic Chemistry* **2009,** *46* (2), 243-250.
29. Brooker, S.; Dunbar, G. S.; Jameson, G. B., Synthesis, Complexation and Cyclisation Reactions of a New Acyclic Diamide: Observation of Intramolecular Ligand Exchange in a Structurally Characterised Nickel(II) Complex. *Polyhedron* **1999,** *18* (5), 679-688.
30. Wang, Q.-Q.; Day, V. W.; Bowman-James, K., Macrocyclic Influences in CO_2 Uptake and Stabilization. *Organic Letters* **2014,** *16* (15), 3982-3985.

CHAPTER 6

Organic Optoelectronics

6.1.0 Optoelectronics

The interest in optoelectronics and organic photovoltaics (OPV) utilizing conductive polymers has grown greatly over the past decade, expanding from solar cell development to field effect transistors, light emitting diodes, and recently into the field of controllable multiferroics. These materials are particularly alluring in comparison to their inorganic counterparts due to their low-toxicity, light weight, and printable nature. Devices are typically composed of an electron donating material (hole accepting) and an electron accepting material (hole donating) that when interfaced together in respective domains allow for charge generation and transfer.

6.2.0 Optoelectronic Mechanics

When a photon is absorbed, an electron in the donor material's valence band comprised of the highest occupied molecular orbital (HOMO), is promoted to the conduction band (Figure 1a) composed of the lowest unoccupied molecular orbital (LUMO). This process creates a bound electron-hole pair known as an exciton. Excitons can then diffuse through the donor material until they either reach the acceptor material (Figure 1b) or falls back to ground state through recombination of the electron hole pair. If the exciton reaches the acceptor material, the electron can thermodynamically transfer to the LUMO of the acceptor material (Figure 1C) creating a coulombically bound electron-hole pair across the donor and acceptor interface known as a charge transfer (CT) state. The CT state can then be disassociated into free charge carriers (holes and electrons), where holes are transported through donor valance band and electrons are transported through acceptor conduction band. Charges are then collected at their respective electrodes in the device (Figure 1d).[1] If charge is not transferred, it can be lost through thermal or radiative decay.

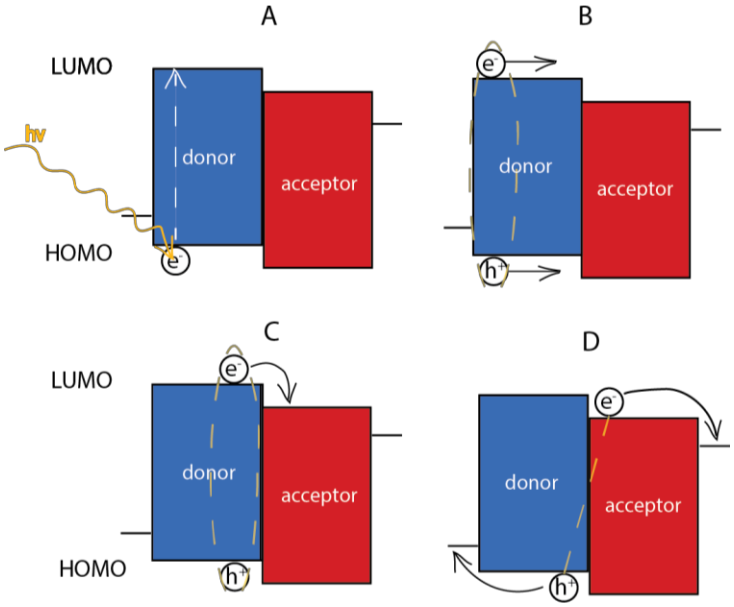

Figure 1. Charge generation through photon absorption (A), exciton diffusion to donor-acceptor interface (B), charge separation at interface (C) and charge transport and collection at electrodes.

To construct an effective OPV device several energetic factors need to be taken into account when choosing materials. Firstly, the donor and acceptor materials' valance and conduction bands should match one another in what is known as a type II heterojunction. This is where the LUMO of the acceptor is slightly lower in energy than the donor LUMO and the donor HOMO is slightly greater in energy than the acceptor HOMO. The energetic mismatch between the LUMOs of the donor and acceptor material provides an energetic driving force to separate coulombically bound exciton and thus allowing charge transfer. The binding energy, E_b, of an exciton in organic semiconductors has been reported to be ~0.5 eV, which has been shown to be higher than that of inorganic silicon systems of ~0.1 eV.[2-3] It has been reported that a minimum offset of 0.3 eV is needed as a primary energetic driving force to ensure charge transfer, however, over 0.5 eV has been shown to be not entirely beneficial and simply results in energy loss.[4] Typically 0.3 eV is the target offset between donor and acceptor systems.

Efficiency of an OPV device is based on the power output (P_{out}) in regard to power input (P_{in}) of a device as seen in Equation 1. The P_{out} is influenced in the OPV cell by the fill factor (FF), the short circuit current (J_{SC}) and the open circuit voltage (V_{OC}). Tuning these properties in the cell can be achieved by tuning electronic properties and morphological interfaces within the cell components.

$$\eta = \frac{P_{out}}{P_{in}} = FF\ \frac{(J_{SC})(V_{OC})}{P_{in}} \qquad \textbf{Eq 1.}$$

Open circuit voltage, V_{OC}, is defined by the voltage when no current is flowing through the device which is entirely dependent on the potential difference between donor and acceptor (Figure 2). A larger potential difference influences a higher V_{OC} and can subsequently increase efficiency. However, increasing the potential difference between donor HOMO and acceptor LUMO typically calls for increasing the donor HOMO-LUMO bandgap. This can have an adverse effect, where photoabsorption is decreased by lowering the spectral absorption overlap with the solar absorption spectrum resulting in decreased efficiency. It is therefore important to balance the two factors leading to an ideal bandgap of 1.5 eV.[4-5]

Another property that has an effect on efficiency is short circuit current, which is the maximum current achieved at zero applied voltage. This is governed by the internal charge transport process that include photoabsorption, charge densities, and charge collection that is influenced by charge movement through interfaces. The maximum power output is affected heavily by resistances in the material and cell composition known as shunt and series resistance. Shunt resistance (R_{SH}) is caused by photocurrent loss that is from current that is diverted by trap states of edge effects in the device. Series resistance (R_S) represents a loss in photocurrent through poor interface and material mobility. Taking these into account, at the point of maximum

power on the curvature of the *J-V* curve in Figure 2, the voltage at maximum power (V_{pm}) and the current at maximum power (J_{pm}) can be obtained.

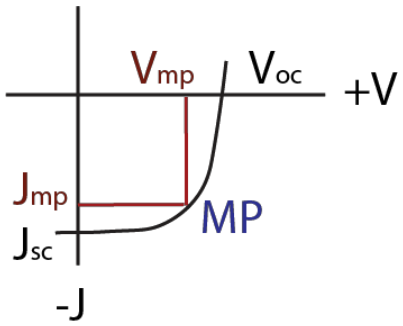

Figure 2. Representation of a *J-V* curve with relationship of short circuit current (J_{SC}), open circuit voltage (V_{OC}), maximum power current (J_{mp}), and maximum power voltage (V_{mp}) to maximum power generated (MP).

When these are divided by the V_{OC} and J_{SC}, the fill factor can be determined which relates the maximum power obtained in the cell to the theoretical power generated as seen in Equation 2. The fill factor's relationship to actual power and theoretical power is then directly proportional to overall cell efficiency. Idealized cells contain low resistances with high V_{OC} and J_{SC} to increase power output, which all depends on the electronic properties of the chosen donor and acceptors as well as their interface construction.

$$FF = \frac{(J_{mp})(V_{mp})}{(J_{sc})(V_{oc})} \qquad \textbf{Eq. 2}$$

6.3.0 Donors and acceptors

Many advancements have been made in OPV devices which cover a range of small molecule and polymer materials. To achieve an ideal OPV device, not only must the band gaps between the donor and acceptor materials be tuned for correct energetic offset but the blend of

the materials as well as interface must also be considered. How the materials will energetically align and how well they interact with one another depends on their intrinsic electronic and physical properties.

Fullerene and its derivatives are commonly used in OPV cells as electron acceptors due to its high electron affinity which is attributed to its low-lying LUMO at 4.2 eV. They also exhibit high electron mobility. Another attractive attribute that makes fullerene an idea acceptor is that it has a triply degenerate HOMO, which makes it capable of reversible reduction for up to six electrons material.[6] Fullerene can also be modified to improve solubility and interfacial interactions amongst donors with little impact on the electronic properties. One such modified fullerene that is commonly used in OPV devices is phenyl-C_{61}-butyric acid methyl ester (PCBM), **2**.[7]

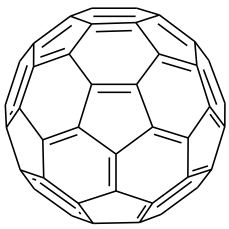

1

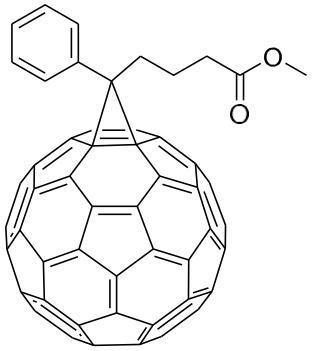

2

Desirable attributes for polymer donor to pair with fullerene based acceptors is a band offset to drive charge separation, charge carrier mobility, and the ability to form bicontinuous crystalline domains. Microphase separation of donor and acceptor domains is important so that donor and acceptor interface will promote charge separation and transport which will be described in greater detail in subsequent sections. p-Phenylenevinylene (PPV) polymers were

initially investigated as a suitable donor material for fullerene acceptors. Poly[2- methoxy,5-(2'-ethyl-hexyloxy)-p-phenyl-ene vinylene] (MEM-PPV), **3**, was one of the first C_{60}-conductive polymer charge transfer systems reported by Wudl and coworkers in 1992.[1] PPV polymer systems tend to exhibit a lower miscibility with fullerene derivatives, thus increasing their propensity of macrophase separation which can decrease charge separation. Poly-3-hexylthiophene (P3HT), **4**, was found to be an improvement in comparison to PPV based polymers because it has an increased miscibility with fullerene derivatives leading to a decrease in macrophase separation. It also has a lower donor bandgap of 2.0 eV as opposed to 2.2 eV in PPV, thereby improving photon absorption.[8-9] P3HT exhibits the ability to form π-π stacks between the polymer chains leading to enhanced crystallinity which increases its hole mobility thereby improving photocurrent. *Regioregularity*, wherein there is a high degree of order to the hexyl tails of each polymer unit, will further increase the π-π stacking degree of P3HT and thus can further increase crystallinity.[10-12]

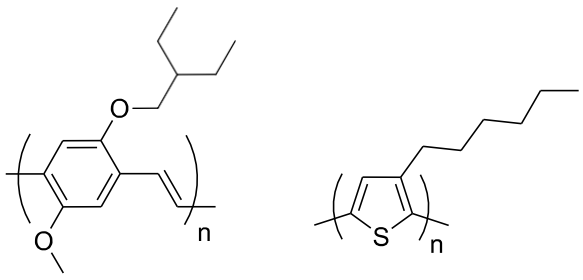

3 **4**

6.4.0 Interface

Interface between donor and acceptor domains is imperative to the effective exciton generation, separation and charge transport which govern the overall device performance. A limiting factor to this process is the exciton's diffusion length in organic materials due to strong coulombic attractions between hole and electron of the exciton which is approximately 10 nm of

diffusion of the excitons through the donor material.[13] If the acceptor interface is not reachable within this diffusion constraint recombination will occur and any potential charge transfer will be lost. Tang developed the first bilayer heterojunction in 1986.[14] The initial two-phase donor-acceptor cell systems were composed of a bilayer heterojunction between donor and acceptor where one was layered on top of the other to give two well-defined domains (Figure 3). While giving direct transport of charge carriers to electrodes, this type of cell junction suffers from limited donor and acceptor interface at which exciton can be separated for transport resulting in recombination.

Controlling the interface between the donor and acceptor materials is crucial to achieve 1) maximum interface between the two materials to allow for a greater degree of charge transfer and 2) an optimized domain size allowing for exciton diffusion to occur without recombination. Bulk heterojunction (BHJ) cells are the most prevalent bottom-up composition of optoelectronic devices because they allow for maximum interface between donor and acceptor materials. This design from Alan Heeger in 1995 involves the direct mixing of donor and acceptor materials and solution casting on substrates to provide an increased interfacial donor-acceptor construct (Figure 3).[15] The increase in interface between donor and acceptor domains allowed for a greater amount of charge transfer by creating decreasing overall segregated domain size so that exciton diffusion to interface could occur on a greater scale.

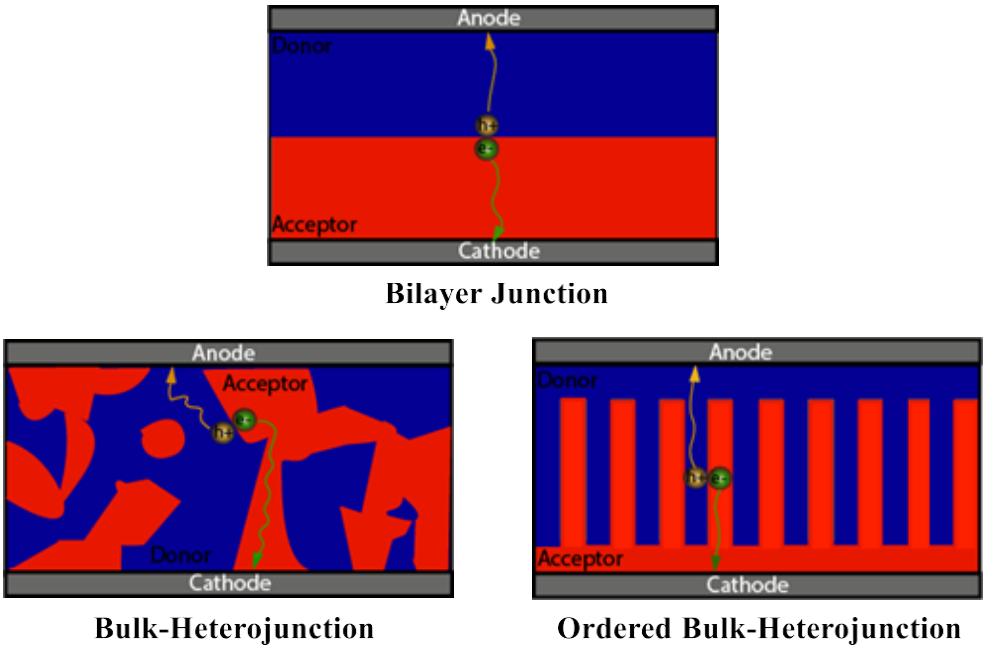

Figure 3. Junction schematic of bilayer junction (top) bulk heterojunction (left) and ordered bulk heterojunction (right).

A disadvantage to the BHJ model of assembly is the islanding effects that occur which disconnects portions of the charge transporting materials from the charge collecting electrodes because a direct charge pathway is denied. Another issue can arise from lack of domain size control upon thermal or solvent annealing of these blends in a BHJ due to the further segregation of donor and acceptor domains. P3HT forms well-defined crystalline stacks from face to face π-π interactions with distances of ~ 3.5 Å between stacks while C_{60} cannot form these ordered stacks as their spherical components are separated by 10.5 Å from their centers. The high propensity of P3HT to form ordered stacking arrays causes incompatibility between the two domains which range from microphase to macrophase segregation between donor and acceptor domains which hinders effective interface degree between the two as well as surpassing the ideal domain length of less than 10 nm for effective exciton transport and separation.[16] It is in this regard that an interest in ordered BHJs has arisen as the ideal OPV junction wherein domain size is ordered and

controlled into two well defined domains with maximum interface while providing ideal transport paths (Figure 3).[17-18]

Obtaining an optimal interface for donor and acceptor domains wherein there exists a large interface between the two while still exhibiting a bicontinuous network for charge separation and transport is a challenge. The ideal method to produce these cells is with the bottom-up assembly approach where the materials would be constructed so that after deposition they would self-assemble into the desired domains. In this respect methods to control domain size active layer competition, post-processing treatments, and block copolymers have garnered much attention. The self-assembly characteristics of these processes allows for interfacial control between donor and acceptor layers to enhance photovoltaic efficiencies.[17, 19]

6.4.1 Morphological Control

The extent of phase segregation in OPV devices composed of polymer and fullerene active layers are heavily dependent on not only the donor and acceptor components, but also on how the film is processed. Donor and acceptor ratio, concentration, solvent, and post coating processing such as thermal and solvent annealing can greatly affect the efficiency of an OPV device.

Ratio of materials and their inherent miscibility together can impact the degree of segregation. PPV and fullerene have shown high degrees of segregation at low fullerene concentrations. Therefore, to maintain a bicontinuous network, higher concentrations of fullerene are needed to promote effective interface for charge transfer.[9, 20] Whereas the miscibility of P3HT and fullerene is much greater, so a more even 1:1 ratio of components is employed for effective photocurrent production. Due to the importance of miscibility of the two components,

solvent choice is also imperative to the prevention of macrophase segregated domains. In a study comparing chlorobenzene films to toluene, PCBM was found to have lower solubility in toluene which promoted large aggregates of PCBM in the films leading to macrophase segregation with PPV polymers whereas chlorobenzene promoted more even domains.[21]

Thermal and solvent annealing also have a large effect on device efficiency. Thermal annealing can induce macro or micro phase segregation depending on polymer type as well as ratios of donor to acceptor.[22] In PPV/PCBM systems, thermal treatment causes macrophase segregation of the PCBM acceptors due to their lower miscibility with the PPV polymer chains which causes adverse effects on charge diffusion. The glass transition temperature (T_g) of the PPV polymer is 80°C, which poses a significant problem for PPV in devices when exposed to sunlight due to the low thermal stability of the material.[23] In contrast to PPV blends, P3HT exhibits a T_g at ~110°C, thus exhibiting thermal stability in device applications. Furthermore, the baking of P3HT/PCBM cells for a controlled time over the T_g was shown to benefit the cell efficiency performance by increasing crystallinity and diffusing PCBM into microphase segregated domains. These cells were seen to have an increase in efficiency from 1.1% in unannealed cells to almost 5% after thermal annealing treatment.[24-26] Solvent annealing uses solvent vapor pressure to drive the reorganization of polymer chains to increase crystallinity. Vapor pressure of dichlorobenzene allowed polymer chains to self-assemble into ordered domains when compared to unannealed films. It has also been reported that, though thermal annealing can have a stronger effect on crystallinity of the cell and therefore hole mobility, a combination of solvent and thermal annealing can be more beneficial that either singular annealing method.[27-28]

While ratio control and post-processing steps provide necessary microphase segregation, they still lack definite control and depend on processes that can be difficult to carry out when printing on large scale devices. Utilizing materials that can self-assemble into distinct and controlled domains with little post-processing treatment will allow ease of fabrication in OPV applications.

6.4.2 Block Copolymers

Block copolymers (BCP) have been shown as a method controlling domains without a complicated post processing steps and allow for direct interface between both donor and acceptor materials as well as direct transport to electrodes. Bock copolymers are composed of two separate polymer domains covalently linked together upon which the different properties such as solubility inherit to each block as well as block composition ratio can result in the self-assembly into interesting microstructures and domains.

Rod-coil block copolymers are composed of both a conjugated conducting block (referred to as rod) and an insulating block (referred to as coil). The differences in physical properties and the ratio between these two blocks allow for a high degree of self-assembly into different domain shapes.[29] Lamellar nanostructures can provide organized interfaces as seen in Figure 4 with controllable domain orientation and size tuned to the 10 nm exciton diffusion limitation.[30] Since the “coil” block in rod-coil BCP is an insulating block, several methods have been used to introduce acceptor materials in order to obtain the necessary heterojunction needed for charge transfer.

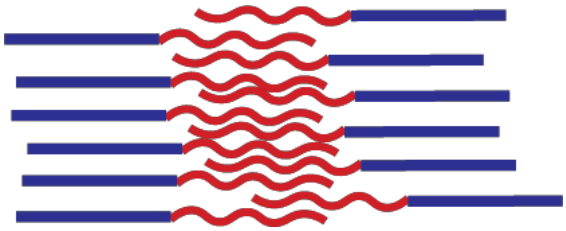

Figure 4. Lamellar alignment of rod-coil BCP leading to microphase segregation.

One method involves grafting an acceptor onto the coil block to utilize its inherent self-assembly, but still have an electron acceptor component for charge separation and transport. Hadziioannou and coworkers demonstrated the linkage of fullerene to a polystyrene (PS) coil block that was covalently joined to a PPV-based rod block poly[(2,5-di(2′-ethyl)hexyloxy)-1,4-phenylenevinylene] (DEH-PPV).[31-32] The resultant DEH-PPV-b-poly(BA-statC60MS, **5**, exhibited photoluminescence (PL) quenching that suggests charge transfer between the PPV donor and the fullerene. However, the surface morphology, as seen through atomic force microscopy (AFM), failed to exhibit the desired lamellar structures for effective charge transport due to fullerene nanocrystal aggregates driving the self-assembly. It was surmised that by using a rod polymer that displayed greater rod-rod intermolecular interaction by π-π stacking such as P3HT, the lamellar architecture could be achieved. From this, Jo and coworkers covalently linked PCBM to a methyl methacrylate (MMA) and 2-hydroxyethyl methacrylate (HEMA) coil unit with P3HT as the rod unit to form P3HT-b-P(MMA-r-HEMA), **6**.[33] The resulting BCP **6**, did not display the fullerene nanocrystals that were seen in BCP **5**, but instead formed self-assembled domains that were the almost ideal 15 nm in size. This was attributed to the further separation of the PCBM from the coil chain whereas C_{60} was directly linked to the coil chain in BCP **5**. The use of rod-coil fullerene linked systems also have the potential to provide long-term

stability of the cell components. This is accomplished by decreasing phase segregation over time when used as compatibilizing agents to increase miscibility between the polymer systems and fullerene derivative by decreasing interfacial energy.[34]

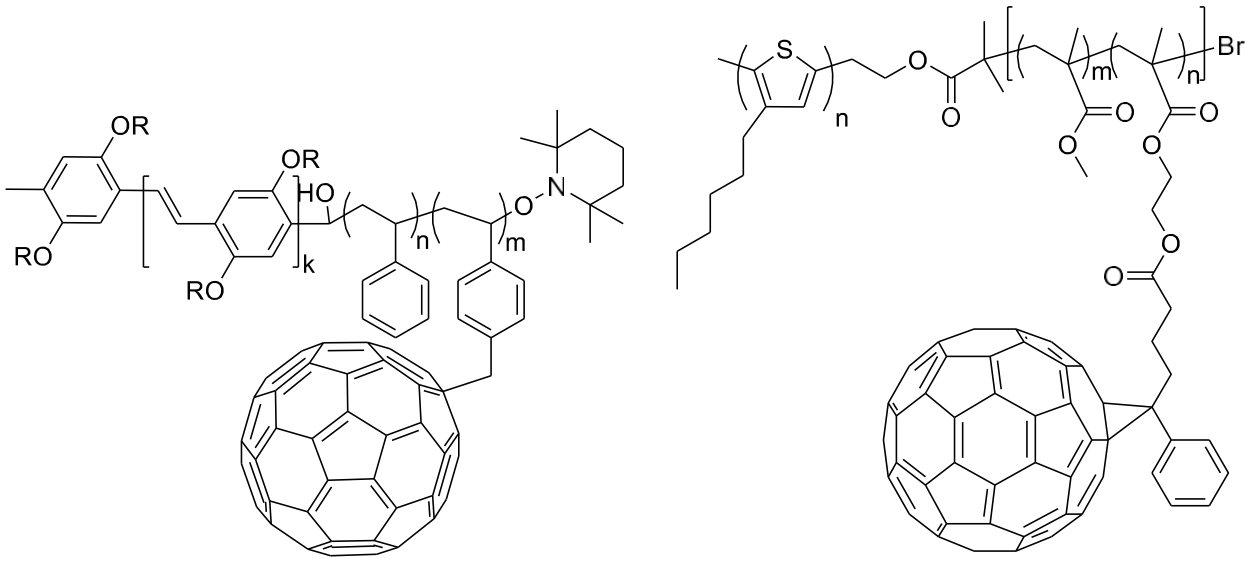

5 **6**

Another method employed for rod-coil BCP is by using a sacrificial coil block such as polylactide (PLA) or PS solely for the purposes of driving the self-assembled architecture. It can then be chemically etched away after which an acceptor material may be backfilled in its place. Poly-3-alkylthiophene has been polymerized with to PLA to result in P3AT-b-PLA BCP, **7**.[35] BCP **7** was shown to form well-ordered domains ~35 nm in size. The PLA was etched away using NaOH to leave vacancies in the films. C_{60} was successfully loaded into the templated P3AT films and displayed PL quenching. However, this method had drawbacks which included the difficulty to control the amount of fullerene in the vacancies as well as the appearance of defects in domain size due to collapse of parts of the P3AT template during processing.[36]

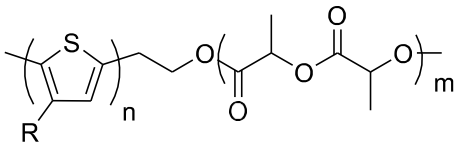

7

To overcome the flaws of rod-coil BCPs, interest shifted to all conjugated rod-rod BCPs. Rod-rod BCPs have the desirable quality of being fully conductive for charge transport while still displaying self-assembly into lamellar shapes. This eliminates the rod-coil BCP insulating block that can hamper charge transport and eliminates the need for poorly controlled chemical etching. In early results Hashimoto demonstrated that rod-rod BCP form lamellar microstructures naturally which allows for controlled microsegregation in even simple systems of P3AT with different aliphatic tail structures on each block.[19, 37] While having many desirable properties, all conjugated BCPs tend to be more synthetically challenging than their insulating counterparts through joining two conjugated domains and incorporating an acceptor unit for PV applications. Donor-acceptor linked diblock copolymers have been approached in two ways: 1) by using two different polymer blocks with different electronic properties to drive charge transfer and 2) linking fullerene to a conjugated block with a functional handle.[3, 38]

Ren and coworkers reported a polythiophene-based all conjugated BCP wherein P3HT was used as a donor block and a polythiophene with an electron withdrawing carboxylate group directly on the thiophene backbone, P3HT-b-P3HCT, served as an acceptor material, **8**.[39] The electron withdrawing unit tuned the band structure of the carboxylate block so that it exhibited the band offset of 0.5 eV to provide the driving force of required for charge transfer between the two blocks. Due to the direct and large interfacial area between the crystalline P3HT block and the acceptor block, a room temperature excitonic magnetic field effect (MFE) was observed where an external magnetic field can be used to tune the inherent current production of a device.

This was due to fast and large amounts of charge transfer states and a highly organized donor and acceptor interface exhibited by the self-assembly of the material.[40]

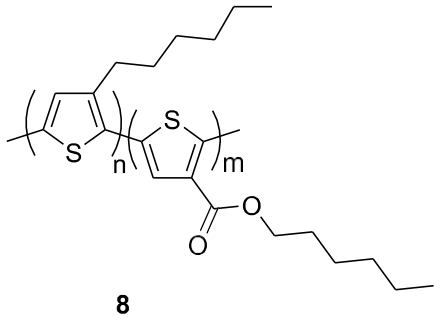

8

Fullerene linked all conjugated BCPs have been explored as single component devices as seen by Hashimoto with P3HT rods wherein one block exhibited C_{60} linkage on the chain tail. These cells reported optimal microphase segregation between fullerene and P3HT domains.[41] These single component cells can be limited by fast recombination of charge due to close interfaces and the poor extent of C_{60} that can be loaded onto a chain for effective domain size and ratio to donor.[10, 42] Chen and coworkers took a different approach by using C_{60}-linked P3HT BCPs as a compatibilizing unit instead of a single component material. They developed a block copolymer comprised of P3HT and poly-6-bromo-3-hexylthiophene (PBr3HT).[43] The bromide tail was converted post-polymerization to an azide, then used to link into fullerene. The resulting P3C_{60}HT-b-P3HT BCP, **9**, was used as a compatibilizing compound to control phase segregation between free C_{60} and P3HT homopolymer. Without post-polymerization annealing, P3HT:C_{60} films that included BCP **9** as a compatibilizing agent demonstrated a unique ability to self-assemble into small, controlled domains. BCP **9** additives containing P3HT:C_{60} cells were reported to have power conversion efficiencies of 2.56% while annealing and additive free cells were reported to have an efficiency of only 0.48%.

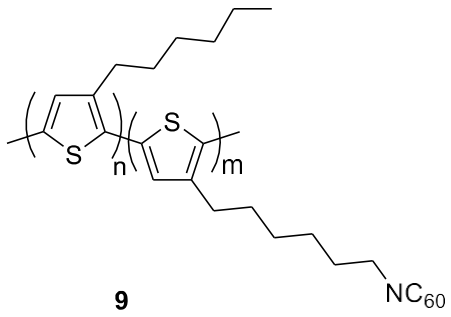

9

Further advancement of block copolymer incorporation into OPV devices can allow for further control of cell domains and morphologies. BCP materials can eliminate the requirement for post-processing steps in cell fabrication and enhance long-term stability of materials by locking desirable microphase segregated architectures in place. These qualities provide real world applications of device manufacturing and processing for cell usage.

6.5.0 Magnetoconductance in Optoelectronics

Enhancement of charge carrier density provides a unique opportunity in organic optoelectronic materials by shifting interest to the application of room temperature magnetoresistance. In these organic semiconducting charge transfer devices, an induced magnetoconductance (MC) is observed wherein external magnetic fields can be utilized to tune the resultant current generation of a cell. The effect of MC on a device is described in Equation 3, where MC is a function of an external magnetic field, J(H) is the current density with applied magnetic field and J(0) is the current without an applied magnetic field.[44]

$$MC(H) = \frac{[J(H) - J(0)]}{J(0)} \qquad \textbf{\textit{Eq. 3}}$$

Upon excitation in a cell, singlet and triplet excitons are produced. As demonstrated by Koopmans and Hu groups, an external magnetic field can tune singlet to triplet ratios which can have a positive or negative effect on photocurrent.[45] For instance, an increase in the degree of

intersystem crossing can produce a higher degree of triplet excitons and CTs.[46] Triplet excitons and CTs exhibit a longer lifetime which can interact and scatter charges. This produces a negative MC when the application of a magnetic field lowers current generations.[47]

Utilizing highly ordered fully conjugated organic components in charge transfer complexes due to their weak hyperfine interaction and low spin-orbit coupling has proven to be an effective way of eliciting a magnetic field effect on device performance. The crystallization of P3HT and C_{60} domains and ordering of these materials has been shown to be imperative to the acquisition and degree of this magnetic field effect that has been observed in 1D P3HT nanowire components when mixed with C_{60}.[40] A fully conjugated BCP **9** that was described in the previous section also exhibited the highly ordered donor and acceptor domains that produced fast charge transfer complexes.[39] Further investigation into the field of organic materials with larger donor-acceptor interface that produces fast charge transfer can aid in the development of organic sensors and memories, as well as a further understanding of magnetoresistance materials.

6.6.0 Ren group BCP crystals

The following chapter will entail my work in the Ren group to synthesize P3HT-C_{60} linked block copolymers in different block ratios. The resulting P3HT-P3C_{60}HT BCP's were analyzed for morphology and spectral properties that reduced phase segregation. Through the incorporation of P3HT-C_{60} BCP into homopolymer P3HT and free C_{60} domains, segregated domains could be minimized. An induced crystal growth through seeding and sonication was then used to generate large crystals composed of both P3HT and PCBM. The highly ordered donor and acceptor interfaces could then be examined for magnetoresistance in organic materials.

References

1. Sariciftci, N. S.; Smilowitz, L.; Heeger, A. J.; Wudl, F., Photoinduced Electron Transfer from a Conducting Polymer to Buckminsterfullerene. *Science* **1992,** *258* (5087), 1474-1476.
2. Arkhipov, V. I.; Bässler, H., Exciton Dissociation and Charge Photogeneration in Pristine and Doped Conjugated Polymers. *physica status solidi (a)* **2004,** *201* (6), 1152-1187.
3. Facchetti, A., Polymer Donor–Polymer Acceptor (All-Polymer) Solar Cells. *Materials Today* **2013,** *16* (4), 123-132.
4. Koster, L. J. A.; Mihailetchi, V. D.; Blom, P. W. M., Ultimate Efficiency of Polymer/Fullerene Bulk Heterojunction Solar Cells. *Applied Physics Letters* **2006,** *88* (9), 093511.
5. Soci, C.; Hwang, I. W.; Moses, D.; Zhu, Z.; Waller, D.; Gaudiana, R.; Brabec, C. J.; Heeger, A. J., Photoconductivity of a Low-Bandgap Conjugated Polymer. *Advanced Functional Materials* **2007,** *17* (4), 632-636.
6. Allemand, P. M.; Koch, A.; Wudl, F.; Rubin, Y.; Diederich, F.; Alvarez, M. M.; Anz, S. J.; Whetten, R. L., Two Different Fullerenes have the same Cyclic Voltammetry. *Journal of the American Chemical Society* **1991,** *113* (3), 1050-1051.
7. Hummelen, J. C.; Knight, B. W.; LePeq, F.; Wudl, F.; Yao, J.; Wilkins, C. L., Preparation and Characterization of Fulleroid and Methanofullerene Derivatives. *The Journal of Organic Chemistry* **1995,** *60* (3), 532-538.
8. Mazzio, K. A.; Luscombe, C. K., The Future of Organic Photovoltaics. *Chemical Society Reviews* **2015,** *44* (1), 78-90.
9. Thompson, B. C.; Fréchet, J. M. J., Polymer–Fullerene Composite Solar Cells. *Angewandte Chemie International Edition* **2008,** *47* (1), 58-77.
10. Zhou, H.; Yang, L.; You, W., Rational Design of High Performance Conjugated Polymers for Organic Solar Cells. *Macromolecules* **2012,** *45* (2), 607-632.
11. Kim, Y.; Cook, S.; Tuladhar, S. M.; Choulis, S. A.; Nelson, J.; Durrant, J. R.; Bradley, D. D. C.; Giles, M.; McCulloch, I.; Ha, C.-S.; Ree, M., A Strong Regioregularity Effect in Self-Organizing Conjugated Polymer Films and High-Efficiency Polythiophene:Fullerene Solar Cells. *Nat Mater* **2006,** *5* (3), 197-203.
12. Österbacka, R.; An, C. P.; Jiang, X. M.; Vardeny, Z. V., Two-Dimensional Electronic Excitations in Self-Assembled Conjugated Polymer Nanocrystals. *Science* **2000,** *287* (5454), 839-842.
13. Mikhnenko, O. V.; Azimi, H.; Scharber, M.; Morana, M.; Blom, P. W. M.; Loi, M. A., Exciton Diffusion Length in Narrow Bandgap Polymers. *Energy & Environmental Science* **2012,** *5* (5), 6960-6965.
14. Tang, C. W., Two-layer Organic Photovoltaic Cell. *Applied Physics Letters* **1986,** *48* (2), 183-185.
15. Sariciftci, N. S.; Braun, D.; Zhang, C.; Srdanov, V. I.; Heeger, A. J.; Stucky, G.; Wudl, F., Semiconducting Polymer-Buckminsterfullerene Heterojunctions: Diodes, Photodiodes, and Photovoltaic Cells. *Applied Physics Letters* **1993,** *62* (6), 585-587.
16. Venkataraman, D.; Yurt, S.; Venkatraman, B. H.; Gavvalapalli, N., Role of Molecular Architecture in Organic Photovoltaic Cells. *The Journal of Physical Chemistry Letters*

2010, *1* (6), 947-958.
17. Tseng, Y.-C.; Darling, S. B., Block Copolymer Nanostructures for Technology. *Polymers* **2010,** *2* (4), 470.
18. Scharber, M. C.; Sariciftci, N. S., Efficiency of Bulk-Heterojunction Organic Solar Cells. *Progress in Polymer Science* **2013,** *38* (12), 1929-1940.
19. Scherf, U.; Adamczyk, S.; Gutacker, A.; Koenen, N., All-Conjugated, Rod-Rod Block Copolymers-Generation and Self-Assembly Properties. *Macromolecular Rapid Communications* **2009,** *30* (13), 1059-1065.
20. Yu, G.; Gao, J.; Hummelen, J. C.; Wudl, F.; Heeger, A. J., Polymer Photovoltaic Cells: Enhanced Efficiencies via a Network of Internal Donor-Acceptor Heterojunctions. *Science* **1995,** *270* (5243), 1789-1791.
21. Shaheen, S. E.; Brabec, C. J.; Sariciftci, N. S.; Padinger, F.; Fromherz, T.; Hummelen, J. C., 2.5% Efficient Organic Plastic Solar Cells. *Applied Physics Letters* **2001,** *78* (6), 841-843.
22. Padinger, F.; Rittberger, R. S.; Sariciftci, N. S., Effects of Postproduction Treatment on Plastic Solar Cells. *Advanced Functional Materials* **2003,** *13* (1), 85-88.
23. Yang, X.; van Duren, J. K. J.; Janssen, R. A. J.; Michels, M. A. J.; Loos, J., Morphology and Thermal Stability of the Active Layer in Poly(p-phenylenevinylene)/Methanofullerene Plastic Photovoltaic Devices. *Macromolecules* **2004,** *37* (6), 2151-2158.
24. Ma, W.; Yang, C.; Gong, X.; Lee, K.; Heeger, A. J., Thermally Stable, Efficient Polymer Solar Cells with Nanoscale Control of the Interpenetrating Network Morphology. *Advanced Functional Materials* **2005,** *15* (10), 1617-1622.
25. Li, G.; Shrotriya, V.; Huang, J.; Yao, Y.; Moriarty, T.; Emery, K.; Yang, Y., High-Efficiency Solution Processable Polymer Photovoltaic Cells by Self-organization of Polymer Blends. *Nature Materials* **2005,** *4* (11), 864-868.
26. Reyes-Reyes, M.; Kim, K.; Carroll, D. L., High-Efficiency Photovoltaic Devices Based on Annealed Poly(3-hexylthiophene) and 1-(3-methoxycarbonyl)-propyl-1- phenyl-(6,6)C_{61} Blends. *Applied Physics Letters* **2005,** *87* (8), 083506.
27. Shrotriya, V.; Yao, Y.; Li, G.; Yang, Y., Effect of self-organization in polymer/fullerene bulk heterojunctions on solar cell performance. *Applied Physics Letters* **2006,** *89* (6), 063505.
28. Zhao, Y.; Xie, Z.; Qu, Y.; Geng, Y.; Wang, L., Solvent-vapor Treatment Induced Performance Enhancement of Poly(3-hexylthiophene):Methanofullerene Bulk-Heterojunction Photovoltaic Cells. *Applied Physics Letters* **2007,** *90* (4), 043504.
29. Lee, M.; Cho, B.-K.; Zin, W.-C., Supramolecular Structures from Rod−Coil Block Copolymers. *Chemical Reviews* **2001,** *101* (12), 3869-3892.
30. Olsen, B. D.; Li, X.; Wang, J.; Segalman, R. A., Near-surface and Internal Lamellar Structure and Orientation in Thin Films of Rod-Coil Block Copolymers. *Soft Matter* **2009,** *5* (1), 182-192.
31. de Boer, B.; Stalmach, U.; van Hutten, P. F.; Melzer, C.; Krasnikov, V. V.; Hadziioannou, G., Supramolecular Self-Assembly and Opto-Electronic Properties of Semiconducting Block Copolymers. *Polymer* **2001,** *42* (21), 9097-9109.
32. Barrau, S.; Heiser, T.; Richard, F.; Brochon, C.; Ngov, C.; van de Wetering, K.; Hadziioannou, G.; Anokhin, D. V.; Ivanov, D. A., Self-Assembling of Novel Fullerene-

Grafted Donor– Acceptor Rod−Coil Block Copolymers. *Macromolecules* **2008,** *41* (7), 2701-2710.
33. Lee, J. U.; Cirpan, A.; Emrick, T.; Russell, T. P.; Jo, W. H., Synthesis and Photophysical Property of Well-defined Donor-Acceptor Diblock Copolymer based on Regioregular Poly(3- hexylthiophene) and Fullerene. *Journal of Materials Chemistry* **2009,** *19* (10), 1483-1489.
34. Sivula, K.; Ball, Z. T.; Watanabe, N.; Fréchet, J. M. J., Amphiphilic Diblock Copolymer Compatibilizers and Their Effect on the Morphology and Performance of Polythiophene:Fullerene Solar Cells. *Advanced Materials* **2006,** *18* (2), 206-210.
35. Boudouris, B. W.; Frisbie, C. D.; Hillmyer, M. A., Nanoporous Poly(3-alkylthiophene) Thin Films Generated from Block Copolymer Templates. *Macromolecules* **2008,** *41* (1), 67-75.
36. Botiz, I.; Darling, S. B., Self-Assembly of Poly(3-hexylthiophene)-block-polylactide Block Copolymer and Subsequent Incorporation of Electron Acceptor Material. *Macromolecules* **2009,** *42* (21), 8211-8217.
37. Zhang, Y.; Tajima, K.; Hirota, K.; Hashimoto, K., Synthesis of All-Conjugated Diblock Copolymers by Quasi-Living Polymerization and Observation of Their Microphase Separation. *Journal of the American Chemical Society* **2008,** *130* (25), 7812-7813.
38. Yamamoto, S.; Yasuda, H.; Ohkita, H.; Benten, H.; Ito, S.; Miyanishi, S.; Tajima, K.; Hashimoto, K., Charge Generation and Recombination in Fullerene-Attached Poly(3-hexylthiophene)-Based Diblock Copolymer Films. *The Journal of Physical Chemistry C* **2014,** *118* (20), 10584-10589.
39. Lohrman, J.; Liu, Y.; Duan, S.; Zhao, X.; Wuttig, M.; Ren, S., All Conjugated Copolymer Excitonic Multiferroics. *Advanced Materials* **2013,** *25* (5), 783-787.
40. Ren, S.; Wuttig, M., Organic Exciton Multiferroics. *Advanced Materials* **2012,** *24* (6), 724-727.
41. Miyanishi, S.; Zhang, Y.; Tajima, K.; Hashimoto, K., Fullerene Attached All-Semiconducting Diblock Copolymers for Stable Single-component Polymer Solar Cells. *Chemical Communications* **2010,** *46* (36), 6723-6725.
42. Miyanishi, S.; Zhang, Y.; Hashimoto, K.; Tajima, K., Controlled Synthesis of Fullerene-Attached Poly(3-alkylthiophene)-Based Copolymers for Rational Morphological Design in Polymer Photovoltaic Devices. *Macromolecules* **2012,** *45* (16), 6424-6437.
43. Chan, S.-H.; Lai, C.-S.; Chen, H.-L.; Ting, C.; Chen, C.-P., Highly Efficient P3HT: C60 Solar Cell Free of Annealing Process. *Macromolecules* **2011,** *44* (22), 8886-8891.
44. Qin, W.; Gao, K.; Yin, S.; Xie, S. J., Investigating the Magnetic Field Effect on Electron-Hole pair in Organic Semiconductor Devices. *Journal of Applied Physics* **2013,** *113* (19), 193901.
45. Hu, B.; Wu, Y., Tuning Magnetoresistance between Positive and Negative Values in Organic Semiconductors. *Nat Mater* **2007,** *6* (12), 985-991.
46. Janssen, P.; Cox, M.; Wouters, S. H. W.; Kemerink, M.; Wienk, M. M.; Koopmans, B., Tuning Organic Magnetoresistance in Polymer-Fullerene Blends by Controlling Spin Reaction Pathways. *Nature Communications* **2013,** *4*, 2286.
47. Qin, W.; Chen, X.; Li, H.; Gong, M.; Yuan, G.; Grossman, J. C.; Wuttig, M.; Ren, S., Room Temperature Multiferroicity of Charge Transfer Crystals. *ACS Nano* **2015,** *9* (9), 9373-9379.

CHAPTER 7

C_{60}-linked P3HT Block Copolymers for Use in Magnetoconductive Charge Transfer Crystals

Reproduced with permission from: Qin, W.; Chen, X.; Lohrman, J.; Gong, M.; Yuan, G.; Wuttig, M.; Ren, S., *Nano Research* **2016,** *9* (4), 925-932. DOI 10.1007/s12274-015-0975-8

This work was accomplished in conjunction with Wei Qin. Data collected from this author will be marked with an (*).

7.1.0 Introduction

Enhancement of charge carrier density has a unique opportunity in organic optoelectronic materials by shifting interest to the application of multiferroics. In these organic semiconducting charge transfer devices, an induced magnetoconductance is observed wherein external magnetic fields can be utilized to tune the resultant current generation of a cell.

As was mentioned in Chapter 6, fullerene-linked all conjugated block copolymers have been shown to act as compatibilizing agents to reduce macrophase segregation in polymer-fullerene composite devices.[1-2] Previous work by the Ren group has shown that organized pristine charge transfer complexes using P3HT and C_{60} demonstrate an inherent room temperature magnetoresistance. Initial investigations used acetonitrile to induce aggregation and then sonication to promote organization in P3HT to form 1D nanowires for magnetoelectric devices when mixed with P3HT.[3] Following this, crystal growth was studied by using both P3HT and C_{60} in the aggregation and ordering process to obtain charge transfer crystals (CTC) with donor and acceptor domains.[4] The CTC facilitated the molecular packing of segregated well-ordered C_{60} and pristine P3HT lattices allowing for a generous interface between the two crystal component domains. The well-ordered CTCs produced a negative magnetoconductance when a magnetic field was applied to the device.

Room temperature organic magnetoelectronics provide an opportunity to make printable, flexible devices to be used in sensors and memory applications. It was the goal of this work to synthesize and incorporate the block copolymer into magnetoresponsive CTCs. To increase the interface between C_{60} and P3HT within the CTC, all conjugated P3HT block copolymers with C_{60} linkage (P3HT-b-P3C_{60}HT) take advantage of the compatibilization and nanostructure self-

assembly that has been previously reported. [1] P3HT-b-P3C_{60}HT was used as a dopant into a 1:1 mixture of homopolymer P3HT and free C_{60} to co-crystalize the two domains together as opposed to the segregated stacking that was previously observed. The aggregation of CT materials was accomplished by the addition of acetonitrile, then ordered through sonication and aging (Figure 1).

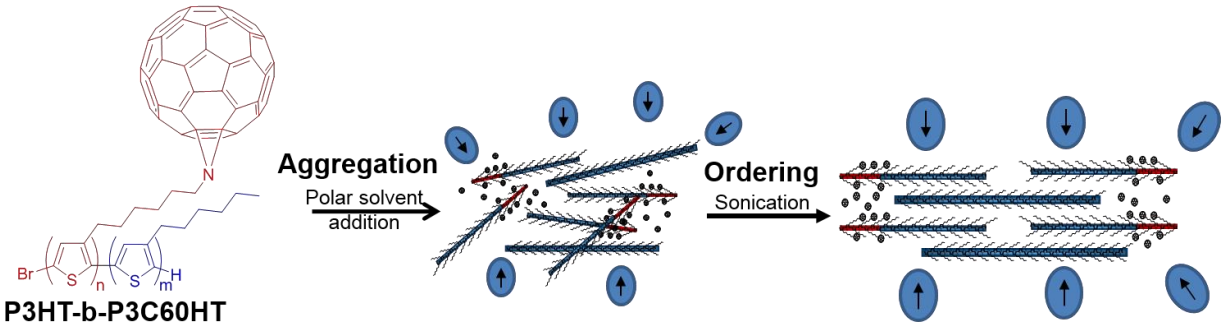

Figure 1. Polymer ordering and crystals growth through solvent-induced aggregation and sonication to induce organization.[5]

BCP-doped cocrystals of P3HT and C_{60} have the potential to increase charge transfer in an organized crystalline system that can lead to magnetoresistance effects. The synthesis, fabrication, and study of these devices will be explored in this chapter. This work was detailed in a publication from the Ren group in Nano Research.[5]

7.2.0 Experimental

General

Fullerene was purchased from Nano-C Inc. and P3HT (M104) was purchased from Ossila. TEM and cell data was collected by Dr. Wei Qin, a postdoctoral scholar in the Ren group.

7.2.1 Synthesis

All monomer reactions were carried out in air with reagent grade solvents unless otherwise indicated. Monomer preparation and polymerization were performed with synthetic procedures were based on the works of Chan and Hashimoto with modifications to produce specific block ratios.[1, 6] Grigniard reagents were titrated before every use to ensure actuate concentrations. Polymerizations and post polymerization reactions were carried out on schlenk line under argon. Anhydrous THF was used for polymerization.

Synthesis of 2,5-dibromo-3-hexylthiophene. 7.a(Br$_2$3HT).

Scheme 1. Synthesis of 2,5-dibromo-3-hexylthiophene **7.a**(Br$_2$3HT) monomer.

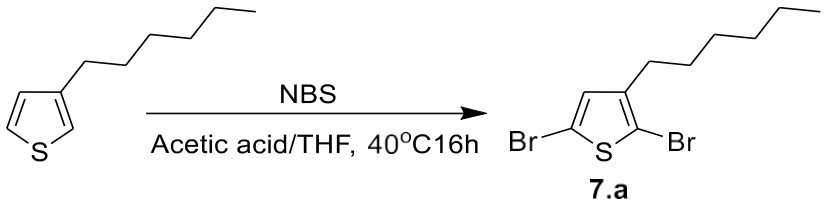

7.a

A solution of 3-hexylthiophene (2.34 g, 14.1 mmol) was prepared in 30 mL of a 1:1 mixture of THF:acetic acid. N-bromoscuccinimide (5.77 g, 34.1 mmol) was added in 1 portion then was heated to 40°C and stirred for 12 hours. The mixture was poured into water and extracted with ethyl acetate, then washed with saturated sodium chloride and brine. The product was further purified with column chromatography in hexanes then dried over magnesium sulfate to produce a **7.a**(Br$_2$3HT) as a yellow oil (4.002 g, 87.6%). ^{1}H NMR (400 MHz, $CDCl_3$, ppm): 6.79 (s, 1H), 2.52 (t, 2H), 1.55 (m, 2H), 1.31 (m, 2H), 0.91 (t, 3H).

Synthesis of 3-(6-bromohexyl)thiophene. 7.b(3BrHT).

Scheme 2. Synthesis of 3-(6-bromohexyl)thiophene **7.b**(3BrHT).

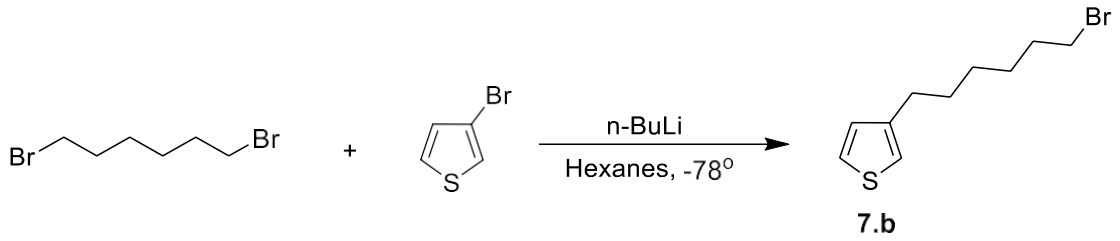

A solution of 3-bromothiophene (4 mL, 42.7 mmol) in 60 mL dry hexanes under argon was cooled to -78°C. A 1.6 mM n-BuLi in THF (26.7 mL, 42.7 mmol) was added dropwise then stirred 10 minutes. Dry THF added dropwise until a white precipitate evolves then stirred for one hour. The reaction was warmed to 0°C then 2 mL of dry THF was added along with 1,6-dibromohexane (26 mL, 170.1 mmol) as precipitiate dissolves and stirred for 2 hours then extracted with chloroform. Solvent was removed and excess 1,6-dibromohexane was removed via vacuum distillation to yield **7.b**(3BrHT) as a yellow oil and further purified with column chromatography in hexanes. ^{1}H NMR (400 MHz, $CDCl_3$, ppm): 7.26 (d, 2H), 6.94 (d, 2H), 3.42 (t, 2H), 2.65 (t, 2H), 1.87 (m, 2H), 1.65 (m, 2H) 1.48 (m, 2H), 1.37 (m, 2H).

Synthesis of 2,5-dibromo-3-(6-bromohexyl)thiophene. 7.c($Br_2$3BrHT).

Scheme 3. Synthesis of 3-(6-bromohexyl)thiophene **7.c**($Br_2$3BrHT).

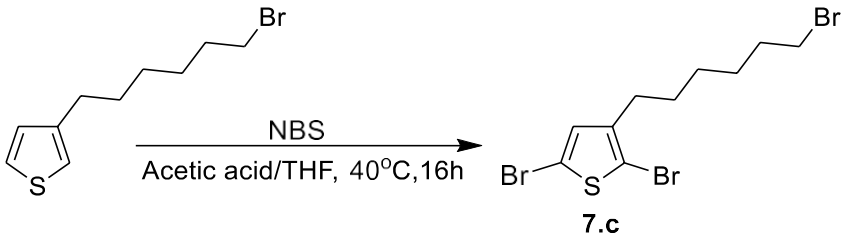

A solution of 3-hexyl-6-bromothiophene (1.98 g, 8.0 mmol) was prepared with 30 mL of a 1:1 mixture of THF:acetic acid. N-bromoscuccinimide (3.12 g, 17.6 mmol) was added in 1 portion then was heated to 40°C and stirred for 12 hours. The mixture was poured into water and extracted with ethyl acetate, then washed with saturated sodium bicarbonate and brine. The product was further purified with column chromatography in hexanes then dried over magnesium sulfate to produce a yellow oil (1.104 g, 34.1%). ^{1}H NMR (400 MHz, $CDCl_3$, ppm): 6.78 (s, 1H), 3.42 (t, 2H), 2.53 (t, 2H), 1.89 (m, 2H), 1.57 (m, 2H), 1.48 (m, 2H), 1.37 (t, 2H).

General synthesis for 7.1(P3HT-b-P3BrHT).

Scheme 4. BCP polymerization of **7.1**(P3HT-b-P3BrHT).

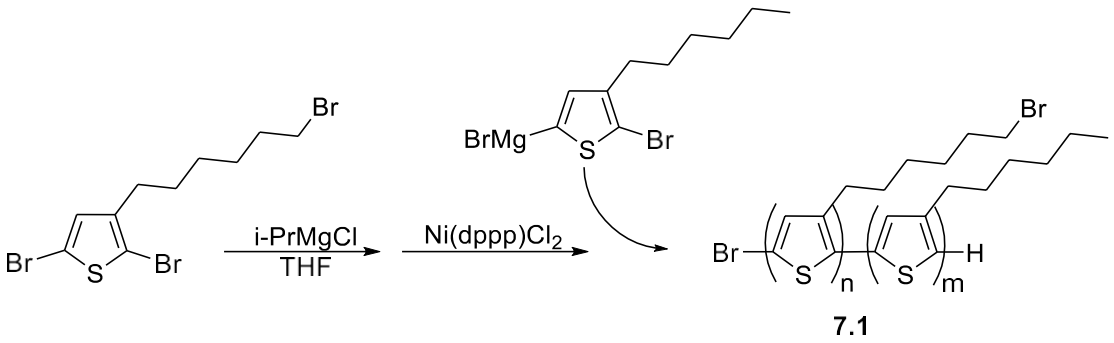

7.1

The monomer **7.c**($Br_2$3BrHT) (0.4 mmol) was added to a 100 mL schlenk flask under argon with 20 mL dry THF. Flask was cooled to 0° C. i-PrMgCl (0.4 mmol) was added dropwise and then stirred for 30 min at room temperature. Ni(dppp)Cl_2 (0.8% total monomer mol) was added via cannula and stirred for 1 h at 50° C. In a separate flask, **7.a**($Br_2$3HT) (1.6 mmol) was added under argon with 70 mL of dry THF. Flask was cooled to 0°C. i-PrMgCl (1.6 mmol) was added and stirred for 30 min at room temperature. It was then added to the original polymerization flask via cannula and continued to stir at 50° C for 5 h. 10% HCl was added to the reaction vessel to precipitate the polymer. It was then washed in a soxhulet with methanol and hexanes and extracted with chloroform then solvent was removed under reduced pressure to

yield **7.1**(P3HT-b-P3BrHT) as a purple solid. Yield 0.15g (M_w: 11,000) ^{1}H NMR (400 MHz, $CDCl_3$): 6.99 (s, 1H), 3.44 (t, 2H), 2.82 (t, 2H), 1.91 (m, 2H), 1.73 (m, 2H), 1.55 (m, 2H), 1.45 (m, 2H), 1.36 (m, 2H), 0.92 (t, 3H).

Synthesis of 7.2(P3HT-b-P3N$_3$HT).

Scheme 5. BCP polymerization of **7.2**(P3HT-b-P3N$_3$HT).

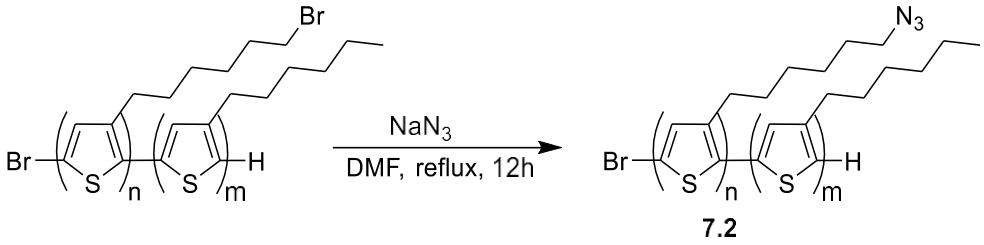

7.2

7.1(P3HT-b-P3BrHT) (338 mg)was placed in a 100 mL round bottom flask with anhydrous DMF. 2 g of sodium azide added to flask. Flask was purged with argon on schlenk line then heated to reflux overnight. Flask was cooled to room temperature and poured into 200 mL methanol. Polymer was filtered and washed with methanol in a soxhulet and extracted with chloroform then solvent was removed to yield **7.2**(P3HT-b-P3N$_3$HT) (290 mg). ^{1}H NMR (400 MHz, $CDCl_3$): 6.99 (s, 1H), 3.29 (t, 2H), 2.82 (t, 2H), 1.72 (m, 2H), 1.64 (m, 2H), 1.56 (m, 2H), 1.46 (m 2H), 1.36 (m, 2H), 1.27 (m, 2H), 0.92 (t, 3H).

Synthesis of 7.3(P3HT-b-P3C$_{60}$HT).

Scheme 6. BCP polymerization of **7.3**(P3HT-b-P3C$_{60}$HT).

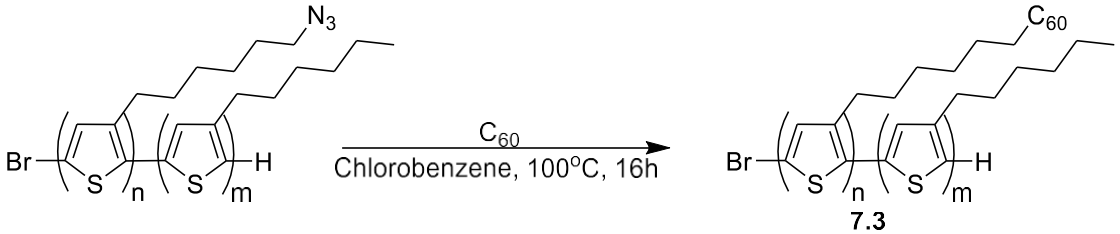

7.3

7.2(P3HT-b-P3N_3HT) (290 mg) was added to a 3-neck round bottom flask with anhydrous chlorobenzene under argon. An excess C_{60} (260 mg) was added to the flask and argon was bubbled through for 20 min. The reaction was heated to 100 °C overnight then cooled. It was washed with water once and then dried with anhydrous sodium sulfate. Solvent was removed via rotovap and the polymer was diluted in THF. The product was hot filtered via suction filtration to remove unbound C_{60} then solvent was removed again. This process was repeated 3 times and final polymer was dried under vacuum overnight Yield (110 mg). ^{1}H NMR (400 MHz, $CDCl_3$): 6.99 (s, 1H), 2.82 (t, 2H), 2.52 (m, 2H), 1.72 (m, 2H), 1.61 (m, 2H), 1.36 (m, 2H), 0.90 (m, 3H).

7.2.2 Cell Preparation

Organic Co-Crystal Solution Preparation.

7.3(P3HT-b-P3HC_{60}T) was dissolved by 1,2-dichlorobenzene (1,2-DCB), then BCP solution is used to dissolve thiophene to form 20 mg/mL concentration thiophene solution, and the fullerene was added into the solution at the weight ratio fullerene:thiophene 1:1. After 10 hours of stirring, acetonitrile was added into the mixed solution (10% in volume) followed by a low power sonication (45 minutes) wherein the solution became a dark purple. The solution then was aged in the dark under nitrogen for 2 days.

Device Fabrication

Indium tin oxide (ITO) glass substrates were cleaned then coated with poly(3,4-etylenediaminedioxythiophene) polystyrene sulfonate (PDOT:PSS) by spin coating at in a nitrogen glovebox for 1 minute at 3600 rpm. Solvent annealing took place in a sealed container after 1 day then the cells were baked at 150°C for 10 minutes. The crystal solution active layer

was applied by spin coating at 2000 rpm for 1 minute after which Aluminum electrodes were applied via thermal evaporation.

7.3.0 Results and Discussion

The interest for this project had a two-pronged approach. First, a series of C_{60}-linked P3HT block copolymers, **7.3**(P3HT-b-P3C_{60}HT), were synthesized with variable ratios of P3HT to C_{60}-linked P3HT. The ratio that yielded the greatest degree of nanowires was decerned by morphological analysis after which **7.3**(P3HT-b-P3C_{60}HT) was applyed as a compatibalizing agent**7.3** for growth of large room temperature multiferroic charge transfer co-crystals.

7.3.1 BCP Synthesis and Characterization

Synthesis of **7.3**(P3HT-b-P3HC_{60}T) was accomplished a method published by Chan and coworkers.[1] The **7.a**($Br_2$3HT) monomer was polymerized first into a quasi-living chain by Grignard metathesis (GRIM), then the second Grignard prepared **7.c**($Br_2$3BrHT) monomer was introduced to the living chain and grew off of it allowing for two distinct blocks. Block ratio was controlled by adjusting the molar feed ratio of the monomers for both **7.a**($Br_2$3HT) and **7.c**($Br_2$3BrHT). The resulting block ratios observed were found to be close to the input molar ratios of each monomer. The polymer that deviated the most was that of the 9% obtained **7.3**(P3HT-b-P3HC_{60}T) polymer, where the feed ratio was at 15% (Table 1) which was monitored by ^{1}H NMR integrations of the terminal CH_3 on the P3HT block at 0.92 ppm and the Br adjacent CH_2 at 3.42 ppm on the P3C_{60}HT. Functionalized block composition higher than 30% C_{60}-functionalized block was briefly explored but was abandoned. This was due to a higher degree of crosslinking and insolubility in these blocks especially after post-polymerization reactions, which made for less homogenous coatings.

Table 1. Resultant functionalized block composition based on molar feed ratios for **7.c**($Br_2$3BrHT). and **7.a**($Br_2$3HT) monomers.

Functionalized block ratios	**7.c**($Br_2$3BrHT) feed	**7.a**($Br_2$3HT) feed
30%	1.23 mmols	2.50 mmols
20%	0.74 mmols	2.96 mmols
9%	0.61 mmols	3.22 mmols
5%	0.25 mmols	3.20 mmols

Hot filtration of the polymer in the final synthetic step removes any untethered C_{60} leaving only the desired **7.3**(P3HT-b-P3HC_{60}T) product.[7] The UV-Vis spectra in Figure 2 confirm the presence of both C_{60}, with the peak at 330 nm, and P3HT, at 450 nm, in each of the **7.3**(P3HT-b-P3HC_{60}T) polymers. The BCP with the larger ratios of C_{60} functionalized block produced a stronger C_{60} peak at 330 nm.

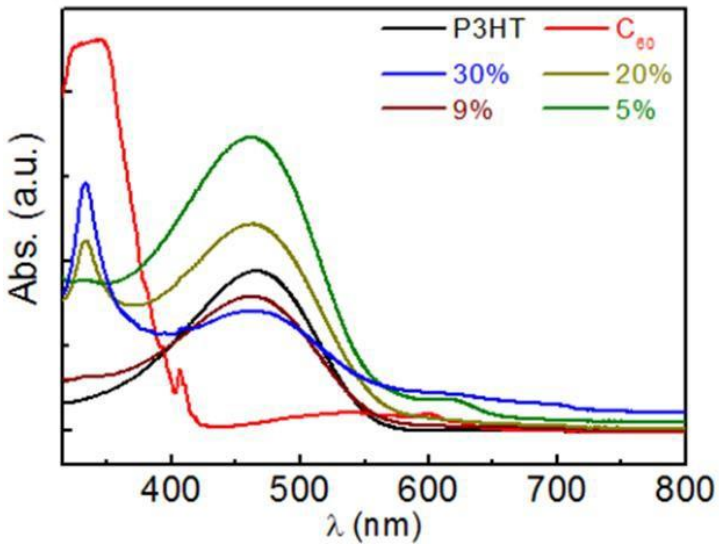

Figure 2. UV-Vis absorption spectra of BCP **7.3**(P3HT-b-P3HC_{60}T) at 5%, 9%, 20%, and 30%, pure P3HT, and pure C_{60} in chloroform.

Thin films of the polymers were prepared by creating 10 mg/mL solutions of the polymers which were then spin-coated onto silicon substrates then thermally annealed at 150°C. During preparation of the substrates it was noted that the polymer coatings with the higher ratios of C_{60} blocks set down as less uniform thin films with aggregate artifacts. This is likely due to a slightly higher degree of cross linking and aggregation.

Contact mode AFM of the 9%, 20% and 30% C_{60}-functionalized block ratio polymers showed the appearance of nanostructures in the form of nanowires, as has been reported in other all-conjugated BCP systems.[1-2, 6] The 9% **7.3**(P3HT-b-P3HC_{60}T) ratio displayed a dense and well-defined network of nanowires having a desirable narrow domain width of around 30 nm (Figure 3). The 20% and 30% ratios exhibited more scare networks that were thicker in width. It was also observed that the 30% BCP produced less uniform films with larger artifacts on this surface. This was likely due to enhanced crosslinking between BCP chains with increased functionalized blocks. Due to the higher density of microstructures in the 9% BCP and the uniform film coatings, it was the block ratio used in continued cocrystalization experiments.

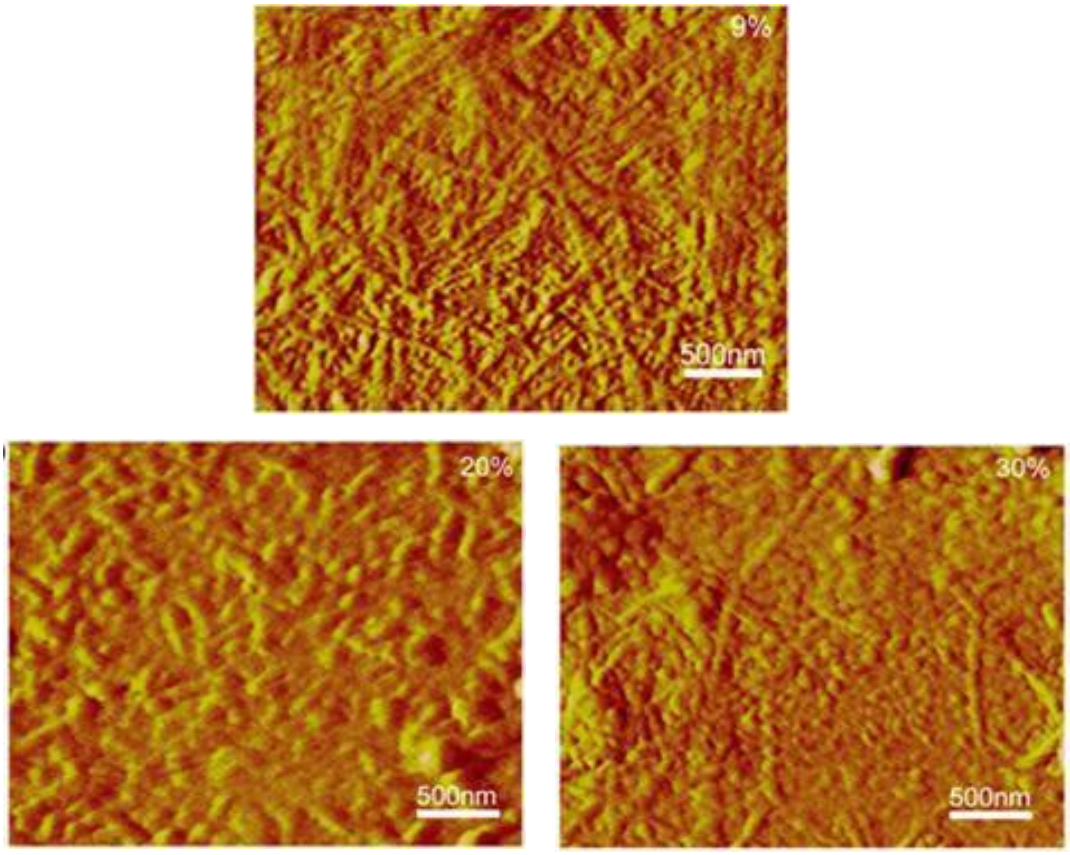

Figure 3. AFM phase images from 9%, 20%, and 30% BCP **7.3**(P3HT-b-P3HC$_{60}$T) polymer thin films.

7.3.2 Co-Crystallization

A 20 mg/mL solution of P3HT in 1,2-dichlorobenzene was prepared and a 1:1 mass equivalent of C_{60} was added to the solution. Using the 9% **7.3**(P3HT-b-P3HC$_{60}$T) BCP as a compatibilizer, solutions were prepared with dopant ratios of 0, 0.1, 0.15, and 0.5 into the P3HT:C_{60} mixture. The resultant solution was stirred for 10 hours in the dark within a nitrogen glovebox. After stirring, acetonitrile was added into the solution as 10% of the solution volume to induce an aggregation of the P3HT, BCP, and C_{60} components. Sonication for 45 minutes allowed the breakup of aggregates, and the solution was then permitted to stand and age in the glovebox for 2 days which cause a slow ordering of aggregates into cocrystal seeds.

The crystalline component solutions were then spin-coated onto silicon substrates and thermally annealed. In Table 2 the variation in crystal size with the different BCP dopant ratios is reported. The crystal aggregates obtained without the addition of the BCP dopant were of an average size of 8 μm in length with an aspect ratio of 3.4, whereas the highest dopant ratio yielded a lower density of crystals an average length of 14.7 μm and aspect ratio of 3.6. After 0.15 ratio of dopant was added there was a stagnation of growth in length at that point and proved to only increase width and thickness in subsequent larger dopant ratios yielding a lower density of crystals.

Table 2. Crystal dimensions at different BCP dopant ratios **7.3**(P3HT-b-P3HC$_{60}$T) to P3HT:C$_{60}$ mixed.*

BCP ratio	Length (μm)	Width (μm)	Thickness (μm)
0.00	8.00	2.30	0.37
0.10	8.80	2.30	0.51
0.15	14.60	3.50	0.73
0.50	14.70	3.98	0.77

Micron scale sized crystals formed in the aggregate solution after sonication induced ordering which is seen in the optical microscope image in Figure 4. These large crystals, when analyzed by TEM, reveal an internal component made up of a high density of nanowires.

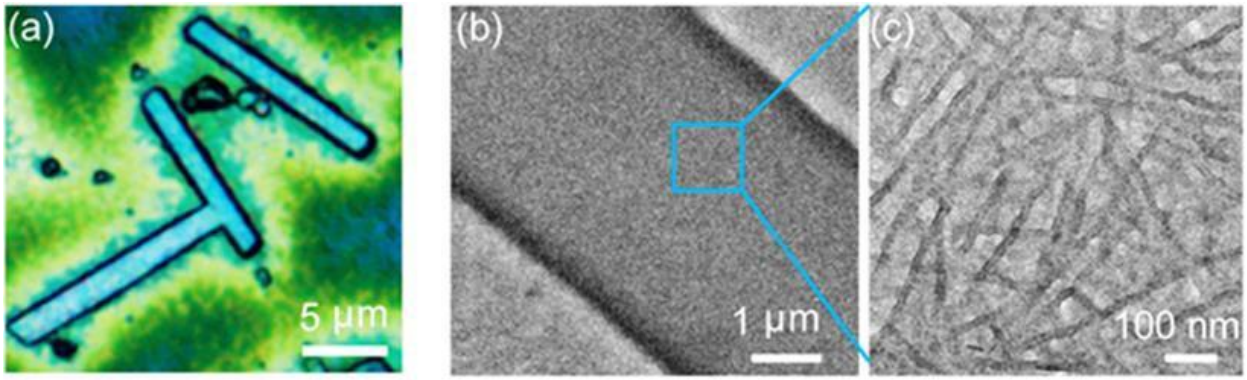

Figure 4. Optical microscope image of BCP doped P3HT:C_{60} crystals (a) and TEM images of crystal (b) with expansion showing component nanowires within large co-crystals (c).[5]*

7.3.3 BCP Co-Crystal Devices

PV cells were made by spin coating the BCP doped P3HT:C_{60} active layer on a layer of PEDOT:PSS as a hole blocking layer on ITO glass upon (Figure 5a). J-V curve revealed that the cocrystal solution with the BCP dopant produced an improvement in power conversion efficiency (PCE) when compared with the previous charge transfer crystals reported by Wei Qin in the Ren group without the use of the BCP dopant.[4] The fill factor and J_{SC} of the device is substantially improved as evidenced by the *JV* curve. This led to a PCE of 0.46% that was obtained with 0.15 BCP dopant ratio in the crystal (Figure 5b). When this is compared with BHJ composite cells of P3HT:PCBM that have previously shown PCE of ~ 5%, it is clearly significantly lower in device efficiency. This is likely due to large recombination rates in the mixed domains.[8] However, the P3HT:C_{60}:BCP-doped cocrystals exhibited magnetoconductive properties that were not observed in typical BHJ cells of P3HT and C_{60} components.

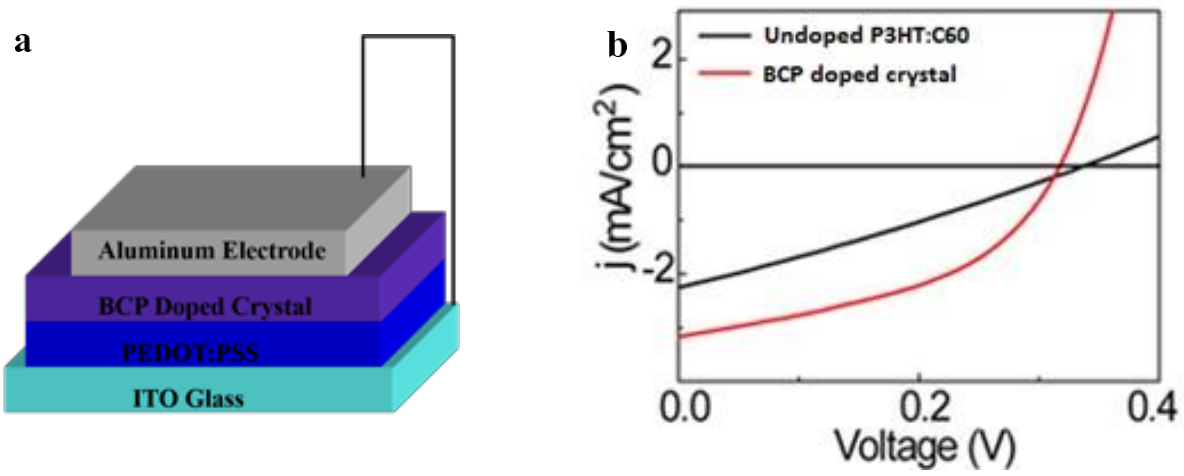

Figure 5. Diagram of cell composition (a) and a current density for the BCP doped crystal and the undoped P3HT:C_{60} crystal (b).[5]*

The **7.3**(P3HT-b-P3HC_{60}T)-doped cocrystal devices demonstrated a unique ability for the current produced in the cell to be modulated in the influence of a small external magnetic field. The large interface and ordering of crystalline domains within the BCP-doped cocrystal produce a gratuitous amount of CTs whose singlet to triplet ratio can be tuned with the application of an external magnetic field. This is shown by Equation 1 where MC is defined by the change in current under an external magnetic field in comparison to the unaltered current production of the cell.

$$MC(H) = \frac{[J(H) - J(0)]}{J(0)} \qquad \textbf{\textit{Eq 1.}}$$

With an increase in triplet charge transfers, the longer lifetimes of the CTs can induce scattering of charge carriers, thus lowering produced current.[9-11] This is exemplified in a negative MC at the application of 1000 Oe as seen in Figure 7. The MC was found to be greater than that of the CTC without BCP dopant that was reported by Qin.[4] While the undoped CTC crystals

were organized into segregated stacks, the BCP doped crystals allowed for co-crystallization of the P3HT and C_{60} together, providing a greater interface between the two.

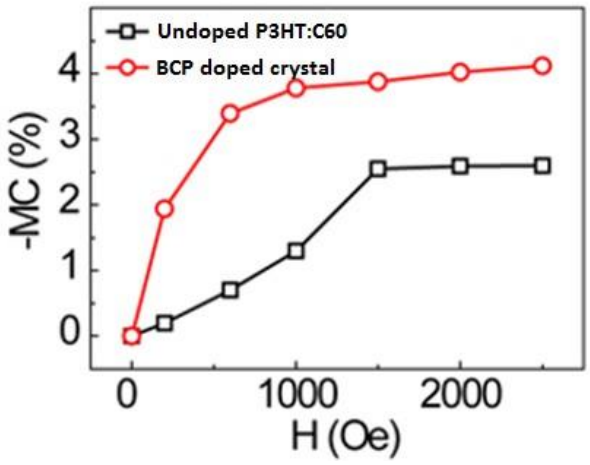

Figure 6. MC effect from an external magnetic field on BCP doped co-crystal vs undoped P3HT:C_{60} CTC crystal.[5]*

7.3.4 BCP:C_{60} Crystal Growth

P3HT:C_{60} BHJ photovoltaic devices are typically fabricated in a 1:1 weight ratio composition. To further investigate some of the previously mentioned co-crystallizations, we looked at the crystal growth of only BCP:C_{60} systems. BCP:C_{60} were mixed in a 1:1 weight ratio and stirred in 1,2-DCB for 10 hours, aggregated with acetonitrile and sonicated for ordering. An initial sample was drop-cast onto silicon substrates and thermally annealed at 150°C for 10 minutes. The AFM of the initial phase crystallization sample yielded hexagonal crystals of fairly uniform size. One possibility for this is that the polymer chains of the 9% **7.3**(P3HT-b-P3HC$_{60}$T) BCP are shorter than those of the P3HT homopolymer that was previously used in the BCP-

doped P3HT:C_{60} co-crystals. This likely affects the size and shape of crystals when the BCP is cocrystalized alone with C_{60}.

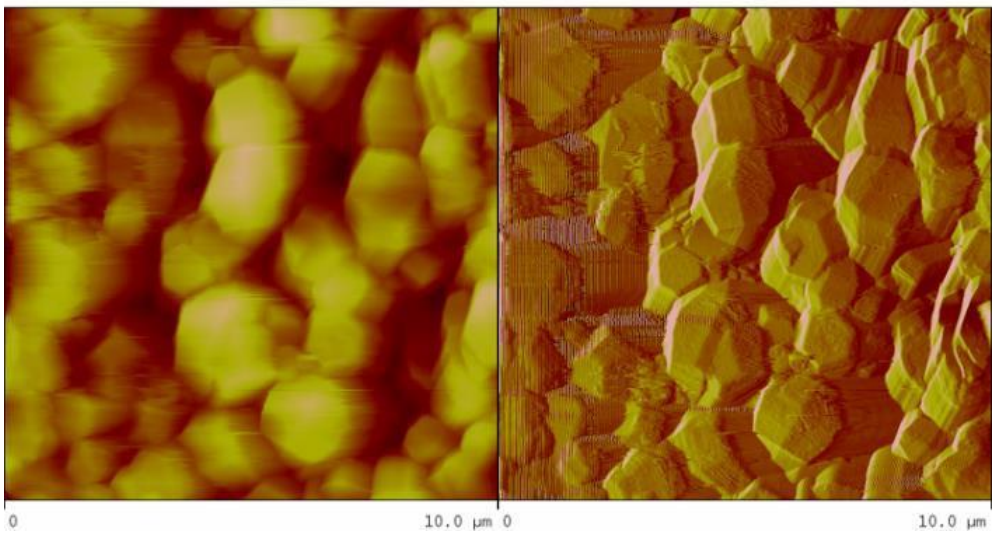

Figure 7. AFM of thermal annealed **7.3**(P3HT-b-P3HC_{60}T)**:C_{60}** thin films.

The resultant solution was aged for two days then dropcast on silicon substrates. Slow solvent annealing in 1,2-DCB for 24 hours resulted induced a large scale crystal growth. Millimeter-sized crystals formed on the substrates that were visible to the naked eye as seen in Figure 9. Vapor pressure of 1,2-DCB propagated the extended ordering and crystal growth from the seed crystals seen in Figure 8. Further investigation into the large BCP-C_{60} co-crystals is required to determine their cell potential and the effect on MC.

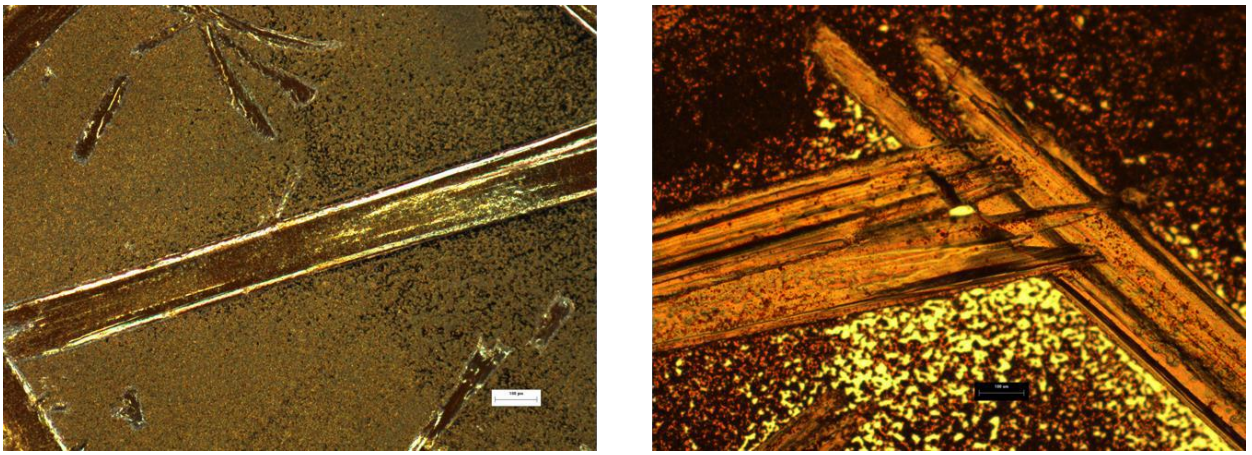

Figure 9. Optical microscope of a) dark field and b) light field large BCP-C_{60} crystals (scale bar 100 μm)

7.5.0 Conclusions

In this chapter, **7.3**(P3HT-b-P3HC_{60}T) BCP were synthesized and investigated for their self-assembly properties in co-crystallizations. 5%, 9%, 20%, and 30% block ratios of P3HT derivative were investigated for morphological properties. BCP-doped co-crystals were produced by aggregation and ordering techniques that resulted in the growth of large unsegregated co-crystals with P3HT and C_{60} with enhanced charge transfer capabilities. Though still low in comparison to BHJ composite cells, higher PEC were achieved in comparison to undoped P3HT:C_{60} CTCs. However, a truly interesting magnetoelectric property was observed wherein the organized BCP-doped charge transfer crystal exhibited tunability of device current by the application of an external magnetic field. This produced a negative MC which was greater than previous P3HT:C_{60} CTC results. It was also shown that hexagonal CTCs can be grown solely with short chains of **7.3**(P3HT-b-P3HC_{60}T) and C_{60} co-crystalized together. Furthermore, slow solvent annealing can propagate crystal growth to the millimeter scale producing macro CT crystals.

References

1. Chan, S.-H.; Lai, C.-S.; Chen, H.-L.; Ting, C.; Chen, C.-P., Highly Efficient P3HT: C_{60} Solar Cell Free of Annealing Process. *Macromolecules* **2011,** *44* (22), 8886-8891.
2. Miyanishi, S.; Zhang, Y.; Tajima, K.; Hashimoto, K., Fullerene Attached All-Semiconducting Diblock Copolymers for Stable Single-component Polymer Solar Cells. *Chemical Communications* **2010,** *46* (36), 6723-6725.
3. Ren, S.; Wuttig, M., Organic Exciton Multiferroics. *Advanced Materials* **2012,** *24* (6), 724-727.
4. Qin, W.; Chen, X.; Li, H.; Gong, M.; Yuan, G.; Grossman, J. C.; Wuttig, M.; Ren, S., Room Temperature Multiferroicity of Charge Transfer Crystals. *ACS Nano* **2015,** *9* (9), 9373-9379.
5. Qin, W.; Chen, X.; Lohrman, J.; Gong, M.; Yuan, G.; Wuttig, M.; Ren, S., External Stimuli Controlled Multiferroic Charge-Transfer Crystals. *Nano Research* **2016,** *9* (4), 925-932.
6. Zhang, Y.; Tajima, K.; Hirota, K.; Hashimoto, K., Synthesis of All-Conjugated Diblock Copolymers by Quasi-Living Polymerization and Observation of Their Microphase Separation. *Journal of the American Chemical Society* **2008,** *130* (25), 7812-7813.
7. Ruoff, R. S.; Tse, D. S.; Malhotra, R.; Lorents, D. C., Solubility of Fullerene (C_{60}) in a Variety of Solvents. *The Journal of Physical Chemistry* **1993,** *97* (13), 3379-3383.
8. Ma, W.; Yang, C.; Gong, X.; Lee, K.; Heeger, A. J., Thermally Stable, Efficient Polymer Solar Cells with Nanoscale Control of the Interpenetrating Network Morphology. *Advanced Functional Materials* **2005,** *15* (10), 1617-1622.
9. Janssen, P.; Cox, M.; Wouters, S. H. W.; Kemerink, M.; Wienk, M. M.; Koopmans, B., Tuning Organic Magnetoresistance in Polymer-Fullerene Blends by Controlling Spin Reaction Pathways. *Nature Communications* **2013,** *4*, 2286.
10. Qin, W.; Gao, K.; Yin, S.; Xie, S. J., Investigating the Magnetic Field Effect on Electron-Hole Pair in Organic Semiconductor Devices. *Journal of Applied Physics* **2013,** *113* (19), 193901.
11. Hu, B.; Wu, Y., Tuning Magnetoresistance between Positive and Negative Values in Organic Semiconductors. *Nature Materials* **2007,** *6* (12), 985-991.

Appendix A:
NMR Spectra

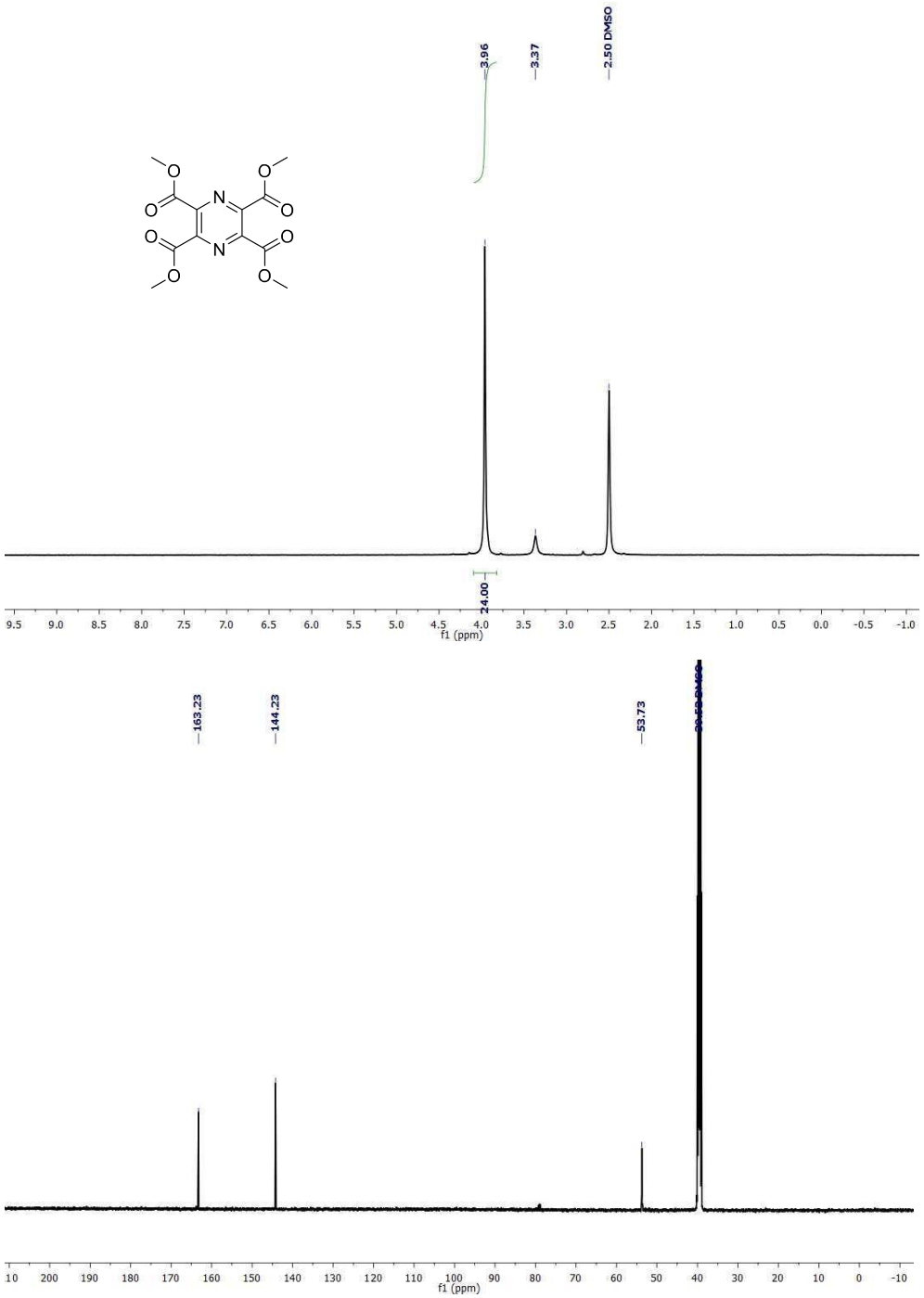

Figure A1. ^{1}H NMR (500 MHz, DMSO-d_6) (top) and ^{13}C NMR (125 MHz, DMSO-d_6) (bottom) of pyrazine-2,3,5,6-tetracarboxylate, **2.a**.

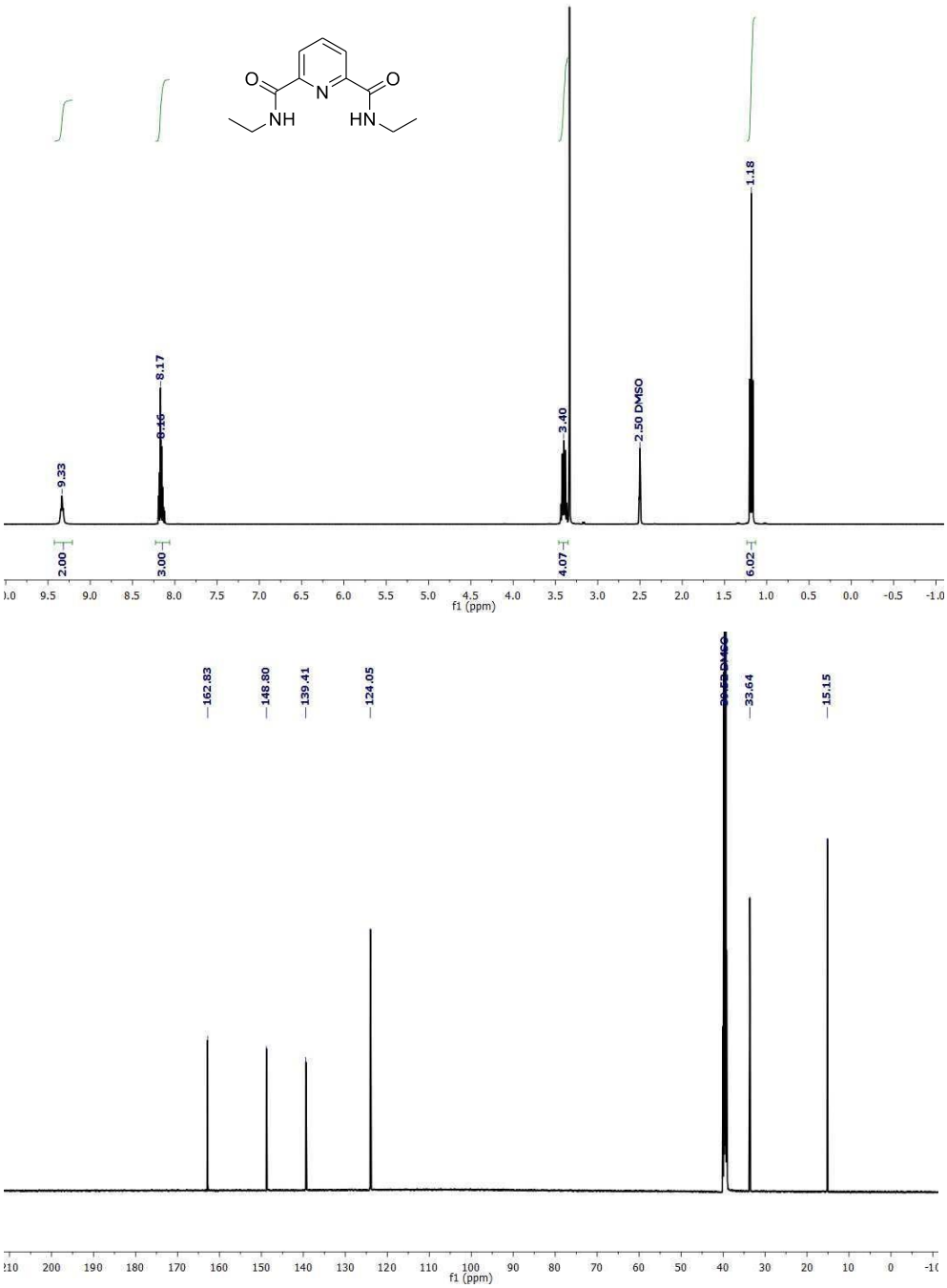

Figure A2. ^{1}H NMR (500 MHz, DMSO-d_6) (top) and ^{13}C NMR (125 MHz, DMSO-d_6) (bottom) of **2.1**(DiEt).

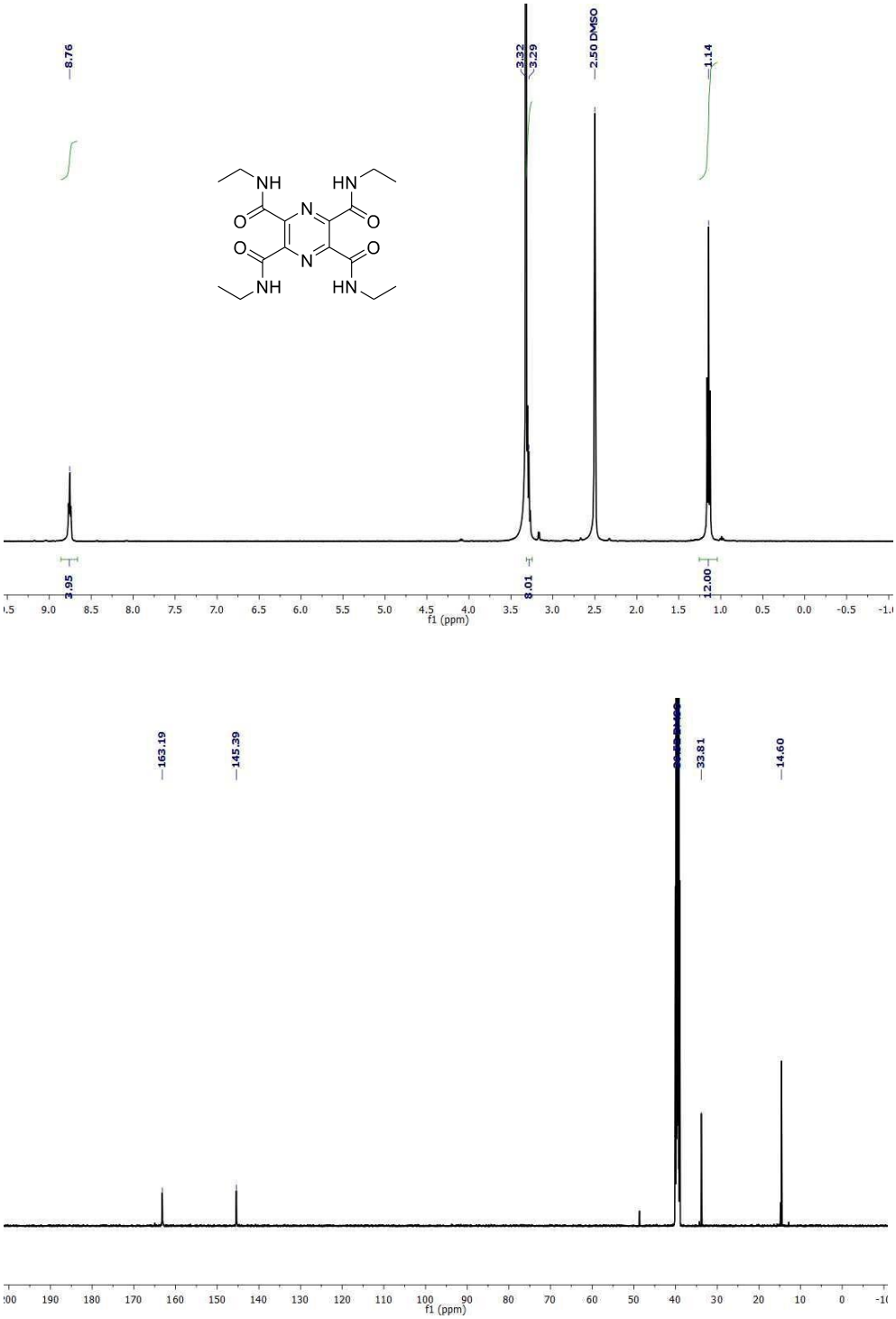

Figure A3. ^{1}H NMR (500 MHz, DMSO-d_6) (top) and ^{13}C NMR (125 MHz, DMSO-d_6) (bottom) of **2.2**(TetraEt).

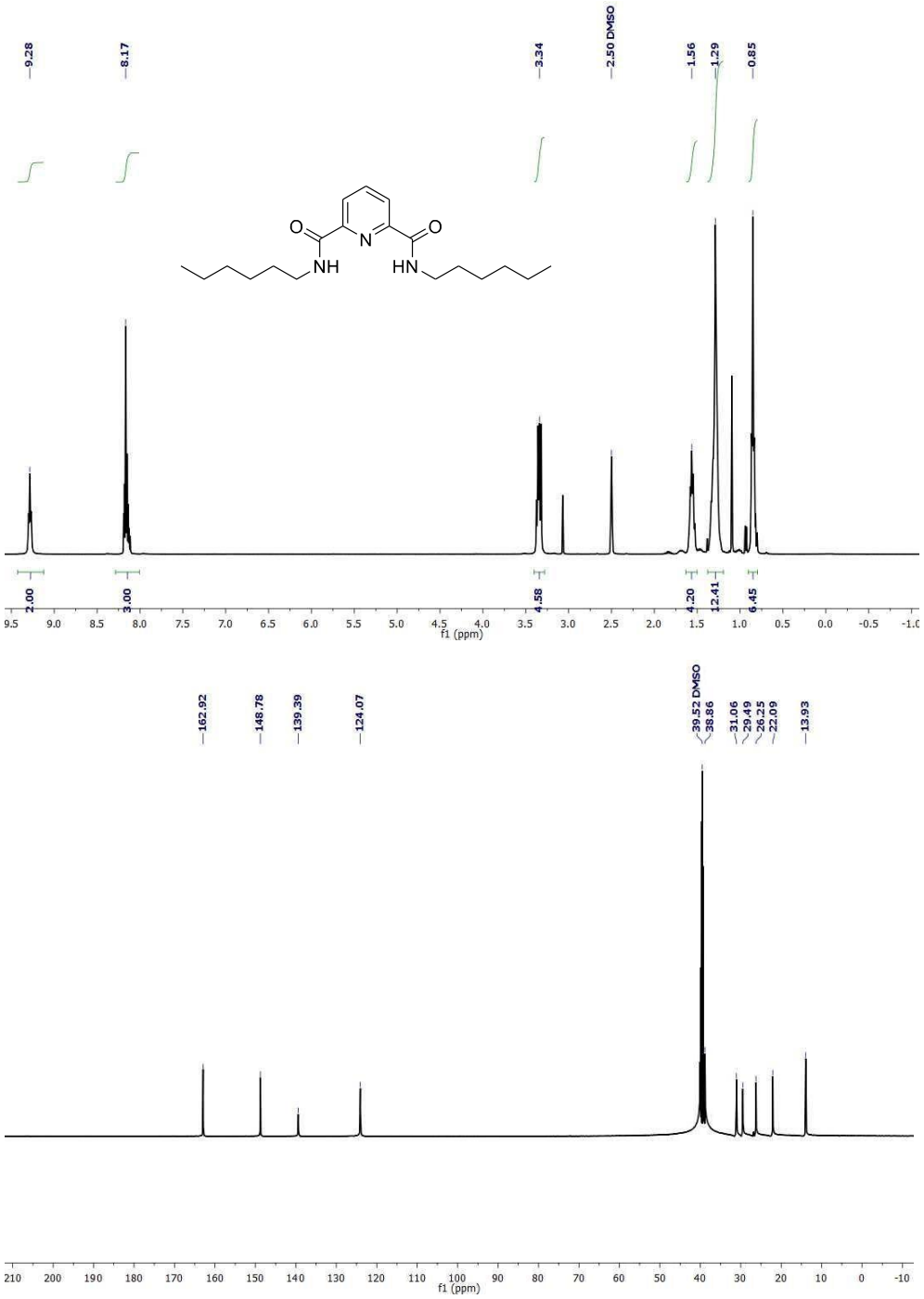

Figure A4. ^{1}H NMR (500 MHz, DMSO-d_6) (top) and ^{13}C NMR (125 MHz, DMSO-d_6) (bottom) **2.3**(DiHex).

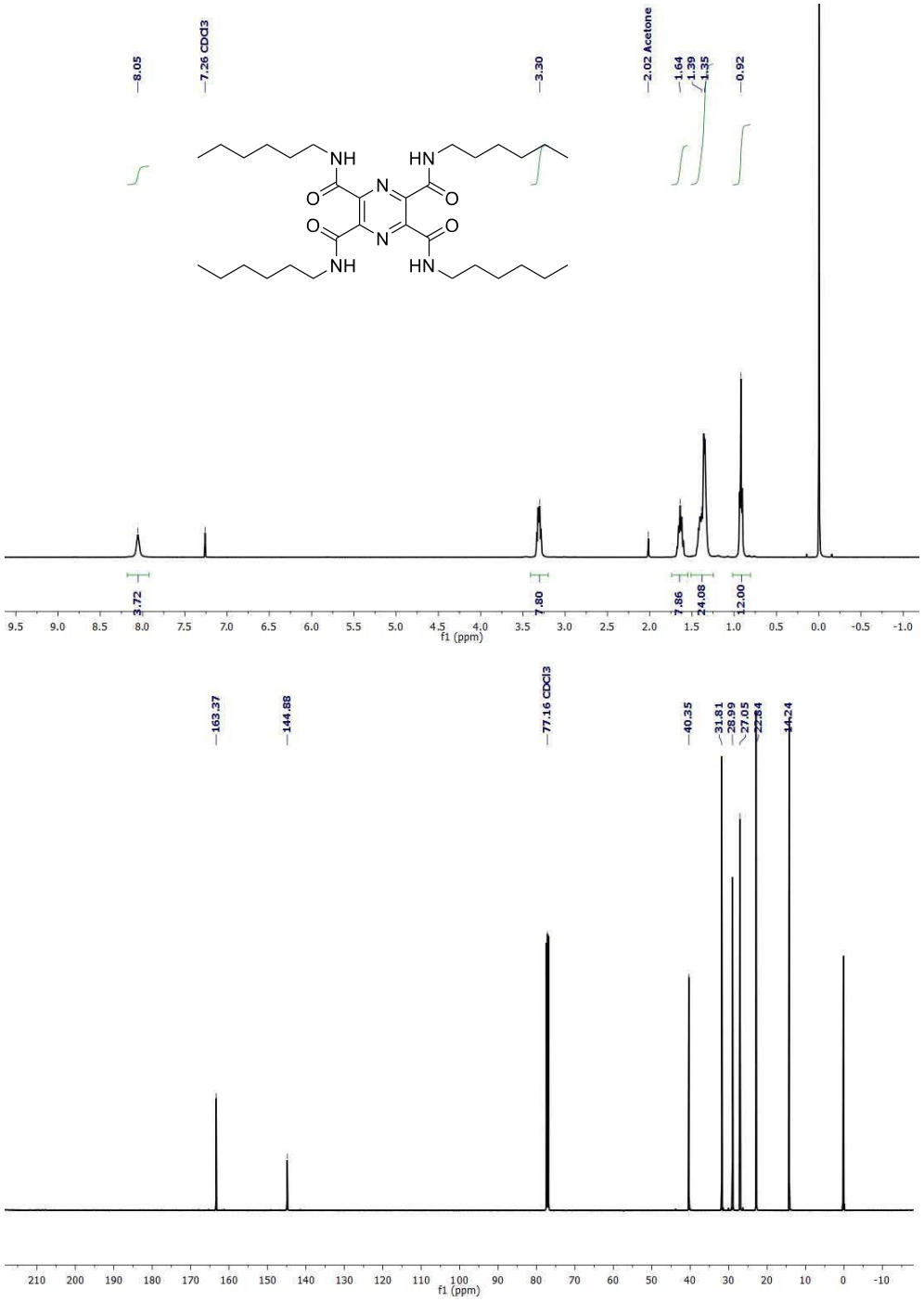

Figure A5. ^{1}H NMR (500 MHz, DMSO-d_6) (top) and ^{13}C NMR (125 MHz, DMSO-d_6) (bottom) **2.4**(TetraHex).

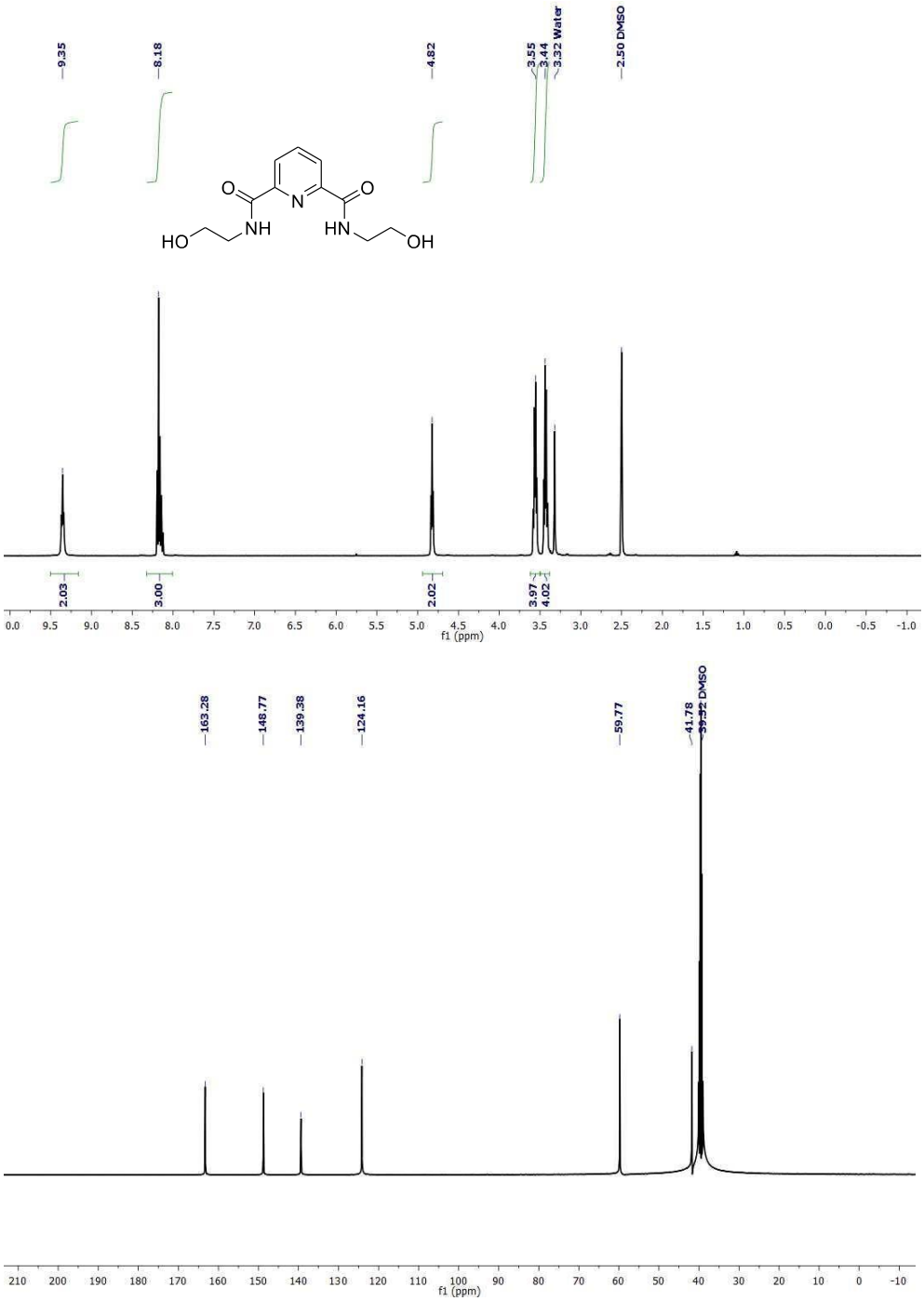

Figure A6. ^{1}H NMR (500 MHz, DMSO-d_6) (top) and ^{13}C NMR (125 MHz, DMSO-d_6) (bottom) of **2.5**(DiEtOH).

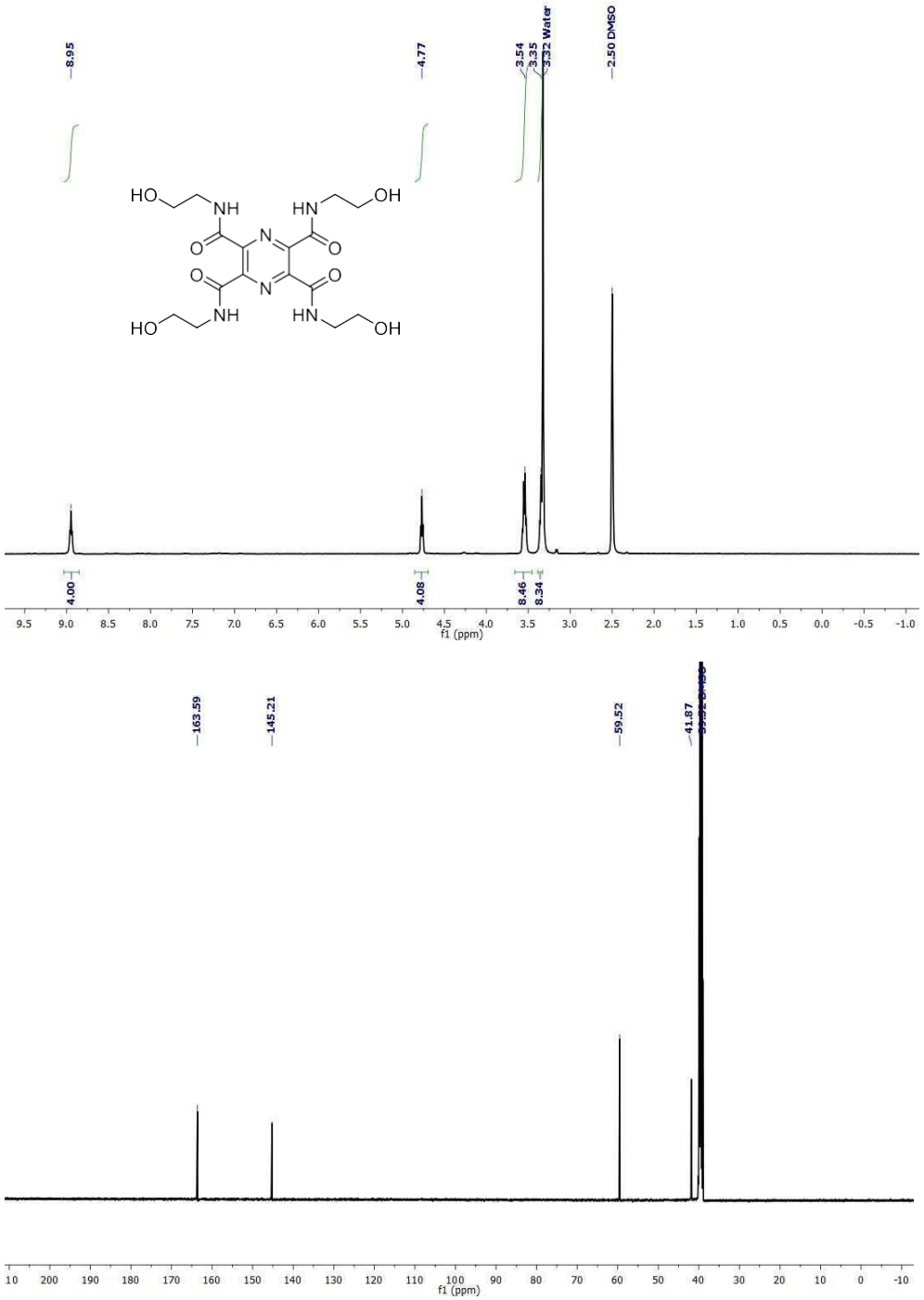

Figure A7. ^{1}H NMR (500 MHz, DMSO-d_6) (top) and ^{13}C NMR (125 MHz, DMSO-d_6) (bottom) of **2.6**(TetraEtOH)**.**

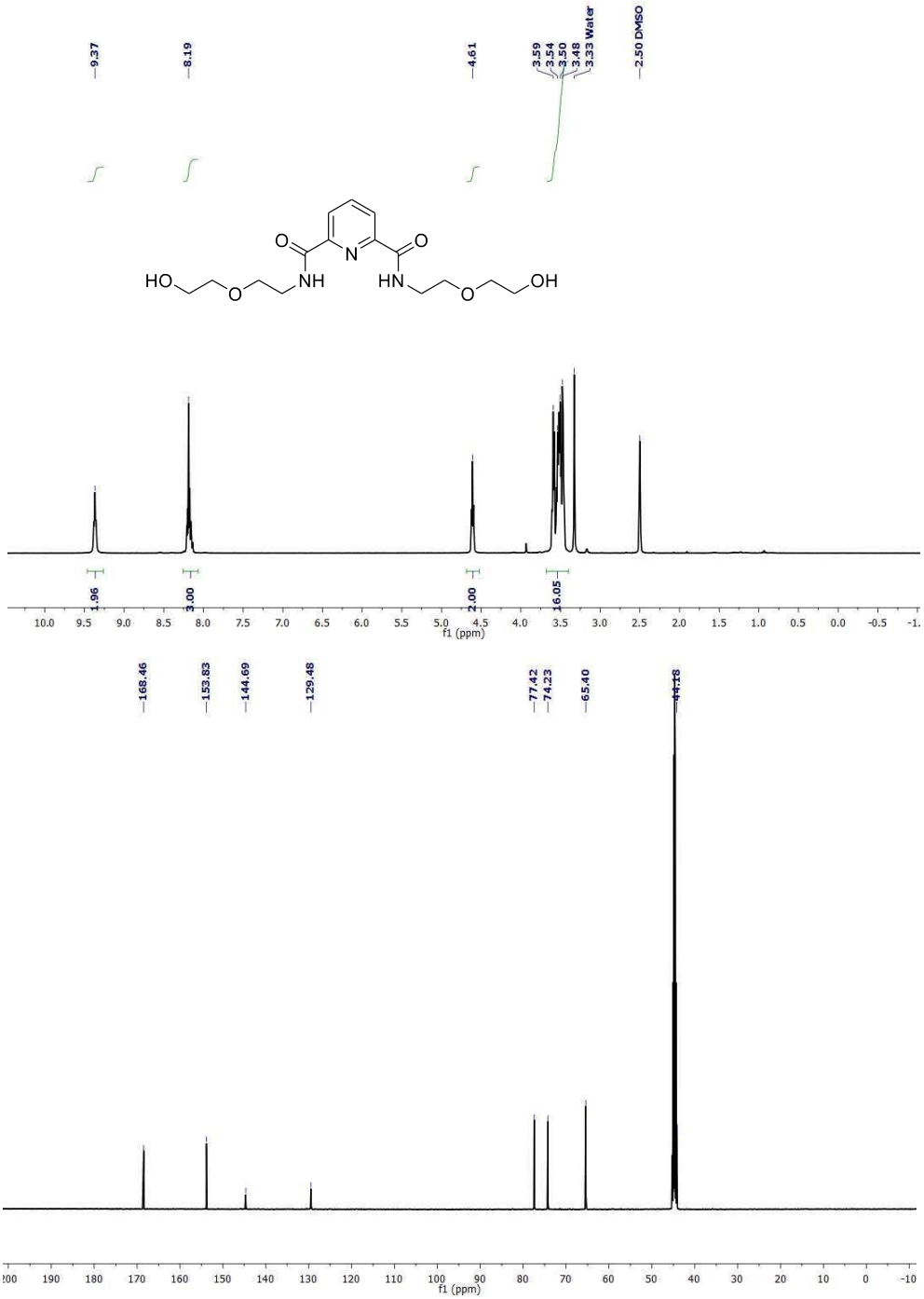

Figure A8. ^{1}H NMR (500 MHz, DMSO-d_6) (top) and ^{13}C NMR (125 MHz, DMSO-d_6) (bottom) of **2.7**(DiGly)**.**

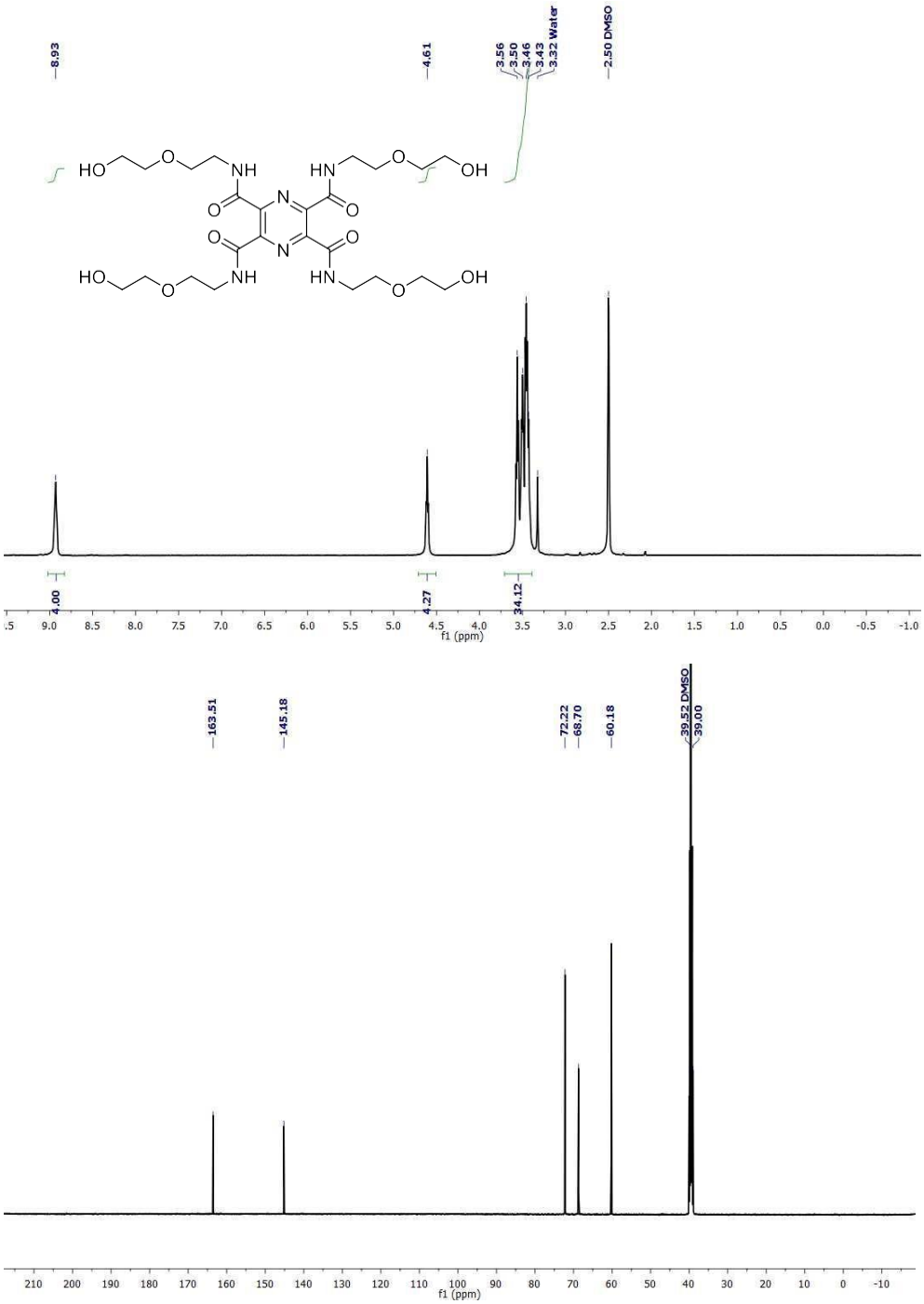

Figure A9. ^{1}H NMR (500 MHz, DMSO-d_6) (top) and ^{13}C NMR (125 MHz, DMSO-d_6) (bottom) of **2.8**(TetraGly)**.**

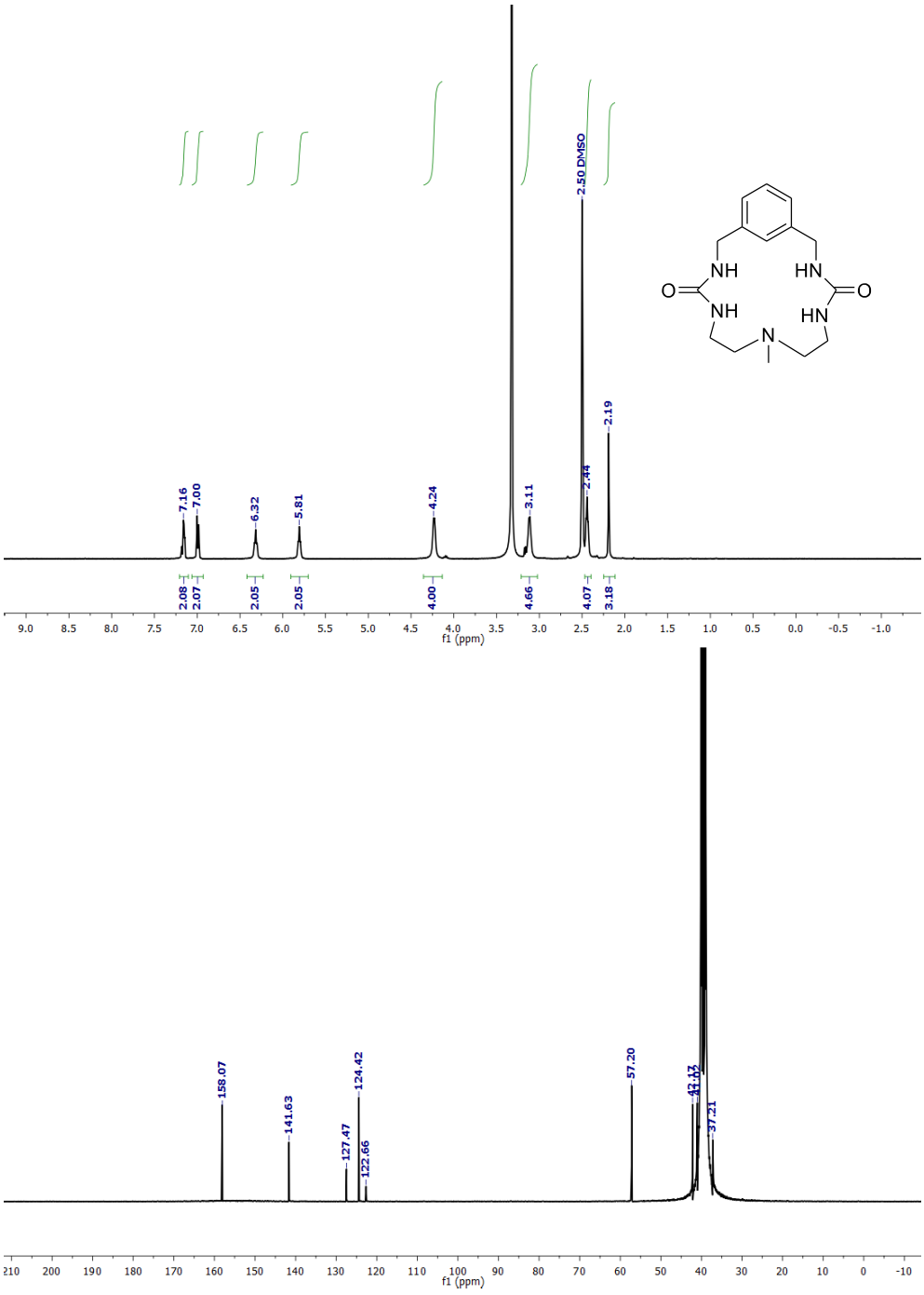

Figure A10. ^{1}H NMR (500 MHz, DMSO-d_6) (top) and ^{13}C NMR (125 MHz, DMSO-d_6) (bottom) of **3.1.**

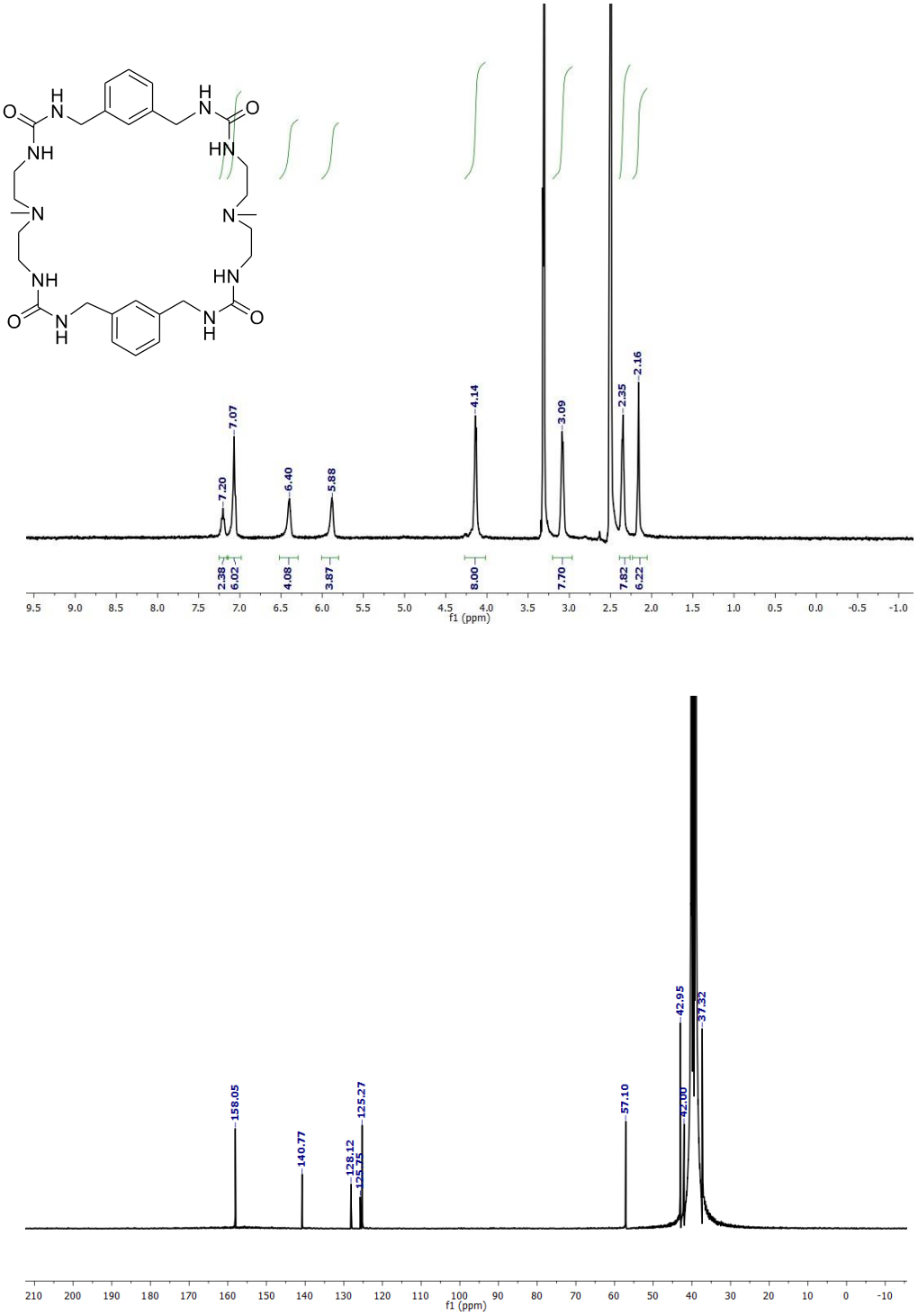

Figure A11. ^{1}H NMR (500 MHz, DMSO-d_6) (top) and ^{13}C NMR (125 MHz, DMSO-d_6) (bottom) of **3.2.**

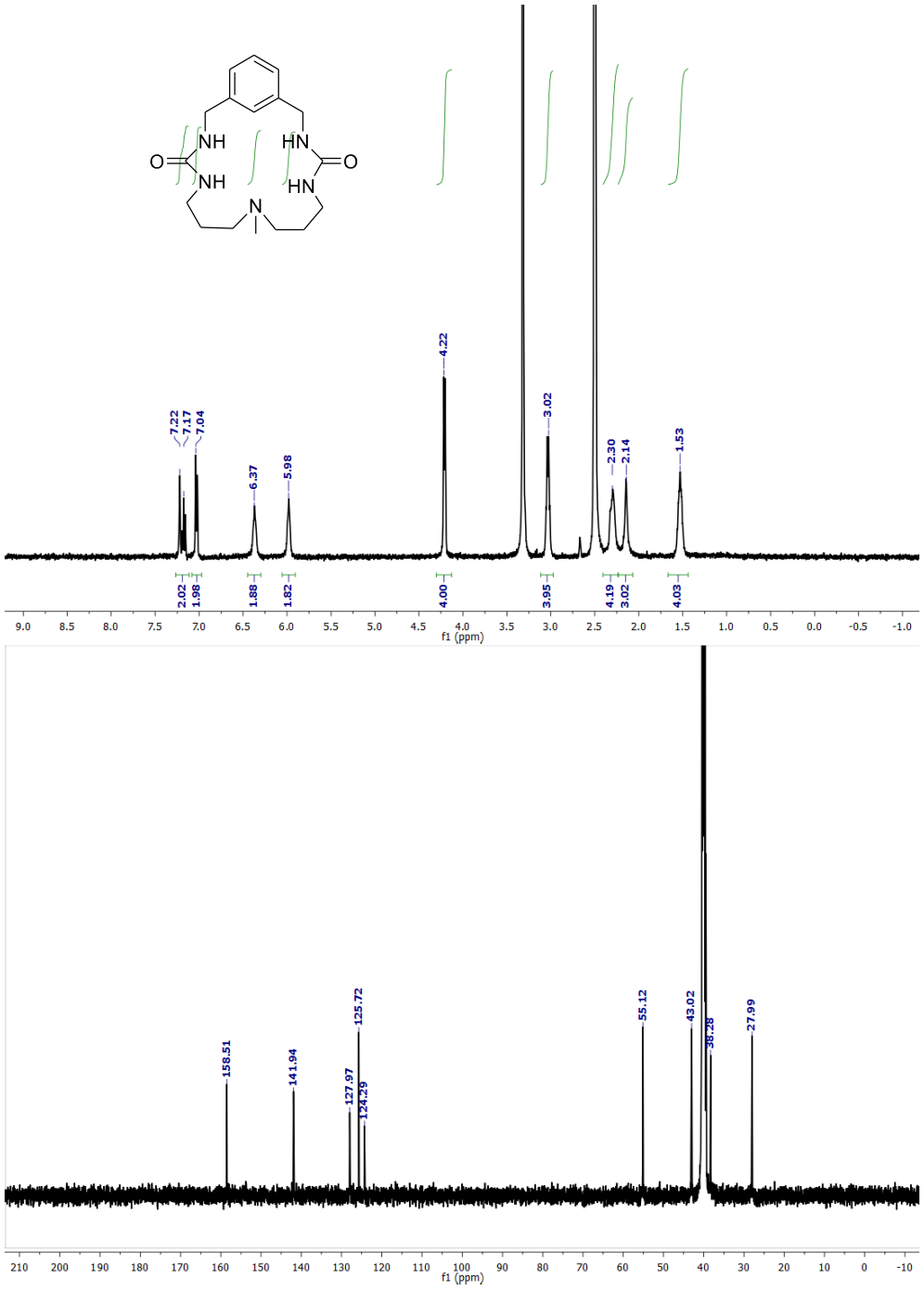

Figure A12. ^{1}H NMR (500 MHz, DMSO-d_6) (top) and ^{13}C NMR (125 MHz, DMSO-d_6) (bottom) of **3.3**.

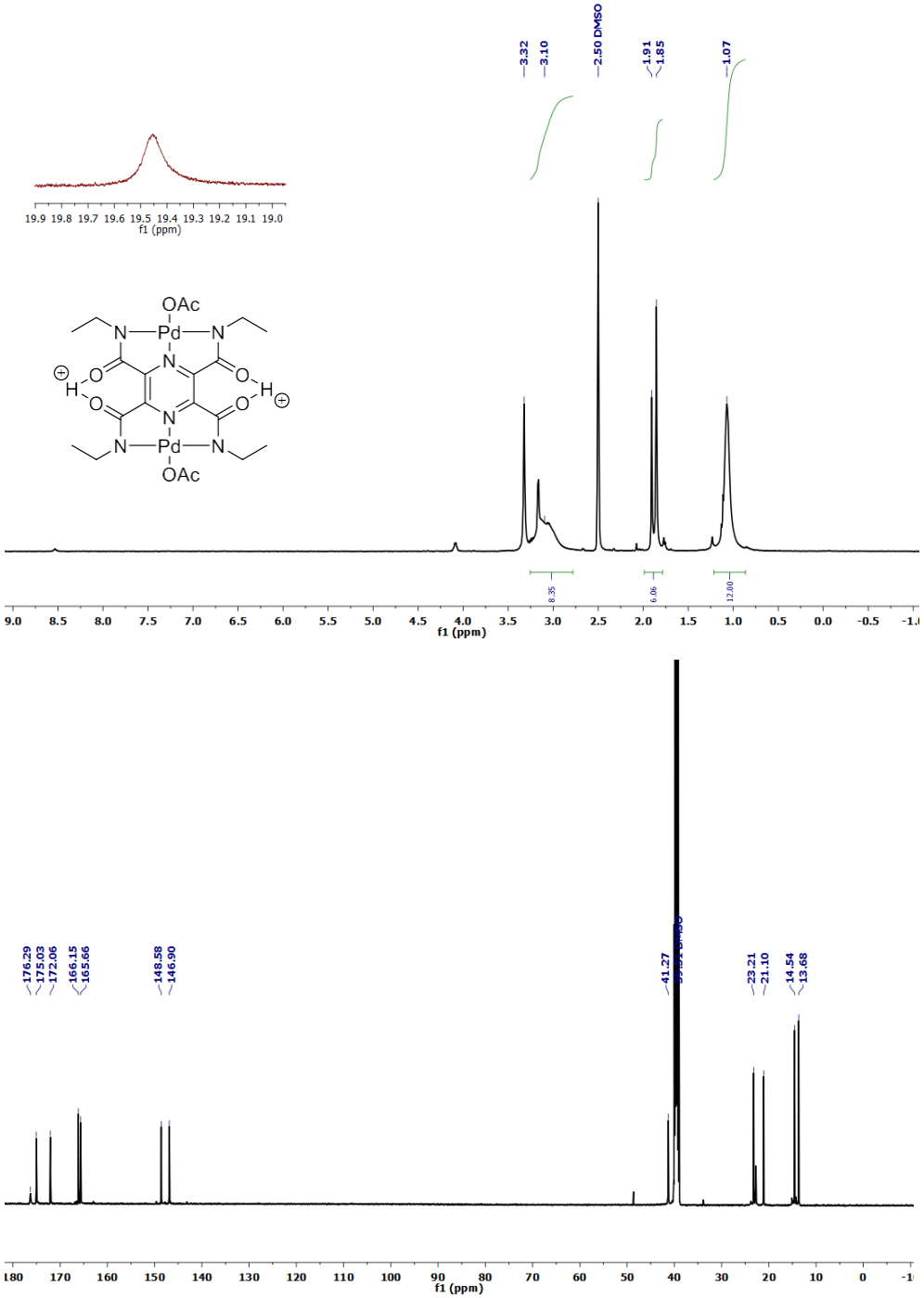

Figure A13. ^{1}H NMR (500 MHz, DMSO-d_6) (top) and ^{13}C NMR (125 MHz, DMSO-d_6) (bottom) of **5.1.**

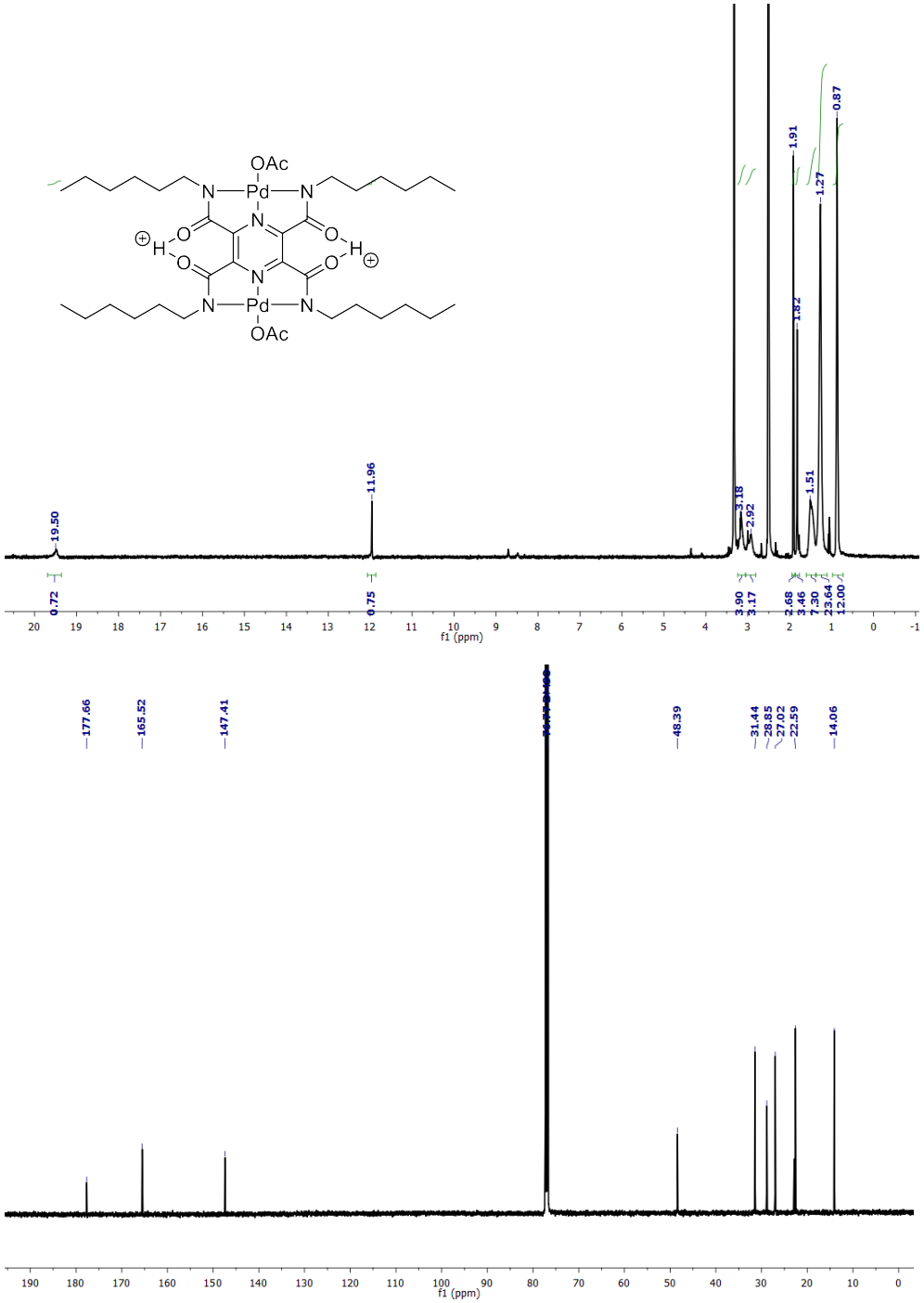

Figure A14. ^{1}H NMR (500 MHz, DMSO-d_6) (top) and ^{13}C NMR (125 MHz, DMSO-d_6) (bottom) of **5.2.**

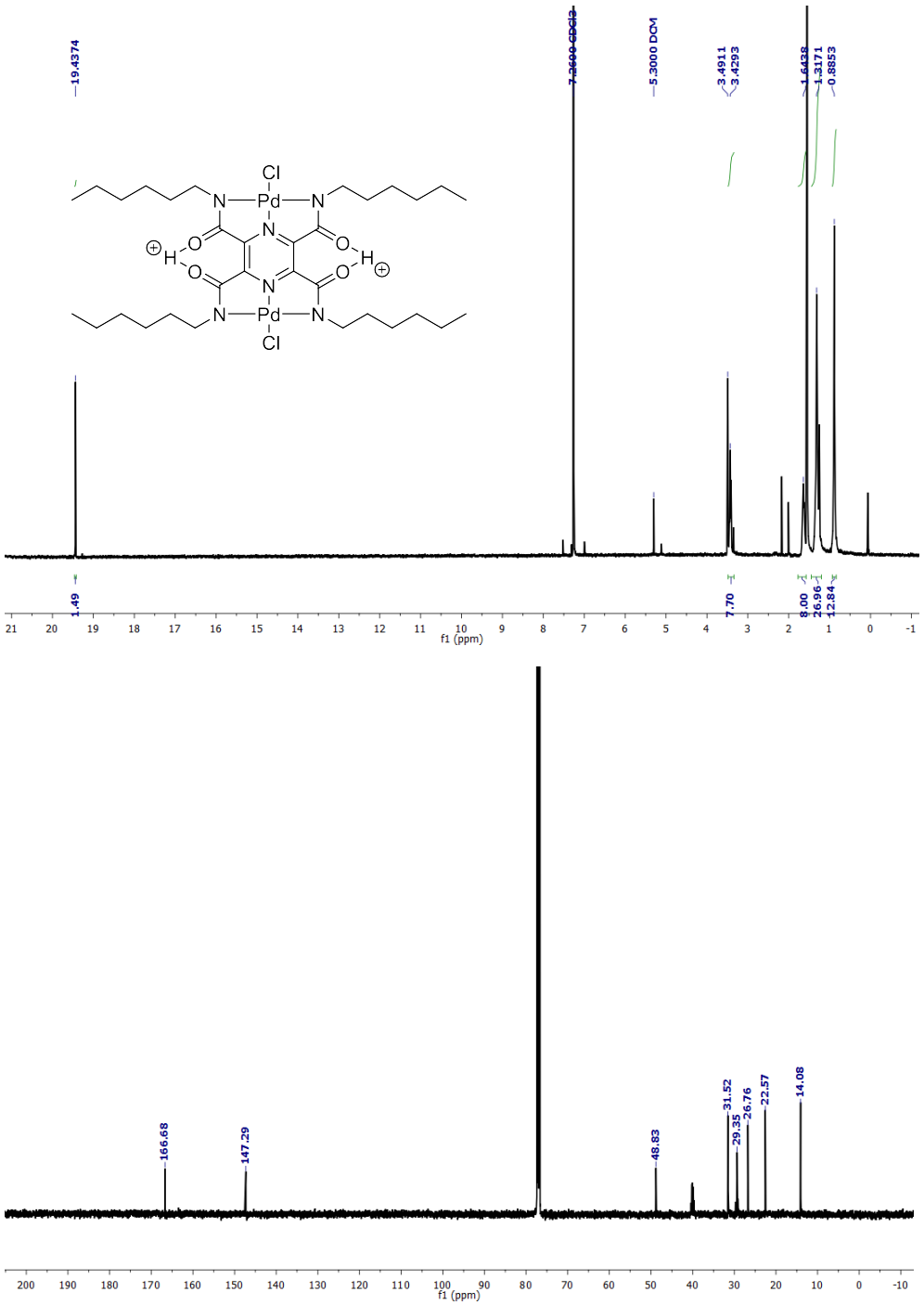

Figure A15. ^{1}H NMR (500 MHz, $CDCl_3$) (top) and ^{13}C NMR (125 MHz, $CDCl_3$) (bottom) of **5.3.**

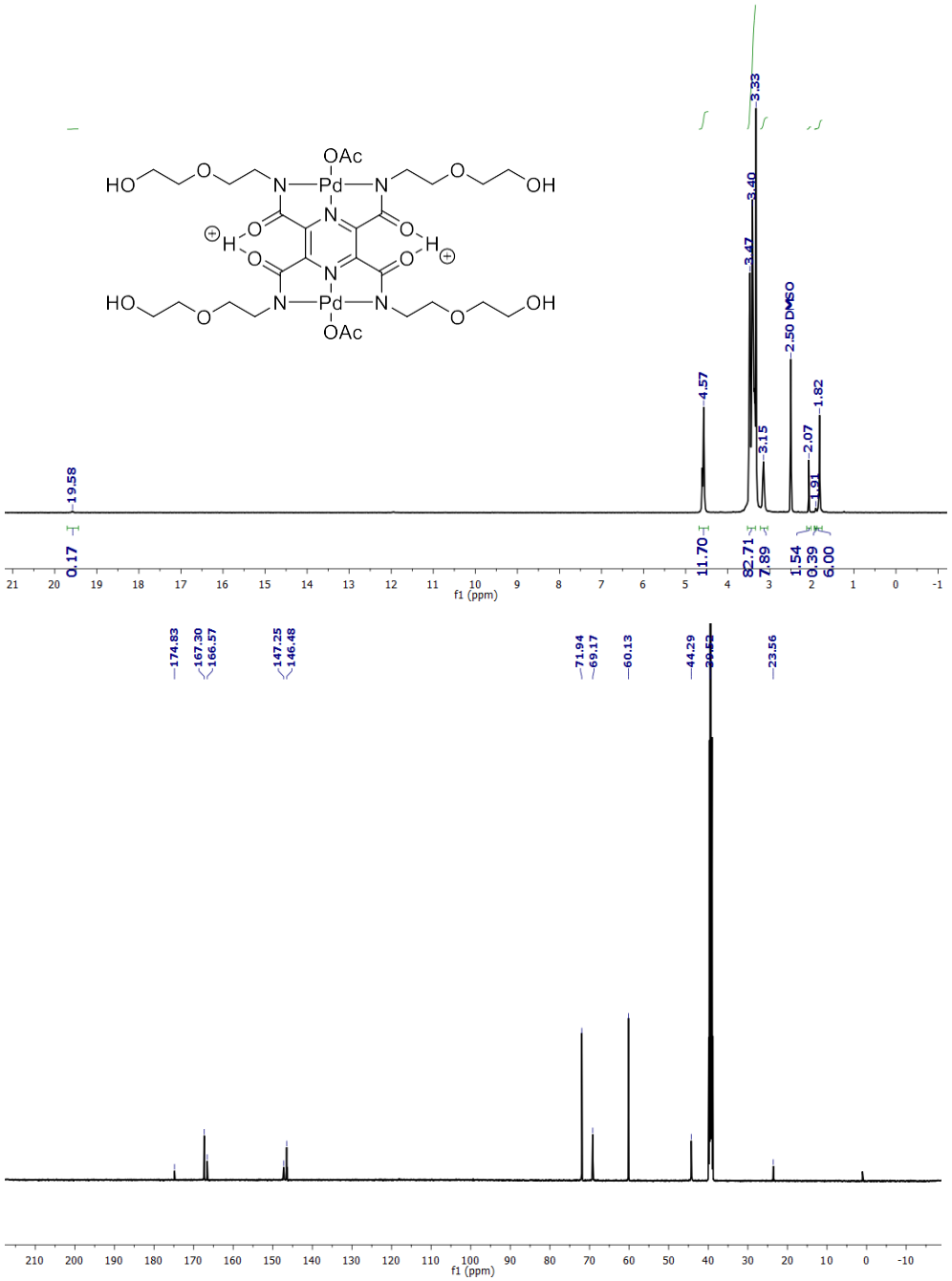

Figure A16. ^{1}H NMR (500 MHz, DMSO-d_6) (top) and ^{13}C NMR (125 MHz, DMSO-d_6) (bottom) of **5.4.**

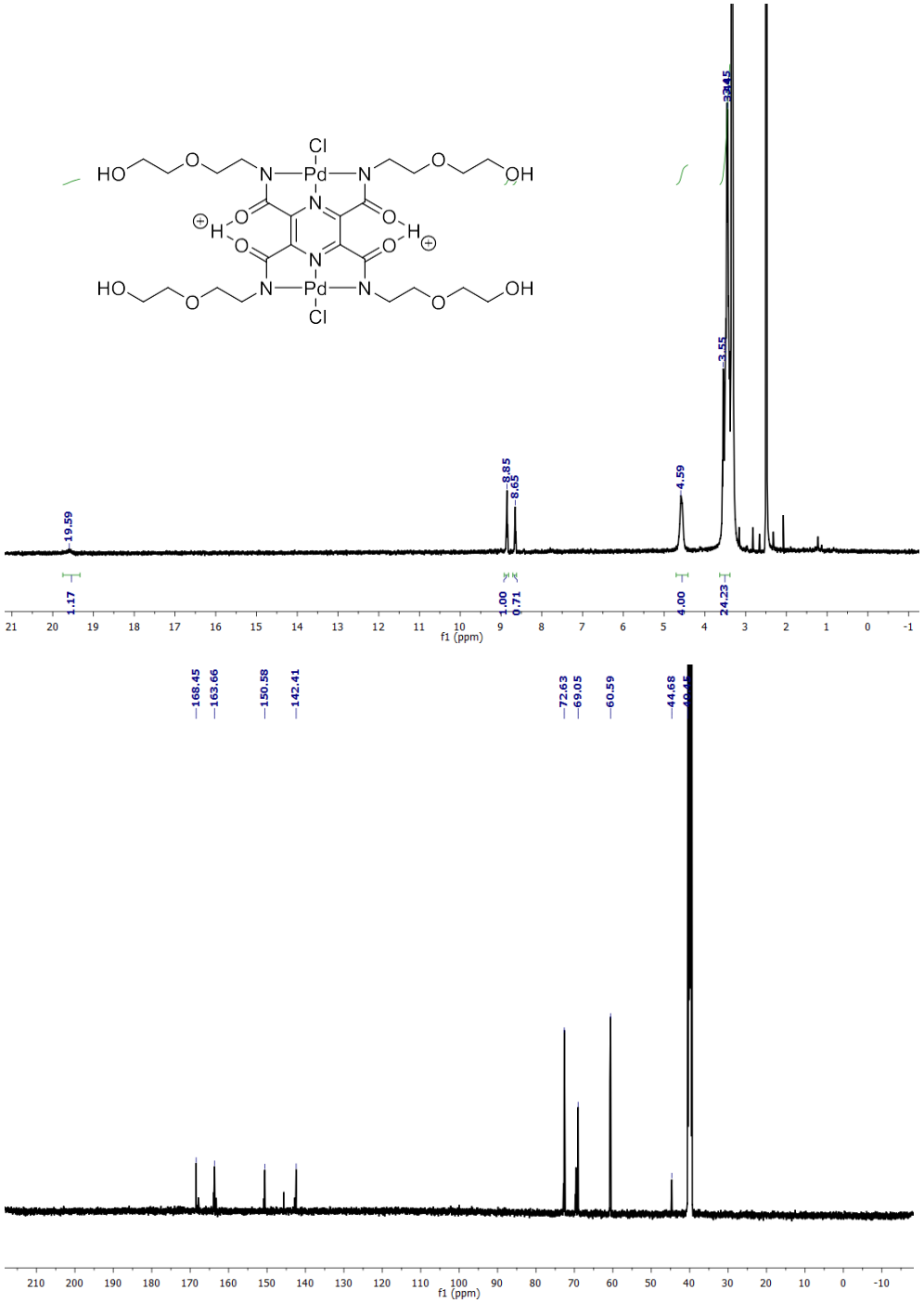

Figure A17. ^{1}H NMR (500 MHz, DMSO-d_6) (top) and ^{13}C NMR (125 MHz, DMSO-d_6) (bottom) of **5.5.**

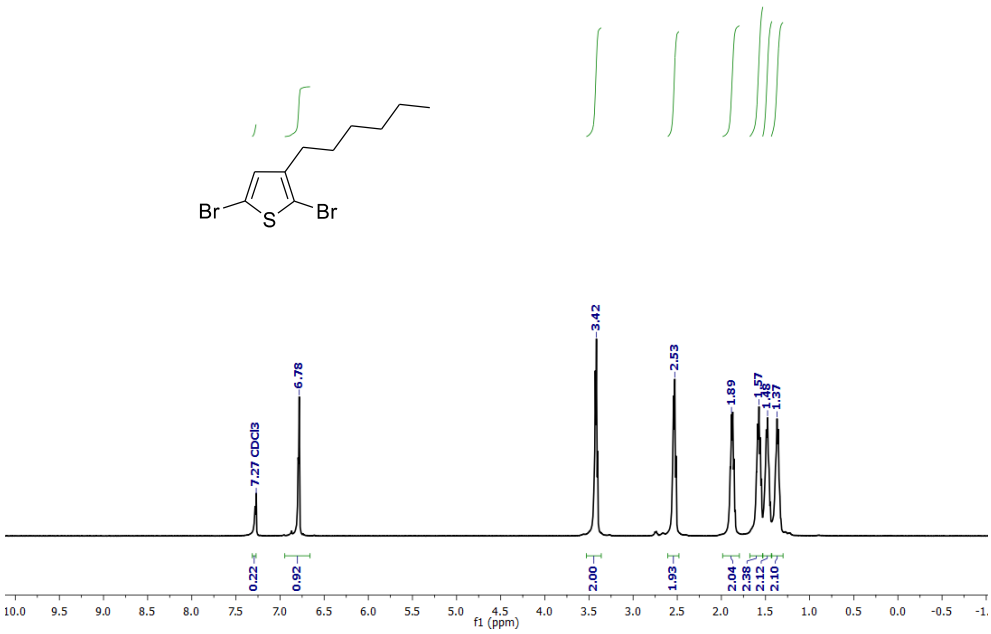

Figure 18. ^{1}H NMR (500 MHz, DMSO-d_6) of **7.a**($Br_2$3HT).

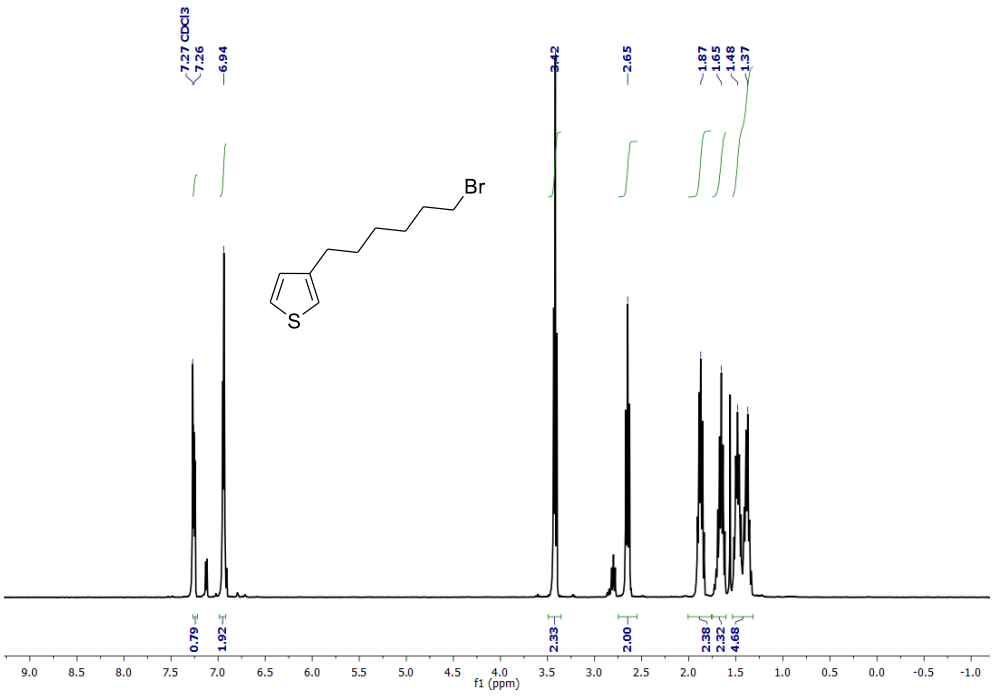

Figure 19. ^{1}H NMR (500 MHz, DMSO-d_6) of **7.b**(3BrHT).

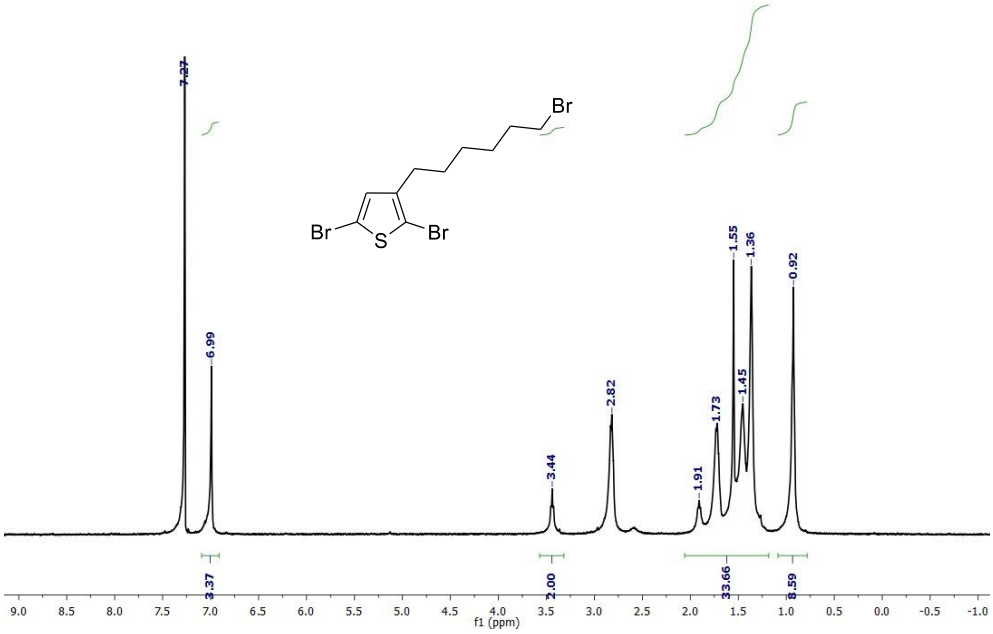

Figure 20. ^{1}H NMR (500 MHz, DMSO-d_6) of **7.c**($Br_2$3BrHT).

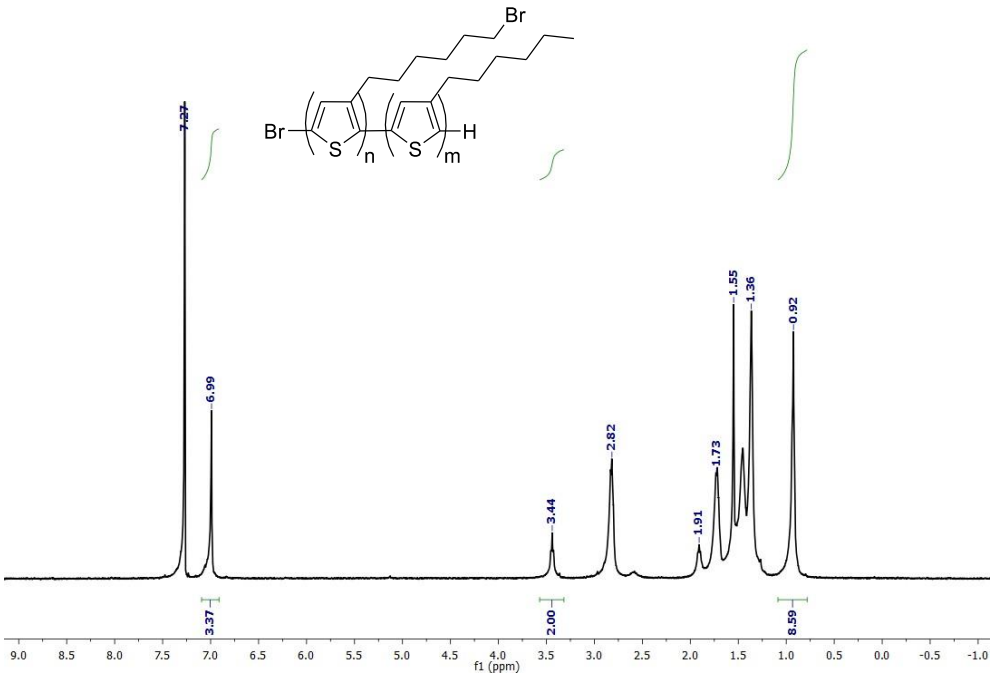

Figure 21. ^{1}H NMR (500 MHz, DMSO-d_6) of **7.1**(P3HT-b-P3BrHT).

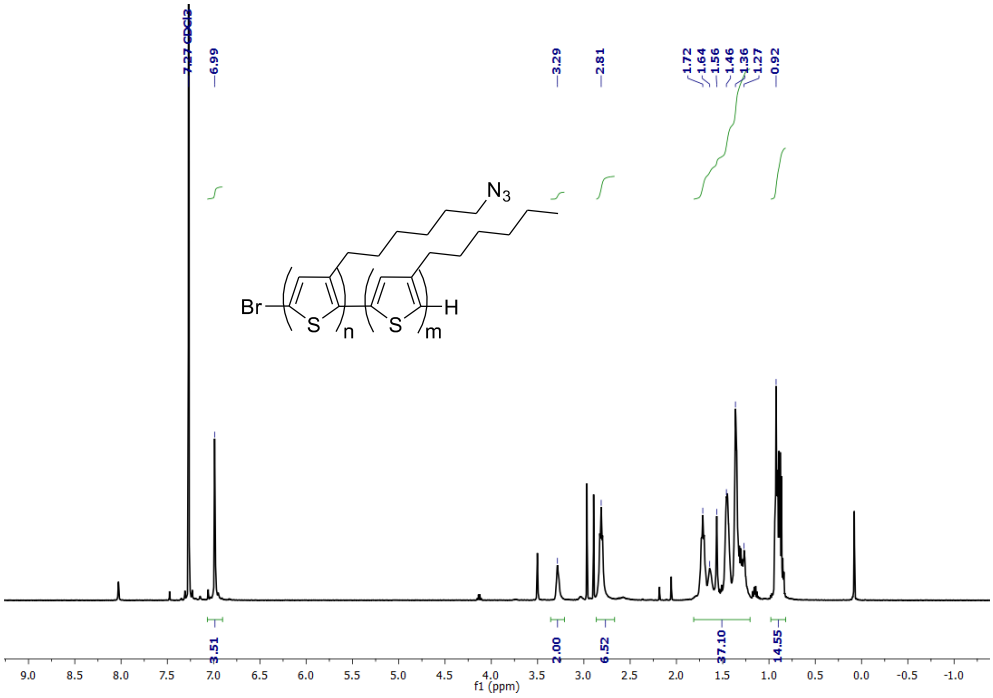

Figure 22. ^{1}H NMR (500 MHz, DMSO-d_6) of **7.2**(P3HT-b-P3N$_3$HT).

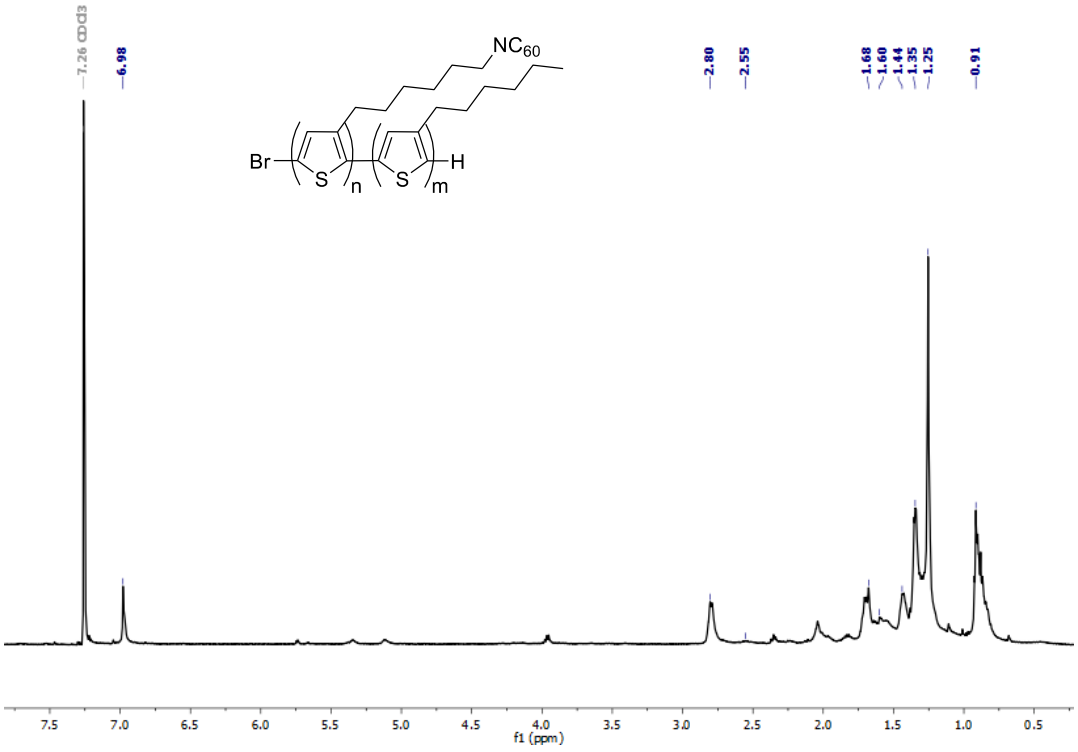

Figure 23. ^{1}H NMR (500 MHz, DMSO-d_6) of **7.3**(P3HT-b-P3C$_{60}$HT).

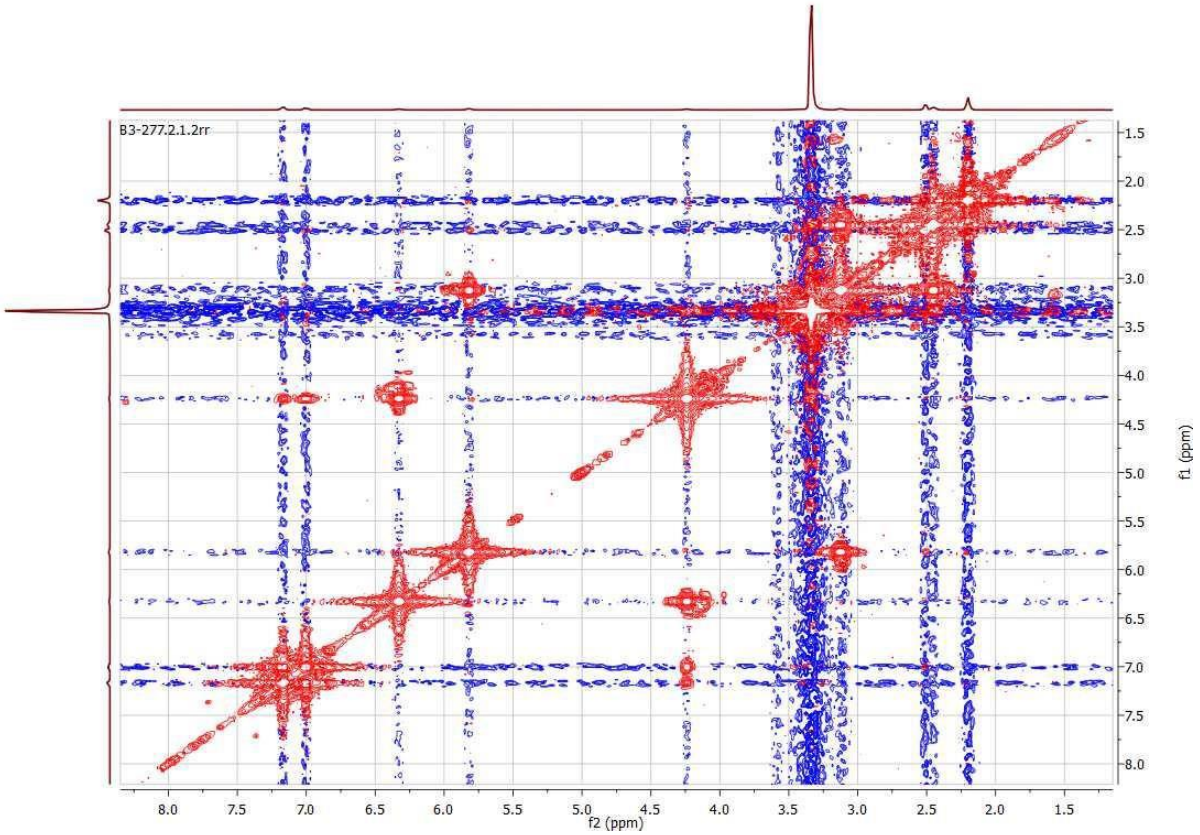

Figure A24. ^{1}H COSY NMR spectrum for compound **3.1**.

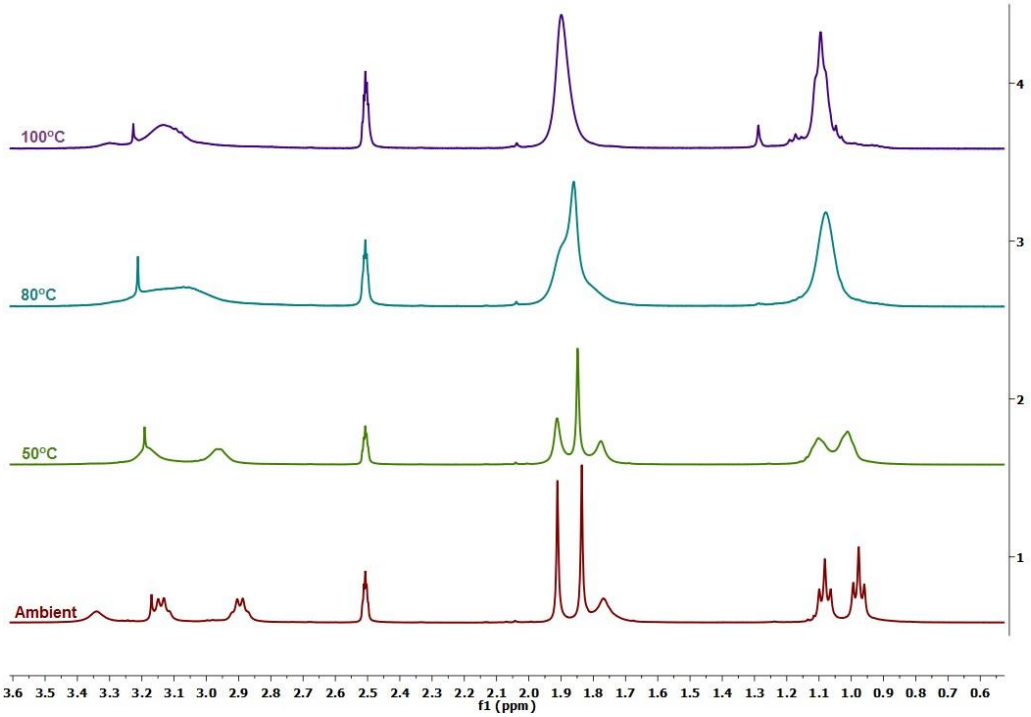

Figure A25. ^{1}H NMR study on **5.1** at ambient temperature, 50°C, 80°C, and 100°C.

Appendix B:
Additional Titration Data

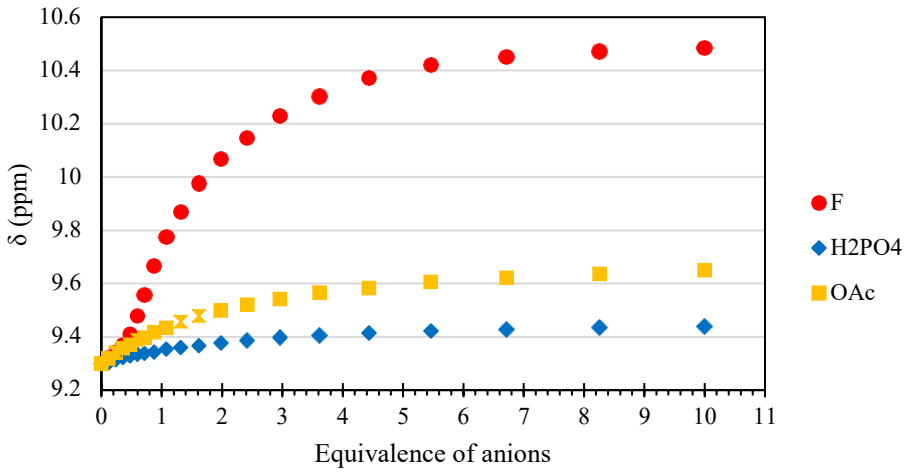

Figure B1. Plot of NH chemical shift of **2.3**(DiHex) upon increasing concentration of anions F^- (red), OAc^- (yellow), and $H_2PO_4^-$ (blue) in 9:1 CD_3CN:DMSO-d_6.

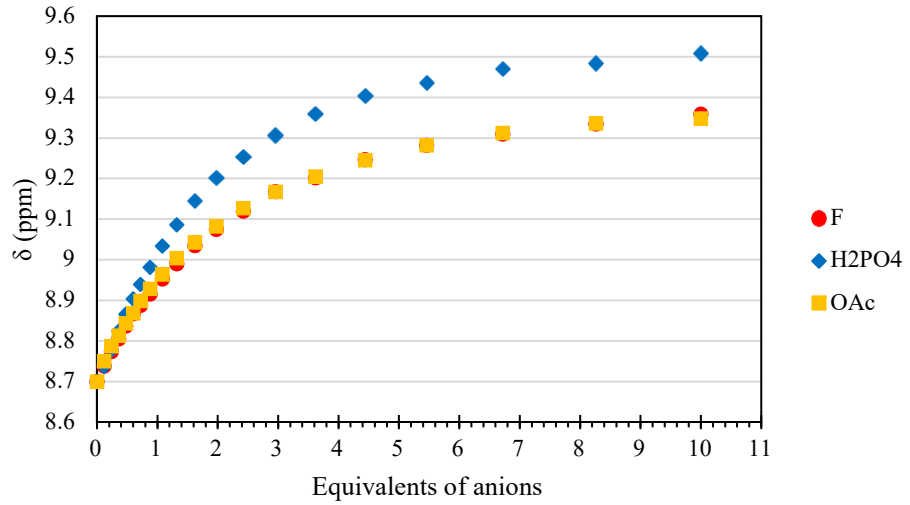

Figure B2. Plot of NH chemical shift of **2.4**(TetraHex) upon increasing concentration of anions F^- (red), OAc^- (yellow), and $H_2PO_4^-$ (blue) in 9:1 CD_3CN:DMSO-d_6.

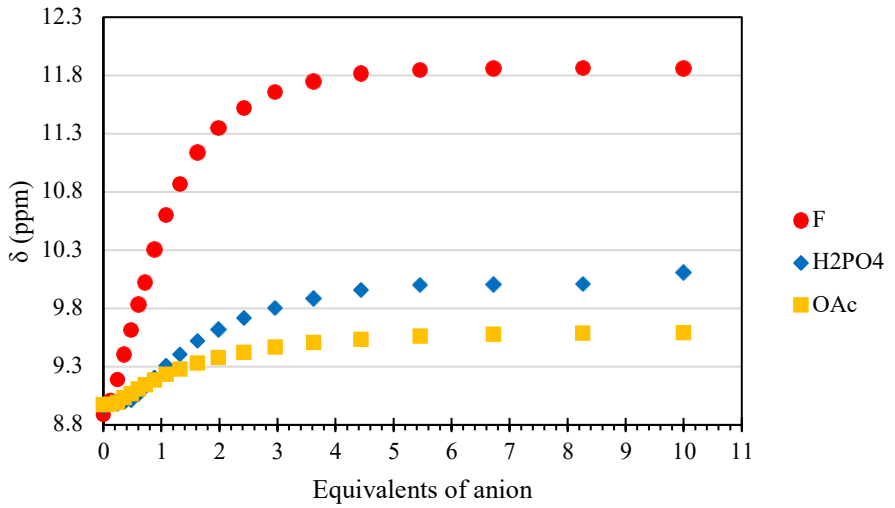

Figure B3. Plot of NH chemical shift of **2.7**(DiGly) upon increasing concentration of anions F^- (red), OAc^- (yellow), and $H_2PO_4^-$ (blue) in 9:1 CD_3CN:DMSO-d_6.

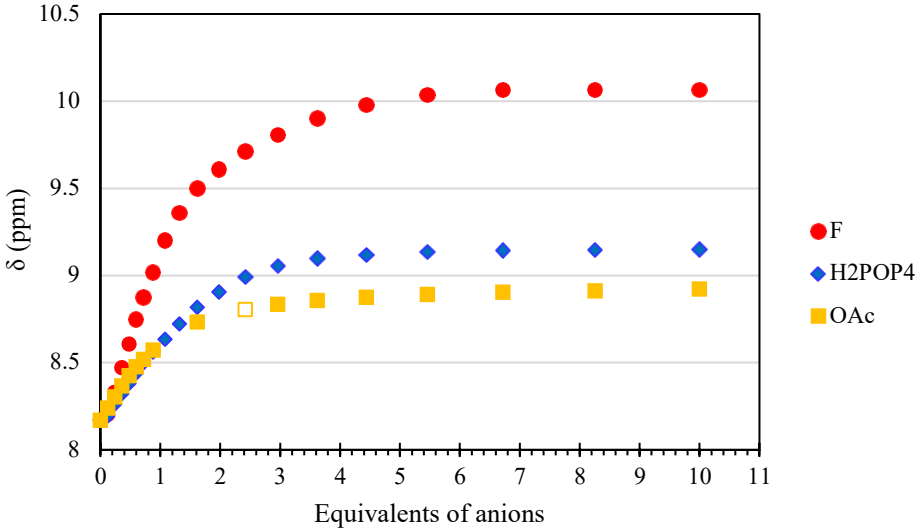

Figure B4. Plot of NH chemical shift of **2.8**(TetraGly) upon increasing concentration of anions F^- (red), OAc^- (yellow), and $H_2PO_4^-$ (blue) in 9:1 CD_3CN:DMSO-d_6.

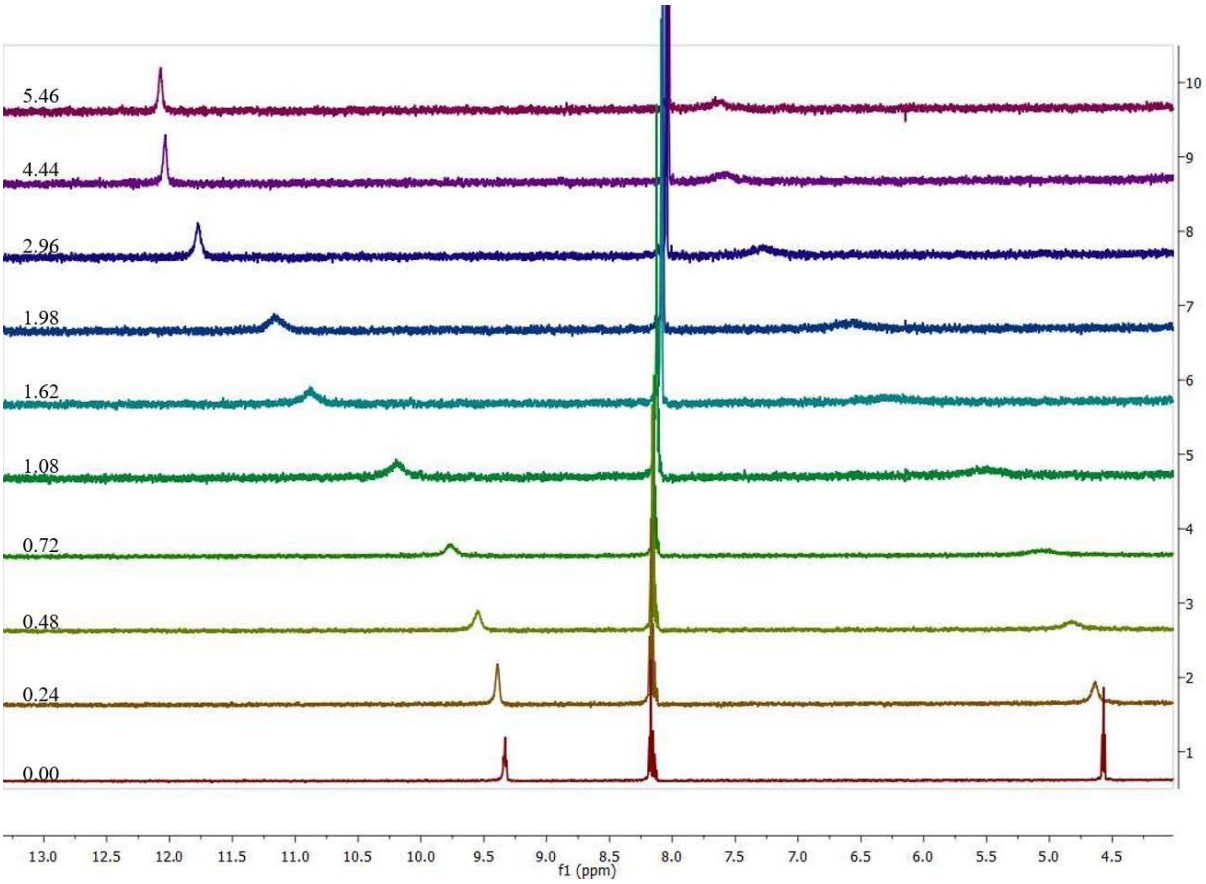

Figure B5. Titration spectra of 2.5(DiEtOH) with TBAF in DMSO-d_6.

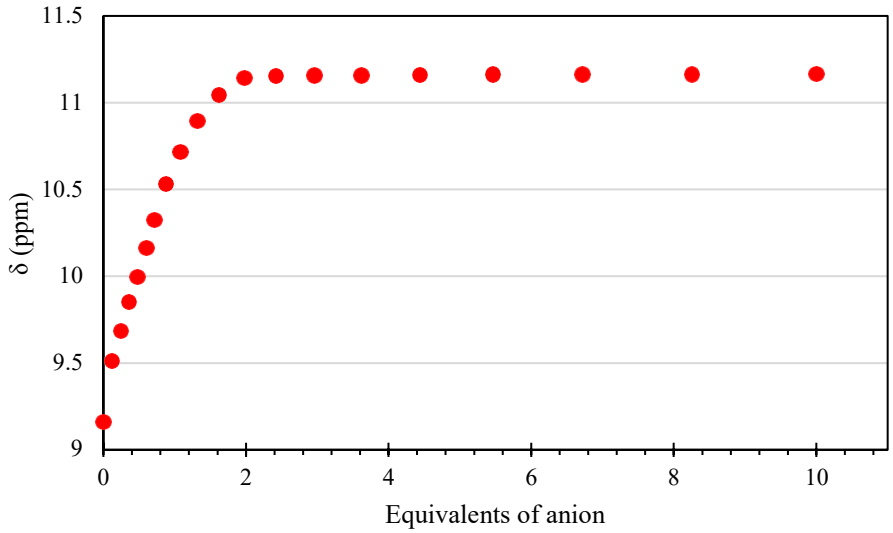

Figure B6. Plot of NH chemical shift of **2.5**(DiEtOH) upon increasing concentration of anions F^- in DMSO-d_6.

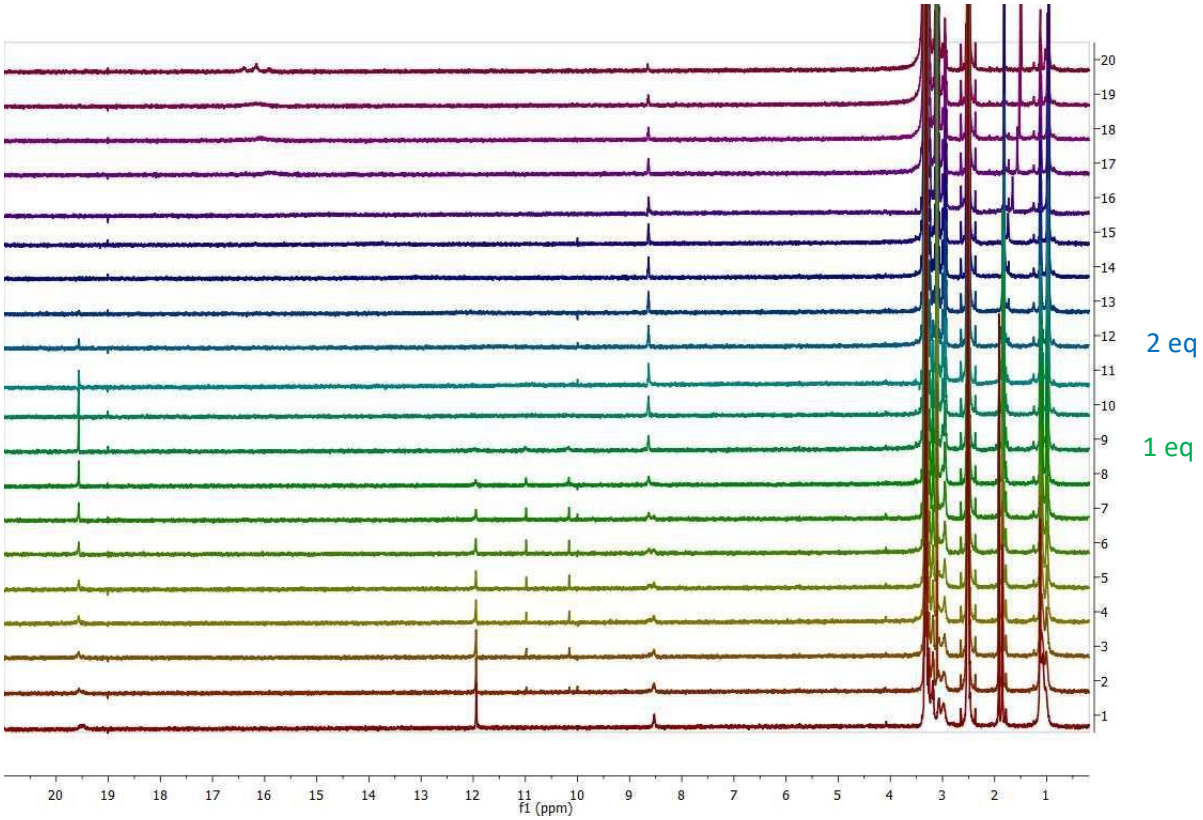

Figure B7. Titration spectra **5.1** with TBAF in DMSO-d_6.

Appendix C:
Crystallographic Data

Table C1. Crystal data and structure refinement for 7.6(TetraEtOH).

Empirical formula	C16 H26 N6 O9	
Formula weight	446.43	
Temperature	200(2) K	
Wavelength	1.54178 Å	
Crystal system	Monoclinic	
Space group	$P2_1/c$	
Unit cell dimensions	a = 8.7091(6) Å	□= 90°.
	b = 24.6511(16) Å	□= 94.492(3)°.
	c = 9.7352(7) Å	□ = 90°.
Volume	2083.6(2) $Å^3$	
Z	4	
Density (calculated)	1.423 Mg/m^3	
Absorption coefficient	1.004 mm^{-1}	
F(000)	944	
Crystal size	0.450 x 0.055 x 0.025 mm^3	
Theta range for data collection	3.586 to 70.069°.	
Index ranges	-10<=h<=8, -29<=k<=28, -11<=l<=10	
Reflections collected	23676	
Independent reflections	3853 [R(int) = 0.0606]	
Completeness to theta = 66.000°	99.5 %	
Absorption correction	Multi-scan	
Max. and min. transmission	1.000 and 0.461	
Refinement method	Full-matrix least-squares on F^2	

Data / restraints / parameters	3853 / 0 / 384
Goodness-of-fit on F^2	1.024
Final R indices [I>2sigma(I)]	R1 = 0.0511, wR2 = 0.1429
R indices (all data)	R1 = 0.0561, wR2 = 0.1480
Extinction coefficient	n/a
Largest diff. peak and hole	0.246 and -0.313 e.$Å^{-3}$

Table C2. Atomic coordinates (x 10^4) and equivalent isotropic displacement parameters ($Å^2$x 10^3) for 7.6(TetraEtOH). U(eq) is defined as one third of the trace of the orthogonalized U^{ij} tensor.

	x	y	z	U(eq)
O(1)	4728(2)	4412(1)	8187(2)	39(1)
O(2)	-146(2)	4406(1)	2114(2)	38(1)
O(3)	-1176(2)	3420(1)	3626(2)	32(1)
O(4)	5781(2)	3412(1)	6762(2)	33(1)
O(5)	4769(2)	6197(1)	9502(2)	34(1)
O(6)	487(2)	6137(1)	318(2)	40(1)
O(7)	601(2)	1936(1)	3114(2)	34(1)
O(8)	3943(2)	1907(1)	7175(2)	32(1)
N(1)	4377(2)	5142(1)	6792(2)	22(1)
N(2)	786(2)	5161(1)	3203(2)	22(1)
N(3)	2426(2)	4568(1)	5078(1)	17(1)
N(4)	765(2)	3067(1)	2490(2)	22(1)
N(5)	3770(2)	3044(1)	7782(2)	21(1)

N(8)	2286(2)	3449(1)	5161(2)	19(1)
C(1)	4213(2)	4622(1)	7109(2)	20(1)
C(2)	3283(2)	4293(1)	6024(2)	17(1)
C(4)	1495(2)	4297(1)	4172(2)	18(1)
C(5)	629(2)	4628(1)	3055(2)	21(1)
C(6)	192(2)	3395(1)	3397(2)	20(1)
C(7)	1372(2)	3731(1)	4248(2)	18(1)
C(9)	3264(2)	3723(1)	6033(2)	18(1)
C(10)	4392(2)	3380(1)	6919(2)	20(1)
C(11)	5153(2)	5525(1)	7753(2)	26(1)
C(12)	4025(3)	5792(1)	8647(2)	29(1)
C(13)	63(2)	5545(1)	2213(2)	26(1)
C(14)	1166(3)	5719(1)	1176(2)	33(1)
C(15)	-204(3)	2682(1)	1669(2)	27(1)
C(16)	-726(2)	2211(1)	2520(2)	30(1)
C(17)	4702(2)	2658(1)	8628(2)	25(1)
C(18)	5240(2)	2187(1)	7798(2)	27(1)
O(1W)	7224(2)	4124(1)	5138(2)	28(1)

Table C3. Bond lengths [Å] for 7.6(TetraEtOH).

O(1)-C(1)	1.224(2)	N(3)-C(4)	1.330(2)	C(12)-H(12B)	0.94(3)
O(2)-C(5)	1.224(2)	N(4)-C(6)	1.324(2)	C(13)-C(14)	1.509(3)
O(3)-C(6)	1.230(2)	N(4)-C(15)	1.464(2)	C(13)-H(13A)	0.98(3)
O(4)-C(10)	1.233(2)	N(4)-H(4N)	0.89(3)	C(13)-H(13B)	0.99(3)

O(5)-C(12)	1.423(2)	N(5)-C(10)	1.326(2)	C(14)-H(14A)	0.99(3)
O(5)-H(5O)	0.89(3)	N(5)-C(17)	1.463(2)	C(14)-H(14B)	0.99(3)
O(6)-C(14)	1.424(2)	N(5)-H(5N)	0.85(3)	C(15)-C(16)	1.517(3)
O(6)-H(6O)	0.91(3)	N(8)-C(9)	1.338(2)	C(15)-H(15A)	1.05(3)
O(7)-C(16)	1.423(3)	N(8)-C(7)	1.341(2)	C(15)-H(15B)	0.99(3)
O(7)-H(7O)	0.84(3)	C(1)-C(2)	1.515(2)	C(16)-H(16A)	1.01(3)
O(8)-C(18)	1.418(2)	C(2)-C(9)	1.406(2)	C(16)-H(16B)	0.99(3)
O(8)-H(8O)	0.86(3)	C(4)-C(7)	1.401(2)	C(17)-C(18)	1.511(3)
N(1)-C(1)	1.327(2)	C(4)-C(5)	1.513(2)	C(17)-H(17A)	1.02(2)
N(1)-C(11)	1.457(2)	C(6)-C(7)	1.515(2)	C(17)-H(17B)	0.98(3)
N(1)-H(1N)	0.86(2)	C(9)-C(10)	1.513(2)	C(18)-H(18A)	0.97(2)
N(2)-C(5)	1.328(2)	C(11)-C(12)	1.513(3)	C(18)-H(18B)	1.00(3)
N(2)-C(13)	1.458(2)	C(11)-H(11A)	1.00(3)	O(1W)-H(1W1)	0.92(3)
N(2)-H(2N)	0.87(3)	C(11)-H(11B)	0.97(3)	O(1W)-H(1W2)	0.91(3)
N(3)-C(2)	1.325(2)	C(12)-H(12A)	1.01(3)		

Table C4. Bond angles [°] for 7.6(TetraEtOH).

C(12)-O(5)-H(5O)	111.5(17)	O(3)-C(6)-C(7)	119.96(16)	O(6)-C(14)-H(14A)	108.3(17)
C(14)-O(6)-H(6O)	111.6(18)	N(4)-C(6)-C(7)	115.07(16)	C(13)-C(14)-H(14A)	108.0(18)
C(16)-O(7)-H(7O)	113(2)	N(8)-C(7)-C(4)	120.52(16)	O(6)-C(14)-H(14B)	110.9(17)
C(18)-O(8)-H(8O)	114(2)	N(8)-C(7)-C(6)	114.86(15)	C(13)-C(14)-H(14B)	109.1(17)
C(1)-N(1)-C(11)	121.96(17)	C(4)-C(7)-C(6)	124.55(16)	H(14A)-C(14)-H(14B)	111(2)
C(1)-N(1)-H(1N)	118.9(15)	N(8)-C(9)-C(2)	120.56(16)	N(4)-C(15)-C(16)	112.48(17)
C(11)-N(1)-H(1N)	118.7(15)	N(8)-C(9)-C(10)	115.60(15)	N(4)-C(15)-H(15A)	105.4(13)
C(5)-N(2)-C(13)	122.31(17)	C(2)-C(9)-C(10)	123.67(16)	C(16)-C(15)-H(15A)	110.8(13)
C(5)-N(2)-H(2N)	116.4(16)	O(4)-C(10)-N(5)	124.85(17)	N(4)-C(15)-H(15B)	109.7(16)
C(13)-N(2)-H(2N)	121.2(16)	O(4)-C(10)-C(9)	119.60(16)	C(16)-C(15)-H(15B)	109.7(17)
C(2)-N(3)-C(4)	119.03(15)	N(5)-C(10)-C(9)	115.49(16)	H(15A)-C(15)-H(15B)	109(2)

C(6)-N(4)-C(15)	121.89(17)	N(1)-C(11)-C(12)	111.23(16)	O(7)-C(16)-C(15)	108.59(17)
C(6)-N(4)-H(4N)	119.2(18)	N(1)-C(11)-H(11A)	110.5(16)	O(7)-C(16)-H(16A)	110.3(15)
C(15)-N(4)-H(4N)	118.8(18)	C(12)-C(11)-H(11A)	109.3(15)	C(15)-C(16)-H(16A)	110.7(15)
C(10)-N(5)-C(17)	121.83(17)	N(1)-C(11)-H(11B)	111.1(16)	O(7)-C(16)-H(16B)	109.5(16)
C(10)-N(5)-H(5N)	119.6(18)	C(12)-C(11)-H(11B)	110.8(16)	C(15)-C(16)-H(16B)	105.6(17)
C(17)-N(5)-H(5N)	118.5(18)	H(11A)-C(11)-H(11B)	104(2)	H(16A)-C(16)-H(16B)	112(2)
C(9)-N(8)-C(7)	118.28(15)	O(5)-C(12)-C(11)	110.83(17)	N(5)-C(17)-C(18)	112.42(16)
O(1)-C(1)-N(1)	124.67(18)	O(5)-C(12)-H(12A)	107.8(17)	N(5)-C(17)-H(17A)	103.1(13)
O(1)-C(1)-C(2)	120.72(16)	C(11)-C(12)-H(12A)	107.7(18)	C(18)-C(17)-H(17A)	113.0(13)
N(1)-C(1)-C(2)	114.60(16)	O(5)-C(12)-H(12B)	110.8(17)	N(5)-C(17)-H(17B)	109.1(15)
N(3)-C(2)-C(9)	120.61(16)	C(11)-C(12)-H(12B)	107.4(17)	C(18)-C(17)-H(17B)	109.5(15)
N(3)-C(2)-C(1)	116.86(15)	H(12A)-C(12)-H(12B)	112(2)	H(17A)-C(17)-H(17B)	110(2)
C(9)-C(2)-C(1)	122.48(16)	N(2)-C(13)-C(14)	111.30(17)	O(8)-C(18)-C(17)	109.40(16)
N(3)-C(4)-C(7)	120.64(16)	N(2)-C(13)-H(13A)	109.1(15)	O(8)-C(18)-H(18A)	110.5(14)
N(3)-C(4)-C(5)	116.75(15)	C(14)-C(13)-H(13A)	108.6(15)	C(17)-C(18)-H(18A)	111.3(13)
C(7)-C(4)-C(5)	122.58(16)	N(2)-C(13)-H(13B)	109.0(16)	O(8)-C(18)-H(18B)	109.4(15)
O(2)-C(5)-N(2)	124.77(17)	C(14)-C(13)-H(13B)	112.4(16)	C(17)-C(18)-H(18B)	108.3(16)
O(2)-C(5)-C(4)	120.77(16)	H(13A)-C(13)-H(13B)	106(2)	H(18A)-C(18)-H(18B)	108(2)
N(2)-C(5)-C(4)	114.45(16)	O(6)-C(14)-C(13)	109.97(18)	H(1W1)-O(1W)-H(1W2)	107(3)
O(3)-C(6)-N(4)	124.86(17)				

Table C5. Anisotropic displacement parameters ($Å^2 x\ 10^3$) for 7.6(TetraEtOH). The anisotropic displacement factor exponent takes the form: $-2\pi^2[h^2 a^{*2} U^{11} + ... + 2 h k a^* b^* U^{12}]$

	U^{11}	U^{22}	U^{33}	U^{23}	U^{13}	U^{12}
O(1)	57(1)	22(1)	32(1)	6(1)	-25(1)	-7(1)
O(2)	53(1)	22(1)	34(1)	-3(1)	-25(1)	3(1)
O(3)	21(1)	31(1)	44(1)	-11(1)	0(1)	-1(1)

O(4)	23(1)	30(1)	45(1)	14(1)	-1(1)	1(1)
O(5)	60(1)	22(1)	19(1)	-3(1)	-3(1)	-11(1)
O(6)	73(1)	27(1)	21(1)	6(1)	1(1)	18(1)
O(7)	29(1)	22(1)	52(1)	11(1)	5(1)	0(1)
O(8)	28(1)	21(1)	48(1)	-12(1)	3(1)	-1(1)
N(1)	32(1)	12(1)	22(1)	0(1)	-4(1)	-3(1)
N(2)	30(1)	14(1)	22(1)	2(1)	-5(1)	2(1)
N(3)	22(1)	12(1)	18(1)	0(1)	0(1)	0(1)
N(4)	26(1)	14(1)	25(1)	-3(1)	-2(1)	-3(1)
N(5)	24(1)	13(1)	25(1)	3(1)	-1(1)	2(1)
N(8)	23(1)	12(1)	23(1)	0(1)	-2(1)	0(1)
C(1)	24(1)	15(1)	21(1)	1(1)	-3(1)	0(1)
C(2)	21(1)	12(1)	18(1)	2(1)	0(1)	-1(1)
C(4)	22(1)	13(1)	18(1)	-2(1)	0(1)	2(1)
C(5)	26(1)	16(1)	20(1)	-1(1)	-3(1)	2(1)
C(6)	25(1)	12(1)	23(1)	1(1)	-3(1)	-1(1)
C(7)	19(1)	13(1)	22(1)	-1(1)	-1(1)	1(1)
C(9)	20(1)	12(1)	21(1)	1(1)	0(1)	1(1)
C(10)	24(1)	11(1)	24(1)	-1(1)	-4(1)	0(1)
C(11)	29(1)	17(1)	30(1)	-5(1)	-4(1)	-5(1)
C(12)	37(1)	26(1)	24(1)	-6(1)	1(1)	-10(1)
C(13)	31(1)	18(1)	27(1)	4(1)	-4(1)	8(1)
C(14)	44(1)	30(1)	24(1)	8(1)	4(1)	13(1)
C(15)	34(1)	18(1)	27(1)	-4(1)	-9(1)	-4(1)
C(16)	27(1)	19(1)	43(1)	-3(1)	-6(1)	-6(1)

C(17)	34(1)	15(1)	24(1)	2(1)	-7(1)	4(1)
C(18)	27(1)	17(1)	37(1)	1(1)	-4(1)	4(1)
O(1W)	42(1)	13(1)	30(1)	1(1)	2(1)	-1(1)

Table C6. Hydrogen coordinates (x 10^4) and isotropic displacement parameters ($Å^2$x 10^3) for 7.6(TetraEtOH).

	x	y	z	U(eq)
H(5O)	5130(30)	6060(11)	10310(30)	39(7)
H(6O)	210(30)	6012(11)	-550(30)	48(8)
H(7O)	390(40)	1713(13)	3730(30)	57(9)
H(8O)	4160(40)	1690(13)	6530(40)	61(9)
H(1N)	3920(30)	5264(9)	6040(20)	20(5)
H(2N)	1380(30)	5271(10)	3900(30)	27(6)
H(4N)	1770(30)	3065(11)	2410(30)	47(8)
H(5N)	2800(30)	3042(10)	7820(30)	38(7)
H(11A)	5690(30)	5810(11)	7240(30)	41(7)
H(11B)	5980(30)	5349(11)	8320(30)	41(7)
H(12A)	3210(40)	5976(12)	8020(30)	58(9)
H(12B)	3610(30)	5517(11)	9180(30)	45(7)
H(13A)	-260(30)	5868(11)	2710(30)	36(6)
H(13B)	-880(30)	5381(11)	1770(30)	46(7)
H(14A)	2100(40)	5869(12)	1690(30)	54(8)

H(14B)	1430(30)	5400(12)	620(30)	54(8)
H(15A)	480(30)	2545(10)	900(30)	34(6)
H(15B)	-1110(30)	2873(11)	1230(30)	48(8)
H(16A)	-1380(30)	2343(10)	3260(30)	40(7)
H(16B)	-1310(30)	1967(12)	1860(30)	52(8)
H(17A)	3990(30)	2544(9)	9350(20)	26(6)
H(17B)	5590(30)	2847(10)	9070(30)	38(7)
H(18A)	5900(30)	2307(9)	7110(20)	23(5)
H(18B)	5850(30)	1937(11)	8430(30)	43(7)
H(1W1)	7840(30)	3918(13)	4620(30)	52(8)
H(1W2)	6730(30)	3892(12)	5680(30)	51(8)

Table C7. Torsion angles [°] for 7.6(TetraEtOH).

C(11)-N(1)-C(1)-O(1)	-2.8(3)	O(3)-C(6)-C(7)-N(8)	106.9(2)
C(11)-N(1)-C(1)-C(2)	175.99(16)	N(4)-C(6)-C(7)-N(8)	-69.5(2)
C(4)-N(3)-C(2)-C(9)	2.9(2)	O(3)-C(6)-C(7)-C(4)	-70.1(2)
C(4)-N(3)-C(2)-C(1)	-174.64(15)	N(4)-C(6)-C(7)-C(4)	113.6(2)
O(1)-C(1)-C(2)-N(3)	162.23(18)	C(7)-N(8)-C(9)-C(2)	2.6(2)
N(1)-C(1)-C(2)-N(3)	-16.6(2)	C(7)-N(8)-C(9)-C(10)	-172.93(15)
O(1)-C(1)-C(2)-C(9)	-15.3(3)	N(3)-C(2)-C(9)-N(8)	-5.7(3)
N(1)-C(1)-C(2)-C(9)	165.90(17)	C(1)-C(2)-C(9)-N(8)	171.75(16)
C(2)-N(3)-C(4)-C(7)	2.6(2)	N(3)-C(2)-C(9)-C(10)	169.45(16)
C(2)-N(3)-C(4)-C(5)	-175.79(15)	C(1)-C(2)-C(9)-C(10)	-13.1(3)
C(13)-N(2)-C(5)-O(2)	-1.8(3)	C(17)-N(5)-C(10)-O(4)	-1.7(3)
C(13)-N(2)-C(5)-C(4)	178.67(16)	C(17)-N(5)-C(10)-C(9)	175.25(15)
N(3)-C(4)-C(5)-O(2)	173.67(18)	N(8)-C(9)-C(10)-O(4)	114.21(19)

C(7)-C(4)-C(5)-O(2)	-4.7(3)	C(2)-C(9)-C(10)-O(4)	-61.1(2)
N(3)-C(4)-C(5)-N(2)	-6.7(2)	N(8)-C(9)-C(10)-N(5)	-62.9(2)
C(7)-C(4)-C(5)-N(2)	174.93(17)	C(2)-C(9)-C(10)-N(5)	121.78(19)
C(15)-N(4)-C(6)-O(3)	-1.3(3)	C(1)-N(1)-C(11)-C(12)	-90.5(2)
C(15)-N(4)-C(6)-C(7)	174.78(16)	N(1)-C(11)-C(12)-O(5)	-175.22(16)
C(9)-N(8)-C(7)-C(4)	2.9(3)	C(5)-N(2)-C(13)-C(14)	-95.9(2)
C(9)-N(8)-C(7)-C(6)	-174.18(16)	N(2)-C(13)-C(14)-O(6)	-173.68(17)
N(3)-C(4)-C(7)-N(8)	-5.6(3)	C(6)-N(4)-C(15)-C(16)	-71.9(2)
C(5)-C(4)-C(7)-N(8)	172.61(16)	N(4)-C(15)-C(16)-O(7)	-59.1(2)
N(3)-C(4)-C(7)-C(6)	171.10(16)	C(10)-N(5)-C(17)-C(18)	-73.8(2)
C(5)-C(4)-C(7)-C(6)	-10.6(3)	N(5)-C(17)-C(18)-O(8)	-59.8(2)

Table C8. Hydrogen bonds for 7.6(TetraEtOH) [Å and °].

D-H...A	d(D-H)	d(H...A)	d(D...A)	<(DHA)
O(5)-H(5O)...O(1)#1	0.89(3)	1.87(3)	2.712(2)	157(2)
O(6)-H(6O)...O(2)#2	0.91(3)	1.84(3)	2.716(2)	161(3)
O(7)-H(7O)...O(6)#3	0.84(3)	1.89(3)	2.708(2)	163(3)
O(8)-H(8O)...O(5)#4	0.86(3)	1.87(3)	2.697(2)	161(3)
N(1)-H(1N)...O(1W)#5	0.86(2)	2.10(2)	2.889(2)	152(2)
N(2)-H(2N)...N(3)	0.87(3)	2.23(2)	2.665(2)	110.8(19)
N(2)-H(2N)...O(1W)#5	0.87(3)	2.10(3)	2.878(2)	150(2)
N(4)-H(4N)...O(8)#6	0.89(3)	1.92(3)	2.809(2)	177(3)
N(5)-H(5N)...O(7)#7	0.85(3)	1.96(3)	2.804(2)	174(3)
O(1W)-H(1W1)...O(3)#8	0.92(3)	1.82(3)	2.728(2)	170(3)

O(1W)-H(1W2)...O(4)	0.91(3)	1.82(3)	2.732(2)	178(3)

Symmetry transformations used to generate equivalent atoms:

#1 -x+1,-y+1,-z+2 #2 -x,-y+1,-z #3 -x,y-1/2,-z+1/2

#4 -x+1,y-1/2,-z+3/2 #5 -x+1,-y+1,-z+1 #6 x,-y+1/2,z-1/2

#7 x,-y+1/2,z+1/2 #8 x+1,y,z

Table C9. Crystal data and structure refinement for 3.1.

Empirical formula	C15 H25 N5 O3	
Formula weight	323.40	
Temperature	228(2) K	
Wavelength	0.71073 Å	
Crystal system	Monoclinic	
Space group	$P2_1/n$	
Unit cell dimensions	a = 10.821(2) Å	□= 90°.
	b = 8.5582(19) Å	□= 95.168(3)°.
	c = 18.291(4) Å	□ = 90°.
Volume	1687.0(6) $Å^3$	
Z	4	
Density (calculated)	1.273 Mg/m^3	
Absorption coefficient	0.091 mm^{-1}	
F(000)	696	
Crystal size	0.600 x 0.550 x 0.420 mm^3	
Theta range for data collection	2.236 to 29.573°.	

Index ranges	-15<=h<=15, -11<=k<=11, -25<=l<=25
Reflections collected	18956
Independent reflections	4708 [R(int) = 0.0316]
Completeness to theta = 25.242°	100.0 %
Absorption correction	Multi-scan
Max. and min. transmission	1.000 and 0.887
Refinement method	Full-matrix least-squares on F^2
Data / restraints / parameters	4708 / 0 / 308
Goodness-of-fit on F^2	1.011
Final R indices [I>2sigma(I)]	R1 = 0.0406, wR2 = 0.0988
R indices (all data)	R1 = 0.0608, wR2 = 0.1119
Extinction coefficient	n/a
Largest diff. peak and hole	0.287 and -0.171 e.$Å^{-3}$

Table C10. Atomic coordinates (x 10^4) and equivalent isotropic displacement parameters ($Å^2$x 10^3) for 3.1. U(eq) is defined as one third of the trace of the orthogonalized U^{ij} tensor.

	x	y	z	U(eq)
O(1)	3363(1)	4267(1)	2322(1)	46(1)
O(2)	3853(1)	7239(1)	-672(1)	36(1)
N(1)	5510(1)	8074(1)	1890(1)	32(1)
C(2)	6415(1)	6891(2)	2149(1)	38(1)
C(3)	5821(2)	5481(2)	2477(1)	43(1)
N(4)	5284(1)	4433(1)	1914(1)	42(1)

C(5)	4138(1)	3814(1)	1904(1)	32(1)
N(6)	3898(1)	2667(1)	1404(1)	34(1)
C(7)	2692(1)	1937(2)	1249(1)	40(1)
C(8)	2031(1)	2442(1)	526(1)	32(1)
C(9)	2043(1)	4017(1)	325(1)	28(1)
C(10)	1398(1)	1388(2)	55(1)	39(1)
C(11)	770(1)	1904(2)	-596(1)	41(1)
C(12)	777(1)	3467(2)	-785(1)	36(1)
C(13)	1428(1)	4545(1)	-325(1)	27(1)
C(14)	1425(1)	6261(1)	-529(1)	28(1)
N(15)	2166(1)	7233(1)	-10(1)	26(1)
C(16)	3399(1)	7445(1)	-82(1)	25(1)
N(17)	4074(1)	7978(1)	523(1)	33(1)
C(18)	5415(1)	8124(2)	547(1)	35(1)
C(19)	5876(1)	8940(2)	1254(1)	37(1)
C(20)	5217(2)	9105(2)	2480(1)	48(1)
O(1W)	2731(1)	2112(2)	3357(1)	44(1)

Table C11. Bond lengths [Å] for 3.1.

O(1)-C(5)	1.2468(15)	C(7)-C(8)	1.5086(19)	C(14)-H(14B)	0.979(14)
O(2)-C(16)	1.2374(14)	C(7)-H(7A)	0.953(17)	N(15)-C(16)	1.3649(15)
N(1)-C(20)	1.4507(17)	C(7)-H(7B)	0.995(17)	N(15)-H(15N)	0.879(15)
N(1)-C(2)	1.4581(17)	C(8)-C(10)	1.3851(19)	C(16)-N(17)	1.3494(15)
N(1)-C(19)	1.4643(17)	C(8)-C(9)	1.3969(16)	N(17)-C(18)	1.4533(16)
C(2)-C(3)	1.515(2)	C(9)-C(13)	1.3852(16)	N(17)-H(17N)	0.890(16)

C(2)-H(2A)	1.007(17)	C(9)-H(9)	0.968(14)	C(18)-C(19)	1.5152(18)
C(2)-H(2B)	1.006(16)	C(10)-C(11)	1.388(2)	C(18)-H(18A)	0.993(16)
C(3)-N(4)	1.4473(18)	C(10)-H(10)	0.952(17)	C(18)-H(18B)	0.988(15)
C(3)-H(3A)	0.981(16)	C(11)-C(12)	1.382(2)	C(19)-H(19A)	0.996(17)
C(3)-H(3B)	1.013(17)	C(11)-H(11)	0.986(17)	C(19)-H(19B)	1.027(16)
N(4)-C(5)	1.3465(17)	C(12)-C(13)	1.3964(17)	C(20)-H(20A)	1.000(17)
N(4)-H(4N)	0.855(17)	C(12)-H(12)	0.978(15)	C(20)-H(20B)	0.97(2)
C(5)-N(6)	1.3502(17)	C(13)-C(14)	1.5151(16)	C(20)-H(20C)	1.041(19)
N(6)-C(7)	1.4523(18)	C(14)-N(15)	1.4489(15)	O(1W)-H(1W1)	0.83(2)
N(6)-H(6N)	0.878(16)	C(14)-H(14A)	1.002(15)	O(1W)-H(1W2)	0.87(2)

Table C12. Bond angles [°] for 3.1.

C(20)-N(1)-C(2)	111.50(11)	C(8)-C(7)-H(7B)	109.2(9)	C(16)-N(15)-H(15N)	114.9(10)
C(20)-N(1)-C(19)	112.10(12)	H(7A)-C(7)-H(7B)	106.5(13)	C(14)-N(15)-H(15N)	117.9(10)
C(2)-N(1)-C(19)	112.80(11)	C(10)-C(8)-C(9)	118.75(12)	O(2)-C(16)-N(17)	122.38(11)
N(1)-C(2)-C(3)	112.66(12)	C(10)-C(8)-C(7)	121.79(12)	O(2)-C(16)-N(15)	122.26(11)
N(1)-C(2)-H(2A)	110.1(9)	C(9)-C(8)-C(7)	119.46(12)	N(17)-C(16)-N(15)	115.26(10)
C(3)-C(2)-H(2A)	109.4(9)	C(13)-C(9)-C(8)	121.69(11)	C(16)-N(17)-C(18)	121.22(10)
N(1)-C(2)-H(2B)	110.3(9)	C(13)-C(9)-H(9)	121.2(8)	C(16)-N(17)-H(17N)	116.4(10)
C(3)-C(2)-H(2B)	107.8(9)	C(8)-C(9)-H(9)	117.1(8)	C(18)-N(17)-H(17N)	116.4(10)
H(2A)-C(2)-H(2B)	106.4(13)	C(8)-C(10)-C(11)	120.13(12)	N(17)-C(18)-C(19)	108.42(11)
N(4)-C(3)-C(2)	111.73(12)	C(8)-C(10)-H(10)	117.8(10)	N(17)-C(18)-H(18A)	111.2(9)
N(4)-C(3)-H(3A)	105.5(9)	C(11)-C(10)-H(10)	122.0(9)	C(19)-C(18)-H(18A)	110.8(9)
C(2)-C(3)-H(3A)	111.1(9)	C(12)-C(11)-C(10)	120.65(12)	N(17)-C(18)-H(18B)	110.1(8)
N(4)-C(3)-H(3B)	109.7(10)	C(12)-C(11)-H(11)	119.0(10)	C(19)-C(18)-H(18B)	109.1(9)
C(2)-C(3)-H(3B)	108.0(10)	C(10)-C(11)-H(11)	120.4(10)	H(18A)-C(18)-H(18B)	107.1(13)
H(3A)-C(3)-H(3B)	110.9(13)	C(11)-C(12)-C(13)	120.16(13)	N(1)-C(19)-C(18)	110.71(11)
C(5)-N(4)-C(3)	124.35(12)	C(11)-C(12)-H(12)	120.1(9)	N(1)-C(19)-H(19A)	108.2(10)
C(5)-N(4)-H(4N)	117.2(11)	C(13)-C(12)-H(12)	119.7(9)	C(18)-C(19)-H(19A)	109.3(9)

C(3)-N(4)-H(4N)	117.9(11)	C(9)-C(13)-C(12)	118.61(11)	N(1)-C(19)-H(19B)	112.9(9)
O(1)-C(5)-N(4)	122.56(13)	C(9)-C(13)-C(14)	121.21(10)	C(18)-C(19)-H(19B)	108.4(9)
O(1)-C(5)-N(6)	122.87(12)	C(12)-C(13)-C(14)	120.16(11)	H(19A)-C(19)-H(19B)	107.1(13)
N(4)-C(5)-N(6)	114.57(11)	N(15)-C(14)-C(13)	113.97(10)	N(1)-C(20)-H(20A)	108.9(10)
C(5)-N(6)-C(7)	124.05(12)	N(15)-C(14)-H(14A)	107.4(8)	N(1)-C(20)-H(20B)	109.4(11)
C(5)-N(6)-H(6N)	116.3(10)	C(13)-C(14)-H(14A)	110.2(8)	H(20A)-C(20)-H(20B)	106.7(15)
C(7)-N(6)-H(6N)	118.0(10)	N(15)-C(14)-H(14B)	107.6(8)	N(1)-C(20)-H(20C)	111.2(10)
N(6)-C(7)-C(8)	113.27(11)	C(13)-C(14)-H(14B)	108.7(8)	H(20A)-C(20)-H(20C)	109.3(14)
N(6)-C(7)-H(7A)	106.5(10)	H(14A)-C(14)-H(14B)	108.7(11)	H(20B)-C(20)-H(20C)	111.2(16)
C(8)-C(7)-H(7A)	110.5(10)	C(16)-N(15)-C(14)	120.06(10)	H(1W1)-O(1W)-H(1W2)	103.9(18)
N(6)-C(7)-H(7B)	110.7(9)				

Table C13. Anisotropic displacement parameters ($Å^2$x 10^3) for 3.1. The anisotropic displacement factor exponent takes the form: $-2\pi^2[h^2 a^{*2}U^{11} + ... + 2 h k a^* b^* U^{12}]$

	U^{11}	U^{22}	U^{33}	U^{23}	U^{13}	U^{12}
O(1)	53(1)	39(1)	51(1)	8(1)	29(1)	8(1)
O(2)	32(1)	51(1)	26(1)	-3(1)	9(1)	-7(1)
N(1)	33(1)	36(1)	27(1)	-2(1)	-1(1)	2(1)
C(2)	32(1)	39(1)	41(1)	0(1)	-4(1)	1(1)
C(3)	54(1)	40(1)	34(1)	2(1)	0(1)	1(1)
N(4)	44(1)	42(1)	44(1)	-9(1)	17(1)	-6(1)
C(5)	38(1)	26(1)	35(1)	11(1)	11(1)	6(1)
N(6)	29(1)	33(1)	40(1)	5(1)	7(1)	4(1)

C(7)	34(1)	32(1)	55(1)	16(1)	5(1)	-1(1)
C(8)	25(1)	25(1)	45(1)	4(1)	10(1)	0(1)
C(9)	24(1)	24(1)	35(1)	-1(1)	4(1)	-1(1)
C(10)	36(1)	23(1)	60(1)	-3(1)	14(1)	-3(1)
C(11)	41(1)	36(1)	48(1)	-15(1)	11(1)	-12(1)
C(12)	35(1)	41(1)	32(1)	-5(1)	5(1)	-8(1)
C(13)	23(1)	27(1)	31(1)	-2(1)	7(1)	-3(1)
C(14)	26(1)	30(1)	28(1)	3(1)	1(1)	-2(1)
N(15)	28(1)	25(1)	27(1)	1(1)	6(1)	-1(1)
C(16)	28(1)	23(1)	26(1)	3(1)	5(1)	0(1)
N(17)	29(1)	46(1)	25(1)	-3(1)	6(1)	-5(1)
C(18)	29(1)	46(1)	30(1)	-2(1)	4(1)	-4(1)
C(19)	39(1)	36(1)	35(1)	1(1)	-2(1)	-7(1)
C(20)	56(1)	52(1)	36(1)	-10(1)	1(1)	11(1)
O(1W)	54(1)	50(1)	29(1)	4(1)	10(1)	-10(1)

Table C14. Hydrogen coordinates (x 10^4) and isotropic displacement parameters ($Å^2$x 10^3) for 3.1.

	x	y	z	U(eq)
H(2A)	7049(15)	7355(19)	2525(9)	49(4)
H(2B)	6884(15)	6514(19)	1733(9)	49(4)
H(3A)	5132(15)	5794(18)	2759(9)	47(4)
H(3B)	6486(16)	4910(20)	2800(9)	57(5)

H(4N)	5754(15)	4086(19)	1599(9)	47(4)
H(6N)	4455(14)	2524(17)	1090(8)	37(4)
H(7A)	2217(15)	2207(19)	1644(9)	47(4)
H(7B)	2769(15)	780(20)	1255(9)	52(4)
H(9)	2500(13)	4727(16)	661(7)	32(3)
H(10)	1419(14)	310(20)	192(8)	48(4)
H(11)	323(15)	1160(20)	-933(9)	53(4)
H(12)	325(13)	3822(18)	-1242(8)	39(4)
H(14A)	557(14)	6681(17)	-567(7)	35(4)
H(14B)	1757(13)	6372(16)	-1007(8)	32(3)
H(15N)	1958(14)	7274(17)	443(8)	36(4)
H(17N)	3762(14)	7806(17)	950(9)	39(4)
H(18A)	5816(14)	7085(18)	512(8)	39(4)
H(18B)	5645(14)	8751(18)	126(8)	41(4)
H(19A)	5504(15)	10000(20)	1262(9)	53(4)
H(19B)	6819(15)	9082(18)	1261(8)	49(4)
H(20A)	4915(15)	8460(20)	2885(9)	51(4)
H(20B)	4538(18)	9790(20)	2306(10)	67(5)
H(20C)	5991(17)	9740(20)	2684(10)	64(5)
H(1W1)	2880(17)	2770(20)	3041(11)	59(5)
H(1W2)	2430(20)	1320(30)	3100(12)	82(7)

Table C15. Torsion angles [°] for 3.1.

C(20)-N(1)-C(2)-C(3)	84.69(15)	C(10)-C(11)-C(12)-C(13)	0.6(2)

C(19)-N(1)-C(2)-C(3)	-148.14(12)	C(8)-C(9)-C(13)-C(12)	0.35(17)
N(1)-C(2)-C(3)-N(4)	79.38(16)	C(8)-C(9)-C(13)-C(14)	178.66(11)
C(2)-C(3)-N(4)-C(5)	-132.79(14)	C(11)-C(12)-C(13)-C(9)	-1.09(18)
C(3)-N(4)-C(5)-O(1)	10.7(2)	C(11)-C(12)-C(13)-C(14)	-179.42(12)
C(3)-N(4)-C(5)-N(6)	-169.23(12)	C(9)-C(13)-C(14)-N(15)	3.23(16)
O(1)-C(5)-N(6)-C(7)	6.05(18)	C(12)-C(13)-C(14)-N(15)	-178.49(10)
N(4)-C(5)-N(6)-C(7)	-173.97(12)	C(13)-C(14)-N(15)-C(16)	87.73(13)
C(5)-N(6)-C(7)-C(8)	106.02(15)	C(14)-N(15)-C(16)-O(2)	21.53(16)
N(6)-C(7)-C(8)-C(10)	137.88(13)	C(14)-N(15)-C(16)-N(17)	-161.99(10)
N(6)-C(7)-C(8)-C(9)	-42.72(18)	O(2)-C(16)-N(17)-C(18)	-9.13(18)
C(10)-C(8)-C(9)-C(13)	0.86(17)	N(15)-C(16)-N(17)-C(18)	174.39(11)
C(7)-C(8)-C(9)-C(13)	-178.56(11)	C(16)-N(17)-C(18)-C(19)	172.80(11)
C(9)-C(8)-C(10)-C(11)	-1.32(19)	C(20)-N(1)-C(19)-C(18)	-144.50(12)
C(7)-C(8)-C(10)-C(11)	178.08(13)	C(2)-N(1)-C(19)-C(18)	88.64(13)
C(8)-C(10)-C(11)-C(12)	0.6(2)	N(17)-C(18)-C(19)-N(1)	57.81(15)

Symmetry transformations used to generate equivalent atoms:

Table C16. Hydrogen bonds for 3.1 [Å and °].

D-H...A	d(D-H)	d(H...A)	d(D...A)	<(DHA)
N(4)-H(4N)...O(2)#1	0.855(17)	2.115(17)	2.9092(15)	154.2(15)
N(6)-H(6N)...O(2)#1	0.878(16)	2.057(16)	2.8826(15)	156.4(13)
N(15)-H(15N)...O(1W)#2	0.879(15)	2.195(15)	3.0176(16)	155.7(13)
N(17)-H(17N)...O(1W)#2	0.890(16)	2.223(16)	3.0469(15)	153.7(13)
O(1W)-H(1W1)...O(1)	0.83(2)	1.94(2)	2.7716(15)	175.4(18)
O(1W)-H(1W2)...O(1)#3	0.87(2)	2.07(2)	2.9342(16)	169(2)

Symmetry transformations used to generate equivalent atoms:

#1 -x+1,-y+1,-z #2 -x+1/2,y+1/2,-z+1/2 #3 -x+1/2,y-1/2,-z+1/2

Table C17. Crystal data and structure refinement for 2.2(TetraEt).

Empirical formula	C16 H24 N6 O4	
Formula weight	364.41	
Temperature	296(2) K	
Wavelength	1.54178 Å	
Crystal system	Triclinic	
Space group	P-1	
Unit cell dimensions	a = 17.1327(12) Å	□= 109.215(3)°.
	b = 23.4368(17) Å	□= 91.596(3)°.
	c = 29.688(2) Å	□ = 102.410(2)°.
Volume	10930.9(14) Å^3	
Z	22	
Density (calculated)	1.218 Mg/m^3	
Absorption coefficient	0.746 mm^{-1}	
F(000)	4268	
Crystal size	0.460 x 0.060 x 0.020 mm^3	
Theta range for data collection	1.585 to 68.257°.	
Index ranges	-17<=h<=20, -25<=k<=27, -35<=l<=26	
Reflections collected	83687	
Independent reflections	37073 [R(int) = 0.0495]	

Completeness to theta = 66.000°	95.7 %
Absorption correction	Multi-scan
Max. and min. transmission	1.000 and 0.766
Refinement method	Full-matrix least-squares on F^2
Data / restraints / parameters	37073 / 1 / 2845
Goodness-of-fit on F^2	1.016
Final R indices [I>2sigma(I)]	R1 = 0.0628, wR2 = 0.1830
R indices (all data)	R1 = 0.1051, wR2 = 0.2076
Extinction coefficient	n/a
Largest diff. peak and hole	0.551 and -0.414 e.$Å^{-3}$

Table C18. Atomic coordinates (x 10^4) and equivalent isotropic displacement parameters ($Å^2$x 10^3) for 2.2(TetraEt). U(eq) is defined as one third of the trace of the orthogonalized U^{ij} tensor.

	x	y	z	U(eq)
O(1H)	9063(1)	-1548(1)	-3624(1)	92(1)
O(2H)	6832(2)	163(1)	-4038(1)	98(1)
O(3H)	6064(1)	-1099(1)	-4933(1)	97(1)
O(4H)	7540(1)	-1966(1)	-3106(1)	85(1)
N(1H)	8976(1)	-687(1)	-3024(1)	80(1)
N(2H)	7790(2)	-18(2)	-4536(1)	100(1)
N(3H)	7926(1)	-708(1)	-3850(1)	70(1)

N(4H)	5319(2)	-1795(2)	-4642(1)	94(1)
N(5H)	6552(2)	-2612(1)	-3681(1)	92(1)
N(8H)	6601(1)	-1697(1)	-4057(1)	66(1)
C(1H)	8701(2)	-1157(1)	-3426(1)	69(1)
C(2H)	7909(2)	-1166(1)	-3671(1)	66(1)
C(4H)	7281(2)	-745(1)	-4131(1)	70(1)
C(5H)	7273(2)	-159(2)	-4242(1)	78(1)
C(6H)	5967(2)	-1382(2)	-4645(1)	80(1)
C(7H)	6640(2)	-1266(1)	-4264(1)	69(1)
C(9H)	7218(2)	-1642(1)	-3748(1)	63(1)
C(10H)	7112(2)	-2101(1)	-3486(1)	71(1)
C(11H)	9765(2)	-560(2)	-2764(1)	92(1)
C(12H)	10287(3)	37(2)	-2748(2)	126(1)
C(13H)	7895(3)	559(2)	-4641(2)	127(2)
C(14H)	7351(5)	548(4)	-5003(3)	236(4)
C(15H)	4604(2)	-1984(3)	-4991(2)	127(2)
C(16H)	4465(5)	-2629(4)	-5281(3)	284(6)
C(17H)	6370(3)	-3101(2)	-3468(2)	139(2)
C(18H)	5594(5)	-3309(4)	-3441(4)	259(5)

Table C19. Bond lengths [Å] for 2.2(TetraEt).

O(1H)-C(1H)	1.216(3)	N(5H)-H(5HN)	0.86	C(13H)-H(13S)	0.97
O(2H)-C(5H)	1.216(3)	N(8H)-C(9H)	1.336(3)	C(14H)-H(14Y)	0.96
O(3H)-C(6H)	1.236(4)	N(8H)-C(7H)	1.337(4)	C(14H)-H(14Z)	0.96
O(4H)-C(10H)	1.238(3)	C(1H)-C(2H)	1.515(4)	C(14H)-H(15S)	0.96
N(1H)-C(1H)	1.320(4)	C(2H)-C(9H)	1.395(4)	C(15H)-C(16H)	1.435(8)
N(1H)-C(11H)	1.459(4)	C(4H)-C(7H)	1.391(4)	C(15H)-H(15T)	0.97
N(1H)-H(1HN)	0.86	C(4H)-C(5H)	1.515(4)	C(15H)-H(15U)	0.97
N(2H)-C(5H)	1.329(4)	C(6H)-C(7H)	1.509(4)	C(16H)-H(17R)	0.96
N(2H)-C(13H)	1.461(5)	C(9H)-C(10H)	1.505(4)	C(16H)-H(17S)	0.96
N(2H)-H(2HN)	0.86	C(11H)-C(12H)	1.473(6)	C(16H)-H(17T)	0.96
N(3H)-C(4H)	1.337(4)	C(11H)-H(11Q)	0.97	C(17H)-C(18H)	1.330(8)
N(3H)-C(2H)	1.341(4)	C(11H)-H(11R)	0.97	C(17H)-H(17U)	0.97
N(4H)-C(6H)	1.309(4)	C(12H)-H(12Y)	0.96	C(17H)-H(17V)	0.97
N(4H)-C(15H)	1.471(5)	C(12H)-H(12Z)	0.96	C(18H)-H(18Y)	0.96
N(4H)-H(4HN)	0.86	C(12H)-H(13Q)	0.96	C(18H)-H(18Z)	0.96
N(5H)-C(10H)	1.308(4)	C(13H)-C(14H)	1.392(8)	C(18H)-H(19A)	0.96
N(5H)-C(17H)	1.464(5)	C(13H)-H(13R)	0.97		

Table C20. Bond angles [°] for 2.2(TetraEt).

C(1H)-N(1H)-C(11H)	124.1(2)	O(2H)-C(5H)-N(2H)	124.7(3)	C(11H)-C(12H)-H(12Z)	109.5
C(1H)-N(1H)-H(1HN)	117.9	O(2H)-C(5H)-C(4H)	118.4(3)	H(12Y)-C(12H)-H(12Z)	109.5
C(11H)-N(1H)-H(1HN)	117.9	N(2H)-C(5H)-C(4H)	116.8(3)	C(11H)-C(12H)-H(13Q)	109.5
C(5H)-N(2H)-C(13H)	122.6(3)	O(3H)-C(6H)-N(4H)	125.5(3)	H(12Y)-C(12H)-H(13Q)	109.5
C(5H)-N(2H)-H(2HN)	118.7	O(3H)-C(6H)-C(7H)	119.5(3)	H(12Z)-C(12H)-H(13Q)	109.5
C(13H)-N(2H)-H(2HN)	118.7	N(4H)-C(6H)-C(7H)	115.0(3)	C(14H)-C(13H)-N(2H)	115.5(5)
C(4H)-N(3H)-C(2H)	117.9(3)	N(8H)-C(7H)-C(4H)	120.5(2)	C(14H)-C(13H)-H(13R)	108.4
C(6H)-N(4H)-C(15H)	123.4(4)	N(8H)-C(7H)-C(6H)	116.6(3)	N(2H)-C(13H)-H(13R)	108.4

C(6H)-N(4H)-H(4HN)	118.3	C(4H)-C(7H)-C(6H)	122.9(3)	C(14H)-C(13H)-H(13S)	108.4
C(15H)-N(4H)-H(4HN)	118.3	N(8H)-C(9H)-C(2H)	120.2(3)	N(2H)-C(13H)-H(13S)	108.4
C(10H)-N(5H)-C(17H)	122.7(3)	N(8H)-C(9H)-C(10H)	116.7(3)	H(13R)-C(13H)-H(13S)	107.5
C(10H)-N(5H)-H(5HN)	118.6	C(2H)-C(9H)-C(10H)	123.1(2)	C(13H)-C(14H)-H(14Y)	109.5
C(17H)-N(5H)-H(5HN)	118.6	O(4H)-C(10H)-N(5H)	125.2(3)	C(13H)-C(14H)-H(14Z)	109.5
C(9H)-N(8H)-C(7H)	118.6(3)	O(4H)-C(10H)-C(9H)	118.7(3)	H(14Y)-C(14H)-H(14Z)	109.5
O(1H)-C(1H)-N(1H)	124.7(3)	N(5H)-C(10H)-C(9H)	116.1(3)	C(13H)-C(14H)-H(15S)	109.5
O(1H)-C(1H)-C(2H)	119.0(3)	N(1H)-C(11H)-C(12H)	112.4(3)	H(14Y)-C(14H)-H(15S)	109.5
N(1H)-C(1H)-C(2H)	116.1(2)	N(1H)-C(11H)-H(11Q)	109.1	H(14Z)-C(14H)-H(15S)	109.5
N(3H)-C(2H)-C(9H)	120.9(2)	C(12H)-C(11H)-H(11Q)	109.1	C(16H)-C(15H)-N(4H)	111.0(4)
N(3H)-C(2H)-C(1H)	115.4(3)	N(1H)-C(11H)-H(11R)	109.1	C(16H)-C(15H)-H(15T)	109.4
C(9H)-C(2H)-C(1H)	123.5(3)	C(12H)-C(11H)-H(11R)	109.1	N(4H)-C(15H)-H(15T)	109.4
N(3H)-C(4H)-C(7H)	120.8(3)	H(11Q)-C(11H)-H(11R)	107.8	C(16H)-C(15H)-H(15U)	109.4
N(3H)-C(4H)-C(5H)	115.0(3)	C(11H)-C(12H)-H(12Y)	109.5	N(4H)-C(15H)-H(15U)	109.4
C(7H)-C(4H)-C(5H)	123.9(3)				

Table C21. Anisotropic displacement parameters ($Å^2 x\ 10^3$) for 2.2(TetraEt). The anisotropic displacement factor exponent takes the form: $-2\pi^2[h^2 a^{*2} U^{11} + ... + 2 h k a^* b^* U^{12}]$

	U^{11}	U^{22}	U^{33}	U^{23}	U^{13}	U^{12}
O(1H)	87(1)	102(2)	86(1)	9(1)	5(1)	53(1)
O(2H)	117(2)	108(2)	105(2)	52(1)	46(1)	71(2)
O(3H)	100(2)	141(2)	76(1)	47(2)	18(1)	64(2)
O(4H)	104(2)	94(1)	68(1)	27(1)	11(1)	45(1)

N(1H)	72(1)	78(2)	84(2)	12(1)	1(1)	33(1)
N(2H)	111(2)	111(2)	113(2)	62(2)	48(2)	58(2)
N(3H)	72(1)	76(2)	73(1)	27(1)	16(1)	36(1)
N(4H)	74(2)	126(2)	79(2)	27(2)	-1(1)	32(2)
N(5H)	107(2)	90(2)	81(2)	37(2)	14(2)	13(2)
N(8H)	66(1)	81(2)	57(1)	17(1)	16(1)	34(1)
C(1H)	70(2)	73(2)	68(2)	19(1)	11(1)	34(1)
C(2H)	69(2)	73(2)	60(2)	16(1)	14(1)	37(1)
C(4H)	69(2)	84(2)	69(2)	26(1)	20(1)	42(2)
C(5H)	80(2)	93(2)	80(2)	38(2)	21(2)	42(2)
C(6H)	71(2)	107(2)	68(2)	22(2)	12(1)	46(2)
C(7H)	68(2)	88(2)	60(2)	22(1)	20(1)	43(2)
C(9H)	69(2)	70(2)	56(1)	15(1)	17(1)	34(1)
C(10H)	80(2)	78(2)	62(2)	20(1)	21(1)	37(2)
C(11H)	85(2)	94(2)	90(2)	21(2)	-8(2)	25(2)
C(12H)	104(3)	137(4)	118(3)	40(3)	-10(2)	-3(3)
C(13H)	149(4)	132(4)	139(4)	78(3)	46(3)	63(3)
C(14H)	306(10)	210(7)	201(7)	118(6)	-82(7)	20(7)
C(15H)	91(3)	178(5)	103(3)	28(3)	-13(2)	49(3)
C(16H)	207(7)	232(8)	296(10)	-79(8)	-156(7)	103(7)
C(17H)	146(4)	141(4)	137(4)	82(3)	15(3)	-4(3)
C(18H)	205(8)	308(11)	328(11)	244(10)	0(7)	-18(7)

Table C22. Hydrogen coordinates (x 10^4) and isotropic displacement parameters ($Å^2$x 10^3) for 2.2(TetraEt).

	x	y	z	U(eq)
H(1HN)	8669	-440	-2907	96
H(2HN)	8074	-276	-4670	120
H(4HN)	5311	-1965	-4426	113
H(5HN)	6280	-2663	-3945	111
H(11Q)	10024	-893	-2919	110
H(11R)	9699	-553	-2439	110
H(12Y)	10798	100	-2575	189
H(12Z)	10364	29	-3069	189
H(13Q)	10039	370	-2589	189
H(13R)	7853	890	-4350	152
H(13S)	8434	662	-4730	152
H(14Y)	7467	945	-5046	354
H(14Z)	7397	231	-5297	354
H(15S)	6815	460	-4916	354
H(15T)	4138	-1914	-4822	152
H(15U)	4677	-1732	-5196	152
H(17R)	3997	-2742	-5505	426
H(17S)	4923	-2698	-5453	426
H(17T)	4384	-2879	-5079	426
H(17U)	6579	-3449	-3656	166
H(17V)	6651	-2943	-3148	166
H(18Y)	5528	-3626	-3298	389

H(18Z)	5382	-2971	-3248	389
H(19A)	5310	-3478	-3757	389

Table C23. Torsion angles [°] for 2.2(TetraEt).

C(11H)-N(1H)-C(1H)-O(1H)	1.7(5)	N(3H)-C(4H)-C(7H)-C(6H)	-169.1(2)
C(11H)-N(1H)-C(1H)-C(2H)	-173.0(3)	C(5H)-C(4H)-C(7H)-C(6H)	17.7(4)
C(4H)-N(3H)-C(2H)-C(9H)	-4.4(4)	O(3H)-C(6H)-C(7H)-N(8H)	-161.3(3)
C(4H)-N(3H)-C(2H)-C(1H)	170.2(2)	N(4H)-C(6H)-C(7H)-N(8H)	17.6(4)
O(1H)-C(1H)-C(2H)-N(3H)	-107.8(3)	O(3H)-C(6H)-C(7H)-C(4H)	17.9(4)
N(1H)-C(1H)-C(2H)-N(3H)	67.2(3)	N(4H)-C(6H)-C(7H)-C(4H)	-163.2(3)
O(1H)-C(1H)-C(2H)-C(9H)	66.6(4)	C(7H)-N(8H)-C(9H)-C(2H)	-4.4(3)
N(1H)-C(1H)-C(2H)-C(9H)	-118.4(3)	C(7H)-N(8H)-C(9H)-C(10H)	174.0(2)
C(2H)-N(3H)-C(4H)-C(7H)	-5.1(4)	N(3H)-C(2H)-C(9H)-N(8H)	9.4(4)
C(2H)-N(3H)-C(4H)-C(5H)	168.7(2)	C(1H)-C(2H)-C(9H)-N(8H)	-164.7(2)
C(13H)-N(2H)-C(5H)-O(2H)	1.2(6)	N(3H)-C(2H)-C(9H)-C(10H)	-168.8(2)
C(13H)-N(2H)-C(5H)-C(4H)	-174.7(4)	C(1H)-C(2H)-C(9H)-C(10H)	17.1(4)
N(3H)-C(4H)-C(5H)-O(2H)	-104.8(3)	C(17H)-N(5H)-C(10H)-O(4H)	-0.9(5)
C(7H)-C(4H)-C(5H)-O(2H)	68.7(4)	C(17H)-N(5H)-C(10H)-C(9H)	-179.4(4)
N(3H)-C(4H)-C(5H)-N(2H)	71.3(4)	N(8H)-C(9H)-C(10H)-O(4H)	-158.7(2)
C(7H)-C(4H)-C(5H)-N(2H)	-115.2(3)	C(2H)-C(9H)-C(10H)-O(4H)	19.6(4)
C(15H)-N(4H)-C(6H)-O(3H)	0.2(5)	N(8H)-C(9H)-C(10H)-N(5H)	19.9(4)
C(15H)-N(4H)-C(6H)-C(7H)	-178.6(3)	C(2H)-C(9H)-C(10H)-N(5H)	-161.8(3)
C(9H)-N(8H)-C(7H)-C(4H)	-5.0(4)	C(1H)-N(1H)-C(11H)-C(12H)	116.0(4)
C(9H)-N(8H)-C(7H)-C(6H)	174.2(2)	C(5H)-N(2H)-C(13H)-C(14H)	-84.3(7)
N(3H)-C(4H)-C(7H)-N(8H)	10.1(4)	C(6H)-N(4H)-C(15H)-C(16H)	116.1(7)
C(5H)-C(4H)-C(7H)-N(8H)	-163.1(2)	C(10H)-N(5H)-C(17H)-C(18H)	132.4(7)

Table C24. Hydrogen bonds for 2.2(TetraEt) [Å and °].

D-H...A	d(D-H)	d(H...A)	d(D...A)	<(DHA)
N(1H)-H(1HN)...O(3G)	0.86	2.11	2.928(3)	159.8
N(2H)-H(2HN)...O(2I)	0.86	2.05	2.893(4)	166.3
N(4H)-H(4HN)...O(1G)	0.86	2.19	2.945(4)	147.0
N(5H)-H(5HN)...O(4I)	0.86	2.13	2.914(4)	151.9
N(1I)-H(1IN)...O(1H)	0.86	2.24	3.010(4)	149.3
N(2I)-H(2IN)...O(2J)	0.86	2.19	3.000(4)	157.5
N(4I)-H(4IN)...O(3H)	0.86	2.08	2.910(4)	160.8

Symmetry transformations used to generate equivalent atoms:

#1 -x,-y,-z #2 -x+1,-y+1,-z #3 -x+1,-y,-z-1

#4 x+1,y-1,z-1 #5 x-1,y+1,z+1

Table C25. Crystal data and structure refinement for 5.1.

Empirical formula	C20 H28 N6 O8 Pd2	
Formula weight	693.28	
Temperature	296(2) K	
Wavelength	1.54178 Å	
Crystal system	Triclinic	
Space group	P-1	
Unit cell dimensions	a = 7.0644(15) Å	□= 73.952(6)°.
	b = 9.275(2) Å	□= 73.576(7)°.

	c = 10.340(2) Å □ = 80.210(6)°.
Volume	621.4(2) $Å^3$
Z	1
Density (calculated)	1.853 Mg/m^3
Absorption coefficient	12.179 mm^{-1}
F(000)	346
Crystal size	0.110 x 0.095 x 0.050 mm^3
Theta range for data collection	4.594 to 70.313°.
Index ranges	-8<=h<=8, -11<=k<=11, -10<=l<=12
Reflections collected	14533
Independent reflections	2193 [R(int) = 0.0500]
Completeness to theta = 66.000°	96.5 %
Absorption correction	Multi-scan
Max. and min. transmission	1.000 and 0.573
Refinement method	Full-matrix least-squares on F^2
Data / restraints / parameters	2193 / 0 / 171
Goodness-of-fit on F^2	1.147
Final R indices [I>2sigma(I)]	R1 = 0.0354, wR2 = 0.0874
R indices (all data)	R1 = 0.0357, wR2 = 0.0878
Extinction coefficient	0.0081(7)
Largest diff. peak and hole	1.126 and -1.344 $e.Å^{-3}$

Table C26. Atomic coordinates (x 10^4) and equivalent isotropic displacement parameters ($Å^2$x 10^3) for 5.1. U(eq) is defined as one third of the trace of the orthogonalized U^{ij} tensor.

	x	y	z	U(eq)
Pd	1392(1)	2534(1)	-621(1)	37(1)
O(1)	1457(5)	383(4)	3387(3)	55(1)
O(2)	5903(5)	1598(4)	-3844(3)	57(1)
O(3)	-730(4)	4181(3)	-1082(4)	55(1)
O(4)	-2624(6)	2490(4)	-943(5)	86(1)
N(1)	528(4)	1950(3)	1495(3)	41(1)
N(2)	3532(4)	1038(3)	-253(3)	35(1)
N(3)	3022(5)	2637(4)	-2588(3)	44(1)
C(1)	1716(5)	911(4)	2073(4)	40(1)
C(2)	3495(5)	349(4)	1081(3)	35(1)
C(3)	4960(5)	749(4)	-1346(3)	36(1)
C(4)	4642(5)	1722(4)	-2713(3)	42(1)
C(5)	-1272(6)	2553(4)	2389(4)	48(1)
C(6)	-2951(6)	1619(5)	2700(5)	58(1)
C(7)	2534(7)	3628(5)	-3875(4)	53(1)
C(8)	1258(8)	2891(6)	-4384(5)	66(1)
C(9)	-2275(5)	3789(4)	-1223(4)	46(1)
C(10)	-3698(7)	5061(7)	-1752(6)	72(1)

Table C27. Bond lengths [Å] 5.1.

Pd-N(2)	1.917(3)	N(2)-C(2)	1.345(4)	C(6)-H(6C)	0.96
Pd-O(3)	2.007(3)	N(3)-C(4)	1.301(5)	C(7)-C(8)	1.494(7)

Pd-N(3)	2.020(3)	N(3)-C(7)	1.487(4)	C(7)-H(7A)	0.97
Pd-N(1)	2.038(3)	C(1)-C(2)	1.499(4)	C(7)-H(7B)	0.97
O(1)-C(1)	1.281(5)	C(2)-C(3)#1	1.393(5)	C(8)-H(8A)	0.96
O(1)-H(1O)	0.77(7)	C(3)-C(2)#1	1.393(5)	C(8)-H(8B)	0.96
O(2)-C(4)	1.275(5)	C(3)-C(4)	1.506(4)	C(8)-H(8C)	0.96
O(3)-C(9)	1.265(5)	C(5)-C(6)	1.497(6)	C(9)-C(10)	1.501(6)
O(4)-C(9)	1.210(5)	C(5)-H(5A)	0.97	C(10)-H(10A)	0.96
N(1)-C(1)	1.297(5)	C(5)-H(5B)	0.97	C(10)-H(10B)	0.96
N(1)-C(5)	1.471(4)	C(6)-H(6A)	0.96	C(10)-H(10C)	0.96
N(2)-C(3)	1.341(5)	C(6)-H(6B)	0.96		

Table C28. Bond angles [°] for 5.1.

N(2)-Pd-O(3)	176.62(10)	N(2)-C(2)-C(1)	112.4(3)	N(3)-C(7)-H(7A)	109.5
N(2)-Pd-N(3)	80.59(12)	C(3)#1-C(2)-C(1)	129.8(3)	C(8)-C(7)-H(7A)	109.5
O(3)-Pd-N(3)	97.12(13)	N(2)-C(3)-C(2)#1	117.6(3)	N(3)-C(7)-H(7B)	109.5
N(2)-Pd-N(1)	80.57(12)	N(2)-C(3)-C(4)	112.9(3)	C(8)-C(7)-H(7B)	109.5
O(3)-Pd-N(1)	101.64(13)	C(2)#1-C(3)-C(4)	129.5(3)	H(7A)-C(7)-H(7B)	108.1
N(3)-Pd-N(1)	161.12(13)	O(2)-C(4)-N(3)	126.4(3)	C(7)-C(8)-H(8A)	109.5
C(1)-O(1)-H(1O)	116(5)	O(2)-C(4)-C(3)	120.0(3)	C(7)-C(8)-H(8B)	109.5
C(9)-O(3)-Pd	117.0(3)	N(3)-C(4)-C(3)	113.5(3)	H(8A)-C(8)-H(8B)	109.5
C(1)-N(1)-C(5)	118.7(3)	N(1)-C(5)-C(6)	111.2(3)	C(7)-C(8)-H(8C)	109.5
C(1)-N(1)-Pd	114.2(2)	N(1)-C(5)-H(5A)	109.4	H(8A)-C(8)-H(8C)	109.5
C(5)-N(1)-Pd	127.1(3)	C(6)-C(5)-H(5A)	109.4	H(8B)-C(8)-H(8C)	109.5
C(3)-N(2)-C(2)	124.6(3)	N(1)-C(5)-H(5B)	109.4	O(4)-C(9)-O(3)	123.5(4)
C(3)-N(2)-Pd	117.6(2)	C(6)-C(5)-H(5B)	109.4	O(4)-C(9)-C(10)	121.3(4)
C(2)-N(2)-Pd	117.8(2)	H(5A)-C(5)-H(5B)	108	O(3)-C(9)-C(10)	115.2(4)
C(4)-N(3)-C(7)	118.2(3)	C(5)-C(6)-H(6A)	109.5	C(9)-C(10)-H(10A)	109.5
C(4)-N(3)-Pd	115.4(2)	C(5)-C(6)-H(6B)	109.5	C(9)-C(10)-H(10B)	109.5
C(7)-N(3)-Pd	126.5(3)	H(6A)-C(6)-H(6B)	109.5	H(10A)-C(10)-H(10B)	109.5

O(1)-C(1)-N(1)	124.4(3)	C(5)-C(6)-H(6C)	109.5	C(9)-C(10)-H(10C)	109.5
O(1)-C(1)-C(2)	120.6(3)	H(6A)-C(6)-H(6C)	109.5	H(10A)-C(10)-H(10C)	109.5
N(1)-C(1)-C(2)	114.9(3)	H(6B)-C(6)-H(6C)	109.5	H(10B)-C(10)-H(10C)	109.5
N(2)-C(2)-C(3)#1	117.8(3)	N(3)-C(7)-C(8)	110.8(3)		

Symmetry transformations used to generate equivalent atoms:

#1 -x+1,-y,-z

Table C29. Anisotropic displacement parameters ($Å^2$x 10^3) for 5.1. The anisotropic displacement factor exponent takes the form: $-2\pi^2[h^2 a^{*2}U^{11} + ... + 2 h k a^* b^* U^{12}]$

	U^{11}	U^{22}	U^{33}	U^{23}	U^{13}	U^{12}
Pd	33(1)	34(1)	44(1)	-4(1)	-18(1)	-2(1)
O(1)	55(2)	65(2)	37(1)	-10(1)	-9(1)	5(1)
O(2)	60(2)	68(2)	34(1)	0(1)	-18(1)	4(1)
O(3)	49(2)	38(2)	82(2)	-7(1)	-31(1)	-2(1)
O(4)	74(2)	55(2)	145(4)	-7(2)	-64(2)	-17(2)
N(1)	36(1)	40(2)	48(2)	-13(1)	-11(1)	-1(1)
N(2)	33(1)	38(2)	35(1)	-4(1)	-13(1)	-6(1)
N(3)	49(2)	42(2)	41(1)	1(1)	-24(1)	-2(1)
C(1)	37(2)	40(2)	43(2)	-12(1)	-10(1)	-5(1)
C(2)	33(2)	40(2)	34(1)	-5(1)	-13(1)	-7(1)
C(3)	35(2)	40(2)	35(1)	-5(1)	-16(1)	-5(1)

C(4)	47(2)	47(2)	34(2)	-1(1)	-18(1)	-8(2)
C(5)	45(2)	47(2)	49(2)	-18(2)	-7(2)	2(2)
C(6)	45(2)	56(2)	64(2)	-9(2)	-4(2)	-6(2)
C(7)	66(2)	45(2)	45(2)	5(2)	-29(2)	-1(2)
C(8)	82(3)	67(3)	57(2)	-5(2)	-44(2)	-2(2)
C(9)	40(2)	46(2)	48(2)	-4(2)	-15(1)	-3(2)
C(10)	53(2)	78(3)	77(3)	-1(2)	-28(2)	10(2)

Table C30. Hydrogen coordinates (x 10^4) and isotropic displacement parameters ($Å^2$x 10^3) for 5.1.

	x	y	z	U(eq)
H(1O)	2200(100)	-270(80)	3620(70)	90(20)
H(5A)	-1650	3581	1929	57
H(5B)	-998	2570	3252	57
H(6A)	-4116	2056	3257	87
H(6B)	-2604	613	3195	87
H(6C)	-3209	1588	1845	87
H(7A)	3749	3845	-4589	63
H(7B)	1845	4575	-3688	63
H(8A)	762	3612	-5107	99
H(8B)	166	2524	-3630	99
H(8C)	2028	2064	-4742	99
H(10A)	-3429	5982	-1617	108

H(10B)	-5031	4856	-1254	108
H(10C)	-3543	5158	-2724	108

Table C31. Torsion angles [°] for 5.1.

C(5)-N(1)-C(1)-O(1)	-1.4(5)	Pd-N(2)-C(3)-C(4)	1.7(4)
Pd-N(1)-C(1)-O(1)	179.8(3)	C(7)-N(3)-C(4)-O(2)	1.3(6)
C(5)-N(1)-C(1)-C(2)	179.2(3)	Pd-N(3)-C(4)-O(2)	-179.4(3)
Pd-N(1)-C(1)-C(2)	0.4(4)	C(7)-N(3)-C(4)-C(3)	-178.7(3)
C(3)-N(2)-C(2)-C(3)#1	-0.6(6)	Pd-N(3)-C(4)-C(3)	0.7(4)
Pd-N(2)-C(2)-C(3)#1	179.3(2)	N(2)-C(3)-C(4)-O(2)	178.5(3)
C(3)-N(2)-C(2)-C(1)	179.8(3)	C(2)#1-C(3)-C(4)-O(2)	-0.3(6)
Pd-N(2)-C(2)-C(1)	-0.3(4)	N(2)-C(3)-C(4)-N(3)	-1.5(5)
O(1)-C(1)-C(2)-N(2)	-179.5(3)	C(2)#1-C(3)-C(4)-N(3)	179.7(3)
N(1)-C(1)-C(2)-N(2)	0.0(4)	C(1)-N(1)-C(5)-C(6)	-86.9(4)
O(1)-C(1)-C(2)-C(3)#1	0.9(6)	Pd-N(1)-C(5)-C(6)	91.7(4)
N(1)-C(1)-C(2)-C(3)#1	-179.6(3)	C(4)-N(3)-C(7)-C(8)	91.8(5)
C(2)-N(2)-C(3)-C(2)#1	0.6(6)	Pd-N(3)-C(7)-C(8)	-87.4(4)
Pd-N(2)-C(3)-C(2)#1	-179.3(2)	Pd-O(3)-C(9)-O(4)	8.8(6)
C(2)-N(2)-C(3)-C(4)	-178.4(3)	Pd-O(3)-C(9)-C(10)	-172.2(3)

Symmetry transformations used to generate equivalent atoms:

#1 -x+1,-y,-z

Table C32. Crystal data and structure refinement for 2.8(TetraGly).

Empirical formula	C24 H40 N6 O12
Formula weight	604.62

Temperature	228(2) K
Wavelength	0.71073 Å
Crystal system	Monoclinic
Space group	$P2_1/c$
Unit cell dimensions	a = 11.0587(19) Å □= 90°.
	b = 14.955(3) Å □= 101.133(2)°.
	c = 8.8548(15) Å □ = 90°.
Volume	1436.9(4) $Å^3$
Z	2
Density (calculated)	1.397 Mg/m^3
Absorption coefficient	0.113 mm^{-1}
F(000)	644
Crystal size	0.490 x 0.330 x 0.180 mm^3
Theta range for data collection	1.877 to 30.521°.
Index ranges	-15<=h<=15, -21<=k<=21, -10<=l<=12
Reflections collected	11257
Independent reflections	4320 [R(int) = 0.0541]
Completeness to theta = 27.500°	99.4 %
Absorption correction	Multi-scan
Max. and min. transmission	1.000 and 0.622
Refinement method	Full-matrix least-squares on F^2
Data / restraints / parameters	4320 / 0 / 270
Goodness-of-fit on F^2	1.031
Final R indices [I>2sigma(I)]	R1 = 0.0521, wR2 = 0.1312
R indices (all data)	R1 = 0.1028, wR2 = 0.1725

Extinction coefficient	n/a
Largest diff. peak and hole	0.335 and -0.284 e.Å^{-3}

Table C33. Atomic coordinates (x 10^4) and equivalent isotropic displacement parameters (Å^{2}x 10^3) for 2.8(TetraGly). U(eq) is defined as one third of the trace of the orthogonalized U^{ij} tensor.

	x	y	z	U(eq)
O(1)	2022(1)	1084(1)	2808(2)	44(1)
O(2)	609(1)	-1695(1)	7916(2)	44(1)
O(3)	3683(1)	-1290(1)	1418(2)	44(1)
O(4)	3970(2)	-3179(1)	563(2)	60(1)
O(5)	-1750(1)	-3284(1)	7517(2)	39(1)
O(6)	-3873(2)	-2140(1)	7937(2)	57(1)
N(1)	2949(2)	-186(1)	3826(2)	33(1)
N(2)	-177(2)	-2404(1)	5677(2)	32(1)
N(3)	956(1)	-602(1)	5017(2)	28(1)
C(1)	2028(2)	400(1)	3575(2)	28(1)
C(2)	949(2)	194(1)	4320(2)	26(1)
C(4)	11(2)	-802(1)	5697(2)	26(1)
C(5)	147(2)	-1687(1)	6546(2)	28(1)
C(6)	4048(2)	-77(1)	3168(2)	34(1)
C(7)	3878(2)	-363(1)	1518(3)	38(1)
C(8)	3506(3)	-1615(2)	-120(3)	50(1)
C(9)	3086(3)	-2561(2)	-156(4)	58(1)

C(10)	-22(2)	-3312(1)	6277(3)	39(1)
C(11)	-1229(2)	-3744(1)	6389(2)	40(1)
C(12)	-2962(2)	-3582(2)	7591(3)	46(1)
C(13)	-3499(2)	-2973(2)	8628(3)	47(1)

Table C34. Bond lengths [Å] for 2.8(TetraGly).

O(1)-C(1)	1.226(2)	N(2)-C(10)	1.456(2)	C(8)-H(8A)	0.99(3)
O(2)-C(5)	1.221(2)	N(2)-H(2N)	0.89(2)	C(8)-H(8B)	1.01(3)
O(3)-C(7)	1.403(2)	N(3)-C(4)	1.337(2)	C(9)-H(9A)	1.04(3)
O(3)-C(8)	1.423(3)	N(3)-C(2)	1.339(2)	C(9)-H(9B)	0.90(3)
O(4)-C(9)	1.406(3)	C(1)-C(2)	1.503(2)	C(10)-C(11)	1.503(3)
O(4)-H(40)	0.86(3)	C(2)-C(4)#1	1.396(2)	C(10)-H(10A)	0.96(2)
O(5)-C(11)	1.423(2)	C(4)-C(2)#1	1.396(2)	C(10)-H(10B)	0.98(2)
O(5)-C(12)	1.426(2)	C(4)-C(5)	1.515(2)	C(11)-H(11A)	1.02(2)
O(6)-C(13)	1.413(3)	C(6)-C(7)	1.498(3)	C(11)-H(11B)	0.95(2)
O(6)-H(6O)	0.81(3)	C(6)-H(6A)	1.01(2)	C(12)-C(13)	1.496(4)
N(1)-C(1)	1.330(2)	C(6)-H(6B)	0.98(2)	C(12)-H(12A)	1.01(2)
N(1)-C(6)	1.455(2)	C(7)-H(7A)	0.97(2)	C(12)-H(12B)	1.01(2)
N(1)-H(1N)	0.90(2)	C(7)-H(7B)	1.05(2)	C(13)-H(13A)	1.00(2)
N(2)-C(5)	1.328(2)	C(8)-C(9)	1.487(4)	C(13)-H(13B)	0.98(3)

Table C35. Bond angles [°] for 2.8(TetraGly).

C(7)-O(3)-C(8)	112.90(17)	N(1)-C(6)-H(6A)	108.6(12)	N(2)-C(10)-H(10A)	108.6(13)
C(9)-O(4)-H(40)	114.1(18)	C(7)-C(6)-H(6A)	108.4(12)	C(11)-C(10)-H(10A)	109.2(13)
C(11)-O(5)-C(12)	113.09(16)	N(1)-C(6)-H(6B)	106.8(12)	N(2)-C(10)-H(10B)	107.6(13)

C(13)-O(6)-H(6O)	110(2)	C(7)-C(6)-H(6B)	108.8(12)	C(11)-C(10)-H(10B)	110.2(13)
C(1)-N(1)-C(6)	122.09(16)	H(6A)-C(6)-H(6B)	110.6(17)	H(10A)-C(10)-H(10B)	108.8(19)
C(1)-N(1)-H(1N)	119.5(15)	O(3)-C(7)-C(6)	109.43(17)	O(5)-C(11)-C(10)	108.90(16)
C(6)-N(1)-H(1N)	118.3(15)	O(3)-C(7)-H(7A)	111.4(14)	O(5)-C(11)-H(11A)	106.7(13)
C(5)-N(2)-C(10)	122.81(17)	C(6)-C(7)-H(7A)	113.2(13)	C(10)-C(11)-H(11A)	112.6(13)
C(5)-N(2)-H(2N)	115.9(15)	O(3)-C(7)-H(7B)	108.6(12)	O(5)-C(11)-H(11B)	110.4(13)
C(10)-N(2)-H(2N)	121.2(15)	C(6)-C(7)-H(7B)	109.4(13)	C(10)-C(11)-H(11B)	110.7(13)
C(4)-N(3)-C(2)	118.13(15)	H(7A)-C(7)-H(7B)	104.6(18)	H(11A)-C(11)-H(11B)	107.5(19)
O(1)-C(1)-N(1)	124.38(17)	O(3)-C(8)-C(9)	109.3(2)	O(5)-C(12)-C(13)	108.99(18)
O(1)-C(1)-C(2)	119.63(15)	O(3)-C(8)-H(8A)	108.0(15)	O(5)-C(12)-H(12A)	110.8(13)
N(1)-C(1)-C(2)	115.99(15)	C(9)-C(8)-H(8A)	109.4(15)	C(13)-C(12)-H(12A)	110.8(13)
N(3)-C(2)-C(4)#1	121.40(15)	O(3)-C(8)-H(8B)	109.3(16)	O(5)-C(12)-H(12B)	108.2(14)
N(3)-C(2)-C(1)	116.78(15)	C(9)-C(8)-H(8B)	110.6(15)	C(13)-C(12)-H(12B)	108.1(13)
C(4)#1-C(2)-C(1)	121.81(15)	H(8A)-C(8)-H(8B)	110(2)	H(12A)-C(12)-H(12B)	109.9(19)
N(3)-C(4)-C(2)#1	120.48(15)	O(4)-C(9)-C(8)	115.4(2)	O(6)-C(13)-C(12)	112.8(2)
N(3)-C(4)-C(5)	114.10(15)	O(4)-C(9)-H(9A)	103.7(15)	O(6)-C(13)-H(13A)	110.9(14)
C(2)#1-C(4)-C(5)	125.27(15)	C(8)-C(9)-H(9A)	109.1(15)	C(12)-C(13)-H(13A)	106.9(13)
O(2)-C(5)-N(2)	125.62(17)	O(4)-C(9)-H(9B)	105(2)	O(6)-C(13)-H(13B)	105.0(16)
O(2)-C(5)-C(4)	118.90(16)	C(8)-C(9)-H(9B)	107.4(19)	C(12)-C(13)-H(13B)	109.1(16)
N(2)-C(5)-C(4)	115.30(15)	H(9A)-C(9)-H(9B)	116(2)	H(13A)-C(13)-H(13B)	112(2)
N(1)-C(6)-C(7)	113.67(17)	N(2)-C(10)-C(11)	112.36(18)		

Symmetry transformations used to generate equivalent atoms:

#1 -x,-y,-z+1

Table C36. Anisotropic displacement parameters ($Å^2 x\ 10^3$) for 2.7(TetraGly). The anisotropic displacement factor exponent takes the form: $-2\pi^2 [\ h^2 a^{*2} U^{11} + ... + 2\ h\ k\ a^*\ b^*\ U^{12}\ ]$

	U^{11}	U^{22}	U^{33}	U^{23}	U^{13}	U^{12}

O(1)	43(1)	34(1)	60(1)	16(1)	27(1)	5(1)
O(2)	53(1)	46(1)	30(1)	6(1)	3(1)	2(1)
O(3)	61(1)	32(1)	41(1)	-3(1)	14(1)	2(1)
O(4)	60(1)	43(1)	70(1)	-16(1)	-5(1)	7(1)
O(5)	39(1)	42(1)	37(1)	-2(1)	10(1)	-10(1)
O(6)	39(1)	49(1)	85(1)	22(1)	18(1)	-3(1)
N(1)	36(1)	28(1)	40(1)	4(1)	20(1)	3(1)
N(2)	47(1)	25(1)	28(1)	5(1)	15(1)	1(1)
N(3)	30(1)	25(1)	31(1)	0(1)	11(1)	0(1)
C(1)	31(1)	25(1)	32(1)	-1(1)	14(1)	-1(1)
C(2)	31(1)	24(1)	26(1)	-2(1)	9(1)	-3(1)
C(4)	28(1)	26(1)	25(1)	-1(1)	9(1)	-1(1)
C(5)	29(1)	30(1)	29(1)	4(1)	13(1)	2(1)
C(6)	33(1)	30(1)	43(1)	-1(1)	17(1)	0(1)
C(7)	45(1)	32(1)	42(1)	3(1)	21(1)	2(1)
C(8)	54(2)	48(1)	44(1)	-7(1)	2(1)	3(1)
C(9)	53(2)	47(1)	68(2)	-17(1)	-3(1)	5(1)
C(10)	55(1)	26(1)	43(1)	6(1)	24(1)	7(1)
C(11)	58(1)	28(1)	37(1)	2(1)	13(1)	-4(1)
C(12)	40(1)	43(1)	53(1)	8(1)	7(1)	-12(1)
C(13)	38(1)	49(1)	57(2)	14(1)	17(1)	-4(1)

Table C37. Hydrogen coordinates (x 10^4) and isotropic displacement parameters ($Å^2$x 10^3) for 2.8(TetraGly).

	x	y	z	U(eq)
H(40)	4470(30)	-2969(18)	1350(30)	69(9)
H(6O)	-3280(30)	-1881(19)	7720(30)	75(9)
H(1N)	2880(20)	-684(16)	4380(30)	55(7)
H(2N)	-480(20)	-2299(15)	4690(30)	47(6)
H(6A)	4292(19)	573(15)	3240(20)	40(6)
H(6B)	4693(19)	-446(13)	3780(20)	33(5)
H(7A)	3220(20)	-39(16)	840(30)	50(6)
H(7B)	4680(20)	-213(15)	1100(30)	53(6)
H(8A)	2860(20)	-1244(17)	-760(30)	61(7)
H(8B)	4300(30)	-1566(17)	-510(30)	72(8)
H(9A)	2880(20)	-2778(18)	-1290(30)	71(8)
H(9B)	2470(30)	-2590(20)	370(30)	77(10)
H(10A)	500(20)	-3294(14)	7280(30)	40(6)
H(10B)	390(20)	-3657(15)	5590(30)	46(6)
H(11A)	-1860(20)	-3707(16)	5390(30)	49(6)
H(11B)	-1115(19)	-4358(16)	6650(20)	46(6)
H(12A)	-2950(20)	-4218(16)	7970(30)	52(7)
H(12B)	-3490(20)	-3539(16)	6520(30)	55(7)
H(13A)	-2860(20)	-2890(15)	9580(30)	47(6)
H(13B)	-4260(30)	-3242(18)	8850(30)	72(8)

Table C38. Torsion angles [°] for 2.7(TetraGly).

C(6)-N(1)-C(1)-O(1)	-1.5(3)	C(2)#1-C(4)-C(5)-O(2)	-82.7(2)
C(6)-N(1)-C(1)-C(2)	179.45(16)	N(3)-C(4)-C(5)-N(2)	-82.5(2)
C(4)-N(3)-C(2)-C(4)#1	0.3(3)	C(2)#1-C(4)-C(5)-N(2)	102.0(2)
C(4)-N(3)-C(2)-C(1)	179.69(15)	C(1)-N(1)-C(6)-C(7)	-79.9(2)
O(1)-C(1)-C(2)-N(3)	173.78(17)	C(8)-O(3)-C(7)-C(6)	179.66(18)
N(1)-C(1)-C(2)-N(3)	-7.2(2)	N(1)-C(6)-C(7)-O(3)	-66.2(2)
O(1)-C(1)-C(2)-C(4)#1	-6.8(3)	C(7)-O(3)-C(8)-C(9)	-169.9(2)
N(1)-C(1)-C(2)-C(4)#1	172.26(16)	O(3)-C(8)-C(9)-O(4)	-69.0(3)
C(2)-N(3)-C(4)-C(2)#1	-0.3(3)	C(5)-N(2)-C(10)-C(11)	108.4(2)
C(2)-N(3)-C(4)-C(5)	-175.94(15)	C(12)-O(5)-C(11)-C(10)	173.62(17)
C(10)-N(2)-C(5)-O(2)	0.4(3)	N(2)-C(10)-C(11)-O(5)	-66.2(2)
C(10)-N(2)-C(5)-C(4)	175.32(16)	C(11)-O(5)-C(12)-C(13)	-171.52(18)
N(3)-C(4)-C(5)-O(2)	92.7(2)	O(5)-C(12)-C(13)-O(6)	75.2(2)

Symmetry transformations used to generate equivalent atoms:

#1 -x,-y,-z+1

Table C39. Hydrogen bonds for 2.8(TetraGly) [Å and °].

D-H...A	d(D-H)	d(H...A)	d(D...A)	<(DHA)
O(4)-H(40)...O(6)#2	0.86(3)	2.09(3)	2.898(3)	156(3)
O(6)-H(6O)...O(1)#1	0.81(3)	1.96(3)	2.765(2)	171(3)
N(1)-H(1N)...O(4)#3	0.90(2)	2.22(2)	2.991(2)	142(2)
N(2)-H(2N)...O(2)#4	0.89(2)	2.63(2)	3.062(2)	110.8(17)
N(2)-H(2N)...O(5)#4	0.89(2)	2.32(2)	3.168(2)	160(2)
C(6)-H(6A)...O(6)#1	1.01(2)	2.57(2)	3.452(3)	146.1(15)

C(8)-H(8A)...O(2)#5	0.99(3)	2.63(3)	3.339(3)	128.9(18)
C(10)-H(10B)...O(2)#4	0.98(2)	2.48(2)	3.185(3)	128.7(17)

Symmetry transformations used to generate equivalent atoms:

#1 -x,-y,-z+1 #2 x+1,-y-1/2,z-1/2 #3 x,-y-1/2,z+1/2

#4 x,-y-1/2,z-1/2 #5 x,y,z-1

Table C40. Crystal data and structure refinement for 5.5.

Empirical formula	C24 H42 Cl2 N6 O14 Pd2	
Formula weight	922.33	
Temperature	200(2) K	
Wavelength	1.54178 Å	
Crystal system	Monoclinic	
Space group	$P2_1/c$	
Unit cell dimensions	a = 6.8976(4) Å	□= 90°.
	b = 22.8703(12) Å	□= 94.609(2)°.
	c = 10.5306(5) Å	□ = 90°.
Volume	1655.83(15) $Å^3$	
Z	2	
Density (calculated)	1.850 Mg/m^3	
Absorption coefficient	10.914 mm^{-1}	
F(000)	932	
Crystal size	0.260 x 0.020 x 0.015 mm^3	
Theta range for data collection	3.865 to 70.108°.	

Index ranges	-7<=h<=8, -27<=k<=24, -12<=l<=12
Reflections collected	19101
Independent reflections	2993 [R(int) = 0.0598]
Completeness to theta = 66.000°	97.5 %
Absorption correction	Multi-scan
Max. and min. transmission	1.000 and 0.480
Refinement method	Full-matrix least-squares on F^2
Data / restraints / parameters	2993 / 0 / 299
Goodness-of-fit on F^2	1.044
Final R indices [I>2sigma(I)]	R1 = 0.0403, wR2 = 0.1077
R indices (all data)	R1 = 0.0414, wR2 = 0.1089
Extinction coefficient	n/a
Largest diff. peak and hole	1.790 and -0.801 e.$Å^{-3}$

Table C41. Atomic coordinates (x 10^4) and equivalent isotropic displacement parameters ($Å^2$x 10^3) for 5.5. U(eq) is defined as one third of the trace of the orthogonalized U^{ij} tensor.

	x	y	z	U(eq)
Pd	3860(1)	653(1)	4120(1)	21(1)
Cl	6676(1)	1063(1)	3512(1)	30(1)
O(1)	3103(3)	472(1)	7914(2)	29(1)
O(2)	-251(4)	26(1)	1453(2)	34(1)
O(3)	4386(3)	1833(1)	7522(2)	28(1)
O(4)	867(4)	2527(1)	7819(3)	49(1)

O(5)	1367(3)	1503(1)	978(2)	31(1)
O(6)	-1294(5)	2393(1)	-40(4)	47(1)
N(1)	4396(4)	718(1)	6042(3)	22(1)
N(2)	2531(4)	450(1)	2380(3)	24(1)
N(3)	1539(4)	278(1)	4647(2)	20(1)
C(1)	3057(5)	489(1)	6695(3)	23(1)
C(2)	1374(4)	221(1)	5902(3)	22(1)
C(4)	251(4)	69(1)	3729(3)	21(1)
C(5)	855(5)	192(1)	2416(3)	24(1)
C(6)	6069(5)	1002(1)	6731(3)	26(1)
C(7)	5879(5)	1663(2)	6743(3)	28(1)
C(8)	4370(6)	2454(2)	7651(4)	35(1)
C(9)	2746(6)	2638(2)	8434(4)	40(1)
C(10)	3219(6)	574(2)	1121(3)	28(1)
C(11)	3182(5)	1225(2)	830(3)	29(1)
C(12)	-117(6)	1383(2)	-14(4)	35(1)
C(13)	-1773(6)	1794(2)	125(4)	40(1)
O(1W)	515(5)	1468(2)	5971(4)	58(1)

Table C42. Bond lengths [Å] for 5.5.

Pd-N(3)	1.936(2)	N(1)-C(6)	1.465(4)	C(8)-H(8A)	0.94(5)
Pd-N(1)	2.033(3)	N(2)-C(5)	1.301(4)	C(9)-H(9A)	0.95(6)
Pd-N(2)	2.035(3)	N(2)-C(10)	1.471(4)	C(9)-H(9B)	1.02(5)
Pd-Cl	2.2940(7)	N(3)-C(2)	1.342(4)	C(10)-C(11)	1.521(5)

O(1)-C(1)	1.282(4)	N(3)-C(4)	1.347(4)	C(10)-H(10A)	0.95(4)
O(1)-H(1O)	1.13(8)	C(1)-C(2)	1.505(4)	C(10)-H(10B)	0.92(5)
O(2)-C(5)	1.277(4)	C(2)-C(4)#1	1.384(4)	C(11)-H(11A)	0.98(4)
O(3)-C(7)	1.422(4)	C(4)-C(2)#1	1.384(4)	C(11)-H(11B)	0.98(3)
O(3)-C(8)	1.427(4)	C(4)-C(5)	1.502(4)	C(12)-C(13)	1.496(6)
O(4)-C(9)	1.424(6)	C(6)-C(7)	1.517(5)	C(12)-H(12A)	0.88(5)
O(4)-H(4O)	0.79(6)	C(6)-H(6A)	0.94(4)	C(12)-H(12B)	0.94(6)
O(5)-C(11)	1.424(4)	C(6)-H(6B)	0.88(3)	C(13)-H(13A)	0.95(5)
O(5)-C(12)	1.429(5)	C(7)-H(7A)	0.94(4)	C(13)-H(13B)	0.93(5)
O(6)-C(13)	1.422(5)	C(7)-H(7B)	0.97(5)	O(1W)-H(1W1)	0.83(7)
O(6)-H(6O)	0.78(8)	C(8)-C(9)	1.503(5)	O(1W)-H(1W2)	0.79(7)
N(1)-C(1)	1.305(4)	C(8)-H(8B)	1.00(6)		

Table C43. Bond angles [°] for 5.5.

N(3)-Pd-N(1)	80.53(11)	N(3)-C(4)-C(5)	112.2(3)	C(8)-C(9)-H(9B)	111(3)
N(3)-Pd-N(2)	80.47(10)	C(2)#1-C(4)-C(5)	129.7(3)	H(9A)-C(9)-H(9B)	108(4)
N(1)-Pd-N(2)	160.99(11)	O(2)-C(5)-N(2)	126.0(3)	N(2)-C(10)-C(11)	111.6(3)
N(3)-Pd-Cl	177.71(7)	O(2)-C(5)-C(4)	118.9(3)	N(2)-C(10)-H(10A)	110(2)
N(1)-Pd-Cl	99.05(8)	N(2)-C(5)-C(4)	115.1(3)	C(11)-C(10)-H(10A)	108(2)
N(2)-Pd-Cl	99.92(8)	N(1)-C(6)-C(7)	112.3(3)	N(2)-C(10)-H(10B)	107(3)
C(1)-O(1)-H(1O)	108(4)	N(1)-C(6)-H(6A)	112(2)	C(11)-C(10)-H(10B)	112(3)
C(7)-O(3)-C(8)	109.8(3)	C(7)-C(6)-H(6A)	108(2)	H(10A)-C(10)-H(10B)	109(4)
C(9)-O(4)-H(4O)	101(4)	N(1)-C(6)-H(6B)	110(2)	O(5)-C(11)-C(10)	114.6(3)
C(11)-O(5)-C(12)	114.8(3)	C(7)-C(6)-H(6B)	109(2)	O(5)-C(11)-H(11A)	105(2)
C(13)-O(6)-H(6O)	98(7)	H(6A)-C(6)-H(6B)	105(3)	C(10)-C(11)-H(11A)	106(2)
C(1)-N(1)-C(6)	118.7(3)	O(3)-C(7)-C(6)	110.2(3)	O(5)-C(11)-H(11B)	110(2)
C(1)-N(1)-Pd	114.6(2)	O(3)-C(7)-H(7A)	108(2)	C(10)-C(11)-H(11B)	112(2)
C(6)-N(1)-Pd	126.8(2)	C(6)-C(7)-H(7A)	113(2)	H(11A)-C(11)-H(11B)	109(3)

C(5)-N(2)-C(10)	117.7(3)	O(3)-C(7)-H(7B)	108(2)	O(5)-C(12)-C(13)	108.4(3)
C(5)-N(2)-Pd	114.5(2)	C(6)-C(7)-H(7B)	107(3)	O(5)-C(12)-H(12A)	110(3)
C(10)-N(2)-Pd	127.8(2)	H(7A)-C(7)-H(7B)	110(3)	C(13)-C(12)-H(12A)	112(2)
C(2)-N(3)-C(4)	124.7(3)	O(3)-C(8)-C(9)	110.0(3)	O(5)-C(12)-H(12B)	110(3)
C(2)-N(3)-Pd	117.6(2)	O(3)-C(8)-H(8B)	109(3)	C(13)-C(12)-H(12B)	113(4)
C(4)-N(3)-Pd	117.65(19)	C(9)-C(8)-H(8B)	114(3)	H(12A)-C(12)-H(12B)	104(4)
O(1)-C(1)-N(1)	125.3(3)	O(3)-C(8)-H(8A)	110(3)	O(6)-C(13)-C(12)	114.0(3)
O(1)-C(1)-C(2)	120.0(3)	C(9)-C(8)-H(8A)	111(3)	O(6)-C(13)-H(13A)	105(3)
N(1)-C(1)-C(2)	114.7(3)	H(8B)-C(8)-H(8A)	102(4)	C(12)-C(13)-H(13A)	112(3)
N(3)-C(2)-C(4)#1	117.3(3)	O(4)-C(9)-C(8)	113.1(4)	O(6)-C(13)-H(13B)	109(3)
N(3)-C(2)-C(1)	112.6(3)	O(4)-C(9)-H(9A)	113(3)	C(12)-C(13)-H(13B)	106(3)
C(4)#1-C(2)-C(1)	130.2(3)	C(8)-C(9)-H(9A)	108(3)	H(13A)-C(13)-H(13B)	111(4)
N(3)-C(4)-C(2)#1	118.1(3)	O(4)-C(9)-H(9B)	104(3)	H(1W1)-O(1W)-H(1W2)	90(7)

Symmetry transformations used to generate equivalent atoms:

#1 -x,-y,-z+1

Table C44. Anisotropic displacement parameters ($Å^2$x 10^3) for 5.5. The anisotropic displacement factor exponent takes the form: $-2\pi^2[h^2 a^{*2}U^{11} + ... + 2 h k a^* b^* U^{12}]$

	U^{11}	U^{22}	U^{33}	U^{23}	U^{13}	U^{12}
Pd	27(1)	14(1)	21(1)	-1(1)	0(1)	-1(1)
Cl	29(1)	27(1)	36(1)	2(1)	3(1)	-2(1)
O(1)	38(1)	30(1)	19(1)	-1(1)	-6(1)	-8(1)
O(2)	46(1)	36(1)	18(1)	-2(1)	-1(1)	-14(1)
O(3)	34(1)	16(1)	36(1)	-2(1)	4(1)	-3(1)
O(4)	42(2)	51(2)	53(2)	22(1)	6(1)	8(1)

O(5)	36(1)	28(1)	29(1)	-2(1)	-5(1)	0(1)
O(6)	46(2)	40(2)	57(2)	-6(1)	5(2)	6(1)
N(1)	27(1)	16(1)	21(1)	-1(1)	-1(1)	1(1)
N(2)	35(1)	16(1)	20(1)	-1(1)	0(1)	-2(1)
N(3)	30(1)	12(1)	18(1)	-1(1)	-2(1)	1(1)
C(1)	32(2)	15(1)	21(2)	-3(1)	-4(1)	2(1)
C(2)	31(2)	14(2)	20(2)	-3(1)	-2(1)	2(1)
C(4)	33(2)	12(1)	17(1)	-3(1)	-1(1)	2(1)
C(5)	36(2)	20(2)	14(1)	0(1)	2(1)	-1(1)
C(6)	26(2)	21(2)	30(2)	-3(1)	-5(1)	1(1)
C(7)	30(2)	24(2)	29(2)	-1(1)	0(1)	-6(1)
C(8)	40(2)	18(2)	48(2)	-1(2)	6(2)	-3(1)
C(9)	46(2)	25(2)	50(2)	-3(2)	11(2)	1(2)
C(10)	40(2)	22(2)	21(2)	-1(1)	6(2)	-1(1)
C(11)	36(2)	24(2)	26(2)	2(1)	1(1)	-4(1)
C(12)	42(2)	29(2)	32(2)	1(2)	-5(2)	-7(2)
C(13)	32(2)	53(2)	34(2)	3(2)	-2(2)	-7(2)
O(1W)	44(2)	37(2)	90(3)	-2(2)	-10(2)	7(2)

Table C45. Hydrogen coordinates (x 10^4) and isotropic displacement parameters (Å^{2}x 10^3) for 5.5.

	x	y	z	U(eq)

H(1O)	1700(110)	270(40)	8190(80)	110(30)
H(4O)	770(80)	2780(30)	7320(50)	58
H(6O)	-810(110)	2360(40)	-680(80)	90(30)
H(6A)	6240(50)	875(17)	7580(40)	18(8)
H(6B)	7150(50)	907(14)	6390(30)	4(7)
H(7A)	5590(50)	1823(17)	5920(40)	16(8)
H(7B)	7110(60)	1820(20)	7120(40)	35(11)
H(8B)	5680(90)	2590(20)	8000(60)	60(15)
H(8A)	4240(60)	2630(20)	6840(40)	30(10)
H(9A)	2940(70)	3040(20)	8650(50)	48(13)
H(9B)	2780(70)	2400(20)	9250(50)	45(12)
H(10A)	2410(50)	381(17)	480(40)	16(8)
H(10B)	4460(70)	420(20)	1130(40)	34(10)
H(11A)	4090(60)	1407(18)	1470(40)	26(9)
H(11B)	3610(50)	1309(16)	-20(30)	18(8)
H(12A)	-490(60)	1020(20)	30(40)	27(10)
H(12B)	390(80)	1410(30)	-820(60)	59(15)
H(13A)	-2220(70)	1770(20)	950(50)	38(11)
H(13B)	-2740(70)	1690(20)	-500(50)	36(11)
H(1W1)	1390(100)	1670(30)	6310(60)	69
H(1W2)	-60(90)	1750(30)	5730(60)	63(17)

Table C46. Torsion angles [°] for 5.5.

C(6)-N(1)-C(1)-O(1)	-2.4(5)	C(10)-N(2)-C(5)-C(4)	179.0(3)

Pd-N(1)-C(1)-O(1)	179.0(3)	Pd-N(2)-C(5)-C(4)	-2.5(3)
C(6)-N(1)-C(1)-C(2)	178.6(3)	N(3)-C(4)-C(5)-O(2)	-178.9(3)
Pd-N(1)-C(1)-C(2)	0.0(4)	C(2)#1-C(4)-C(5)-O(2)	1.5(5)
C(4)-N(3)-C(2)-C(4)#1	-0.8(5)	N(3)-C(4)-C(5)-N(2)	3.1(4)
Pd-N(3)-C(2)-C(4)#1	-177.4(2)	C(2)#1-C(4)-C(5)-N(2)	-176.6(3)
C(4)-N(3)-C(2)-C(1)	178.8(3)	C(1)-N(1)-C(6)-C(7)	-100.5(4)
Pd-N(3)-C(2)-C(1)	2.2(3)	Pd-N(1)-C(6)-C(7)	77.9(3)
O(1)-C(1)-C(2)-N(3)	179.5(3)	C(8)-O(3)-C(7)-C(6)	173.2(3)
N(1)-C(1)-C(2)-N(3)	-1.4(4)	N(1)-C(6)-C(7)-O(3)	69.6(4)
O(1)-C(1)-C(2)-C(4)#1	-0.9(5)	C(7)-O(3)-C(8)-C(9)	177.9(3)
N(1)-C(1)-C(2)-C(4)#1	178.2(3)	O(3)-C(8)-C(9)-O(4)	-66.7(5)
C(2)-N(3)-C(4)-C(2)#1	0.8(5)	C(5)-N(2)-C(10)-C(11)	109.8(3)
Pd-N(3)-C(4)-C(2)#1	177.4(2)	Pd-N(2)-C(10)-C(11)	-68.6(4)
C(2)-N(3)-C(4)-C(5)	-178.9(3)	C(12)-O(5)-C(11)-C(10)	-74.8(4)
Pd-N(3)-C(4)-C(5)	-2.2(3)	N(2)-C(10)-C(11)-O(5)	-52.4(4)
C(10)-N(2)-C(5)-O(2)	1.1(5)	C(11)-O(5)-C(12)-C(13)	-168.5(3)
Pd-N(2)-C(5)-O(2)	179.6(3)	O(5)-C(12)-C(13)-O(6)	63.7(4)

Symmetry transformations used to generate equivalent atoms:

#1 -x,-y,-z+1

Table C47. Hydrogen bonds for 5.5 [Å and °].

D-H...A	d(D-H)	d(H...A)	d(D...A)	<(DHA)
O(1)-H(1O)...O(2)#1	1.13(8)	1.29(8)	2.413(3)	171(8)
O(4)-H(4O)...O(5)#2	0.79(6)	2.22(6)	2.985(4)	165(6)
O(6)-H(6O)...O(4)#3	0.78(8)	2.07(8)	2.818(5)	162(9)

C(10)-H(10A)...O(2)#4	0.95(4)	2.60(4)	3.539(5)	173(3)
C(11)-H(11A)...Cl	0.98(4)	2.79(4)	3.583(4)	138(3)
O(1W)-H(1W1)...O(3)	0.83(7)	2.37(7)	3.130(5)	154(6)
O(1W)-H(1W1)...O(4)	0.83(7)	2.56(7)	3.105(5)	125(5)
O(1W)-H(1W2)...O(6)#2	0.79(7)	2.26(7)	3.045(5)	172(6)

Symmetry transformations used to generate equivalent atoms:

#1 -x,-y,-z+1 #2 x,-y+1/2,z+1/2 #3 x,y,z-1

#4 -x,-y,-z